

THESE DE DOCTORAT

DAIRY FOULING ON STAINLESS STEEL AND DESIGN
OF ANTIFOULING SURFACES

Encrassement laitier sur acier inoxydable et design de surfaces anti-encrassantes

Thèse préparée et soutenue publiquement à

L'UNIVERSITÉ DE LILLE – SCIENCES ET TECHNOLOGIE

École doctorale Sciences de la Matière, du Rayonnement et de l'Environnement (SMRE)

Pour obtenir le grade de

DOCTEUR

Spécialité : Physique et Sciences des Matériaux

Par

Sawsen ZOUAGHI

Soutenue le 19 Octobre 2018

Devant la commission d'examen composée de :

Pr. Ian Wilson	Rapporteur	University of Cambridge (UK)
Pr. Farzaneh AREFI-KHONSARI	Rapporteur	La Sorbonne (FR)
Dr. Yves ANDRIAENSSENS	Examineur	Chemours (BE)
M. Jean-Jacques SNAPPE	Examineur	Ingredia (FR)
Dr.-Ing. Wolfgang AUGUSTIN	Examineur	Braunschweig University (GE)
Dr. HDR Guillaume DELAPLACE	Examineur	INRA Villeneuve d'Ascq (FR)
Dr. HDR Christophe ANDRE	Co-directeur de thèse	HEI Lille (FR)
Pr. Maude JIMENEZ	Directeur de thèse	Université de Lille (FR)

ACKNOWLEDGEMENTS

First of all, I would like to thank Pr. Patrice Woisel and Pr. Serge Bourbigot for welcoming me in the UMET laboratory and the ISP team, allowing me to be a part of this lab during my PhD. I am also very grateful to Dr. Guillaume Delaplace for his warm welcome in the PIHM team and for all his kindness and advices (even though it seems I exhausted him sometimes).

Then, I address all my thanks to Dr. Christophe André for his help with my articles, presentations and for his availability. Now, I want to acknowledge someone very special: Prof. Maude Jimenez. Maude, you were more than a director, you were a true mentor. Thank you for all the things you taught me, there are so much I could not list them. I will never forget trips we made together, to South Korea and Sweden, nor your life-saving chocolate plates. You gave me a chance and helped me achieve this important work, and I truly hope we will stay in touch and maybe work again together someday.

I would also like to warmly thank Prof. Ian Wilson and Prof. Farzaneh Arefi-Khonsari for their interest in my work and for dedicating their time and expertise to the examination of this manuscript. I am also very grateful to Dr.-Ing. Wolfgang Augustin from Braunschweig University, Dr. Yves Adriaenssens from Chemours and to Dr. Jean-Jacques Snappe from Ingredia for accepting to be a part of my defense jury.

During those three years, several members of UMET gave me substantial help with various parts of my thesis: Séverine Bellayer with the EPMA imaging, Ahmed Addad for the SEM imaging, Brigitte Vermessen with my first attempts to understand and manage university paperwork, Thierry Six with the pilot pasteurizer unit, Joel Lyskawa with polydopamine coatings, Nour-Eddine Chihib and Marwan Abdallah for microbiology tests, Jérôme Frémiot about Life Cycle Assessment approach. I am deeply grateful to every one of them, as I could not have completed this work without their precious help. I would also like to express my gratitude to all the members of the PIHM team who helped me during my thesis. I am also grateful to Nicolas Nuns and Pardis Simon from the UCCS lab for their help with ToF-SIMS and XPS analysis, respectively. A big thank you to all of them.

I would also like to acknowledge the people who accepted to collaborate with me and helped me to put together great papers: Melissa Grunlan and Mikayla Barry from the Texas A&M University, Savvas Hatzikiriakos and Sona Moradi from the University of British Columbia, Yannick Coffinier, Vincent Thomy and Thomas Dargent from IEMN.

A special thank you for my former teachers, Frédéric Chirat from the University of Lille, as well as Krasimir Dimitrov, Peggy Vauchel, Frédéric Krzewinski and Bruno Delbreil from Polytech'Lille, for their guidance during my studies but also during my first steps in teaching. I would also like to acknowledge my students at Polytech'Lille as well as my internship students Thibaud Zilliox and Fatouma Mouzé for the work they did with me and for me. I wish them all the best for their future endeavors.

Now it is time to thank my labmates, people with whom I worked side by side every day. First, my power girls Morgane, Charlotte, Anne-Lise and Laura but also Elodie, Roland, Pierre, Johan, Sophie K, Chi, Tatenda, Pauline, Mariem and Guizem. Whether with few words or long conversations, every one of you once made me smile, or laugh, or feel better, and I thank you for this. I do not forget Nittaya, Laurie and Audrey, who were there when I arrived at the lab and already graduated and with whom I spend great moments. A special thanks to Agnès, who was a true lifejacket during my first days at the lab and quickly became a true friend.

I also address a warm thank you to the senior staff of the lab, Prof. Gaëlle Fontaine, Prof. Sophie Duquesne, Dr. Fabienne Samyn, Dr. Mathilde Casetta, Dr. Fanny Bonnet and Prof. Michel Traisnel for their kindness and advice.

It is now the time to mention my family. First, my grandparents Mamie Dhabia, Granny, and Papy, whom I always want to make proud and who I know always believe in me. I am also grateful to my aunts and uncles Corinne, Titia, Fabien, Diane and Djépi for their support and their never-ending encouragements.

To my sisters, I have so much to say. Maëlle, Léa and Cassandre I think you truly are one of the main reasons I always wanted to do my best and reach high goals. Thank you for this but also for the comfort and encouragement you gave me all along. I do not forget my little niece, Mia, whose smile brightened a lot of hard days.

I am very grateful to my in-law family, Michelle, Philippe, Quentin, Floriane, Théo, Zoé, Violette, Lison but also Mamie Micheline and Papy Michel, for all their kindness and support through these years.

I would like to take some time to thank my father, who most certainly was the trigger of my scientific career, who always pushed me to be the better person (and scientist) I could be; and my mother, who always believed in me and was proud of me, which gave me confidence and helped me achieve this.

Last but so far from least, Félix, my love, thank you for your support, your patience and your tenderness. I could not, in a million years, had done it without you. You were both a motor and a haven. Thank you so much.

TABLE OF CONTENTS

- LIST OF ABBREVIATIONS 5
- GENERAL INTRODUCTION 7
- Chapter 1 - DAIRY FOULING IN THERMAL PROCESSING: MECHANISMS AND IMPACTING FACTORS..... 9
 - Introduction..... 11
 - 1. Dairy fouling composition 13
 - 1.1. Whey proteins 13
 - 1.2. Minerals 16
 - 1.3. Other milk components 18
 - 2. Fouling Mechanisms 19
 - 3. Impacting factors 23
 - 3.1. Fluid composition and characteristics..... 24
 - 3.2. Process characteristics..... 27
 - 3.3. Surface properties of the substrate. 30
 - 4. Cleaning of Dairy Fouling 48
 - Conclusions 51
- Chapter 2 - INFLUENCE OF THE SURFACE PROPERTIES OF STAINLESS STEEL ON DAIRY FOULING 53
 - Introduction..... 55
 - 1. Presentation of the pilot test unit..... 56
 - 1.1. Model fluid..... 56
 - 1.2. Pilot pasteurization rig 57
 - 2. Bacterial adhesion tests..... 60
 - 3. Model surfaces 61
 - 3.1. Surface preparation 61
 - 3.2. Surface characterizations..... 63

4.	Whey protein fouling results	68
4.1.	Impact of physical modifications	71
4.2.	Impact of chemical modifications	76
5.	Bacterial adhesion results.....	78
	Conclusions	80
Chapter 3 - BIOMIMETIC ANTIFOULING SURFACES		83
	Introduction.....	85
1.	Slippery liquid-infused surfaces	86
1.1.	SLIPS-like surface design	87
1.2.	Surface characterizations.....	88
1.3.	Fouling performances	92
2.	Nanotextured plasma coatings	97
2.1.	Atmospheric Pressure Plasma Sprayed Coatings	98
2.2.	Influence of the manufacturing parameters on surface properties.....	99
2.3.	Fouling performances of HMDSO coatings	104
2.4.	Bacterial Adhesion Assay	110
3.	Amphiphilic environment-responsive coatings.....	112
3.1.	Coatings formulation and surface preparation	114
3.2.	Surface properties of PEO-silicone coatings	117
3.3.	Isothermal fouling study	120
3.4.	Clean in place following isothermal fouling study.....	123
3.5.	<i>In situ</i> fouling study.....	124
3.6.	Bacterial Adhesion Assay	125
	Conclusions	127
Chapter 4 - INFLUENCE OF SURFACE MODIFICATION ON THE ENVIRONMENTAL IMPACT OF PASTEURIZATION		129

Introduction.....	131
1. The LCA Approach.....	132
1.1. About LCA	132
1.2. Goals and scope of the present LCA study.....	134
1.3. Description of the investigated systems	137
1.4. Life Cycle Inventories (LCIs)	139
1.5. Method for the LCA analyses.....	143
2. Results of the life cycle assessment.....	145
2.1. Life Cycle Assessment of the REF system.....	145
2.2. Life cycle assessment of Si-PEO system.....	150
Conclusions	154
CONCLUSIONS AND OUTLOOKS.....	155
General Conclusion	157
Outlooks	161
REFERENCES	169
ANNEXES.....	183
ANNEX I	185
ANNEX II	197
ANNEX III	201
ANNEX IV	211
ANNEX V	223
ANNEX VI.....	225
ANNEX VII	231

LIST OF ABBREVIATIONS

AA	Amino acid
APPS	Atmospheric pressure plasma spraying
CAH	Contact angle hysteresis
CCE	Climate change ecosystem
CCH	Climate change human health
CIP	Cleaning in place
Cys	Cysteine
DLC	Diamond-like carbon
EPMA	Electron-probe micro-analysis
EoL	End of life
EEW	Electrical and Electronic waste
FD	Fossil depletion
FU	Functional unit
HT	Human toxicity
IC	Impact category
LCA	Life cycle assessment
LCI	Life cycle inventory
MD	Metal depletion
MF	Model fluid
ML	Mirror-like stainless steel
NAT	Native stainless steel
NLT	Natural land transformation
PD	Polydopamine
PDMS	Poly(dimethylsiloxane)
PECVD	Plasma enhanced chemical vapor deposition

PEG, PEO	Poly(ethylene glycol), Poly(ethylene oxide)
PHE	Plate heat-exchanger
PTFE	Poly(tetrafluoroethylene)
PVA	Poly(vinylamine)
PW	Physiological water
RO	Reverse osmosis
RTV	Room temperature vulcanizing
SEM	Scanning electron microscopy
SFE	Surface free energy
SLIPS	Slippery liquid infused porous surface
SiIML	Fluorosilanized mirror-like stainless steel
SiINAT	Fluorosilanized native stainless steel
SiITEX	Fluorosilanized textured stainless steel
SS	Stainless steel
TEX	Textured stainless steel
ToF-SIMS	Time-of-flight secondary ion mass spectroscopy
TSB	Tryptic soy broth
WCA	Water contact angle
XPS	X-ray photoelectron spectroscopy
α-La	α -Lactalbumin
β-Lg	β -Lactoglobulin
Ra	Arithmetic mean roughness (μm , nm)
Rq	Root mean squared roughness (μm , nm)
θ	Contact angle ($^{\circ}$)
γ	Surface energy (mN/m)

GENERAL INTRODUCTION

One of the greatest challenges of the XXIst century is to fairly provide sustainable and quality food to the growing population of the planet, which will soon reach 10 billion of individuals. With this goal, and due to the increasing demand of emergent countries, food industries and researchers must work to develop eco-efficient and eco-friendly processes.

Among large-scale processed foods, milk and dairy products are of great importance. Indeed, the global milk production is estimated to be 735 billion liters annually, European Union (EU) being one major actor with a production of 156 billion liters^{1,2}. Dairy production has moreover doubled since 2000 and this trend is expected to continue, along with the expanding dairy market³. The European model is an excellent example of dairy industries significance in the global food industry as, according to the European Dairy Association (EDA), dairy products represent more than 12 000 production sites and more than 300 000 direct jobs in the EU⁴.

Indeed, milk and its derivatives present numerous interesting nutritive and functional properties (emulsification, gelation, foaming), and processes for their preparation and transformation have been booming over the past decades. Beyond traditional goods like bottled milk, yoghurt and cheese, the past decades have seen emerging a clear tendency to valorize every by-product of the dairy sector, *e.g.* whey protein, micro- and ultrafiltration permeates or caseins. A remarkable number of highly transformed products – from baby food to sport supplements – indeed contain dairy components⁵.

However, due to their rich water and nutritive content, dairy products are environments of choice for the growth of micro-organisms, which can both spoil the products organoleptic properties and jeopardize consumer's health through foodborne toxi-infections. To ensure the microbiological harmlessness of dairy products, as well as to transform them and extend their shelf-life, thermal treatments are therefore mandatory⁶. As a matter of fact, every dairy product is at least heated once during its transformation⁷ (pasteurization being the most common treatment) and around 91% of worldwide consumed milk passes through this energy-intensive operation⁸. In most production lines, thermal treatment is realized by heat transfer through a conductive material, mainly stainless steel. Particularly, thermal treatments implementing plate heat exchangers (PHE)

are well established and mature processes, which nevertheless present some drawbacks. Notably, fouling, *i.e.* the deposition and accumulation of unwanted material in industrial equipment, burdens heat processes both financially, through oversizing, production loss and cleaning costs⁹; and environmentally, by drastically increasing energy consumption and wastewater volume¹⁰. According to the Environmental Impact of PROducts (EIPRO) analysis, the production and processing of milk and other dairy products indeed accounts for around 5% of global warming potential, 10% of eutrophication potential and 4% of photochemical ozone creation potential across the European Union¹¹. It was also shown that the cost related to production interruption for cleaning can be dominating¹², and that product quality can suffer from fouling, because of the potential presence of detached deposits in the final product¹³. Thus, fouling mitigation solutions, that could help significantly reduce dairy production costs and environmental impact, as well as progressing toward more sustainable and cost-saving thermal processes, are very much sought-after.

Consequently, dairy fouling has been vastly studied since the 1960's and significant efforts have been made in order to elucidate its underlying mechanisms as well as to propose mitigation approaches. In order to contribute to this important research, the purpose of the present thesis work is to explore innovative nonfouling surfaces designed following a biomimetic approach, to study their mode of action in order to further develop antifouling strategies for the dairy sector and to assess the impact of antifouling surfaces on the environmental footprint of dairy thermal treatments

This manuscript therefore organizes in four chapters. Chapter 1 consists in a bibliographic overview of dairy fouling agents, mechanisms and impacting factors. Chapter 2 will then present a fundamental study on the impact of stainless steel surface properties on dairy fouling. In Chapter 3, the surface properties of the selected biomimetic surfaces, as well as their fouling performances will be described. Finally, the impact of surface modification on the global environmental impact of a pasteurization process will be investigated in Chapter 4, through a Life Cycle Assessment study.

Chapter 1 - DAIRY FOULING IN THERMAL PROCESSING: MECHANISMS AND IMPACTING FACTORS

Introduction

Thermal treatments are omnipresent in dairy processing^{14,15}, as they allow to control the microbiological quality and to increase the shelf-life of products. Heating food to high temperatures indeed induces the elimination of spoilage and pathogenic micro-organisms but also the deactivation of enzymes which could rapidly alter the taste, organoleptic properties and nutritive value of the product.

Among thermal treatments, pasteurization is a mild process during which human pathogenic agents are destroyed. In dairy industries, two types of pasteurization are commonly found, according to the temperature range they involve. Low temperature pasteurization consists in heating the product to 63°C for 30 min, whereas classical pasteurization involves temperatures around 72-76°C and 15 to 20 s durations. More recent processes, like High Temperature Short Time (HTST) pasteurization, require higher temperatures (80-90°C) and shorter exposure (around 5 s)¹⁰. Sterilization, on the other hand, allows the elimination of the major part of a product's microbiological flora with temperatures up to 115°C and exposure time of 15 to 20 min. Ultra-High Temperature (UHT) processes involve temperatures up to 150°C and extremely short exposure (2s)⁵. Besides microbiological control, thermal processing is also used for transformation purposes like texturing or evaporation¹⁶. Overall, every dairy product is heated at least once before its commercialization⁷.

However, milk and dairy products tend to foul the industrial equipment when they are exposed to high temperature. The generated deposits burden both the financial and environmental balance of thermal processes. Indeed, heat-induced deposits impair the proper execution of the heat treatment by adding a thermal resistance to the system, increasing processing costs through higher energy and water intake. Overall, about 80% of the total production costs of dairy derivatives are related to fouling¹⁷. Moreover, the mandatory frequent, severe cleaning-in-place (CIP) procedures result in pronounced economic and environmental impacts through production loss and excessive rinsing water, energy and chemicals consumption.

Thus, understanding of fouling phenomenon and its control are major challenges that would allow progressing toward less expensive and more eco-efficient processes. Over the years, a significant research effort has been dedicated to the elucidation of dairy fouling mechanisms and to the identification of the factors that can impact it. This first chapter will focus on the study of dairy fouling, its mechanisms, impacting factors and cleaning.

1. Dairy fouling composition

Milk is a rich and complex bio-emulsion (Figure 1.1) containing colloidal fat and proteins (caseins), as well as soluble sugars, minerals and whey proteins (among which β -lactoglobulin, β -Lg and α -lactalbumine, α -La). Potentially, all milk components might be involved in various phases of thermal milk fouling, depending on their physicochemical properties and especially according to their heat sensitivity. Hence, dairy fouling composition depends in the first place on the considered milk derivative. However, study of milk deposits on heat-transfer surfaces showed that it was mainly composed of minerals and whey proteins. Interestingly, caseins, sugars and fat, which represent over 80% of milk's soluble and colloidal content, are not significant contributors to deposit growth⁵. The following sections will review the main components of dairy fouling and their characteristics.

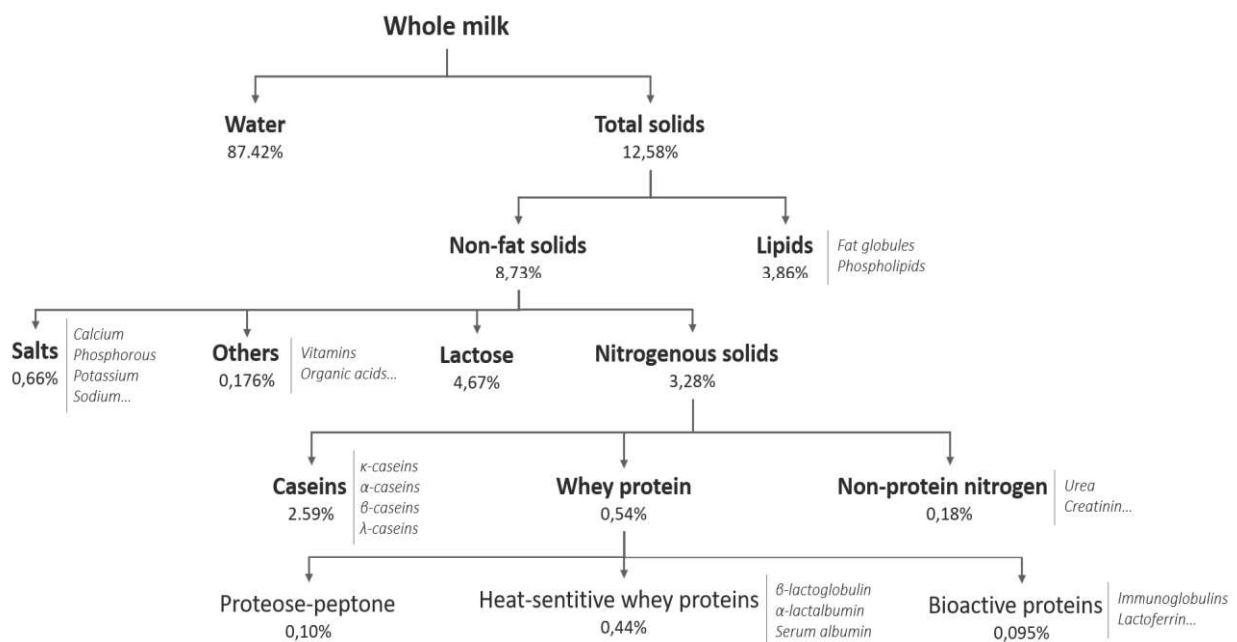


Figure 1.1. Distribution of milk components (adapted from Sadeghinezhad *et al.* (2014)¹²).

1.1. Whey proteins

Whey proteins are the most thermosensitive proteins in milk¹⁸. According to Polat (2009)¹⁹, α -La has the lowest denaturation temperature of all whey proteins, followed by bovine serum albumin (BSA), immunoglobulins and finally β -Lg (77°C^{20,21}). However, inside the pasteurization temperature range, β -Lg unfolds faster than all other whey proteins, hence its preponderant part-taking to fouling¹². As a matter of fact, ever since 1990, a correlation between β -Lg

denaturation and fouling growth has been established²² and numerous studies on dairy fouling are based on the behavior of β -lactoglobulin^{23–32}.

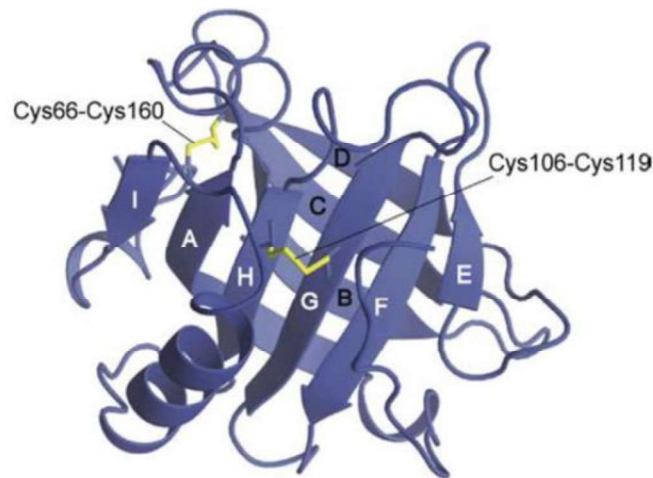


Figure 1.2. β -Lactoglobulin tertiary structure, according to Ikeguchi (2014)³³.

β -Lg (Figure 1.2) is the major component of cow milk soluble protein fraction. Its usual concentration is around 3.5 g/L, although this value may vary geographically, seasonally and with cattle breed⁶. It is a globular protein composed of 162 amino-acids (AA) and its secondary structure consists in 6 to 10% of α -helix, 44 to 52% of β -sheets, 8-10% of turns and 32 to 35% of random coil³⁴. The globular tertiary structure of β -lg is predominantly due to the presence of several cysteine (Cys) residues interacting with each other *via* disulfide bridges (Cys₆₆-Cys₁₆₀ and Cys₁₀₆-Cys₁₁₉). Another cysteine residue located in the inner section of the protein carries a free thiol group^{5,35,36}, which is buried when the protein is under its native form. The quaternary structure of β -Lg greatly depends on environmental parameters such as the temperature, ionic force and pH which have individual and collective effects on the protein association state³⁷. In physiological conditions, the dimeric form is predominant, but β -Lg can also be found in tetrameric, octameric or multimeric state^{34,38}.

Even at room temperature, β -lactoglobulin is capable of irreversible adsorption on stainless steel (SS) in the form of monolayers. Trials at 30°C yielded an irreversible adsorption rate of 1.65 mg/m² within two hours³⁹. Tryptic digestion of adsorbed β -Lg allowed to prove that, in acidic pH ranges, *i.e.* in milk, acidic AA-containing peptides preferentially deposited on SS. Particularly, the T5 peptide fragment (Thr-Pro-**Glu-Asp-Asp-Glu**-Ala-Leu-**Glu**-Lys, residues 125-135), which includes 5 acidic AA (in bold), shows an adsorption behavior very close to that of

native β -Lg. Proteolysis experiments on irreversibly adsorbed β -lg corroborated those findings⁴⁰.

When temperature increases, β -lactoglobulin undergoes gradual changes, detailed by Khaldi (2016)⁵ as follows. At 40°C, the β -Lg irreversibly loses its dimeric quaternary structure, which yields two globular monomers. Between 40 and 55°C, minor modifications occur on the α -helix that masks the buried free thiol group. The protein becomes able to aggregate, however aggregation is negligible at this stage. Above the threshold of 60°C, the break of non-covalent intramolecular bounds induces unfolding, leading to a state commonly referred to as “molten globule”. This state induces significant aggregation. However, the transition from native form to molten globule is reversible, as covalent intramolecular bounds stay unharmed. Above 80°C, β -Lg unfolds irreversibly and above 130°C it loses its secondary structure. All along this process, the different states can occur simultaneously and interaction of molecules in different states is possible. The complexity of β -Lg thermal denaturation possible processes is well illustrated on Figure 1.3.

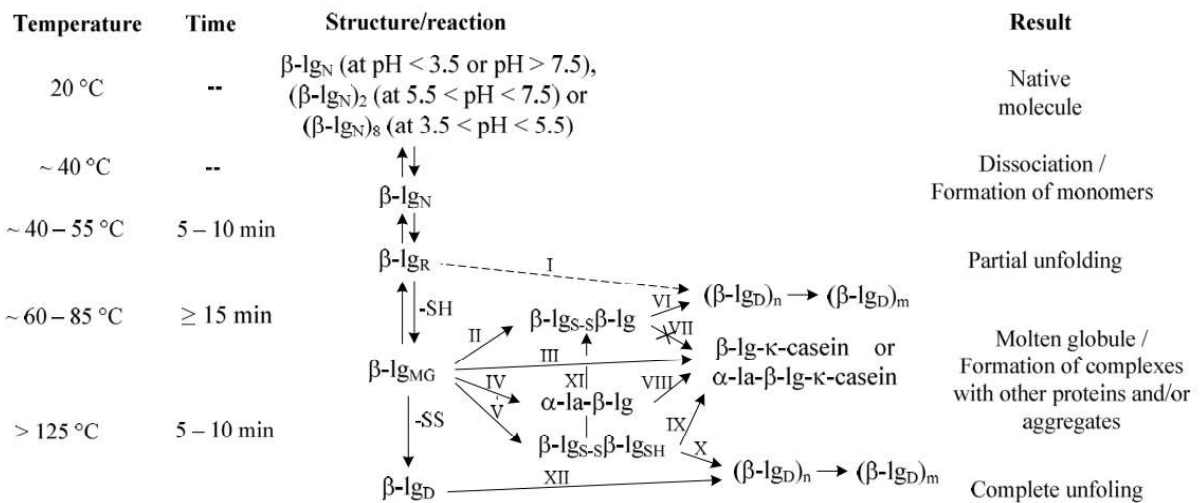


Figure 1.3. Mechanisms of β -Lg thermal denaturation, including the possible interactions with other proteins (from Boxler (2014)¹⁰). β -lg_N: native / β -lg_R: reversible native / β -lg_{MG}: molten globule / β -lg_D: denatured.

As pointed out by Boxler (2014)¹⁰ and Khaldi (2016)⁵, the behavior of β -Lg when subjected to increasing temperature depends on numerous factors such as pH⁴¹, heating conditions (temperature, rate, duration), concentration of protein, ionic strength and ionic composition, as well as hydrodynamic conditions⁴². Particularly, the calcium content has been spotted as a major controlling factor of β -Lg denaturation kinetics^{32,43}. It was indeed proven that an

increase in calcium concentration decreases the unfolding temperature of β -Lg from 83°C to 75°C⁴⁴. Later, Petit *et al.* (2011)⁴⁵ showed that calcium strongly impacts the protein unfolding and aggregation kinetics, pointing toward a catalytic effect of calcium on protein aggregation, through charge exchange phenomena.

The increased reactivity of heated β -Lg enables it to strongly interact with a substrate. In 1995, Itoh *et al.*⁴⁶ studied the adsorption of β -Lg on stainless steel (SS) at various temperatures and proposed a mechanism for protein deposition on stainless steel (Figure 1.4) which states that an unfolded β -Lg molecule can either adsorb on SS or aggregate with another molecule through disulfide bonding. They also point out that deposit build-up is caused by bonding of unfolded β -Lg to already adhered protein.

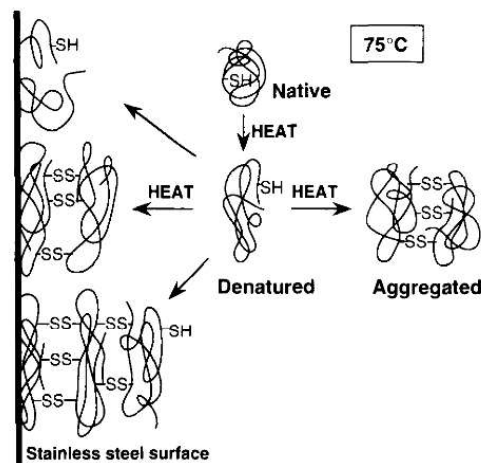


Figure 1.4. Schematic representation of thermally denatured β -Lg adsorption process according to Itoh *et al.* (1995)⁴⁶. ©1995 - Taylor & Francis.

1.2. Minerals

Unanimously, the most important minerals involved in heat-induced dairy fouling phenomena are calcium salts (mainly phosphates $[(Ca^{2+})_3 (PO_4^{3-})_2]$), because of their reverse-solubility to temperature^{12,47-49}, although, calcium carbonates have been shown to take part in deposit build-up in the absence of phosphates³².

Calcium phosphate precipitation and crystallization are intricate processes. Tsuge *et al.* (2002)⁵⁰ indeed reported numerous possible precipitation paths and products, depending on the pH and temperature of the media. They showed that, regardless of the temperature, precipitation did

not occur under pH 5.5. Between pH 5.5 and 7 and under mild temperature (below 35°C), calcium phosphate precipitates in the form of dicalcium phosphate dihydrate. From this point, with increasing pH and temperature, the crystallization products become more and more complex, finally reaching hydroxyapatite $[\text{Ca}_5(\text{PO}_4)_3(\text{OH})]$ ⁴² which is the least soluble calcium phosphate compound^{10,47}. Dey *et al.* (2010)⁵¹ proposed the following five-steps sequence of action for heat-induced calcium phosphate fouling in aqueous solutions:

- Lose aggregation of amorphous pre-nucleation clusters in the bulk
- Adhesion of the clusters on the substrate and formation of a monolayer
- Aggregation and density increase near the substrate
- Nucleation of amorphous particles
- Crystallization.

It is noteworthy that the precipitation and crystallization products of calcium phosphate are at some extent soluble.

However, in complex organic solutions like milk and dairy, the behavior of calcium salts under heating is quite difficult to predict. Figure 1.5 illustrates well this complexity. Calcium can indeed interact with inorganic species, principally phosphate salts, to yield mineral precipitation products like colloidal calcium phosphate or hydroxyapatite⁴². Calcium can also interact with milk organic content (protein, casein, fat) and deposit together with these species⁴⁷.

Anema (2009)⁵² observed that upon heating (from 20 to 80°C), a significant amount of soluble calcium is transferred to casein micelles, triggering a pH drop. This change in pH further encourages the thermal destabilization of the proteins and calcium-sensitive caseins become able to bind on crystalline calcium phosphate. However, Tsuge *et al.* (2002)⁵⁰ noted that the sequestering of calcium phosphate by whey protein delayed calcium precipitation. Nevertheless the authors also point out that the ability of calcium ions to bind β -Lg *via* carboxylic groups promote fouling and its stabilization by favoring the formation of intermolecular bridges between unfolded proteins. This effect was also evidenced by Jimenez *et al.* (2013)³².

Experimentally, the fouling of calcium salts is often investigated through the use of model solutions like simulated milk ultra-filtrate (SMUF)^{29,53,54} or simulated milk (SMUF with added

wey protein)^{55,56}. Generally, it was shown that calcium salts precipitation and fouling was a multi-dependent process, as it was impacted by pH, ionic strength and solution composition. In the case where SMUF was used alone, the authors reported calcium salts destabilization at lower temperatures than in milk, more likely due to the absence of calcium complexing phenomena induced by caseins and whey proteins.

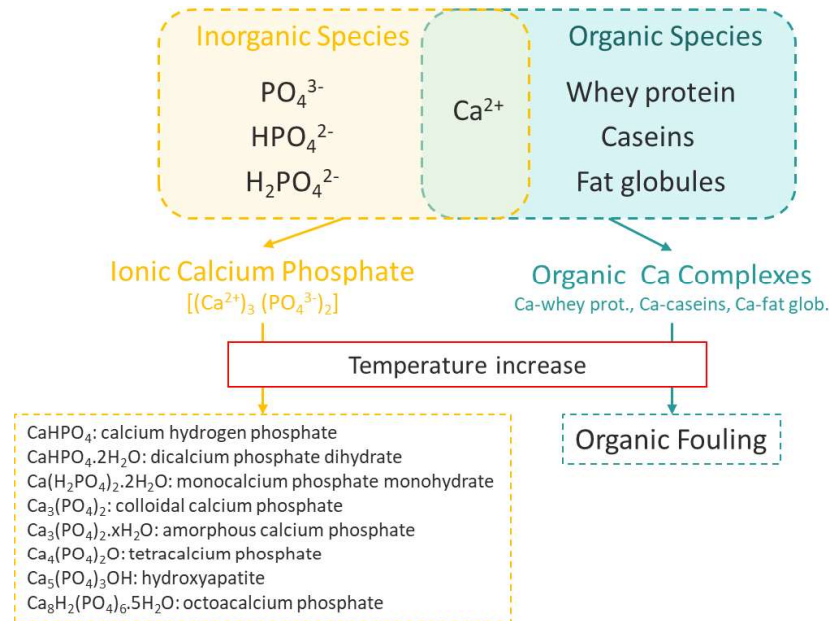


Figure 1.5: Calcium phosphate species in milk and their behavior under heating.

Overall, Boxler (2014) lists three major effects which can, either alone or combined, explain the enhancing effect of calcium on β -Lg denaturation and fouling, namely (i) formation of Ca²⁺-protein complexes due to intermolecular crosslinking; (ii) intramolecular shielding of negative charges on the protein which decreases the electrostatic repulsion phenomena; (iii) bridging between pre-existing deposits and bulk material and (iv) alteration of protein conformation leading to enhanced molecular interaction and aggregation. Khaldi *et al.* (2015, 2016, and 2018)^{4,34,48} indeed demonstrated the considerable impact of calcium on β -Lg unfolding and aggregation kinetics. However, it was found that an excess of calcium could inhibit deposit growth⁵⁸.

1.3. Other milk components

As said earlier, milk is a rich biofluid containing soluble minerals and proteins but also sugars, fat globules and colloidal protein, *i.e.* caseins.

Sugars, and particularly lactose, are generally considered as thermally stable and there is no report on their contribution to fouling. On the other hand, despite the fact that fat and caseins account for 80% of the total colloidal and soluble milk content¹⁰, they usually do not play a significant role in fouling^{7, 18, 59} unless damaged by other environmental variations (heavy shear stress, pH drop).

Caseins can indeed be found in dairy deposits if their thermal resistance has been compromised by pH or ionic strength variations. Once destabilized, they are able to bond with whey proteins or mineral species and therefore can take part to deposit build-up.

As for fat globules, they are generally considered as non-significant part-taker to fouling phenomena⁵⁹. However, similarly to caseins, they can interact with other species if damaged by a pH drop or high shear stress and can thus be trapped into the deposit network. However, it is possible for damaged globules to bond with whey protein and caseins *via* their membrane and as such, participate to fouling.

2. Fouling Mechanisms

Attempts to demystify dairy fouling mechanisms have been made since the 1960's. However, researchers struggled to reach consensus about the course of action of this multi-dependent phenomenon¹⁰. Epstein (1983)⁶⁰ proposed that fouling results from several mechanisms such as molecular adsorption and/or agglomeration, minerals or sugars crystallization or fat deposition, occurring weather consecutively or simultaneously. Further research led to the definition of an ensemble of consecutive or concomitant sub-processes generally accepted by the scientific community^{61, 62}:

- **Bulk Activation**, *i.e.* a change of affinity between soluble material and the surrounding aqueous phase, involving bulk denaturation and aggregation of proteins or precipitation of minerals;
- **Transport** of the activated material to the fluid-substrate interface;
- **Induction** of the fouling process, *i.e.* first deposition of foulant on the substrate;
- **Build-up**, *i.e.* the incorporation of additional fouling material to the pre-existing deposit;
- **Ageing** of the deposit involving thermal reactions, diffusion, re-entrainment, etc.

During the past decades, a particularly rich debate took place around several key steps of the fouling process, namely fouling limiting step, bulk governing reaction and the induction layer composition. Table 1.1 summarizes the different hypotheses formulated on those matters.

Table 1.1. Different controversial aspects of dairy fouling and the corresponding formulated hypotheses (adapted from Bansal and Chen (2006)⁶³, Sadeghinezhad *et al.* (2014)¹² and Boxler (2014)¹⁰).

	Hypothesis	References
Limiting step	Fouling depends on mass transfer and bulk and surface reactions	Toyoda <i>et al.</i> ⁶⁴ , Georgiadis and Macchietto (2000) ⁶⁵ , Bansal and Chen (2005) ⁶⁶
	Fouling depends only on bulk and surface reactions	Belmar-Beiny <i>et al.</i> ⁶⁷ , Jeurink <i>et al.</i> (1996) ²³ , Boxler <i>et al.</i> (2013) ⁶⁸
	Fouling depends only on bulk reactions	de Jong <i>et al.</i> (1992) ⁶⁹ , Belmar-Beiny <i>et al.</i> (1993) ⁶⁷ , Delplace <i>et al.</i> (1994) ⁷⁰ , Delplace <i>et al.</i> (1997) ⁷¹ , Schreier and Fryer ⁷² , Grijspeerdt <i>et al.</i> (2004) ⁷³
Governing bulk reaction	Protein denaturation	Lalande <i>et al.</i> (1985) ⁷⁴ , Hege and Kessler (1986) ⁷⁵ , Arnebrant <i>et al.</i> (1987) ⁷⁶ , Kessler and Bayer (1991) ⁷⁷ , Blanpain-Avet <i>et al.</i> (2012) ⁷⁸ , Jimenez <i>et al.</i> (2013) ³²
	Protein denaturation and aggregation	Belmar-Beiny <i>et al.</i> (1993) ⁶⁷ , Chen <i>et al.</i> (2001) ⁷⁹ , Bansal and Chen (2005) ⁶⁶ , Bansal <i>et al.</i> (2005) ⁸⁰
	Protein aggregation	Lalande et René (1988) ⁶ , Gotham <i>et al.</i> (1992) ⁴¹
Role of Aggregates	Aggregate do not take part to fouling build-up	Blanpain-Avet <i>et al.</i> (2012) ⁸¹ , Jimenez <i>et al.</i> (2013) ³²
	Fouling is caused only by aggregates	Toyoda <i>et al.</i> (1994) ⁶⁴ , Mahdi <i>et al.</i> (2009) ⁸² , Jun and Puri (2006) ⁸³ , Jun and Puri (2007) ⁸⁴
Early fouling stages	Minerals deposit first.	Tissier and Lalande (1986) ⁸⁵ , Britten <i>et al.</i> (1988) ⁸⁶ , Foster <i>et al.</i> (1989), Fryer and Belmar-Beiny (1991) ⁸⁷ ,
	Proteins deposit first.	Delsing and Hiddink (1983) ⁸⁸ , Changani <i>et al.</i> (1997) ²⁵ , Jimenez <i>et al.</i> (2013) ³²

❖ Limiting step.

It is generally admitted that mass transfers, as well as bulk and surface reactions are part of the fouling process. However, their relative importance has been debated. Several works propose that mass transfer and the previously mentioned reactions are all limiting steps in the fouling process^{64–66}, whereas other papers state that only reactions can be limiting^{23, 68,72}.

❖ Governing bulk reaction.

Over the years, it was proposed that fouling depends on mass transfers between the bulk and the substrate, or on bulk and surface reactions, or on both. Similarly, the nature of the governing bulk reaction remained uncertain and was resolved by studying the correlation between β -Lg unfolding and aggregation constants and fouling amounts. Historically, two main kinetic models were used to describe β -Lg hot denaturation. The first one features two consecutive reactions: unfolding (order 1) and aggregation (order 2), which each have their own constant. The second one features one global reaction with only one kinetic constant, which induces a break the Arrhenius plot. Dannenberg and Kessler (1988)⁸⁹ studied the irreversible denaturation kinetics of β -Lg and α -La, which allowed them to show the existence of critical temperatures (80-90°C) at which radical changes of kinetic parameters occur. Later, Petit *et al.* (2011)⁴⁵ came to similar conclusions. In this work, Arrhenius plotting (Figure 1.6) allowed to identify a critical temperature of about 80°C which delimits two fouling regimes. Above 80°C, experimental data fit an aggregation-limited model, meaning that as aggregation increases, less unfolded β -Lg is available for fouling. On the other hand, below 80°C, data fit an unfolding-limited model.

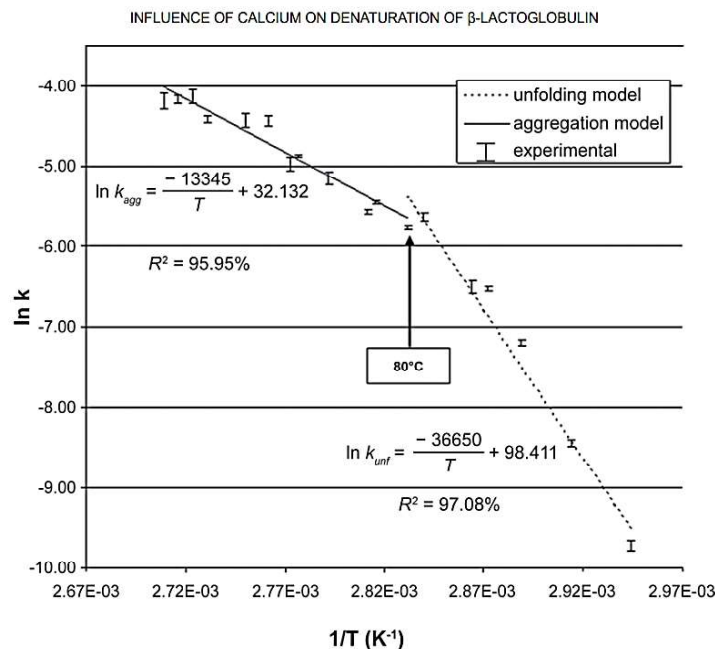


Figure 1.6. Arrhenius plot obtained for a solution of 53.3 g/L β -Lg and 264 mg/kg Ca with T (°K) and k_i the reaction rates ($\text{g}^{1-n} \cdot \text{L}^{n-1} \cdot \text{s}^{-1}$) from Petit *et al.* (2011)⁴⁵. © 2013 – Elsevier.

❖ *Role of aggregates.*

The role of aggregates in fouling is mostly controversial. Indeed, while several pieces of work^{64,82–84} state that dairy fouling only consists in protein aggregates, other sources demonstrated that aggregation enhancement contributed to fouling decrease^{17,71}. Several postulates were made to explain this state of fact, namely that due to their size, the transport of aggregates to the interface may be more difficult than that of single unfolded proteins⁷⁹, or that aggregates were less reactive than single proteins, and thus less prone to bound on existing deposit. Nevertheless, Jun and Puri (2006, 2007)^{83,84} proposed a 2-D predictive model of fouling in a PHE based on this assertion and proved that it is consistent with experimental data. However, the question of whether only aggregated proteins took part to fouling as proposed by Toyoda *et al.* (1994)⁶⁴, or if unfolded protein deposited as well and aggregation took place afterwards, during the ageing of the deposit, long remained unanswered. In an attempt to cast some light on this issue, Blanpain-Avet *et al.* (2012)⁸¹ analyzed isothermal fouling (*i.e.* the substrate is not a heat transfer surface) through RAMAN spectroscopy and found no trace of aggregates in the deposits. The same observation was made later by Jimenez *et al.* (2013)³². The divergence between those sources most probably comes from experimental differences. Jun and Puri (2006, 2007)^{83,84} indeed focused on PHE fouling, *i.e.* fouling on a heated surface, whereas Blanpain-Avet *et al.* (2012)⁸¹ and Jimenez *et al.* (2013)³² studied deposits harvested on non-heated surfaces (isothermal fouling) located after a PHE. Thus, one way to explain the composition difference between heat-transfer surfaces and unheated surfaces would be that unfolded protein deposits in both cases and that thermal energy triggers further aggregation on heated substrate. Overall, additional research, which could benefit from the use of Raman spectroscopy, is needed to elucidate this point.

❖ *Early fouling stages.*

It has been reported that the first micrometer of a deposit layer was principally constituted of mineral⁸⁷. Sandu (1989)⁹⁰ proposed that during the first minute of fouling, a compact layer, mainly composed of calcium phosphate grew on the substrate and acted as an anchor for proteins, leading to two-layered deposits. This kind of two-layered deposit was also reported by several other authors^{23, 25, 61, 81,91}. However, another explanation to these observations was suggested, *i.e.* that protein deposited first and mineral species diffused through the deposit as it ages⁶¹, to crystallize near the interface⁸⁵. This last hypothesis was confirmed by Tissier and

Lalande (1986)⁸⁵ who showed that, for fouling times longer than 1 h, the deposits were composed of two layers (a protein-rich one at the fluid interface and a mineral rich one near the substrate) whereas for shorter fouling time, there no mineral-rich sublayer was found. This is consistent with the findings of Jimenez *et al.* (2013)³² who showed, through a multiscale analysis of one minute to two hours long fouling, that protein adsorbs first on an unheated SS substrate.

3. Impacting factors

Dairy fouling is widely recognized as a multi-dependent process. A review by Sadeghinezhad *et al.* (2013)¹² indeed emphasizes its variability by reporting fourteen different fouling deposit compositions, obtained from fourteen studies with various processing conditions (dairy product type, working temperature and equipment). The numerous factors impacting fouling (Figure 1.7) can be classified into three major categories, namely (i) the processed product composition and characteristics, (ii) the thermal process operating conditions and (iii) the equipment’s surface properties.

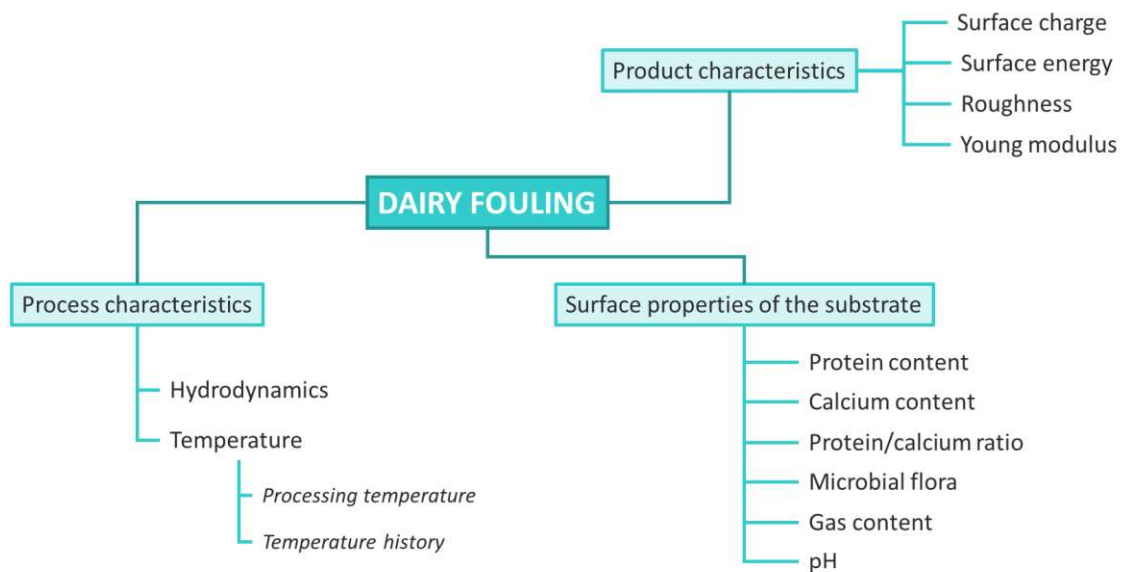


Figure 1.7. Factors impacting dairy fouling.

3.1. Fluid composition and characteristics

3.1.1. Whey protein content

Obviously, whey protein concentration is critical to fouling, as these proteins are one of its major components. Thus, fouling growth has been shown to increase linearly with protein concentration⁹². According to Fickak *et al.* (2011)⁹³, whey protein concentration influences not only the amount of fouling but also its structure (*i.e.* gel hardness) and therefore the cleaning behavior of the deposits. It has been found that an increase in protein concentration leads to a faster forming and firmer deposit^{12, 25,93} and that whey protein fouling with high protein concentration tends to form at lower temperature⁹³.

Studies also showed that reconstituted milk (obtained with powders) was less prone to fouling than fresh milk (25% less in average), because of the partial denaturation and aggregation of whey protein which occurs during drying processes^{12, 25,47}.

3.1.2. Calcium content

The literature reports that calcium content impacts fouling amount, mainly by impacting β -lg denaturation kinetics and the protein's ability to bond with other molecules^{10,57}. Indeed, Ca^{2+} ions are known to lower β -lg unfolding temperature^{94,95} and to promote deposit growth by forming bridges between adsorbed protein and bulk material^{44,94}. Khaldi (2014)⁵ listed four effects explaining the impact of calcium on β -lg denaturation and fouling, namely (i) intermolecular reticulation of carboxylic groups or other negatively charged groups caused by the formation of protein- Ca^{2+} complexes; (ii) shielding effect of Ca^{2+} on negatively charged protein; (iii) conformational changes of the protein caused by Ca^{2+} ions which alter hydrophobic interaction and aggregation and (iv) bridging between bulk protein and pre-existing deposit. Petit *et al.* (2011)⁴⁵ used Arrhenius plots to illustrate the impact of calcium on β -Lg unfolding and aggregation (Figure 1.8).

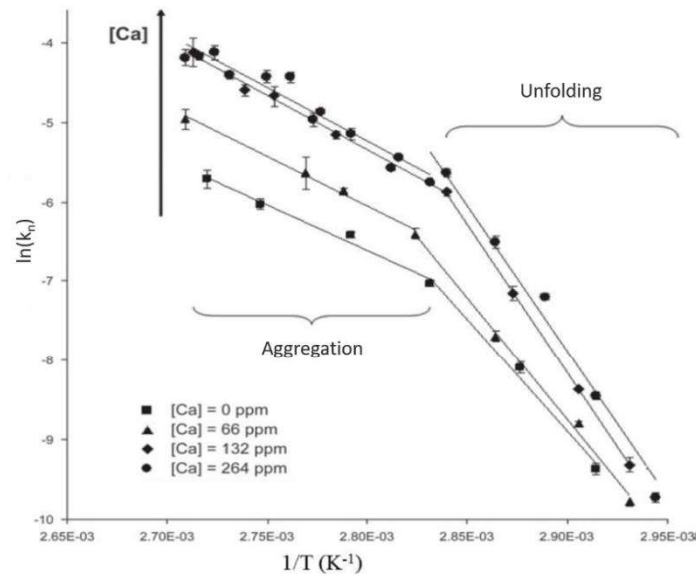


Figure 1.8. Arrhenius plot of β -lg thermal denaturation with several calcium concentrations (from Petit *et al.* (2011)⁴⁵. © 2013 – Elsevier.

Thus, even a slight increase in calcium concentration significantly increases fouling amounts⁹⁶, regardless of the temperature profile⁹⁵. Additionally, Skudder *et al.* (1981)⁴⁹ and Daufin *et al.* (1987)⁹⁷ pointed out that fouling could be limited by adding calcium-complexing additives to a fluid. Jimenez *et al.* (2013)³² also reported that the absence of calcium was shown to prevent build-up after the induction period.

It was also reported that an increased calcium content induces modification of fouling composition, by weakening the electrostatic and steric repulsions between β -lg and caseins^{25,98}, inducing higher fouling amounts and higher casein content in the deposits^{88, 97,99}. On the other hand, a low calcium content decreases caseins heat stability, promoting their disorganization and their participation to deposit growth.

It is noteworthy that a recent study by Khaldi *et al.* (2018)⁴³ highlighted the significance of calcium/protein molar ratio over the calcium concentration alone, for the understanding and predicting of β -lg denaturation and fouling. The author proved that up to a ratio of eleven, this ratio governs the fouling phenomena. Beyond the critical value of eleven, fouling is governed by β -lg concentration which becomes a limiting factor.

Finally, calcium content also proved to modify the physical properties of the deposits. Guérin *et al.* (2007)⁹⁶ showed that low calcium levels yielded soft and spongy deposits, and that higher

calcium levels led to denser and stretchier textures. Those changes in physical properties undoubtedly impact the deposits cleaning behavior.

3.1.3. pH and ionic strength.

The impact of pH on fouling phenomena is complex, as pH influences both mineral and proteinaceous deposition^{12, 25,94}. β -lg adsorption levels are indeed known to increase around its isoelectric point (pH 5.15)^{25,100}. Therefore a pH decrease from the initial value (*i.e.* between 6.6 and 6.8 for cow milk²⁵ and between 6.5 and 7 for the vast majority of dairy products⁵) induces higher fouling amounts. However, in very acid media, intermolecular bonding through disulfide bridges is not possible (pH < 2) and fouling is attenuated. On the other hand, alkaline pH seems to have no effect on protein fouling^{25,94}. pH also influences mineral solubility, as reported by Tung (1998)¹⁰¹. Andritsos *et al.* (2002)⁵⁴ thus showed that mineral fouling only occurs for pH values above 6⁵⁴. Overall, pH does not only impact fouling amount, but also its composition⁴⁹.

In a solution with high ionic strength, the electrostatic repulsions between the proteins are decreased, while thermal denaturation and aggregation are promoted¹⁰². Moreover, ionic strength also impacts the characteristics of the substrate's surface, for example by changing its electrical charge.

3.1.4. Gas content

Generally, the presence of air or gas in milk enhances fouling^{63,103}. Indeed, bubble bursting caused by local boiling or dissolved gases desorption at the solid/liquid interface in thermal treatment plants can significantly increase deposit growth through nucleation. Bursting shocks can also damage caseins and fat globules and facilitate their incorporation in deposits. Thus, air must be prevented to enter in the installation and the use of deaerators is very common¹⁰⁴.

3.1.5. Microbial flora

The presence of bacteria in the processed products impacts fouling¹⁰⁵. Dairy deposits are indeed nutritive media where micro-organisms can settle, either directly on the equipment or inside the deposits and multiply. Biofilms of thermophilic bacteria (*e.g.* *Bacillus stearothermophilus*¹⁰⁵) can therefore develop in the equipment, taking part into the general

fouling process. Moreover, micro-organisms are able to acidify their environment, which is a fouling-promoting factor.

3.2. Process characteristics

Mahdi *et al.* (2009)⁸² highlighted the impact process characteristics on fouling. They reported a preponderant impact of temperature and heating time, but also a strong correlation between fouling and hydrodynamic conditions.

3.2.1. Hydrodynamics

Generally, hydrodynamic conditions are known to impact fouling, as they influence bulk mixing and mass transfers from the bulk to the substrate. It is typically admitted that an increase in turbulence induces fouling reduction and in-line mixers were proven to have a fouling-decreasing effect⁷⁹. Some sources also suggest that enhanced turbulence extend the induction time and thus delay deposit growth^{61,67}. One suggested explanation is that turbulence would decrease the thickness and the volume of the laminar sublayer located near the substrate, which supposedly contains the molecules able to take part to fouling^{25,106}. However, comparisons between two works of Delplace *et al.*, carried out in 1994⁷⁰ and in 1997⁷¹ show no correlation between Reynolds number variation and fouling amount, which somehow questions the sublayer theory. The authors therefore propose that enhanced mixing conditions would promote protein aggregation and thus decrease the amount of unfolded protein available for fouling⁷¹. Finally, it was also postulated that increased turbulence and higher shear stress would enhance re-entrainment of deposits^{25,107}. Nevertheless, Andritsos *et al.* (2002)⁵⁴ pointed out that increased turbulence can have an enhancing effect on mineral fouling. This divergence from observations generally made on protein fouling could be explained by the difference of physical properties between mineral and protein deposits. The latter, being softer, would be more susceptible to re-entrainment compared to denser and harder mineral fouling. This illustrates well the dual impact turbulence can have on fouling, enhancing mass transfer but also promoting re-entrainment.

Finally, equipment geometry has also been proven to have a significant effect on the fouling process as it strongly affects turbulence and flow pathways. Regarding heat treatments in dairy industries, plate heat exchangers (PHE) are preferentially used, because of their compact size,

good mixing features and high heat-transfer efficiency¹². However, they present very narrow channels with contact points between two consecutive plates, which induces the presence of low velocity zones. Those characteristics induce more fouling, and obtained quicker than what can be observed in tubular heat exchangers¹².

3.2.2. Temperature

Temperature is unanimously the most important factor for fouling control. As a matter of fact, both temperature history and processing temperature can impact the fouling process.

3.2.2.1. Temperature history

Temperature history of the processed product also has an impact on fouling. Indeed, maintaining milk for 22h at 4°C has a mitigating effect on fouling amounts during the following heat treatments, most likely due to enzymatic activity. Longer cold holding can even cause a fouling increase, due to bacterial acidification¹².

3.2.2.2. Processing temperature

Milk fouling deposits are generally classified according to the temperature at which they occur^{5,10,13,44}. Formed between 75 and 110°C, Type A fouling is white and has a spongy, foamy appearance. It is composed of 50 to 60% of protein, predominantly β -lactoglobulin^{32, 42,95}. It has been shown that as the temperature approaches 100°C, the casein and mineral content increase^{25, 32, 42,66}. Over 110°C, grey and crumbly Type B, also called “milk stone” deposits are found. They are composed of 70% of minerals (mainly calcium phosphate) and of around 10% of protein.

Consequently, Type A fouling is found mostly in mild temperature processing (classical and High Temperature Short Time (HTST) pasteurization, low-temperature sterilization,) whereas Type B occurs in high temperature treatments like Ultra High Temperature (UHT) and classical sterilization processes. Nevertheless, Barish and Goddard (2013)¹⁰⁸ mention the possibility that both types of fouling can occur simultaneously in HTST processes, due to localized overheating, resulting in a dense and foam-like deposit that is difficult to remove. In addition, as mentioned previously, deposit composition evolves with the processing time. Long temperature exposure may indeed promote heat-induced chemical reactions next to heat-transfer surfaces.

Moreover, it is generally accepted that, with increasing temperature and processing time, the mineral content increases and the protein content decreases²⁵.

Generally, it is considered that an increasing temperature yields higher fouling rates^{42, 67,94,95}. Petit *et al.* (2013)⁴² studied fouling in a pilot heat exchanger and showed that the final fouling mass increased fivefold when the working temperature was increased from 70°C to 95 °C. They correlated this increase with the increase in β -lg denaturation rate (from 50% to almost 100%) in the same temperature interval. However, temperature also controls aggregation (covalent disulfide bonding or hydrophobic interactions)¹⁰⁹ and increases β -Lg aggregation kinetics, as aggregates size increase with the temperature. Consequently, the fouling mass follows a bell shaped distribution with increasing temperature, because, according to the authors, it directly depends on the amount of free unfolded protein⁴². This dual effect of temperature on β -lg chemical behavior was further studied by Khaldi *et al.* (2015)⁹⁵, who revealed a two-steps mechanism through Arrhenius plots of the denaturation kinetics of β -lg versus temperature.

The temperature profile of the process, *i.e.* the temperature increase rate within the channels of a PHE is also a determining factor of the final fouling mass of an installation. Larger temperature differences between the substrate and the fluid core were shown to increase β -lg denaturation and fouling⁴².

It is also important to notice that calcium content was shown to modulate the effect of temperature on dairy fouling⁵⁷. Indeed, temperature increase was shown to have a stronger impact on final deposit mass when the calcium concentration was increased because of the catalytic effect Ca^{2+} has on β -lg denaturation and aggregation kinetics.

Thus, fouling is severely impacted by the characteristics of the product as well as processing conditions. However, fouling is an interfacial phenomenon, and the substrate properties also of great importance.

3.3. Surface properties of the substrate.

3.3.1. Definition of the main surface properties

3.3.1.1. Roughness

Surface roughness is very important for many fundamental issues, such as friction, interfacial flow and adhesion^{110,111}. Overall, more than 50 roughness parameters have been identified and classified between amplitude, spacing and hybrid parameters¹¹¹. Among these different classes, amplitude parameters are usually used to describe surface topographies. Particularly, the arithmetic average height (R_a), also known as center line average (CLA) and the root mean square roughness (R_q or RMS) are the most used roughness parameter. R_a (Equation 1.1) is defined as the absolute deviation of roughness irregularities from the mean line for a given sample length, whereas R_q (Equation 1.2) represents the standard deviation of the distribution of surface heights.

$$R_a = \frac{1}{n} \sum_{i=1}^n |z_i| \quad \text{Equation 1.1}$$

$$R_q = \sqrt{\frac{1}{n} \sum_{i=1}^n z_i^2} \quad \text{Equation 1.2}$$

3.3.1.2. Surface Free Energy

Surface free energy (SFE) is generally defined as the work required to extend the surface of a phase and is expressed in mJ/m^2 or mN/m . SFE is closely linked to the water contact angle (WCA, θ), *i.e.* the angle formed with a surface by the tangent to the drop surface at the triple contact point at the vapor/water/solid interface (Figure 1.9). Roughly, as the SFE of a surface increases, it becomes more hydrophilic and its WCA decreases.

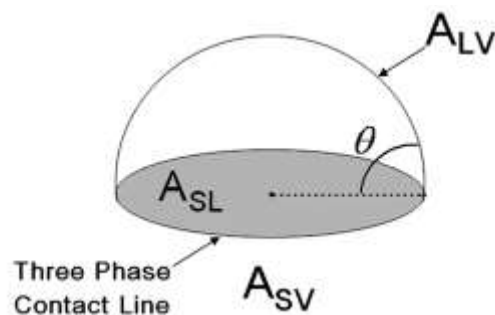


Figure 1.9 : Representation of the contact angle in a three-phase system¹¹². © 2011 – Elsevier.

Surface free energy can be calculated through empirical models from contact angle measures with different probe fluids (Table 1.2). Depending on their complexity, the models allow to calculate the total surface free energy but also to isolate different components which quantify the weight of polar or non-polar interactions in the global surface energy. For example, the two-component Owens, Wendt, Rabel and Kaelble (OWRK) model allows to calculate the dispersive (γ^D) and polar (γ^P) components of the total surface energy (γ^{Total}). Furthermore, the Van Oss, Chaudhury and Good, which is a three-component model, allows to subdivide the polar component into an acid (γ^+) and a basic component (γ^-). Depending on the hypotheses they were built on, some models are more or less fitted to a certain type of surfaces. Thus, Wu's model is considered as particularly well suited for polymer materials, whereas the Van Oss method fits well metallic surfaces.

Table 1.2: Empirical models for SFE determination.

Name	Components	Model
Zisman	One	Measuring several probe liquids' CA and plot the cosine of those angles against the known surface energies, then extrapolate to contact angle equal 0.
Owens, Wendt, Rabel and Kaelble (OWRK)	Two	$\frac{\gamma_L (\cos \theta + 1)}{2\sqrt{\gamma_L^D}} = \frac{\sqrt{\gamma_S^P}\sqrt{\gamma_L^P}}{\sqrt{\gamma_L^D}} + \sqrt{\gamma_S^D}$
Wu	Two	$\gamma_{SL} = \gamma_S + \gamma_L - 4 \left[\frac{\gamma_S^D \gamma_L^D}{(\gamma_S^D + \gamma_L^D)} + \frac{\gamma_S^P \gamma_L^P}{(\gamma_S^P + \gamma_L^P)} \right]$
Van Oss, Chaudhury and Good	Three	$\gamma_L (\cos \theta + 1) = 2 \left[\sqrt{\gamma_L^D \gamma_S^D} + \sqrt{\gamma_L^+ \gamma_S^-} + \sqrt{\gamma_L^- \gamma_S^+} \right]$

3.3.1.3. Wettability

Surface wettability directly depends on its morphology and SFE and is usually characterized by its WCA. The basis for all wetting models is Young equation^{112,113} (Equation 1.3), which states that the surface free energy of a perfectly flat, rigid and homogeneous surface only depends on the interfacial energies of the vapor/liquid/solid system.

$$\cos \theta = \frac{\gamma_{SV} - \gamma_{SL}}{\gamma_{LV}} \quad \text{Equation 1.3}$$

$$\cos \theta^* = r \cos \theta \quad \text{Equation 1.4}$$

$$\cos \theta^* = -1 + \phi_S (\cos \theta + 1) \quad \text{Equation 1.5}$$

However, real surface seldom present perfect homogeneity and smoothness. Wenzel's equation^{112,113} (Equation 1.4) reflects the impact of roughness on wettability by introducing r , a roughness factor, linking the ideal, intrinsic contact angle θ to the observed contact angle θ^* . As r is defined as the ratio of the projected surface on the geometric surface, it is always superior to 1. Thus, Wenzel's equation induces that for a given material, a pre-existing hydrophilic or hydrophobic characteristic will be amplified by an increasing roughness. This most probably comes from the subsequent increase of the contact surface between the material and the fluid⁶⁶. It is nevertheless crucial to note that Wenzel's model applies to homogeneous wetting regime, *i.e.* full contact between the substrate and the wetting fluid. Certain types of morphologies induce a heterogeneous wetting regime, *i.e.* some vapor remains trapped between the fluid and the solid surface. This cases are modelled by Cassie-Baxter's equation (Equation 1.5), which takes into account ϕ_s , the fraction of solid truly in contact with the fluid. According to Bico *et al.*¹¹⁴, the preponderance of heterogeneous or homogeneous wetting regime can be predicted. The authors indeed state that heterogeneous regime is favored when the apparent contact angle, θ^* is superior to the critical value θ_c (Equation 1.6).

$$\cos \theta_c = \frac{1 - \phi_s}{\phi_s - r} \quad \text{Equation 1.6}$$

However, for real surfaces, r and ϕ_s can be difficult to quantify. Researchers then rely on macroscopic approaches (*e.g.* dynamic goniometry) to characterize a surface's wetting regime. Particularly, the contact angle hysteresis (CAH, Figure 1.10), which characterizes adhesion between can be a good wetting regime indicator. Indeed, homogeneous wetting often induces high contact angle hysteresis (CAH) values, whereas low CAH values point toward heterogeneous regime¹¹², mostly because of capillarity phenomena.

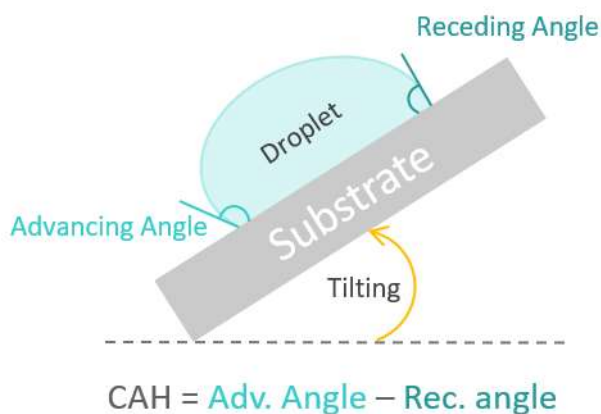


Figure 1.10. Representation of the contact angle hysteresis.

3.3.2. Dairy fouling on modified surfaces

The impact of surface properties on fouling by milk and dairy derivatives has been investigated since the 1970's. Table 1.3 gives an overview of the studies carried out on this matter and underlines the great diversity of possible surface modifications but also the multitude of fouling scenarios. Hence, some of the presented findings contradict one another.

Nevertheless, a large majority of authors point out that surface properties are of great importance in fouling control, especially when the cleaning behavior is considered^{27, 86,115}. Indeed, according to Santos *et al.* (2006)²⁷, surface properties impact the formation of the initial deposit layer, which itself impacts subsequent build-up. Some researchers argue that surface chemical properties only impact the first fouling layer, and that as soon as induction phase is over, only protein-protein interaction governs fouling^{25,116}. However, the first fouling layer also acts as a boundary zone between the substrate and the deposit. Its characteristics may therefore influence the substrate-deposit adhesion strength, the deposit stability and the ease of cleaning. Britten *et al.* (1988)⁸⁶ thus reported that surface properties can impact fouling by extending or shortening the induction period, or by strengthening or weakening protein adhesion to the substrate.

Table 1.3. Literature survey on surface modification impact on milk and dairy fouling study (Adapted from Boxler (2014)¹⁰).

Reference	Substrates	Tested against	Test conditions	Conclusions
Gordon <i>et al.</i> (1968) ¹¹⁷	SS / Teflon	Raw milk	Continuous with recirculation T° _{bulk} =82°C T° _{heating} = 100°C	Teflon was more fouled than SS
Dupeyrat <i>et al.</i> (1987) ¹¹⁸	SS / Polished SS / Glass / Teflon / Polished Teflon / Polyethylene / Silicone resin / Fluorine resin	Whey	Continuous, no recirculation T° _{bulk} = 72°C	Surface did not impact fouling amount
Britten <i>et al.</i> (1988) ⁸⁶	SS / Polished SS / Nylon / PMMA / Polystyrene / Cellulose / Acetate and agarose coatings	Raw whole milk	Batch (60 min) T° _{bulk} = 60°C T° _{heating} = 100°C	Fouling amount did not vary according to the substrate, but fouling adhesion was impacted by surface properties
McGuire and Swartzel (1989) ¹¹⁹	SS / Polished SS / Teflon /Alumino-silicate coatings	Whole milk	Continuous, no recirculation T° _{bulk} = 100°C, 134°C, 154°C	Deposition rate and deposit structure were impacted by the substrate nature.
Kirtley and McGuire (1989) ¹²⁰	SS / PTFE / Polypropylene / Polyethylene / Nylon / Glass	β-Lg in phosphate buffer	Batch (360 min) T° _{bulk} = 30°C	Surface energy was proven to impact native β-Lg adsorption.
Whalgren and Arnebrandt (1990) ¹²¹	Silica / Methylated silica / Polysulfone coatings	β-Lg in phosphate buffer	Batch (60 min) T° _{bulk} = 25°C	Adsorption levels depend on the substrate type.
Yoon and Lund (1994) ¹¹⁶	Ti / SS / Electropolished SS / Teflon / Polysiloxane coatings	Raw whole milk	Continuous in a PHE (72-82 min) T° _{bulk} = 89-90°C	Substrate nature becomes irrelevant once the induction period is over.
Jeurnik <i>et al.</i> (1996) ²³	Chromium oxide	Whey protein concentrate solution β-Lg in water	Continuous (150 s holding) T° _{bulk} = 25, 75-90°C	Protein denaturation is a key phenomenon without which fouling cannot occur.
Karlsson <i>et al.</i> (1996) ²⁴	SS / Chromium oxide / Methylated silica	β-Lg in PBS	Batch (5-30 min) T° _{bulk} = 25°C, 60°C, 73°C, 77°C and 80°C	As build-up progresses, the influence of the substrate decreases.
Murray and Cros (1998) ¹²²	Gold / Octadecyl-mercaptan treated gold	β-Lg and β-casein in imidazole buffer	Continuous (180 min) T° _{bulk} = 25°C	Surface modification induces rearrangement of the protein.

Wu and Nancollas (1997) ⁵³ Wu and Nancollas (1998) ¹²³	PMMA and plasma coated PMMA / FEP and plasma coated FEP / Silicone and plasma coated silicone / Mica, anatase and rutile particles	Calcium phosphate solution	Batch (1140 min) T= 37°C	Surface properties influence nucleation.
Beuf <i>et al.</i> (2003) ¹¹⁵	SS / DLC coatings / SiO _x coatings / Silica coatings / Ni-P-PTFE coatings / Excalibur® coatings / Xylan® coatings / SiF ⁺ coatings / MoS ₂ coatings	Whole milk with whey protein, sugar and xanthan gum	Continuous in a PHE T° _{bulk outlet} = 102°C	Fouling and cleaning were impact by the substrate's surface properties.
Wei <i>et al.</i> (2003) ¹²⁴	SS / Polyethylene glycol / Polyethylenimine	β-Lg in PBS	Batch (60 min) T° _{bulk} = 25°C	Surfaces with high graft densities could prevent native protein adsorption.
Ramachandra <i>et al.</i> (2005) ¹²⁵	SS / TiN	Whey protein or mineral solutions in water	Batch T° _{bulk} =60°C T° _{substrate} =85°C	TiN surfaces presented patchy deposits. It is suggested that bonding mechanisms may differ from one surface to the other.
Premathilaka <i>et al.</i> (2006 and 2007) ²⁶	SS / DLC / Si-DLC coatings by CVD / TiN	Whey protein isolate in water	Continuous, no recirculation (3 min) T° _{bulk} = 55°C T° _{substrate} = 70 °C	Surface modifications induce changes in fouling mechanisms and protein arrangements.
Rosmaninho and Melo (2006) ²⁹	SS / MoS ₂ / SiF ₃ ⁺ / SiO _x / Ni-P-PTFE	Simulated milk ultrafiltrate	Batch (5 and 120 min) T° _{bulk} = 44°C	The impact of surface properties on the induction layer led to different deposit structures.
Santos <i>et al.</i> (2006) ²⁷	SS / SiF ₃ ⁺ / MoS ₂ / TiC ion implantation / DLC sputtered / DLC by CVD / Si-O-DLC by CVD/ Silica sol-gel coatings	Whey protein isolate in PBS	Continuous (20 min) T° _{bulk} = 72°C, 85°C	Adsorption, induction and build-up were impacted by surface properties.
Parbhu <i>et al.</i> (2006) ¹²⁶	SS/ Chromium oxide / Silicate treated chromium oxide	Raw milk	Continuous in a PHE T° _{bulk outlet} = 80°C	Silicate induced lower mineral adhesion and thus lower fouling amounts.
Rosmaninho and Melo (2007) ²⁸	SS / TiN	Whey protein isolate in SMUF	Continuous (1080-1800 min) T° _{bulk} = 48°C, T° _{heating} = 70°C	Deposition rate, final amount and cleaning were influenced by surface properties.
Rosmaninho <i>et al.</i> (2007) ¹²⁷	SS / SiF ₃ ⁺ / Si-O-DLC / SiO _x / Ni-P-PTFE / silica by sol-gel coatings	Calcium phosphate solution / β-lg solution / bacterial suspension / model dairy dessert cream	Batch (120 min) T° _{bulk} = 44°C / 70°C Continuous in a PHE T° _{bulk outlet} = 102°C Lab and pilot-scale	Ni-P-PTFE were the best performers regarding mineral and protein fouling and cleaning. Ni-P-PTFE were the most hydrophobic of all tested

Rosmaninho and Melo (2008) ⁵⁶	SS / SiO _x / Silica / Si-O-DLC by PECVD / MoS ₂ / Ni-P-PTFE coatings	Whey protein isolate in SMUF	Batch (10 and 120 min) T° _{bulk} = 50 and 85°C	surfaces, with low non-polar and polar SFE components. Change in surface properties yielded different induction layers, and therefore different fouling structures.
Rosmaninho <i>et al.</i> (2008) ¹²⁸	SS / TiN coatings	SMUF	Continuous (8400 min) T° _{bulk} = 48°C T° _{heating} = 70	Deposition kinetics and final fouling amount depended on surface properties.
Balasubramanian and Puri (2008, 2009) ^{129,130}	SS / Ni-P-PTFE / Lectrofluor™ / AMCI148-18 coatings	Skim milk	Continuous in a PHE (360 min) T° _{bulk outlet} = 72°C	Coatings reduced fouling amounts by 85 to 95% compared to bare SS.
Mauermann <i>et al.</i> (2009) ³⁰	SS / FEP / PEEK + fluoropolymer / Si-O-DLC by PECVD / Ti-DLC by PVD / Nanocomposite coatings	WPI in water	Batch T° _{bulk} = 80°C	Deposit structure was impacted by surface properties.
Kananeh <i>et al.</i> (2010) ³¹	SS / Electropolished SS / Epoxy-resin coating / Polyurethane coatings / PTFE	Whey protein concentrate in water	Cont.with recirculation (17 min) T° _{bulk} = 45°C T° _{substrate} = 96.5°C Continuous in a PHE (240 min) T° _{bulk outlet} = 85°C	All coated surfaces showed fouling reduction compared to SS except PTFE
Stancl and Zitny (2010) ¹³¹	SS / TiN / Graphite	Skimmed milk	Batch T°=65-75°C	Different levels of fouling were found on the different materials.
Boxler <i>et al.</i> (2011) ¹³²	SS / DLC by PECVD / Si-DLC by PECVD / Si-O-DLC by PECVD	SMUF	Continuous with recirculation (900 min) T° _{bulk} = 50°C	Mineral adsorption, fouling and cleaning were influenced by surface properties.
Jimenez <i>et al.</i> (2012) ¹³³	TMDSO Vacuum plasma coatings / commercial PTFE containing coatings / PTFE-PPS sprayed coating	β-Ig and calcium solution in water	Continuous without recirculation T° _{bulk outlet} =93°C Substrate unheated	Fouling can be limited by low roughness or organized nanostructure. A competition between roughness and SFE for fouling control is suggested.
Rungraeng <i>et al.</i> (2012) ¹³⁴	SS / PTFE / CNT-PTFE	Pasteurized milk	Continuous in a PHE with recirculation (60, 120 and 300 min) T° _{bulk outlet} = 60°C	PTFE and CNT-PTFE showed reduced fouling amounts compared to SS.

Barish and Goddard (2013) ¹⁰⁸	SS / Ni-P-PTFE	Raw milk	Continuous in a PHE (480 min) T° _{bulk outlet} = 85°C	Coated surfaces showed 30 times less deposits than SS.
Patel <i>et al.</i> (2013) ¹³⁵	SS / Doped DLC	Whole milk Skim milk Whey protein isolate	Batch T° _{bulk} = 84°C Continuous in a PHE T° _{bulk outlet} = 84°C	DLC coatings did not show fouling reduction.
Boxler <i>et al.</i> (2013) ¹⁰²	SS / DCL / SICAN® / SICON®	SMUF Whey protein isolate SMUF + whey protein isolate	Batch T° _{bulk} =50°C T° _{substrate} = 80°C, 120°C, 105°C	Surface energy affected the induction layer and further build-up. On optimal γ is suggested.
Boxler <i>et al.</i> (2013) ⁶⁸	SS / DCL / SICAN® / SICON®	SMUF + whey protein isolate	Continuous in a PHE T° _{bulk} = 62-85°C	A quadratic relationship between γ and final fouling amount was found.
Boxler (2014) ¹⁰	SS / Electropolished SS / DLC coating / DLC on electropolished SS / SICAN® coating / SICAN® on electropolished SS / SICON® coating / SICON® on electropolished SS	Raw milk Whey protein isolate SMUF WPI + SMUF	Batch T° _{bulk} = 50°C, 40°C for SMUF T° _{substrate} = 80°C and 120°C for WPI and WPI + SMUF T° _{substrate} = 80°C and 105°C Continuous in PHE with recirculation. T° _{bulk outlet} = 85°C	Surface energy, especially γ and surface roughness influence the initial fouling layer formation, final deposit mass, deposit composition, deposit structure and cleaning behavior.
Barish and Goddard (2014) ¹³⁶	Electroless Ni-PTFE coatings exposed to cleaning solutions	Raw milk	Continuous flow on heated surfaces T°= 81°C	Electroless Ni-PTFE coatings showed antifouling properties, which stayed unchanged after exposure to an alkali sanitizer. The acid sanitizer altered the antifouling properties of the coating.
Huang and Goddard (2015) ¹³⁷	Electroless Ni-PTFE coatings	Raw whole milk Chocolate milk with or without carrageenan	Continuous in a bench-top PHE	Electroless Ni-PTFE coatings showed antifouling properties with both fluids, however, deposits from carrageenan containing milk proved to be harder clean.
Piepiorka-Stepuk <i>et al.</i> (2016) ¹³⁸	SS with different roughness	Whole milk	Batch T° _{bulk} = 90°C	A correlation between the arithmetic mean roughness of the SS and the fouling amount was found.

Boxler (2014)¹⁰ underlines a certain dichotomy in the research presented in Table 1.3, according to the employed scale of analysis. She indeed points out that work based on macroscopic analysis, such as weighing or global chemical analysis of the deposits did not allow identifying an influence of surface properties on fouling amount, composition or superficial structure^{54, 86, 115,116,118}. On the other hand, the use of sophisticated technologies, such as SEM, XPS, QCM or ellipsometry allowed to establish the influence of surface modification on the different steps of the fouling process^{24, 26, 68, 102, 117, 119, 122, 129, 132,136–138}.

3.3.2.1. *Impact of Surface Free Energy.*

It is known that, whenever two phases come in contact, the adsorption of molecules is needed to stabilize the interface, *i.e.* to lower its energy¹³⁹. This adsorption phenomena however depend on the affinity between molecules in question and both phases. As a matter of fact, the adhesion of hydrophilic molecules and particles is generally considered favorable on hydrophobic surfaces¹⁰. Hydrophilic materials can nevertheless attract hydrophilic protein through interactions with electron-donor sites on the surfaces^{27,140}. Globally, SFE can influence the amount of adsorbed protein, the unfolding and denaturation of proteins on or near the surface, the protein-protein binding force in layers close to the substrate and the formation and structuration of further layers^{24,141}. It is also noteworthy that a surface's chemical properties can be altered by the surrounding media. Van Oss (2006)¹⁴⁰ stated that the presence of cations like Ca^{2+} could enhance the hydrophobicity of a surface by acting as an electron-acceptor and neutralizing the electron-donor sites on the surface.

Regarding the impact of SFE on fouling, the well-known Baier curve (Figure 1.11) places the optimal SFE interval for bacteria, food and mineral adhesion between 20 and 30 mN/m. This has been further corroborated in the literature, through the use of the extended Derjaguin-Landau-Verwey-Overbeek (DVLO) theory^{119, 128,142}.

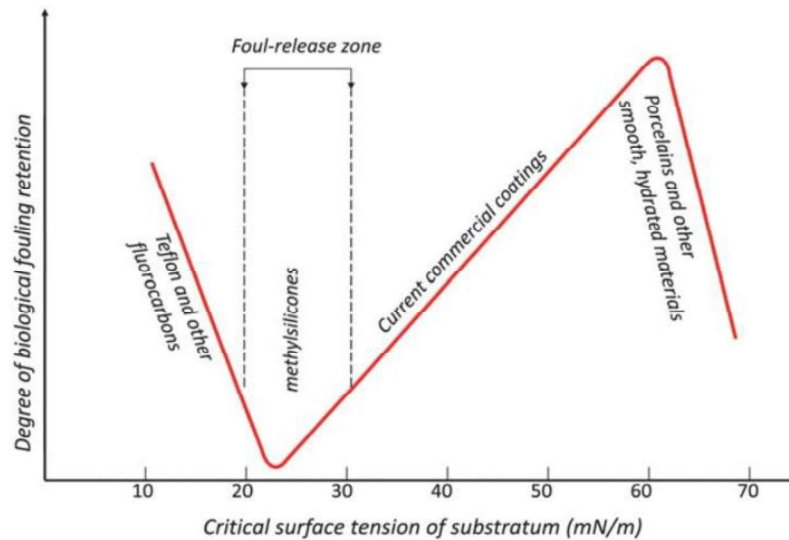


Figure 1.11. Baier's curve, a descriptive correlation between the critical surface tension of a substrate and the degree of biological fouling retention¹⁴³. © 2011 – Royal Society of Chemistry.

The surface free energy of stainless steel, which is the preferred material for food processing equipment¹⁴⁴, is generally considered to be around 40 mN/m. Consequently, most research focused on the reduction of SS substrates SFE, and the reduction of substrate polarity, mostly by means of coating. Low SFE and low-polarity substrates are generally known for their antiadhesive, easy-to-clean and fouling-release properties induced by the weakening of the substrate-deposit adhesion force¹⁰. Table 1.3 indeed presents many examples of silicon-based coatings^{15,18,20,47,98,99,104}, fluoropolymer-based coatings^{22,47, 92, 99–103, 115,116,120} and diamond-like carbon coatings (DLC) (doped or not)^{10, 26,27, 29,30, 56, 68, 102, 115, 132,135}.

❖ *Silicon-based coatings*

From plain silica^{15,47, 98,104} to polysiloxanes¹¹⁶ and SiO_x coatings^{29,56}, silicon-based coatings were investigated in regard to dairy fouling and proven to impact both deposit structure, amount and ease of cleaning. Siloxanes are usually considered as inert species and can thus be considered as good candidates for fouling reduction. However, Rosmaninho *et al.* (2007)¹²⁷ found that SiO_x coatings obtained by a Chemical Vapor Deposition (CVD) process (from hexamethyldisiloxane) presented higher fouling amounts and worse cleaning behavior than bare stainless steel. Yoon and Lund (1994)¹¹⁶ who studied polysiloxane coatings on stainless steel came to the same conclusion, although they did not study cleaning. Interestingly, in the case of Rosmaninho *et al.* (2007)¹²⁷, the

silicon-based coatings were found more hydrophilic than the reference, whereas Yoon *et al.* (1994)¹¹⁶ found that their silicon-based coatings were more hydrophobic than the SS reference. This points out the variability of surface properties, even for similar modifications. However, silicon-based polymers have also been investigated for non-fouling applications outside of dairy processing. For example, Fang *et al.* (2010)¹⁴⁵ showed the efficacy of poly(dimethyl siloxane) (PDMS) against fouling by marine organism. This polymer presents very interesting characteristics such as low surface free energy, low Young's modulus and low surface roughness, but it is quite fragile and does not present good adhesion to the substrate features^{145,146}. To overcome these issues, PDMS is often associated with inorganic particles or chemically cross-linked, but these modification steps can impact other PDMS characteristics and be damageable to the nonfouling properties. Adherence-enhancing strategies that do not challenge antifouling performances have been investigated like blending or cross-linking with other low-energy polymers, like fluoropolymers or polyurethane, that improve mechanical resistance and adhesion to the substrate¹⁴⁶.

❖ *Fluoropolymers*

Fluoropolymers and particularly Teflon – poly(tetrafluoroethylene), PTFE – are generally known for their anti-adhesive properties. However, Gordon *et al.* (1968)¹¹⁷ and Dupeyrat *et al.* (1987)¹¹⁸ studied the fouling behavior of Teflon but did not witness any beneficial effect of the coating on fouling management. However, cleaning was not studied in those two sources. In comparison, autocatalytic Ni-P-PTFE coatings on SS, explored in the European MODSTEEL project^{127,147} showed lower fouling amounts and better cleaning properties than SS. The given reasons are that the hydrophobic Ni-P-PTFE coatings showed low dispersive and electron-donor component (γ^-) SFE components. The authors also underline that the coating beneficially masked the grain boundaries of the underlying SS, modifying the roughness of the substrate.

❖ *Diamond-like coatings*

Both plain and doped, DLC coatings were particularly studied by Boxler *et al.* (2013, 2013 (1), 2014)^{10, 68,102} who proved that this type of coating influenced the fouling initiation, build-up and final amount, as well as the cleaning process. They singled out two preponderant impacting factors:

γ^* (which was shown to have a quadratic relationship with the final fouling mass) and surface roughness, which will be discussed later on. More precisely, an increased roughness was shown to always induce higher deposit amount and surface with lower γ^* were shown to be less fouled. Interestingly, cleaning efficiency was shown to increase with increasing γ^* .

Thus, extensive research was carried out on dairy fouling on modified surfaces and possible antifouling surfaces. It is nevertheless noticeable that high-SFE hydrophilic brushes, that were proven efficient against marine and bacterial fouling^{148,149} were given very little attention in the dairy fouling context. As a matter of fact, to date, only two references report the study of such polymers against β -Lg adsorption, at room temperature^{124,150}, although protein and/or bacterial fouling control through enhanced surface hydrophilicity is widely documented (Table 1.4).

The mechanism of action of hydrophilic coatings rests on the tight bonding of water by polymers immobilized on the surface. As a result, a well-organized layer of hydrated polymer (brush, hydrogel) forms at the solid/liquid interface and prevents fouling agents to reach the substrate. The insertion of a foulant in the brush is indeed prevented by osmotic repulsion and steric hindrance¹⁵¹. Moreover, the compression of hydrated polymer chains by a foulant attracted toward the substrate causes entropy loss to the system¹⁴⁹. The foulant will thus be repelled from the solid surface. Nevertheless, the ability of a brush to prevent fouling depends on two crucial characteristics, namely its thickness and its chain density¹⁵². Extensive research was carried out on poly(ethylene glycol), also known as poly(ethylene oxide) (PEG or PEO) because of its high hydration potential. Poly(vinylamine) (PVA) and similar polymers were also investigated (Table 1.4). It is noticeable that a particular attention was given to the immobilization of hydrophilic polymers on their substrate. A good adhesion between the substrate and the polymers is indeed critical to the sustainability of antifouling properties. Simple adsorption was proven not to be sufficient to achieve long term immobilization¹⁵³. In the case of hydrophilic polymer, immobilization strategies are various, from direct grafting^{154,155} to the use of adhesion promoting primers like bio-inspired polydopamine layers (PD)¹⁵⁶ and plasma polymerization.

Table 1.4. Hydrophilic polymers for protein-repellency.

Polymer(s)	Immobilization technique	Coating type	Substrate	Tested against	Reference
PEG	Grafting on PD primer	Brush	Gold chips Si capillaries	Milk and egg proteins adsorption	Chen <i>et al.</i> (2012) ¹⁵⁷
	Grafting on PD primer	Brush	PES membranes	BSA adsorption	Li <i>et al.</i> (2014) ¹⁵⁸
	Grafting	Brush	Acid-catalyzed silicon	Fibrinogen Adsorption	Chen <i>et al.</i> (2005) ¹⁵⁹
	Grafting on Poly(ethylene imine) primer	Brush	Stainless steel	BSA Adsorption Bacterial adhesion	Caro <i>et al.</i> (2009) ¹⁶⁰
	Catecholate primer	Brush	Stainless steel TiO ₂	Human blood protein Bacterial adhesion	Khalil <i>et al.</i> 2014 ¹⁶¹
	Spin-coating and plasma-mediated cross-linking	Thin film	Stainless steel	Bacterial adhesion	Dong <i>et al.</i> (2005) ¹⁵³
	Plasma-induced grafting	Thin layer	Poly(vinylidene fluoride)	Y-globulin adsorption	Wang <i>et al.</i> (2002) ¹⁶²
Ultra short ethylene oxide	Pulsed plasma polymerization	Ultra thin layer	Polished silicon KBr and PET	BSA and Fibrinogen adsorption	Wu <i>et al.</i> (2000) ¹⁶³
PEGMEMMA + PES	Grafting	Brush	Ultrafiltration membranes	Ultrafiltration of BSA solution	Peng <i>et al.</i> (2011) ¹⁵⁴
Triblock (PEG)-(PPO)-(PEG)	Grafting	Brush	Silicon wafers	BSA and human blood proteins	Norde and Gage (2004) ¹⁵⁵
PEG + Polyallylamine	Grafting on oxidized vinyl silane primer	Dendrimeric	Silicon wafers	BSA adsorption	Dyer <i>et al.</i> (2007) ¹⁶⁴
PEG based polymer	Grafting	Hydrogel	Nanofiltration membranes	BSA and Lysozyme adsorption	Lei and Ulbricht (2014) ¹⁶⁵
PVA	Grafting and dip-coating	Thin layer	Polyamide membrane	BSA, Lysozyme, Sodium Alginate, DTAB, Colloid Ferric hydroxide	Wu <i>et al.</i> (2015) ¹⁶⁶
NH ₂ -terminated polyacrylamide	Grafting on DP prelayer	Brush	Si, SiO ₂ , Ag, Cu, SU8 and PDMS	Static and dynamic adsorption test with BSA	Vu <i>et al.</i> (2014) ¹⁶⁷
Poly(N-vinylpyrrolidone)	Grafting on polyphenol-metal prelayer	Thin layer	Polyamide RO membranes	BSA, Lysozyme and Alginate adsorption	Wu <i>et al.</i> (2015) ¹⁶⁸

Thus, surface energy is a very important parameter regarding fouling and cleaning. Straight comparison of literature data is however complex, due to the multitude of different experimental methods and focus points. SFE must then not be studied alone, but in association with other surface properties, such as surface morphology, charge or elastic modulus.

3.3.2.2. Impact of roughness and morphology.

Roughness and morphology are known to have a direct impact on surface interfacial properties, as they can radically change its apparent wetting features, as mentioned previously, Boxler (2014)¹⁰ states that surface defects on metal substrate, *e.g.* grain boundaries which come from manufacturing processes, are generally larger than individual fouling agents (micro-organisms or molecules), which allow the latter to penetrate the surface relief. This phenomenon is known as interlocking¹⁰, and promotes steadier and denser fouling growth at the base of the deposit. Consequently, heat transfer is affected and so is further build-up¹⁶⁹, resulting in porous superior layers.

In most studies about the consequences of surface properties, SFE and roughness simultaneously vary, which makes it difficult to isolate the effect of one parameter. Yoon and Lund (1994)¹¹⁶ suggested that the effect of roughness was generally weaker than that of surface chemistry while Detry *et al.* (2010)¹⁷⁰ emphasize the controversial influence of roughness on the cleaning behavior of deposits. The authors also points out that deposit located inside surface relief is harder to clean. Overall, as depicted by Boxler (2014), the true effect of roughness on fouling and cleaning of dairy deposit is very difficult to establish. Indeed, even if author generally agree that roughness reduction (*i.e.* Ra) leads to lower fouling amounts and easier cleaning, they sometimes disagree on the roughness range in which the said effect occurs. Britten *et al.* (1968)⁸⁶ suggest that below the threshold of 2 μm , the effect of roughness becomes insignificant, while Leclercq-Perlat and Lalande (1994)¹⁷¹, who studied substrates with Ra comprised between 0.11 μm and 0.8 μm , found that the removal of deposit was eased with lower roughness. On the other hand, Kouider *et al.* (2010)¹⁷² found and optimal Ra of 0.8 μm when working between 0.029 and 3.2 μm .

Dupeyrat *et al.* (1987)¹¹⁸ suggest that a surface's fouling and cleaning behavior results from synergistic interactions between its roughness and surface energy. Furthermore, Jimenez *et al.*

(2012)¹³³ point toward a competition between roughness and SFE for fouling governance and underlined the importance of the roughness scale. These works stress the importance to consider both features to fully comprehend fouling and cleaning phenomena.

Roughness is thus a crucial feature that can increase or decrease fouling, according to the relative size of surface defects and fouling agents. However, its effect is difficult to isolate because, upon surface modification, roughness often varies along with surface energy.

3.3.2.3. Other surface properties.

In the previous sections, the influence of roughness and SFE on fouling was demonstrated. These two surface properties are indeed the most commonly discussed in this context. However, surface charge and elastic modulus should also be mentioned.

❖ *Surface charge*

Considering that proteins are charged molecules, the charge of a substrate should have an impact on protein adhesion and fouling. However, surface charge is dependent on many parameters (surface pre-treatment, cleaning, ageing, surrounding phase characteristics) and delicate to measure. Consequently, experimental literature data about the effect of surface charge or ζ -potential on fouling are scarce and most studies are based on models like the electrical double layer theory.

Developed by Gouy, Chapman and Stern¹⁷³, the electrical double layer theory describes the electrostatic field surrounding a charged particle or surface when immersed in an electrolyte (Figure 1.12) as follows. A compact layer of adsorbed counter-ions forms at the surface and is called the Stern layer. At the vicinity of the Stern layer, a diffuse layer (or Gouy layer) is composed of ions of identical charge as the surface. The Stern and Gouy layers form the electrical double layer. If either the fluid or the surface move in respect to the other, a shear stress is created in the layers, resulting in an electrokinetic potential at the boundary plane between the outer Stern layer (outer Helmholtz layer) and the medium. This potential, known as the ζ -potential, is often used to characterize surface charge, although the relationship between surface charge and ζ -potential is complex. Further research led to the extended DLVO theory, which states that interfacial

interactions are due to Lifshitz-Van der Waals interactions, acid-base interactions and electrostatic double layer interactions.

The ζ -potential depends on several environmental conditions, like pH and ionic strength. It is therefore difficult to measure it, especially in complex solutions. Cai *et al.*¹⁷⁴ carried a comprehensive modelling study of the interactions between different foulant-polymer surface systems and showed that the impact of ζ -potential on adhesion behaviors is much more significant when considering foulant particles on a substrate than when considering two planar entities. The authors also found out that the total interaction energy of a system increases when the absolute value of ζ -potentials increases, and therefore suggest that ζ -potential absolute value decrease could induce fouling mitigation. In other words, charge minimization would lead to fouling mitigation. This is quite verified in the literature, however, charge must not be studied alone, and other surface properties must be taken into account¹⁰.

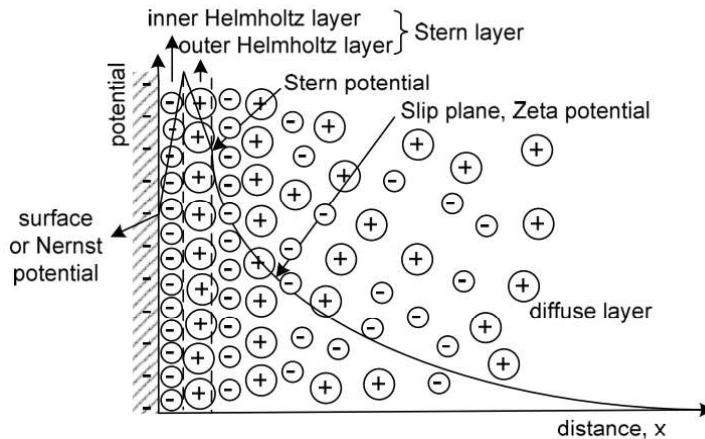


Figure 1.12. Schematic representation of the electrical double layer theory¹⁰.

Coatings containing charged species have been investigated for anti-fouling applications. Single-charge polymers, such as carboxymethyl dextrans (CMD)¹⁷⁵ or cationic polyvinylamine¹⁶⁶ (Figure 1.13) were investigated for protein-repellency and showed mitigated performances. More precisely, McArthur *et al.* (2000)¹⁷⁵, who studied adsorption of lysozyme, human serum albumin, bovine lactoferrin and γ -globulin on negatively charged CMD concluded that, while single charge polymers showed some antifouling properties against one single type of protein, they proved to be inefficient against multi-protein mixtures. Thus, single charge materials can be used to repel

opposed-charge foulants. Since proteins are complex molecules, and their charge can change with environmental variations, single charged polymers might not be the best material to achieve protein-repulsion.

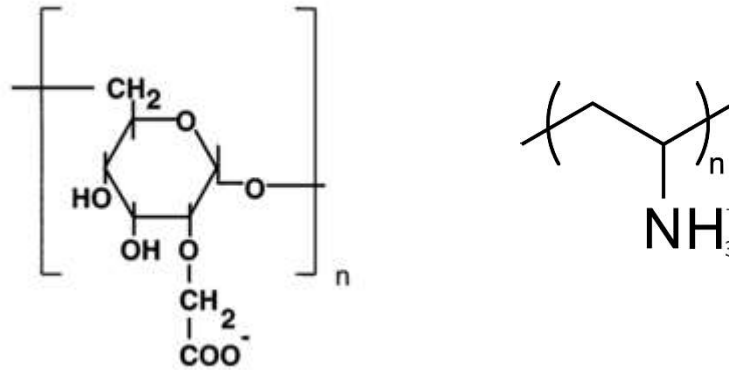


Figure 1.13. Anionic poly(carboxymethyl dextran)¹⁷⁵ (left) and cationic poly(vinylamine) (right).

Thus, attention was drawn to zwitterionic polymers, *i.e.* molecules carrying both positive and negative charges, to address protein-related fouling, because they present the advantage of strong water binding (like neutral hydrophilic polymers) without the inconvenient of carrying an overall net charge¹⁴⁹. As other charged species, zwitterionic polymers are sensitive to their environment, especially to pH and ionic force conditions. Wu *et al.* (2012)¹⁷⁶ demonstrated that the antifouling properties of zwitterionic polybetaines could significantly change when pH value decreases from 7 to 3.5. Moreover, Bengani *et al.* (2015)¹⁷⁷ point out that polyzwitterionic species were more susceptible to dissolve into highly saline media, which questions the sustainability of a zwitterionic coating in those conditions. However, despite the aforementioned drawbacks, several classes of polyzwitterionic polymers were still discussed in the literature for antifouling applications in biological conditions, namely polybetaines^{177–181}, phosphorylcholine^{182,183}, polyampholytes^{184,185}, peptides^{186,187} and polysaccharides¹⁸⁸.

❖ *Elastic modulus*

The elastic modulus E (N/m²) (Equation 1.7), also known as “Young’s modulus” characterizes the stiffness of a solid, that is to say its propensity to elastic deformation. The elastic modulus increases with the stiffness of a material, which implies that a perfectly rigid solid would have an infinite elastic modulus, and conversely, a perfectly elastic material would have a very low modulus. Even

if seldom studied in regard to dairy fouling, E is considered as a key factor for fouling-release properties in marine fouling scenarios^{110,189–191}. It is generally recognized that a low modulus enhances the fouling release properties^{110,146}, as E impacts the critical removal force, *i.e.* the force required to induce adhesion failure between two materials. Brady et al.¹¹⁰ indeed demonstrated a correlation between relative adhesion of several common polymers and $(E\gamma_c)^{1/2}$ where γ_c is the critical surface energy and showed that the lowest relative adhesion was achieved for the lowest E values.

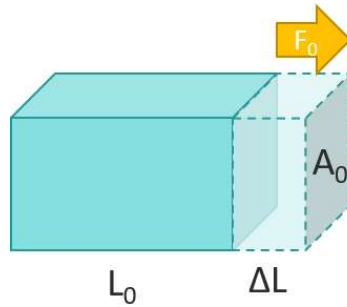


Figure 1.14. Representation of the measurement of the young modulus.

$$E = \frac{F L_0}{A_0 \Delta L}$$

F: exerted force (N)

L₀: initial length (m)

A₀: cross-sectional area (m²)

ΔL: change in length (m)

Equation 1.7

Surface properties, especially roughness and surface free energy proved to be crucial of fouling control. Their tuning would indeed allow either to decrease fouling amounts or to ease cleaning, thus leading to the modification and softening cleaning procedures. These processes are indeed in constant evolution to match both efficiency and cost requirements.

4. Cleaning of Dairy Fouling

Given the omnipresence of fouling in food industries, cleaning of the deposits is considered as a central issue, as it allows maintaining the high hygiene standards of the sector¹⁹² and avoiding cross-contaminations¹⁹³. The first Cleaning-In-Place (CIP) procedures were described in the 1940's and evolved from manual processes requiring the dismantlement of the entire equipment to the current standard automated techniques involving the circulation of cleaning solutions into fouled equipment⁶¹. The aims of CIP procedures are twofold: (i) to restore the initial pressure and heat transfer conditions in the system and (ii) to prevent microbial contamination of the equipment. Fryer and Christian (2005)¹⁹⁴ describe a typical CIP procedures in five steps:

- Pre-rinse: circulation of water to remove loosely bound deposits;
- Detergent cycle: circulation of cleaning chemicals (acidic or alkaline, *i.e.* one step process; or both separated by a water rinse, *i.e.* two-step process)¹⁹⁵;
- Intermediate rinsing: removal of cleaning agents by water circulation, possibly followed by neutralization;
- Sanitization: disinfection of the equipment;
- Final rinsing: removal of sanitizers and all traces of CIP products by water circulation.

CIP operations are water and energy intensive processes which have a negative impact on the environment¹⁹⁶. According to Piepiorka-Stepuk and Diakun (2012)¹⁹⁷, as much as 13.5% of the total energy consumption can be associated with the cleaning of equipment, depending on the nature of the manufactured goods. Indeed, unlike in petrochemical or marine fields, CIP process must be reiterated every five to ten production hours¹⁴⁹. Additionally, some of the chemical cleaning solutions are not biodegradable. As a matter of fact, dairy wastewater treatment can follow several scenarios, including in-plant wastewater treatment units, mechanical treatments, physico-chemical treatments, and biological treatments. All these treatments require inputs in terms of water, energy but also dedicated equipment and operating teams¹⁹⁸ and further increase the impact of CIP procedures on the financial and environmental performances of the global process. CIP procedures should then be carefully defined and calibrated. However, Boxler (2014)¹⁰ points out that most CIP procedures are not optimized and are operated on a semi-empirical basis.

Indeed, the operating sequence of CIP procedures depends greatly, but not only, on the nature of the deposits. Proteinaceous deposits are not water-soluble and require the use of an alkaline solution to hydrolyze them, whereas mineral deposits show variable solubility and are best cleaned by acidic solutions. The efficiency of CIP also depends on many other factors (Figure 1.15), like the cleaning time and temperature as well as hydrodynamic features^{197,199}. Particularly, Gillham *et al.* (2009)²⁰⁰ showed that temperature is a crucial parameter for the cleaning of dairy fouling. Other authors studied the optimal concentration of the cleaning agents^{201,202}, or the impact of hydrodynamic adjustments²⁰³. Boxler (2014)¹⁰ also pointed out the crucial importance of the substrate's surface properties. Indeed, a reduction in the fouling amount or an increase of the ease of cleaning could lead to significant softening of CIP procedures, hence shorter cleaning time, reduced cleaning costs and better environmental balance for thermal processes.

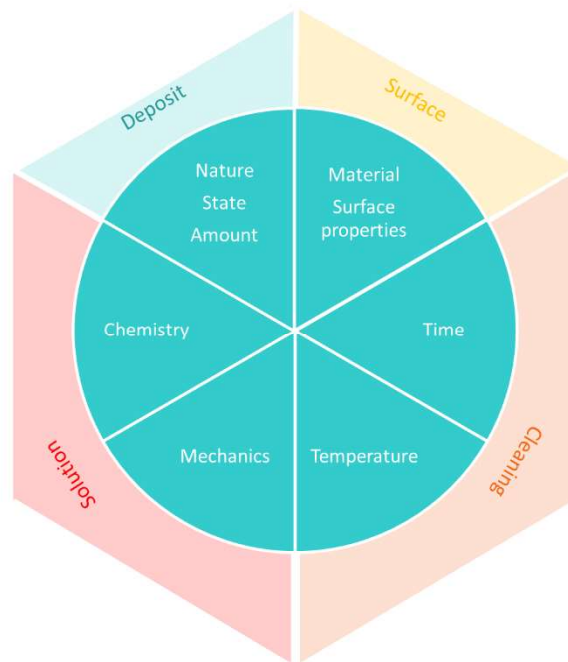


Figure 1.15: Extended Sinner's cleaning cycle according to Boxler (2014)¹⁰.

Adapting the CIP procedures nevertheless requires the quantification of the impact of surface modifications on the cleanability of the deposits. Hence the emergence of mathematical models describing soil cleaning according to several parameters from the Sinner's circle, such as cleaning agent chemistry, the temperature, temperature or mechanical actions¹⁰. Simultaneously, several techniques were developed in order to characterize the adhesion of deposits on the substrates

and their behavior to cleaning, like Fluid Dynamic Gauging (FDG)²⁰⁴ which uses flow data to estimate the adhesive and cohesive strength of a deposit on a substrate or coda wave interferometry²⁰⁵, an ultrasound technique allowing to monitor the formation or the elimination on a deposit.

Conclusions

This first chapter presented a state of the art about dairy fouling, its mechanisms, impacting factors as well as a literature survey on surface modifications targeting its mitigation.

The considerable amount of research focusing on dairy fouling allowed to demystify most of this complex phenomenon, although some controversy persists. Nevertheless, researchers agree on the fact that biofouling in general, and dairy fouling in particular, are multi-dependent phenomena, influenced by an overwhelming number of intrinsic or environmental parameters such as temperature, pH, protein and mineral concentrations, hydrodynamics, microbial flora, etc.

The literature also shows that surface modification is a suitable route to achieve fouling mitigation, even if no true breakthrough has been reported yet. Hydrophobic surfaces like PTFE or DLC have been vastly studied for their fouling-release properties. However, research on non-dairy fouling (marine or biomedical fouling) evokes numerous other alternatives which deserve to be investigated.

Furthermore, it is noticeable that similar works sometimes reach contradictory conclusions, mostly due to subtle experimental differences. Thus, it seems important to establish the impact of SS surface properties on dairy fouling before any antifouling surfaces development. Chapter 2 will therefore be dedicated to the definition of a repeatable fouling testing method and to the study of the influence of roughness and SFE of SS on dairy fouling.

Chapter 2 - INFLUENCE OF THE SURFACE PROPERTIES OF STAINLESS STEEL ON DAIRY FOULING

Introduction

In Chapter 1 the variability and multi-dependence of dairy fouling phenomena were highlighted. The study of literature also pointed out the overwhelming number of surface engineering routes towards fouling mitigation, although experimental variations often prevent direct comparison between different pieces of work.

Consequently, it seems that the clear definition of the test rig, fluids and experimental conditions is crucial to the pertinence of any research about fouling mitigation. Furthermore, it appears judicious to evaluate the impact of surface free energy and roughness on fouling in the defined conditions, before testing any non-fouling surface.

Chapter 2 – which is adapted from the paper entitled “Influence of stainless steel surface properties on whey protein fouling under industrial processing conditions”, published in the *Journal of Food Engineering* in 2018²⁰⁶ (Annex I) – will thus begin by a detailed presentation of the pilot test rig that was used during this project, of the chosen test fluid and operating conditions. The fouling performances of model surfaces of controlled roughness and surface energy, *i.e.* native, mirror polished and textured stainless steel surfaces, fluorosilanized or not, will then be presented and discussed. Multi-scale characterizations of those surfaces before and after fouling, using a wide range of analytical tools (goniometry, SEM, ToF-SIMS, EPMA X-Ray mappings) will be implemented in order to achieve better comprehension of the impact of surface energy and morphology modifications on the fouling behavior, while highlighting their complex interactions in fouling governance.

1. Presentation of the pilot test unit

1.1. Model fluid

Milk, as an animal-sourced biofluid, presents seasonal variation of protein and fat content^{207,208}. Furthermore, fresh milk contains proteolytic enzymes and an important bacterial flora that can trigger important physico-chemical modifications of milk, like clotting or pH drop. Those phenomena are very susceptible to significantly modify the fouling process and deposits amounts. Therefore, in order to ensure repeatability and avoid spoilage, model solutions are often used in fouling studies, instead of fresh milk⁷¹.

Table 2.1. Composition of Promilk 852 FB1, according to the manufacturer.

Compounds	Content (% w/w)
Total protein	80.1
<i>β-lactoglobulin</i>	66.0
<i>α-lactalbumin</i>	13.3
<i>Other</i>	0.8
Lactose	11.0
Lipids	1.0
Total minerals	7.9
<i>Calcium</i>	4.0
<i>Phosphate</i>	2.2
<i>Sodium</i>	1.7

As seen earlier, whey soluble proteins and mainly β -lactoglobulin, are, together with calcium, the main components of dairy fouling deposits^{10,42}. Thus, in the present study, the model fluid (MF) was formulated to approach β -lactoglobulin content in milk, *i.e.* 4 to 6 g/L²⁰⁹. The MF was thus a 1% solution of Whey Protein Concentrate (WPC) powder (Promilk 852 FB1, 80% protein in dry state, Ingredia, France) in reverse osmosis water. Detailed composition of the WPC powder is available in Table 2.1. Moreover, as previous research showed that increasing calcium concentration induces higher fouling levels⁵⁷, the calcium content of MF was adjusted in order to avoid overpressure or blockage in the PHEs while extending the runs duration as far as possible. The calcium content was thus adjusted to 100 ppm by addition of CaCl₂ (Sigma Aldrich). 500 L of

fresh MF were prepared for each fouling run and proteins were left to hydrate for two hours under stirring before testing. The pH of this solution is 6.8, and the calcium and protein contents were checked *via* atomic absorption spectrometry and HPLC (Waters, USA)⁴² respectively.

1.2. Pilot pasteurization rig

A pilot pasteurization rig (Figure 2.1), resulting from the downscaling of an industrial process ($\sim 1/10$) was used for fouling testing throughout the entire project. It is composed of a stirred tank, a volumetric pump (PCM, France) and two plate heat-exchangers (V7 models from Alfa-Laval-Vicarb, France) in a counter-current configuration. PHE 1 is composed of 10 passes, one channel by pass, and pre-heats the treated fluid from room temperature to 60°C. PHE 2 is composed of 5 passes, one channel by pass and heats the model fluid to 85°C, which is a commonly used temperature in classical pasteurization¹⁰. For both PHEs, the equivalent space between two consecutive plates is 3.93 mm. During each fouling test, flow rates, temperatures and pressures were monitored.

Reference and modified stainless steel coupons were placed in a samples-holder, i.e. square pipe of 1 cm² section, directly connected after the heating section. As a consequence, the studied surface were not heated, and the studied deposits resulted from isothermal fouling. The monitoring of the temperature at the outlet of the sample holders showed very little variation of at most 1°C from its target value of 85°C. The studied surfaces were thus submitted to fouling conditions comparable to the holding section of a classic pasteurizer.

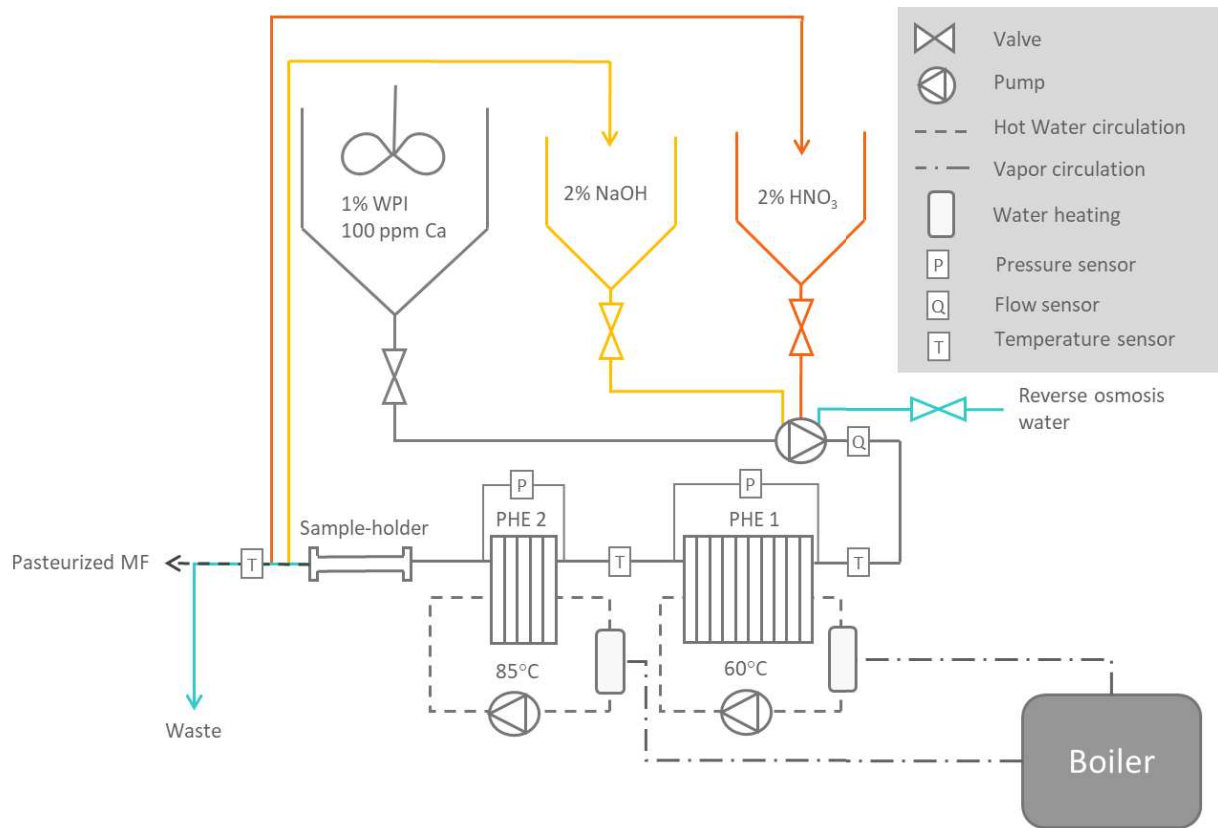


Figure 2.1. Diagram of the pilot pasteurization unit.

For all experiments, the product flow rate was 300 L/h and hot water flow rates were of 900 L/h. Therefore, all tests involved identical temperature profiles in the heat exchangers, which ensures unbiased comparisons between two tests. The Reynolds number inside the sample holders was of 2400 (transient regime). The pilot plant was started and brought to steady-state conditions with circulation of reverse osmosis water, and a by-pass prevented water to pass on the tested samples. Once steady-state was reached, model fluid was circulated and it was only at that point that the by-pass was switched to allow the dairy fluid to foul the samples.

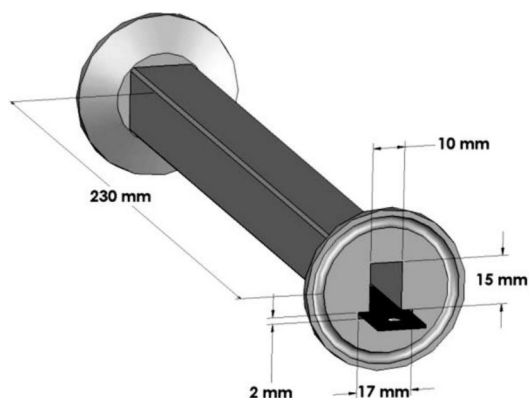


Figure 2.2. Diagram of a sample holder (from Cunault et al. (2015)²¹⁰).

One minute-long experiments were carried out to study the initial steps of deposition. 1.5 hour-long experiments were carried out to observe the deposits structure and compare fouling amounts of the different surfaces.

Cleaning of the installation was performed through cleaning-in-place (CIP) procedures as follows. Firstly, a 20 min pre-rinse with hot water was performed to remove loosely adhered deposit. Then, a 2% (w./v.) NaOH solution was circulated for 15 min to eliminate the organic fouling, followed by an intermediate rinse, and a 2% (w./v.) HNO₃ solution was circulated to remove mineral deposits. All cleaning fluids underwent the same temperature profile as MF, and both the acidic and the alkaline cleaning solutions were recirculated. Fresh solutions were prepared every fifth CIP. Finally, the installation was rinsed and neutralized with the circulation of cold water for 15 min. All solutions were circulated at 300L/h. The tested surfaces were either taken out of the installation before the CIP procedure, after the first rinse or at the end of the CIP, depending on the studied behavior (fouling, fouling release, behavior to clean in place). In the present Chapter, all studied surfaces were taken out of the rig before CIP.

After the fouling tests, the one-minute fouled samples were dehydrated by the critical point method in an E3000 Jumbo Critical Point Dryer (Quorum Technologies). The one-hour fouled samples were stored in a ventilated cold room until they were dry and ready for weighing and further analysis. As the aim of this study was to assess the impact of the substrate's surface properties on its fouling performances, the samples were only used once and the effect of ageing on fouling performances was not investigated.

In each test, at least three replicates of each type of surface were tested. The fouling results presented in the following sections result from three pasteurization tests, performed on different days.

2. Bacterial adhesion tests

In food-related industrial context, control of micro-organisms is extremely important in order to prevent product contamination and illness outbreaks. Food-contacting materials should thus be evaluated for their proneness to retain bacterial cells. For that purpose, bacterial adhesion assays were carried out on the studied substrates. The chosen strains were *Listeria monocytogenes* ATCC 35152 (LM/NCTC, United Kingdom), *Staphylococcus aureus* CIP 4.83, and *Salmonella enterica* CIP 8297 (CRBIP, France), which are well-known foodborne pathogenic bacteria. Those strains were also chosen for their relevance regarding dairy processing and for their diversity, as *S. aureus* is a Gram-positive coccus, *L. monocytogenes* is a rod-shaped Gram-positive strain, and *S. enterica* is a rod-shaped Gram-negative bacterium. All strains were kept frozen until use.

Pre-cultures were done by inoculating 100 µL from defrosted tubes into 5 mL of Tryptic Soy Broth (TSB) and incubated for 24 h at 37°C, which is the optimal growth temperature for mesophilic bacteria. Main cultures were obtained by inoculating 100 µL from pre-cultures into 50 mL of TSB and incubated at 37°C. The bacterial cultures were stopped in the late exponential phase and cells were separated from the supernatant by centrifugation (3000 rpm, 4°C, 10 min). The cells were then washed twice in physiological water (PW) by centrifugation (3000 rpm, 4°C, 10 min). After re-suspension in 20 mL of PW and sonication to ensure optimal cell dispersion, the concentration of the suspension was checked by absorbance measurements (optical density at 620 nm: DO_{620 nm}). The appropriate dilutions were then performed to obtain 10⁷ colony-forming units (CFU) per mL of suspension.

The different substrates were covered with 3 mL of bacterial suspension. After 1h of adhesion, which was carried out at room temperature (21°C) in order to limit further bacterial growth, surfaces were rinsed twice for 1 min with 20 mL of PW on an orbital shaker under low agitation (60 rpm). The adhered cells were then stained with acridine orange (Sigma Aldrich). After 10 min,

samples were rinsed and dried in air at room temperature. Surfaces were then observed with an Olympus BX43 Fluorescence Microscope ($\times 100$), and the adhered cells counted. The presented data are representative of at least three coupons for each kind of surface (50 different microscope fields per coupon).

3. Model surfaces

Reference substrates in this work were $10 \times 16 \times 1 \text{ mm}^3$ and $45 \times 16 \times 1 \text{ mm}^3$ (length \times breadth \times thickness) 316L stainless steel coupons with a 2B finish from Sapim Inox (France). They will be called NAT for “native stainless steel” thereafter. The small surfaces were used for characterization and analysis while the larger ones were used for fouling amounts measurements.

3.1. Surface preparation

3.1.1. Physical modifications

3.1.1.1. Mirror-like polishing

Mirror-like (ML) samples were obtained by polishing NAT surfaces on a rotary polisher (ESC 200 GT, Escil, France) with different grades of silicon carbide abrasive papers (#180 down to #4000) and finally a felt disk impregnated with $\frac{1}{4}$ micron diamond paste (Escil, France). After polishing, mirror-like samples were sonicated in water for ten minutes to remove any leftover silicon carbide particles and left to age at least one week in air before testing.

3.1.1.2. Texturing

Cauliflower-like patterns on stainless steel were obtained through femtosecond laser ablation, performed at the University of British Columbia. The stainless steel surfaces were patterned. Detailed parameters for the laser modification were reported by Kietzig *et al.* (2009)²¹¹, Moradi *et al.* (2013)²¹² and Moradi *et al.* (2015)²¹³. Briefly, an amplified solid-state Ti-Sapphire laser was used to generate ultrashort laser pulses (pulse duration of 120 fs, repetition rate of 1 kHz), with a center wavelength of 800 nm and a Gaussian distribution^{212,213}. The maximum output power was about 2W. Neutral density filters attenuated and adjusted the energy of the laser beam, and the spot size

was 30 μm at the focal point. Laser fluence was set at 480 J/cm^2 . Stainless steel surfaces were moved at 370 $\mu\text{m}/\text{s}$ on a computer-controlled X-Y linear translation stage. Laser texturing was carried out in air (clean room), with the beam normal to the treated surface. Samples were then cleaned for 2 min in an ultrasonic bath and will be referred to as TEX.

3.1.2. Chemical modifications.

Prior to any further modification, NAT, ML and TEX samples were degreased in an acetone/ethanol 50/50 (v./v.) blend, soaked in a 2% v/v RBS 35 detergent (Sigma Aldrich) solution at 65°C for 10 min, then rinsed twice in deionized (DI) water at 50°C for 5 min and finally rinsed twice in DI water at room temperature for 5 min. They were dried in air at room temperature.

In order to decrease their surface energy, NAT, ML and TEX samples were fluorosilanized as follows. Firstly, an atmospheric plasma activation was performed to facilitate fluorosilane adhesion to the substrate and thus increase the fluorosilanization efficiency. Samples were exposed to a low temperature afterglow of an alternative current discharge in nitrogen, with an atmospheric plasma spot device (ULS, Acxys Technologies, France). The nozzle-substrate distance was of 20 mm. The N_2 flow rate was set at 60 L/min and the scanning speed was set at 100 mm/s. Four passes of nitrogen plasma were performed to ensure optimal activation. As the plasma activation induced heating (up to 246°C), the substrates were left to cool down to room temperature before further modification.

Fluorosilanization was then achieved by immersing plasma treated NAT, ML and TEX samples in a 10^{-3} M solution of perfluorodecyltriethoxysilane (PFTES, Sigma Aldrich) in n-hexane (Carlo Erba Reagents) at room temperature for 4 hours. Afterwards, samples were rinsed first under hexane flux (Sigma Aldrich), then under ethanol flux (VWR Chemicals) and finally sonicated for 10 min in ethanol and dried in air at room temperature. The thickness of such self-assembling monolayers is typically in the range of 5 to 10 Å on flat surfaces²¹⁴. Resulting samples are referred to as SilNAT, SilML and SilTEX respectively for native, mirror-like and texturized fluorosilanized samples.

3.2. Surface characterizations

Before fouling tests, water contact angle (WCA), surface energy (SFE) and arithmetic average roughness (Ra) of native and modified stainless steel samples were measured. All experimental methods regarding surface analyses and characterizations are detailed in Annex II. In this chapter, surface free energy was calculated following the Van Oss acid-base approach (see Chapter 1, p. 30). Their surface features are gathered in Table 2.2.

Table 2.2. Water contact angles (WCA), surface free energies (γ) and average roughness (Ra) of native and modified stainless steel.

Samples	WCA (°)	γ^{total} (mN/m)	γ^{LW} (mN/m)	γ^{AB} (mN/m)	γ^+ (mN/m)	γ^- (mN/m)	Ra (μm)
NAT	84.2 ± 2.6	40.5 ± 1.7	38.1 ± 0.3	2.4 ± 1.7	0.4 ± 0.3	3.5 ± 2.5	0.07 ± 0.01
ML	63.9 ± 2.5	42.5 ± 3.8	37.8 ± 1.1	4.7 ± 2.8	0.5 ± 0.5	17.0 ± 5.3	3.10 ⁻³ ± 2.10 ⁻⁴
TEX	0 ± 0			Not possible to determine*			36.0 ± 2.0
SiNAT	111.9 ± 1.1	27.6 ± 3.2	25.5 ± 3.8	2.4 ± 1.5	1.3 ± 0.6	1.1 ± 0.9	0.98 ± 0.09
SiML	105.9 ± 0.8	18.8 ± 4.3	18.6 ± 2.6	0.2 ± 0.2	0	1.8 ± 1.0	4.10 ⁻³ ± 1.10 ⁻³
SiITEX	132.9 ± 1.6			Not possible to determine*			36.0 ± 2.0

*The complex roughness of those samples impacts the apparent contact angle of any liquid droplet on them. Their surface energy therefore could not be calculated through goniometry measurements.

3.2.1. Non-fluorosilanized samples surface properties

Native stainless steel exhibits a WCA of 84.2 ± 2.6°, which is slightly high but still in agreement with values found in the literature (from 75°²¹⁵ to 84°^{108, 147,216}). However, WCA variations from one source to another are not surprising. Indeed, depending on grade and finish, SS surfaces can present very different surface chemistries and morphologies.

As expected, polishing drastically decreases stainless steel's roughness from 0.07 ± 0.01 μm to 3.10⁻³ ± 2.10⁻⁴ μm . Optical microscopy observations revealed that, contrary to NAT, ML samples present no grain boundaries and are very smooth (Figure 2.3). Interestingly, polishing changes the wettability of stainless steel. Indeed, the WCA value of ML samples (63.9 ± 2.5°) is lower than that of native SS (84.2 ± 2.6°). Roughness modifications can cause wettability changes, however, the present variation of WCA with roughness does not fit the theoretical wetting models. Indeed, according to Wenzel's equation (Equation 1.4, p. 31), an increase in roughness leads to an amplification of the pre-existing condition – hydrophilicity (WCA < 90°) or hydrophobicity (WCA > 90°). In the present case, the smoother surface (ML) is hydrophilic (WCA of 63.9 ± 2.5°) and an

increase in roughness should then lead to a decrease of WCA. However, the rougher native stainless steel shows a higher WCA of $84.2 \pm 2.6^\circ$. This divergence from Wenzel's model could be explained by a modification of surface chemistry, caused by the removal of superficial layers during polishing.

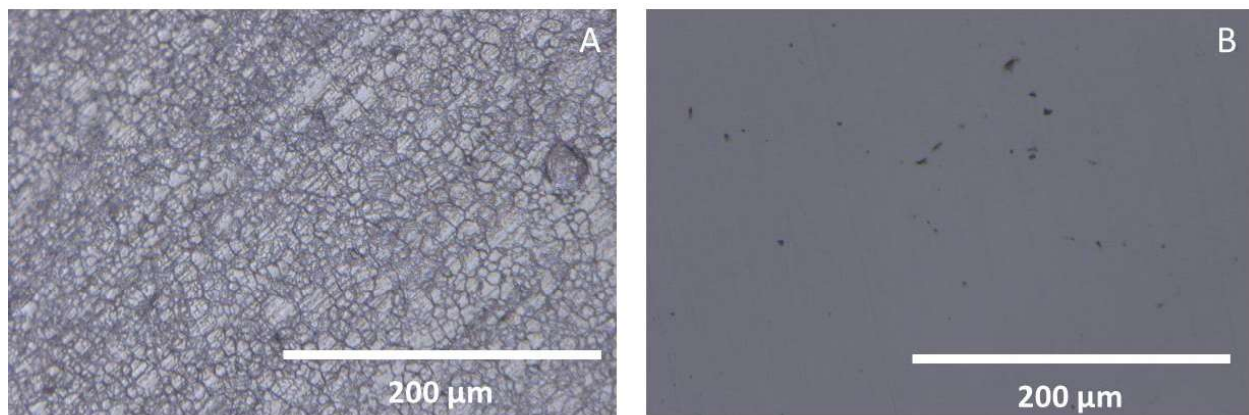


Figure 2.3. Optical microscopy images of native stainless steel (A) and mirror-like stainless steel (B). © 2018 Elsevier.

Statistical analysis (mean comparison *via* Student's test, $\alpha = 0.05$) has shown that the total SFE of native and mirror-like stainless steel did not significantly differ (apart from their electron donor components γ). However, XPS spectroscopy was carried out to determine the chemical composition of NAT and ML samples. The analysis of Fe 2p and Cr 2p XPS spectra was performed following the decomposition proposed by Biesinger *et al.* (2011)²¹⁷. The result of this set of analysis (Table 2.3) shows that the chemical compositions of native and mirror-like stainless steel surfaces are indeed different. What is interesting here is that the proportions of oxide component of Fe (consistent with Fe III (Figure 2.4, A and B)), and of oxide component of Cr (consistent with chromite (Figure 2.4, C and D)) are different between NAT and ML samples. The higher presence of oxides (both iron and chromium oxide) in the native sample is explained by one of the properties of stainless steel, *i.e.* the spontaneous formation of a passive film, rich in oxides, that protects the material from corrosion. The mechanical polishing removes this passive layer, revealing the inner material. Nevertheless, the high content in Chromium of 316L stainless steel (16-18 wt.-%) could lead think that the oxide-rich passive film would rebuild itself after polishing. XPS analyses show here that this is not the case in the time interval between polishing and analysis (one week). It is

probable that the ageing period between polishing and analysis was not long enough to allow the passive film to reform.

Table 2.3. Surface characteristics of native and mirror-like stainless steel as determined by XPS analyses.

Samples	O		Fe		Cr		Ni	
	Total	Fe metal	Fe oxide	Total	Cr metal	Cr oxide		
NAT	77.8%	14.2%	24.8%	75.2%	7.1%	14.1%	85.9%	0.8%
ML	66.4%	19.4%	44.5%	55.2%	10.8%	24.0%	76.0%	3.4%

Overall, the XPS results are consistent with the surface energy measurement, showing that the electron donor component of ML samples was higher than the one of NAT samples. ML samples indeed contain a higher proportion of metal Fe and metal Cr, available for oxidation. The difference in SFE observed between NAT and ML samples can thus be considered as accurate.

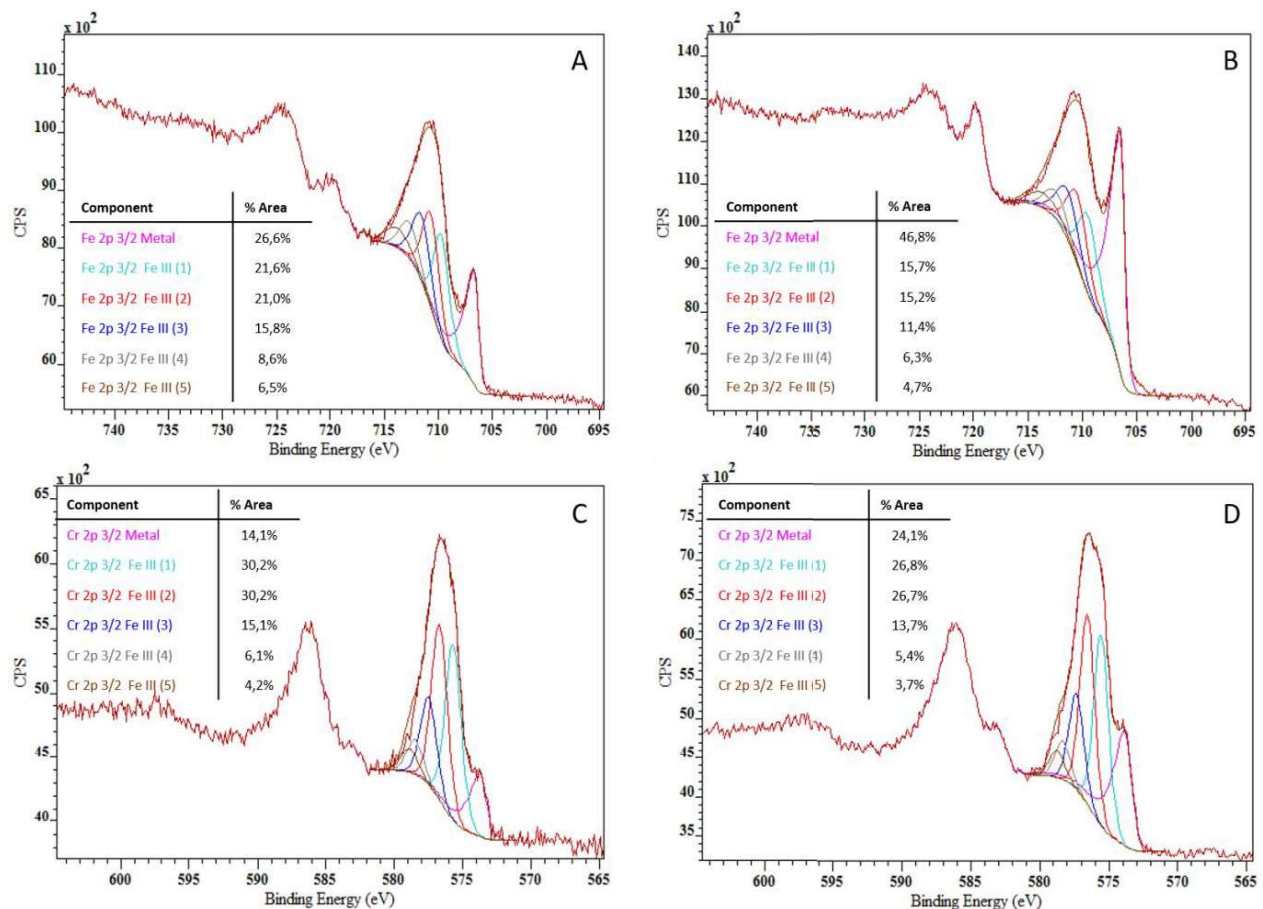


Figure 2.4. XPS spectra of Fe in NAT (A), Fe in ML (B), Cr in NAT (C) and Cr in ML (D). © 2018 Elsevier.

On the other hand, laser textured samples show very high Ra values ($36.0 \pm 2.0 \mu\text{m}$) compared to the reference stainless steel plate. SEM imaging confirms the presence of hierarchical cauliflower-like structures (Figure 2.5). The superhydrophilic properties of textured sample after laser ablation has been reported previously by Kietzig *et al.* (2009)²¹¹, who showed that this low WCA was the combined result of dual-scale morphology and enhanced surface oxidation, both caused by laser ablation. Consequently, the water droplet completely wets the surface and is no longer visible after deposition.

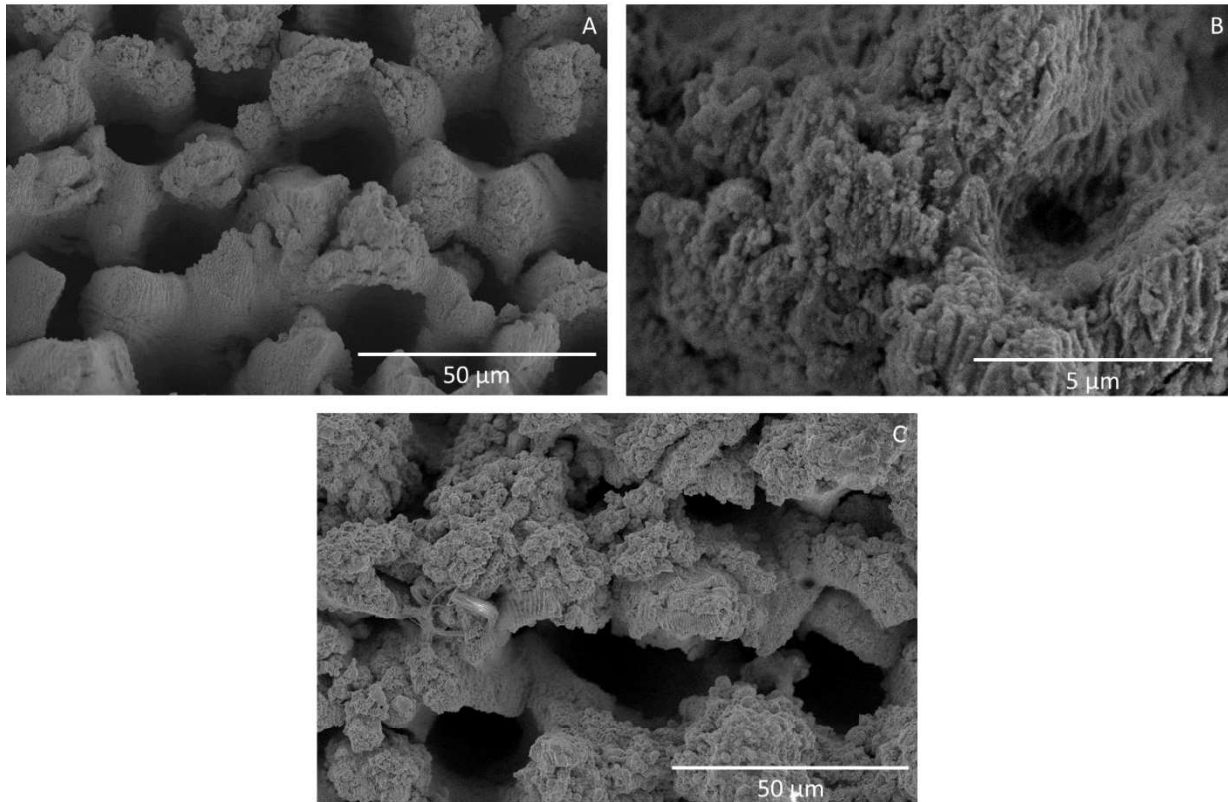


Figure 2.5. SEM pictures of laser textured stainless steel evidencing a micro-roughness (A) supporting a nano-roughness (B), and of fluorosilanized textured stainless steel (C). © 2018 Elsevier.

3.2.1. Fluorosilanized samples surface properties

Fluorosilanization was carried out to increase the hydrophobicity, *i.e.* to lower the surface energy of the substrates. WCA and SFE measures (Table 2.2) indicate that this goal was reached, as SilNAT and SilML showed increased water contact angle (respectively $111.9 \pm 1.1^\circ$ and $105.9 \pm 0.8^\circ$) and reduced SFE (respectively $27.6 \pm 3.2 \text{ mN/m}$ and $18.8 \pm 4.3 \text{ mN/m}$) compared to their untreated

counterparts. It is noteworthy that in this case, the variation of WCA between SilML and SilNAT samples fits Wenzel's model, which highlights the chemical homogeneity of the fluorosilanized surfaces.

Roughness measurements seem to indicate that fluorosilanization causes an increase in surface roughness for all samples, which is surprising, as fluorosilane monolayers are expected to be very thin and not to change surface morphology. Although the roughness disparity between ML ($3.10^{-3} \pm 2.10^{-4} \mu\text{m}$) and SilML ($4.10^{-3} \pm 1.10^{-3} \mu\text{m}$) seems to be insignificant, control SEM imaging (Figure 2.6) was needed to check the appearance of SilNAT surfaces. The fluorosilane layer is visible on Figure 2.6B, and observations at greater magnification (Figure 2.6C) allowed to observe some disperse lumps (around 200 nm in diameter) on the fluorosilane layer. This points out minor local polymerization, however such structures are quite unlikely to be responsible for roughness variation. Given these observations and the rather high standard deviations of the contact profilometer measurements (Table 2.2), the roughness difference between NAT and SilNAT is most likely due to natural surface heterogeneity between SS surfaces.

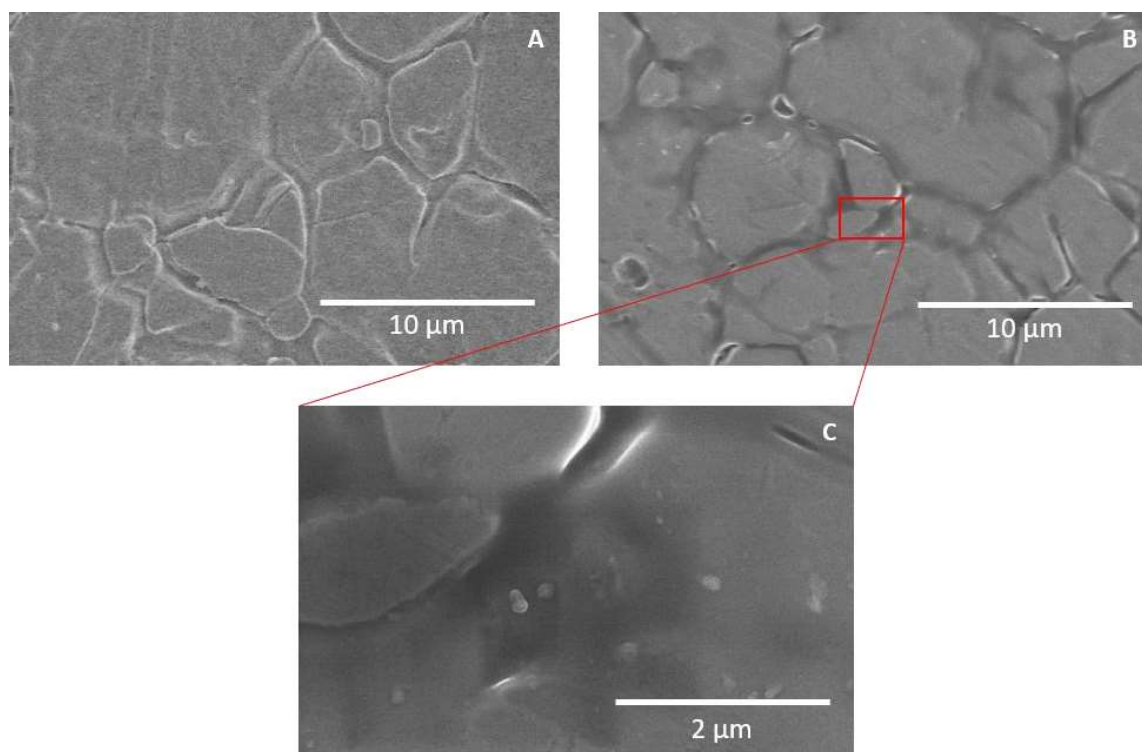


Figure 2.6. SEM micrographs of bare native (A) and native fluorosilanized stainless steel (B) and (C).
© 2018 Elsevier.

Fluorosilanization of textured stainless steel induced a drastic WCA increase (from 0° to $132.9 \pm 1.6^\circ$). SilTEX surfaces can be classified as hyper-hydrophobic and dynamic goniometry measurements revealed a very low contact angle hysteresis (CAH) of $2.6 \pm 0.8^\circ$. The alliance of high WCA and low CAH is characteristic of the suspended Cassie-Baxter wetting regime¹¹², also called “lotus effect”, which is often associated to self-cleaning properties. Such properties would be very interesting regarding fouling management, if they persist through the pasteurization run. Environmental factors, such as temperature, tangential flow and pressure increase could indeed induce destabilization of the suspended Cassie-Baxter state and trigger wetting regime transitions. It is nevertheless interesting to notice that similar surfaces showed good resistance to cell adhesion while immersed in an aqueous media²¹⁸. Chemical modification of textured surfaces did not impact the arithmetic mean roughness, indicating that the chemical treatment resulted in a very thin hydrophobic monolayer. SEM pictures of TEX and SilTEX surfaces confirm these observations (Figure 2.5) as the dual-scale roughness was still visible on treated samples.

NAT, ML, TEX, SilNAT, SilML and SilTEX surfaces were tested in the pilot pasteurizer (Figure 2.1) in isothermal conditions. The fouling results are presented in the following section.

4. Whey protein fouling results

Table 2.4 presents the results obtained for the all samples after 1.5 hour of fouling. NAT is the control sample in all experiments. Throughout the entire manuscript, fouling percentage (F%) was calculated according to Equation 2.1.

Table 2.4. Fouling densities and F% of the different studied surfaces.

Samples	Fouling Density (mg/cm ²)	F%
NAT	30.8 ± 4.0	100
ML	17.2 ± 0.6	56% ($\pm 4\%$)
TEX	151.2 ± 21.2	491% ($\pm 14\%$)
SilNAT	8.7 ± 0.6	28% ($\pm 7\%$)
SilML	5.2 ± 0.4	17% ($\pm 7\%$)
SilTEX	57.4 ± 14.3	186% ($\pm 25\%$)

Results show differences in fouling behavior according to surface properties: fouling is reduced for ML, SilNAT and SilML samples (respectively -44 ± 4 wt.-%, -72 ± 7 wt.-% and -83 ± 7 wt.-%) whereas

the TEX and SilTEX samples present drastic fouling increases of $+391 \pm 14$ wt.-% and $+86 \pm 25$ wt.-% respectively. At this point, a close examination of the fouling/steel interface is needed to clearly establish their origins.

$$F\% = \frac{(M_{Fouling})}{M_{Fouling\ Ref}} \times 100 \quad \text{Equation 2.1.}$$

F%: Percentage of fouling compared to the reference (-)

M_{Fouling}: Deposit mass on modified sample (mg)

M_{Fouling Ref}: Deposit mass on the reference bare stainless steel (mg)

Obviously, roughness plays a crucial role in fouling regulation, as the three samples with lower Ra (ML, SilML and SilNAT) exhibit fouling reduction comprised between -44 ± 4 wt.-% and -83 ± 7 wt.-% compared to the reference. On the other hand, textured samples with higher roughness (TEX and SilTEX) show important fouling increases (up to $+391 \pm 14$ wt.-% for TEX samples).

Surface free energy also appears as a governing factor in the fouling process, as fluorosilanized samples (SilML and SilNAT), which have lower SFE, exhibit better antifouling performances than those of NAT and ML.

However, as shown on Figure 2.7 and Figure 2.8, no straightforward tendency for the effects of roughness or SFE on fouling could be deduced at this point. Cross-comparisons between the model surfaces could help to gain a better understanding of the intricate interactions of roughness and SFE in fouling control.

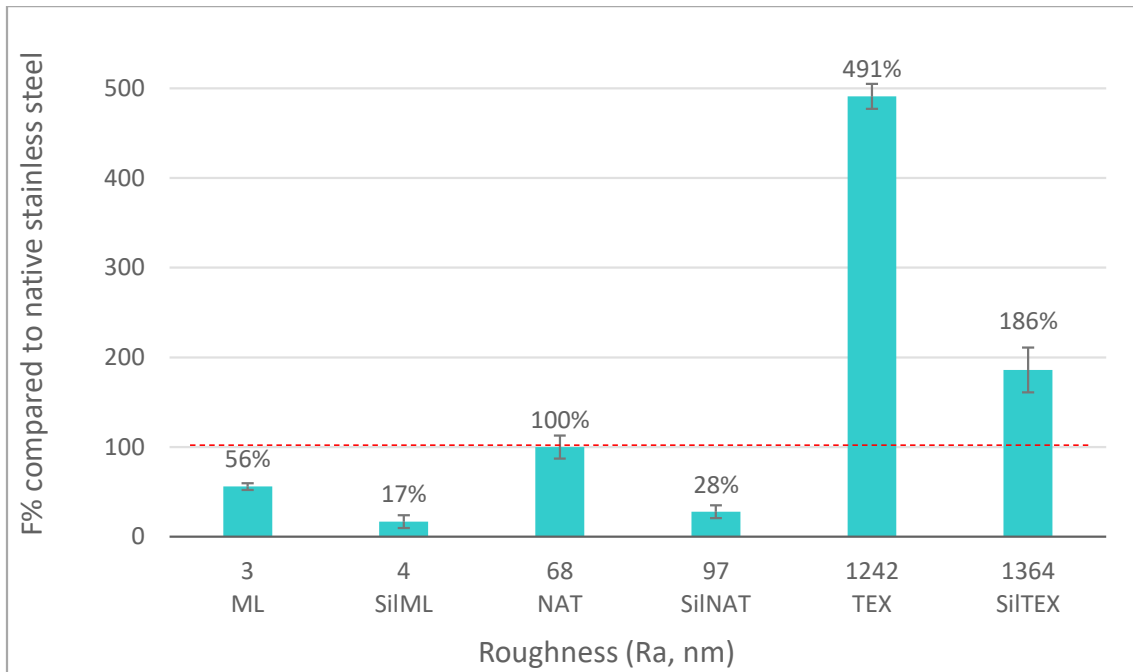


Figure 2.7. Fouling performance of the various modified substrates (wt. %) compared to native stainless steel, plotted against increasing roughness (Ra, nm).

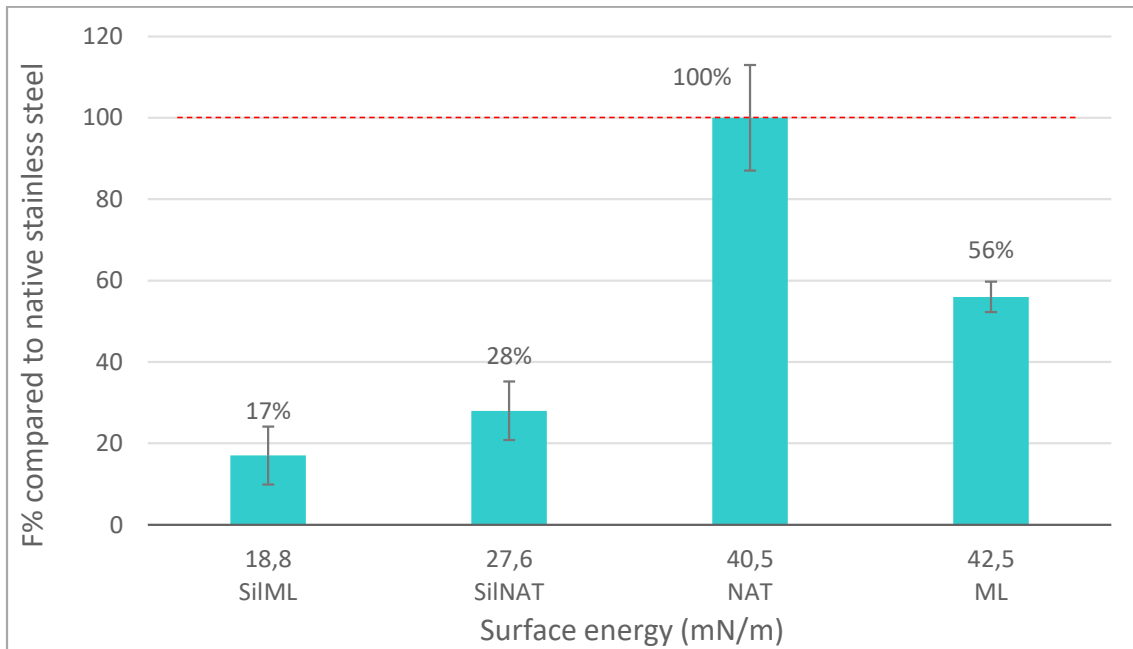


Figure 2.8. Fouling performances of the various modified substrates (wt. %) compared to native stainless steel, plotted against increasing surface free energy (SFE, mN/m).

4.1. Impact of physical modifications

First comparisons were carried out between native (NAT) and mirror polished (ML) samples, showing roughness of $0.07 \pm 0.01 \mu\text{m}$ and $3.10^{-3} \pm 2.10^{-4} \mu\text{m}$, respectively. Their fouling results are consistent with other works¹³⁸ and point out a competition between surface roughness and surface energy for the control of the fouling behavior. Indeed, regarding only the surface free energies, the good anti-fouling performance of mirror-like stainless steel compared to the native reference is surprising, as it is generally accepted that a higher basic component induces more proteinaceous fouling¹²⁷. In this case, ML surfaces, which possess the higher basic component γ^- ($17.0 \pm 5.3 \text{ mN/m}$ versus $3.5 \pm 2.5 \text{ mN/m}$ for native stainless steel) exhibit the lowest amount of fouling. It seems then that in this case, roughness dominates surface energy for fouling control, and that physical phenomena are preponderant in regard of chemical ones.

Indeed, ML and NAT surface present truly different surface morphologies (Figure 2.3) and SEM micrographs of fouled native stainless steel (Figure 2.9A, C and E) show dairy deposits penetration in the grain boundaries. This interlocking phenomenon promotes the formation and anchorage of a steady fouling base-layer, resulting in stable deposit build-up, and inducing the decrease of re-entrainment phenomena¹¹⁰. Mirror-like stainless steel (Figure 2.9B, D and F) presents a smoother surface, free of defects, that does not allow interlocking to happen, as the light scratches visible on Figure 2.9, resulting from the polishing process, are too small for fouling agents to penetrate into them.

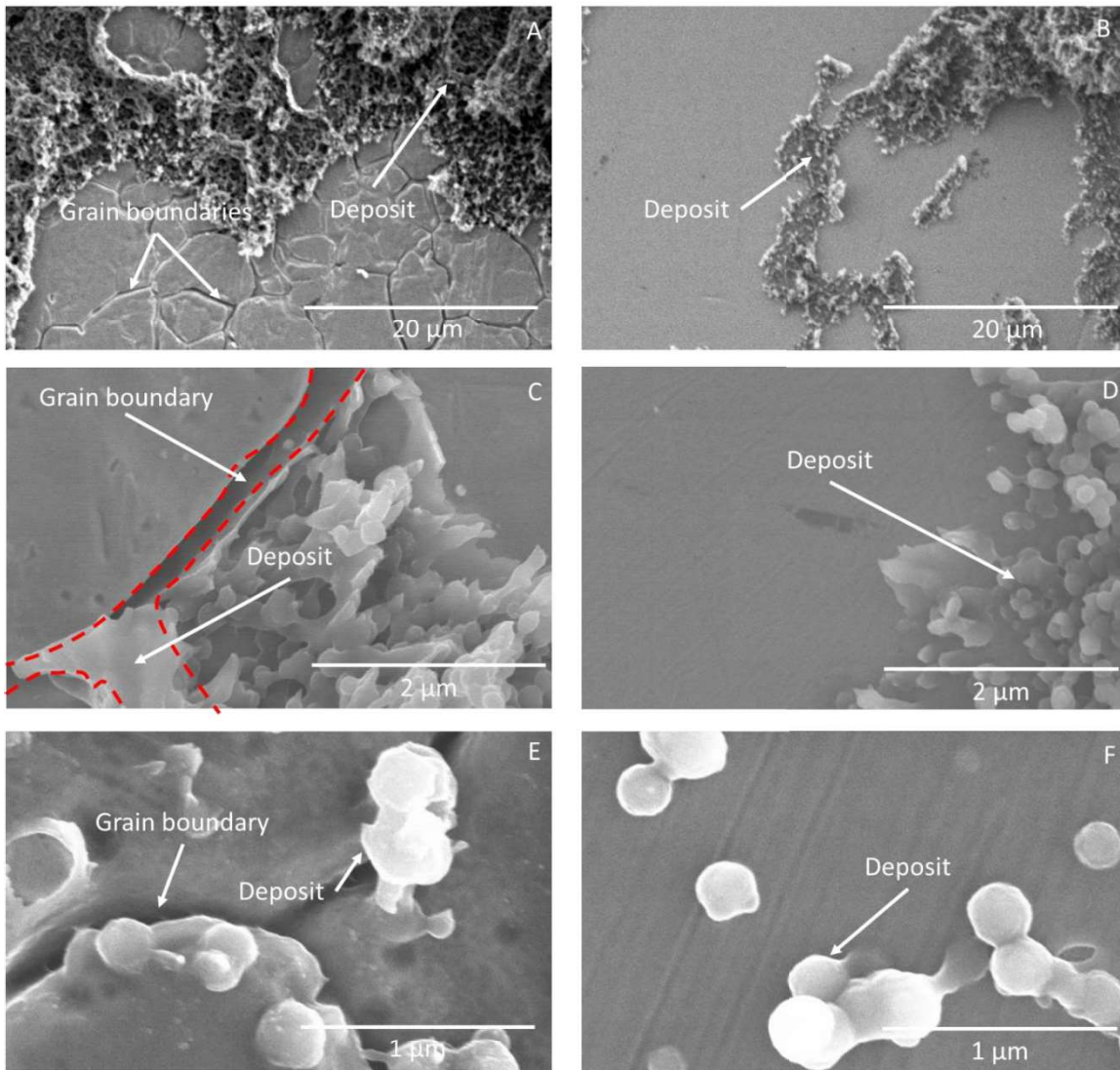


Figure 2.9. SEM micrographs at different magnifications of 1 hour-fouled samples after removal of the top part of the deposit with a cutter; (A), (C) and (E): native stainless steel; (B), (D) and (F): mirror-like stainless steel. © 2018 Elsevier.

Top-view ToF-SIMS iron (substrate) and nitrogen (protein) mappings were carried out on 1 min-fouled NAT and ML samples to investigate the early fouling stages (Figure 2.10).

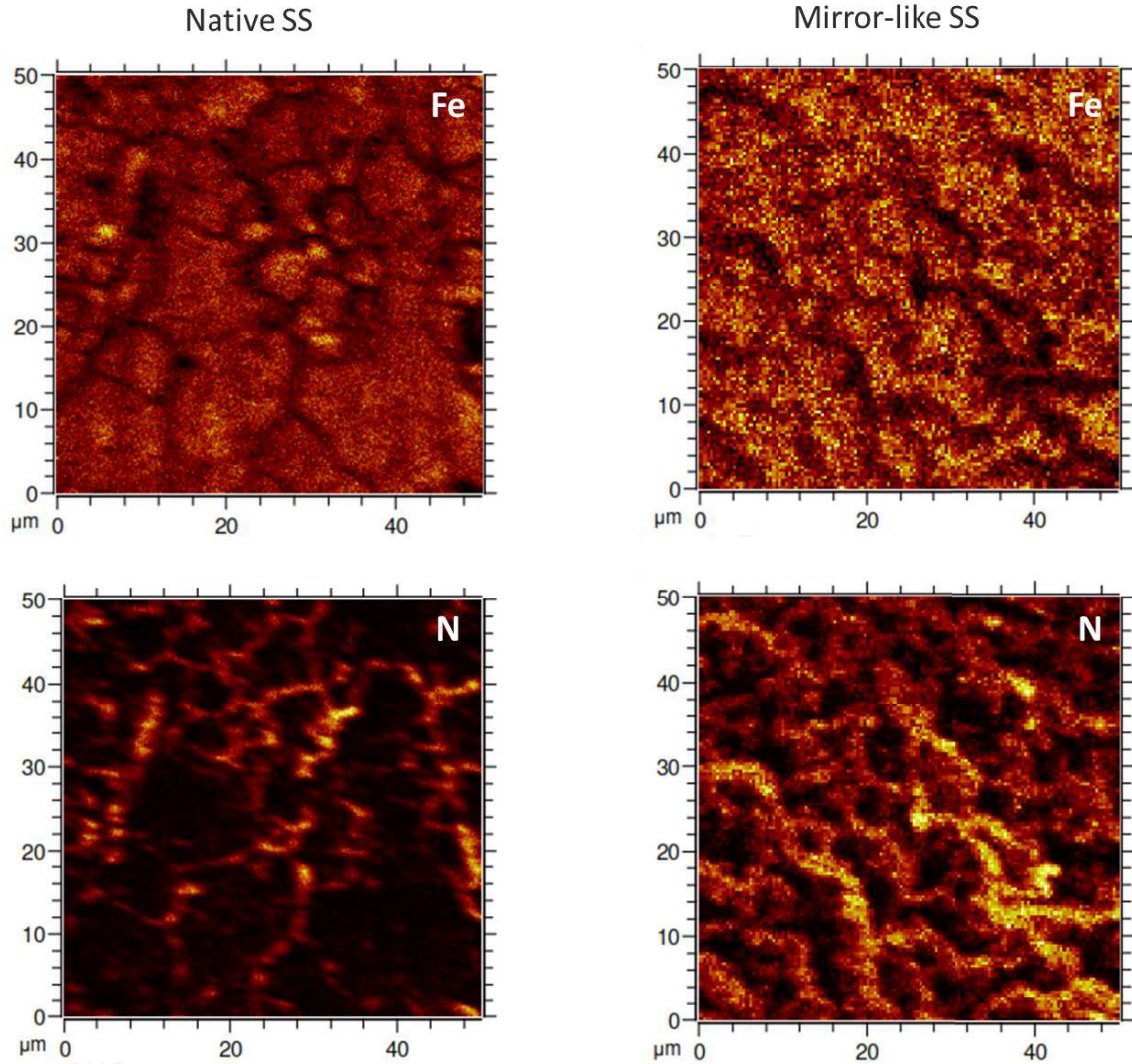


Figure 2.10. ToF-SIMS superficial images of 1-min fouled native and mirror-like. © 2018 Elsevier.

Grain boundaries are well visible on the NAT iron mapping (dark lines) and protein is identified following the same pattern, which corroborates the interlocking hypothesis made earlier. On the other hand, on mirror-like samples, that are free of grain boundaries (Figure 2.3, Figure 2.9), protein is randomly dispersed on the surface. Three dimensional reconstructions of ToF-SIMS depth profiles (Figure 2.11) also confirm those observations.

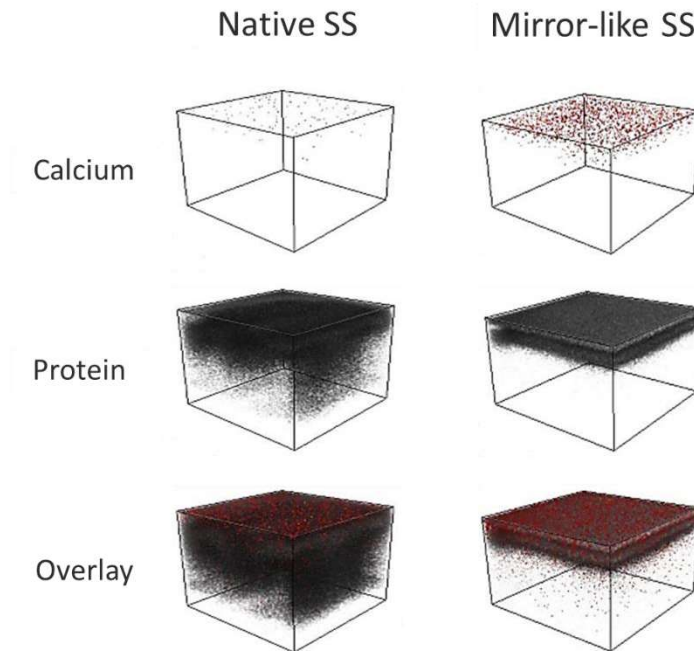


Figure 2.11. ToF-SIMS 3D reconstructions of one minute fouled native and mirror-like samples.

Cross-section X-ray mappings of one-hour fouled samples (Figure 2.12) allowed observing the substrate/deposit interface and the structure of the deposits. While fouling on NAT samples is rather dense and bulky, ML surfaces exhibit more aerated and fragile-looking deposits with a thin, continuous base-layer from which skinny pillars emerge, supporting denser fouling pieces. This mushroom-like structure possibly results from poor anchorage of the deposits on the smooth, low roughness surface of ML. Fouling build-up on such substrate would then be less stable and more susceptible to cohesive failure than the dense deposits on NAT. As a result, ML fouling would be more sensitive to re-entrainment, which can explain the fouling reduction witnessed for the ML surfaces.

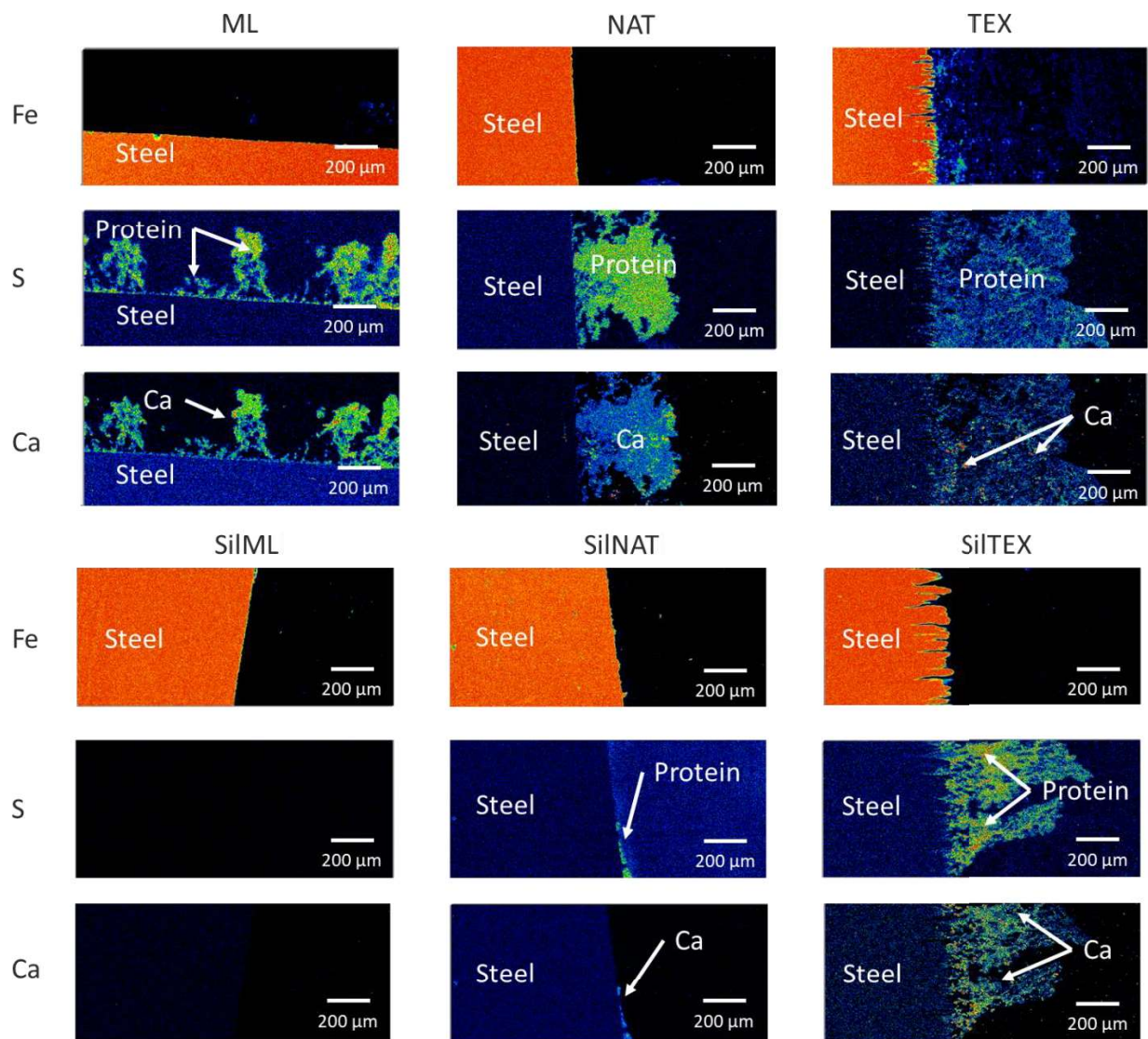


Figure 2.12. Cross-section EPMA X-Ray mappings of 1h-fouled native, mirror-like, and texturized stainless steel, fluorosilvanized or not.

Native and textured samples ($R_a = 1242 \pm 18$ nm) were also compared. Their fouling performances were very different, as TEX samples show an important fouling increase: $+391 \pm 14$ wt.-% compared to the reference. Although high hydrophilicity is often associated with good antifouling performances^{149, 160, 164}, it is important to understand that this applies to highly hydrated polymeric surfaces, like PEG brushes or hydrogels, where the water-polymer organized structure acts as a protein-repellant through steric repulsion. Here, the hydrophilicity of the metallic surface is due to the presence of numerous oxidized sites (like hydroxyl groups for instance) that can interact with unfolded protein and cause its adsorption. The low WCA of TEX surface is then a disadvantage for

fouling performances. Moreover, the morphology of TEX samples, observed on SEM micrographs (Figure 2.5A) and on cross-section X-ray mappings (Figure 2.12), is favorable to fouling increase. Indeed, the craters left by laser impacts on the stainless steel surface show diameters of about 20 to 30 μm , much greater than the size of the unfolded protein clusters (50-60 nm) which are responsible for fouling at its early stages³². Proteinaceous material is then able to penetrate into those holes and to fill them in as observed on Figure 2.12. Interlocking on the textured samples is thus much more pronounced than on native stainless steel, and allied to the good protein adhesion induced by high surface hydrophilicity, provides a very good anchoring to dairy deposit, promoting its build-up.

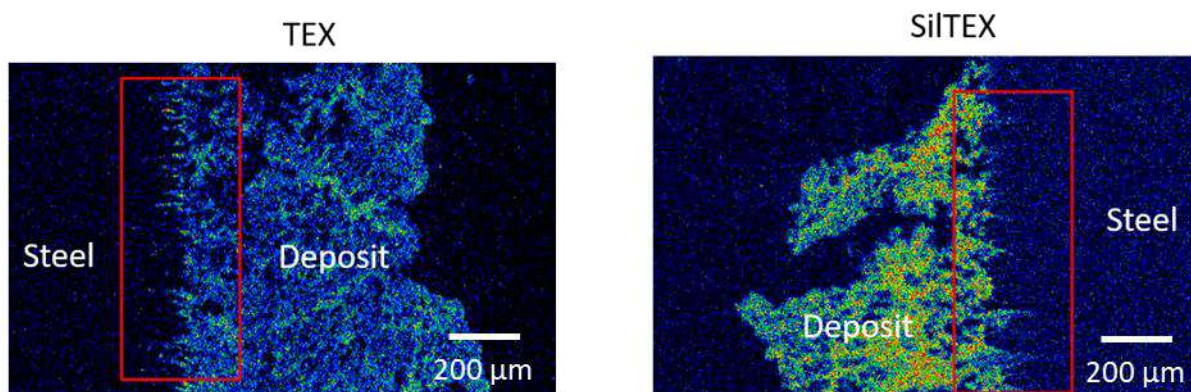


Figure 2.13. Interlocking on TEX and SilTEX samples. © 2018 Elsevier.

4.2. Impact of chemical modifications

The hydrophobicity increase induced by fluorosilanization seems to be an efficient strategy for fouling reduction as all samples treated with PFTES show fouling reduction compared to their untreated counterparts. Such results are consistent with the existing literature^{108,127}. Thus, the good performance of ML samples ($\text{SFE} = 42.5 \pm 3.8 \text{ mN/m}$) is amplified by hydrophobic treatment which yields a fouling reduction of 83 wt.-% for SilML surfaces. The compared performances of smooth ML and rougher, hydrophobic SilNAT samples illustrates well the competition between SFE and roughness for fouling governance. In this case, rougher SilNAT shows greater fouling reduction than smoother but more hydrophilic ML (-72 wt.-% versus -44 wt.-% respectively) evidencing that a favorable surface energy can overcome an unfavorable roughness.

Fluorosilanized native samples SilNAT (SFE of 27.6 ± 3.2 mN/m) also show improved antifouling properties compared to NAT samples (40.5 ± 1.7 mN/m) with a fouling reduction of 72 ± 7 wt.-%, although their arithmetic mean roughness were similar. This case proves the key role of surface energy in fouling regulation.

It is also of high interest to compare untreated (TEX) and treated (SilTEX) laser texturized stainless steels. Fluorosilanization on those samples was performed following a biomimetic approach that yielded hyper-hydrophobic surfaces with high WCA ($132.9 \pm 1.6^\circ$) and low CAH ($2.3 \pm 0.8^\circ$), which, according to the literature^{112,219} points toward self-cleaning properties in air. Nevertheless, the poor performance of SilTEX surfaces and post-fouling analysis showed that the potential self-cleaning properties did not persist through the pilot-scale pasteurization process. Figure 2.12 indeed shows protein material inside the relief of SilTEX samples. It is then clear that SilTEX underwent a wetting regime transition during its stay in the pilot pasteurization equipment. Wetting state transitions are well reported phenomena, where fluid/substrate interface conditions are modified due to environmental factors¹¹⁴. More precisely, environmental changes like variations of pressure, temperature, fluid composition or vibrations can bring the fluid to displace the air entrapped in surface relief. This air is essential for the persistence of suspended Cassie-Baxter's state and is responsible for self-cleaning properties. Its loss leads to the impaled Cassie-Baxter state. This impaled state is characterized by high WCA in association with high CAH, which means that the fluid adheres very much to the surface. In the case of SilTEX samples, the turbulent tangential flow of the MF, allied to temperature increase and to the presence of potentially surface active proteins²²⁰ are most likely to have caused a wetting mode transition during the fouling test, causing the loss of self-cleaning properties. The dual-scale roughness then becomes a disadvantage regarding fouling, explaining the poor performance of SilTEX ($+86 \pm 26$ wt.-%). Nevertheless, the enhanced performance of SilTEX compared to TEX ($+391 \pm 14$ wt.-%) attests that even in this case, hydrophobicity is an advantage against fouling.

5. Bacterial adhesion results.

First of all, the three studied strains, namely *S. aureus*, *L. monocytogenes* and *Salmonella enterica* showed very different adhesion levels on stainless steel. *L. monocytogenes* presents the highest adhesion rate (76.4 ± 8.6 CFU/microscope field) on native stainless steel compared to *S. aureus* (39.3 ± 5.6 CFU/microscope field) and *Salmonella enterica* (15.7 ± 4.4 CFU/microscope field). This preponderance has previously been reported^{221,222} and might be due to the polysaccharide capsule of *L. monocytogenes*. The production of fibrous adhesion-promoting material by this bacterium, even after short adhesion periods (20 min to 1 h) has indeed been reported^{223,224} and can explain the higher cell count of *L. monocytogenes*.

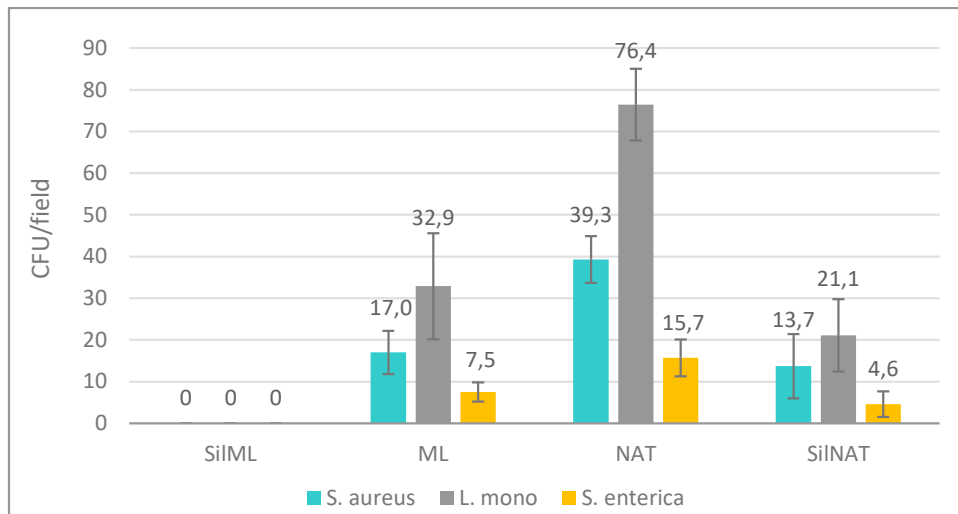


Figure 2.14. Cell counts on SiIML, ML, NAT and SiINAT surfaces after 1 h adhesion in static conditions.

Moreover, the results of the tests on the different substrates highlighted the impact of surface properties on bacterial adhesion²²⁵. Even if their cell counts do not significantly differ from one another, ML and SiINAT substrates still present lower bacterial adhesion than native stainless steel. In the case of ML, the improvement compared to the NAT reference undoubtedly comes from the roughness reduction. Medilanski *et al.* (2002)²²⁶ indeed showed that reduced roughness induces lower micro-organism adhesion. As for SiINAT, the difference in cell count most likely comes from the SFE decrease, as hydrophobic materials have also been shown to prevent bacterial adhesion^{149,227}. Nevertheless, it seems that surface energy and hydrophobicity cannot be considered as

good adhesion predictors. Sinde and Caraballo (2000) indeed witnessed higher adhesion levels of *Salmonella* and *Listeria* strains on hydrophobic rubber and on PTFE. Their work, however, did not consider surface roughness. In the present case, it is noteworthy that SilML, which ally low roughness and low SFE, present the best performance as no cell was retrieved, regardless of the strain.

Conclusions

The main objective of this first Chapter was to assess the impact of surface properties modifications of stainless steel on industrial-like model dairy foulant under isothermal conditions, through the study of model surfaces.

The detailed characterization of those surfaces before and after fouling, allowed to link the surface properties of the steel substrates to their fouling performance. The significant differences in terms of fouling performances observed between the studied samples demonstrates the preponderance of surface properties in fouling governance and highlights the complex interactions of surface energy and morphology in this context.

Several qualitative observations can thus be made: (i) reduction of surface energy decreases whey protein fouling, (ii) reduction of roughness decreases whey protein fouling, (iii) morphology and SFE are interacting and competing to control the fouling behavior of individual surfaces and (iv) surface morphology features – particularly the relative sizes of fouling agents and surface relief – are crucial for fouling control. Mirror-like fluorosilanized samples ($R_a = 4.1$ nm and SFE 18.8 = mN/m) exhibited the best performance, with a reduction of 83wt.-% of final fouling weight compared to the reference, while biomimetic textured surface and native stainless steel exhibited poor fouling behaviors because their morphologies (20 to 30 μm wide craters and ~ 200 nm wide grain boundaries respectively) allowed the penetration of unfolded proteins, favoring interlocking and strong fouling build-up.

It was also demonstrated that (i) “lotus effect” textured surfaces seems not to be suitable for fouling reduction in thermal processes, because of the instability of their particular wetting regime and that (ii) aside from surface free energy considerations, particular care should be given to surface roughness and morphology tailoring. The relative performances of NAT and ML surfaces indeed points out that antifouling performances could be significantly improved by a simple polishing step. Bacterial adhesion tests lead to similar conclusions, i.e. low roughness and low surface energy are favorable to low cell retention.

However, dairy fouling could also be addressed by following other innovating surface engineering routes. Over the past few years, increasing attention was indeed given to biomimetism, *i.e.* the mimicry of natural surfaces, materials and processes in order to solve modern problems. Biomimetic surfaces are at most represented by the overly famous lotus leaf, which was mimicked by SilTEX surfaces in Chapter 2. However, numerous other opportunities exist for biomimetic surface engineering targeting dairy fouling management, and some of them will be explored in Chapter 3.

Chapter 3 - BIOMIMETIC ANTIFOULING SURFACES

Introduction

Literature investigations in Chapter 1 led to the conclusion that the modification of stainless steel could be a suitable route toward dairy fouling mitigation, and this was confirmed in Chapter 2. Consequently, Chapter 3 will explore the design and assessment of innovative surface modification methods targeting fouling control. The most classical approach for dairy fouling management consists in minimizing surface energy (especially polar components) and surface. However, numerous other pathways could be followed to achieve fouling mitigation.

In particular, the remarkable surface properties of several living organisms recently drew the attention of the scientific community toward biomimetic approaches for the design of new functional surfaces, intended to solve issues such as fouling. The most well-known example of biomimetic surface engineering is the superhydrophobic lotus-like surface which presents self-cleaning abilities in certain conditions, due to its particular wetting regime¹¹². Numerous papers indeed report different methods to design synthetic superhydrophobic surfaces through cutting edge technologies, such as lithography²²⁸, vacuum plasma treatments²²⁹, layer-by-layer deposition²³⁰, sol-gel processes^{231,232} or electro-spinning/-spraying²³³. Aside from the overly famous lotus-like surface, the tunable wettability of gecko toes²³⁴ as well as the segregated hydrophilicity/hydrophobicity of *Salvinia* leaves²³⁵ are also worth mentioning, as they have also been studied and mimicked to design functional surfaces. Overall, biomimicry offers multiple possibilities that could be integrated in research strategies aiming at fouling management. Thus, Chapter 3 will present three different biomimetic surfaces designed for fouling mitigation – namely slippery liquid-infused surfaces²³⁶, nano-rough plasma coatings²³⁷ and amphiphile environment-responsive coatings^{1*} – by combining three articles, either published or currently under revision.

^{1*} “Antifouling Amphiphilic Silicone Coatings for Dairy Fouling Mitigation of Stainless Steel” [in revision: Biofouling]

1. Slippery liquid-infused surfaces

As mentioned earlier, bio-inspired surface engineering targeting self-cleaning or anti-adhesive properties, such as Lotus-like surfaces, have been given a great deal of attention recently^{112, 219,238,239} and applications in biofouling management have been investigated^{215,240}. Nevertheless, the key to the self-cleaning properties of these biomimetic surfaces lies with their particular dual-scale roughness which induces a particular wetting state. Unfortunately, as seen in Chapter 2, the drastic conditions of dairy processing (turbulent flows, high temperatures, vibrations) are very likely to cause irreversible wetting state transitions^{114,241,242}, and the loss of self-cleaning properties. However, even if textured lotus-like surface exhibited poor fouling performances as such, they could be used as basis for the design of SLIPS-like surfaces thanks to their particular morphology.

SLIPS (Slippery Liquid Infused Porous Surfaces)^{243,244} are complex biomimetic surfaces inspired by *Nepenthes* pitcher^{243,244}, which are carnivorous plants using different strategies to attract and capture insects. Notably, the peristome of the plant (Figure 3.1A) presents an anisotropic nanostructured morphology which is fully wettable by the nectar secreted by the plant²⁴⁵. As a consequence, the peristome surface is covered with a slippery liquid film, causing insects to fall and slip into the digestive part of the plant. Mimicking this type of surfaces has been identified as a possible way to solve fouling issues, as they theoretically present a robust, perfectly smooth and inert liquid interface, leading to non-adhesive and potentially self-healing properties²⁴⁶. A significant amount of literature has thus been produced on this topic, providing numerous proofs of concepts for synthetic SLIPS²⁴⁶, as well as possible antifouling applications against micro-organisms in the marine sector^{247,248} or against bacteria and blood in the biomedical field^{244,249–252}. These studies reported a wide variety of interesting engineered surfaces which were tested for bio-adhesion *in vitro* or *in vivo*²⁵², although they mostly focused on static or mild flow lab-scale testing.

This section reports the design and fouling testing of SLIPS-like surfaces based on laser textured stainless steel, which were realized in collaboration with the University of British Columbia (Canada) and the *Institut d'Electronique, de Microélectronique et de Nanotechnologie* (IEMN UMR

8520, France), and published in 2017 in *ACS Applied Materials and Interfaces* (Zouaghi et al., 2017²⁵³).

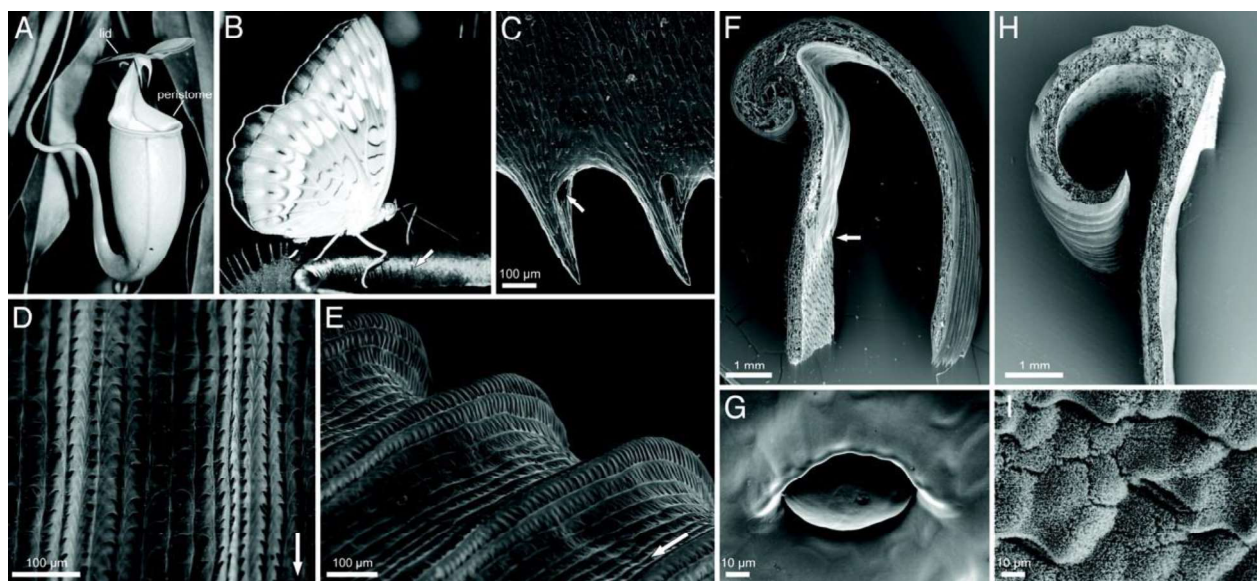


Figure 3.1. *Nepenthes* pitcher and peristome morphology. (A–G) *Nepenthes bicalcarata*. (A) Pitcher. (B) Butterfly (probably *Tanaecia pelea pelea*) harvesting nectar from the peristome surface. (C) Underside of inner margin of peristome with tooth-like projections and nectar pores (arrow). (D and E) Peristome surface with first- and second-order radial ridges. Arrows indicate direction toward the inside of the pitcher (F) Transverse section of peristome. Note the transition from the digestive zone to the smooth surface under the peristome (arrow). (G) Inner pitcher wall with digestive gland at the height of the inner peristome margin (H and I) *N. alata*. (H) Transverse section of peristome. (I) Waxy inner pitcher wall at the height of the inner peristome margin. (From Bohn and Federle (2004)²⁴⁵, ©2004 National Academy of Sciences.)

1.1. SLIPS-like surface design

Native stainless steel coupons (NAT) were used as reference during each fouling test. They were cleaned before use, following the protocol exposed in Chapter 2 (p. 61).

These substrates were then textured using femtosecond laser ablation as detailed in Chapter 2, (p. 61), in order to generate anisotropic cauliflower-like hierarchical micro- and nano-structures at their surface.

The textured surfaces were then treated by a UV/ozone plasma cleaner (UV-O Cleaner, Jetlight Company Inc., 4 mW.cm⁻² at 220 nm) for 20 min to remove any organic contaminant from the surface and to generate hydroxyl groups on it. They were then chemically modified by immersion

in a 10^{-3} M solution of trichloro(1H,1H,2H,2H-perfluorodecyl)silane (Sigma Aldrich) in n-hexane for 4 hours at room temperature in a nitrogen purged glovebox. The resulting samples (SF-TEX) were rinsed once under hexane flow, twice in dichloromethane under stirring and once under ethanol flow. Finally, they were dried under nitrogen flow.

The aim of the texturing and chemical modification steps was to design nanostructured surfaces with enhanced interfacial area and high affinity for impregnation with a hydrophobic lubricant. In the present case, Krytox GPL 103 perfluorinated oil (DuPont, Belgium) was chosen as lubricant because of its chemical inertness, its good durability and its very low surface tension (around 20 mN/m). These features indeed make this oil very likely to (i) resist alkali cleaning procedures and to (ii) present interesting antiadhesive properties. The lubricant was poured dropwise on tilted SF-TEX surfaces until they were covered with it. Samples were left for 15 to 25 min in a tilted position to let the excess oil drip off. The final lubricated surfaces are referred to as “SLIPS-like” in the manuscript, as they are not exactly porous, but textured, like the peristome of *Nepenthes* plants.

1.2. Surface characterizations

Prior to fouling trials, all surfaces were fully characterized. Figure 3.2 illustrates the very different wettability of NAT, TEX, SF-TEX and SLIPS-like surfaces while Table 3.1 gathers the water contact angle (WCA), surface free energy (γ) and arithmetic mean roughness (Ra) and dynamic goniometry features of the different surfaces.

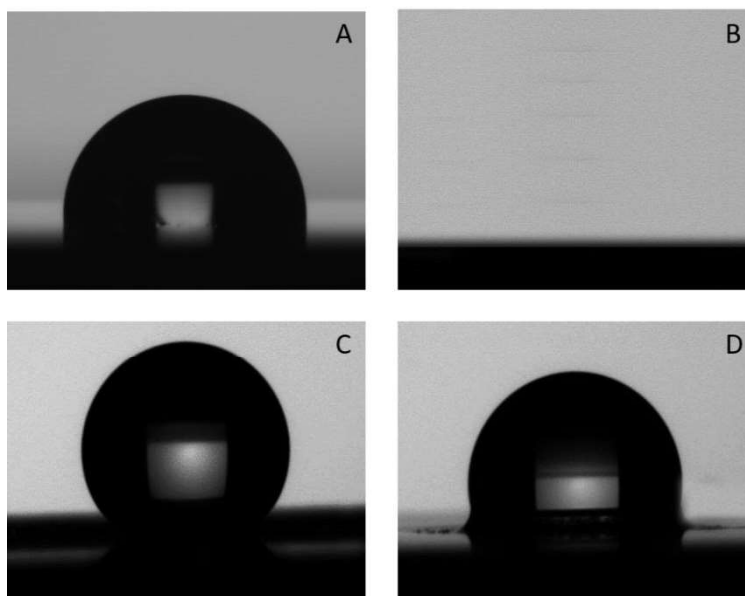


Figure 3.2. Water droplets on native stainless steel, NAT (A), laser-textures stainless steel, TEX (B), fluorosilanized textured stainless steel, SF-TEX (C) and SLIPS-like surface (D). © 2017 ACS.

Native stainless steel presented a water contact angle of $84.2 \pm 2.6^\circ$, and the determination of surface energy with the Van Oss approach revealed a global polar contribution of 2.4 ± 1.7 mN/m, in which the electron donor contribution (γ^-) was quite high (3.5 ± 2.5 mN/m). Significant fouling on native samples can thus be expected, as it has been shown that high electron donor component of the SFE generally induces an increase of protein deposition¹²⁷. Dynamic goniometry measurements performed with 5 μ L droplets revealed that, even at a 90° tilt (which is the maximal tilt that can be obtained with our device), the water droplet neither slides nor rolls from its original position, although it looked quite deformed, as indicated by the CAH of $6.9 \pm 1.9^\circ$. This strong water adhesion to the substrate can result from chemical interactions with the substrate but can also be linked to surface roughness. Indeed, the presence of indents and furrows on a surface can increase a liquid's adhesion through capillarity phenomena. An extreme illustration of this concept is the so-called "Rose Petal effect", where surface morphology induces so high an adherence that the droplet stays in place even on an upside down substrate²⁵⁴. Concerning native stainless steel, profilometer analysis revealed an arithmetic mean roughness of 68 ± 12 nm and SEM images (Chapter 2, Figure 2.6) revealed an uneven relief, with numerous grain boundaries. Those micrometer-scale surface defects allow water to penetrate and can increase water adhesion.

Table 3.1. Surface characteristics of native and modified stainless steel.

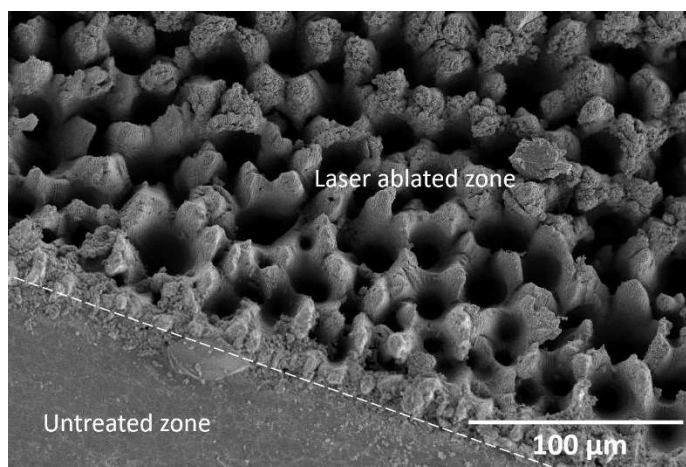
	WCA (°)	γ^{Totale} (mN/m)	γ^{LW} (mN/m)	γ^{AB} (mN/m)	γ^+ (mN/m)	γ^- (mN/m)	Ra (nm)	CAH (°)	Roll/Slide Off angle (°)
NAT	84.2 ± 2.6	40.5 ± 1.7	38.1 ± 0.3	2.4 ± 1.7	0.4 ± 0.3	3.5 ± 2.5	68 ± 12	6.9 ± 1.9	-
TEX	0			ND*			1243 ± 18	-	-
SF-TEX	132.9 ± 1.6			ND*			1364 ± 15	2.6 ± 0.8	5°
SLIPS-like	111.6 ± 1.3	17.4 ± 3.2	18.9 ± 2.2	0.3 ± 0.1	5.10 ^{-3**}	3.7 ± 1.0	ND***	0.6 ± 0.2	2°

*Surface energies are calculated from contact angle measurements with different probe liquids. In the case of TEX and SilTEX samples, the observed contact angle much more results from surface morphology than from surface energy. SFE calculations realized with those apparent contact angles will thus be misleading.

** Standard deviation value too small to be considered.

***Profilometer does not allow measuring roughness on a liquid surface. Nevertheless, a null value is very probable.

The laser texturing of TEX samples was first checked through visual observation. The laser irradiated part of the stainless steel was black-colored, which was meaningful because micro-/nanoscale organized structures have been reported to act as light traps^{255,256}. SEM micrographs of TEX samples (Figure 3.3) further confirmed the success of laser texturing and the dual-scale roughness of the “cauliflower-like” structure. An extreme WCA decrease was observed after texturing (0° for TEX versus 84.2 ± 2.6° for NAT). As stated in Chapter 2, this superhydrophilicity is undoubtedly linked to the high surface oxidation caused by laser irradiation²¹¹, combined to the complex morphology. Figure 3.2B illustrates this phenomenon, the deposited droplet wets so well the TEX surface that it is not visible on the picture anymore.

**Figure 3.3.** SEM micrograph of laser ablated stainless steel (TEX).

SF-TEX sample were then characterized. Fluorosilanzation was performed in order to increase the hydrophobicity of TEX samples and in this way to optimize their wetting by the hydrophobic lubricant. Indeed, chemical modification of textured surfaces by a low surface tension molecule (such as fluorosilanes) is generally recognized to be mandatory for SLIPS design^{244, 249,252}. As previously, WCA measurements prove that fluorosilanzation reached its purpose, as SF-TEX samples present a tremendous water contact angle increase compared to TEX samples ($132.9 \pm 1.6^\circ$ versus 0°). Dynamic goniometry analysis (tilting method) was carried out on SF-TEX samples, revealing a low contact angle hysteresis of $2.6 \pm 0.8^\circ$ (Table 3.1). Together with the high WCA, this low CAH indicates that SF-TEX textured samples are in the suspended Cassie-Baxter's wetting regime^{112, 114,241}, similarly to SilTEX surfaces in Chapter 2.

Analysis of SLIPS-like surfaces showed the great impact of oil impregnation on surface properties. Firstly, a noticeable WCA change was observed, from $132.9 \pm 1.6^\circ$ for SF-TEX down to $111.6 \pm 1.3^\circ$ for SLIP-like surfaces. This change can be explained by the radical interface modifications induced by oil infusion. Indeed, instead of the air-solid composite surface presented by SF-TEX, SLIPS-like surface presents a very smooth liquid interface. Figure 3.2D indeed shows an oil lip pulling up against the edges of the water drop. This pull-up phenomenon has been described in the literature as characteristic of the presence of a thin liquid interfacial film, and of cloaking phenomena, *i.e.* encapsulation of the water droplet in a thin oil film. Smith *et al.* (2013)²⁵⁷ highlighted this phenomenon by dyeing the lubricant with a fluorescent compound, as shown in Figure 3.4.

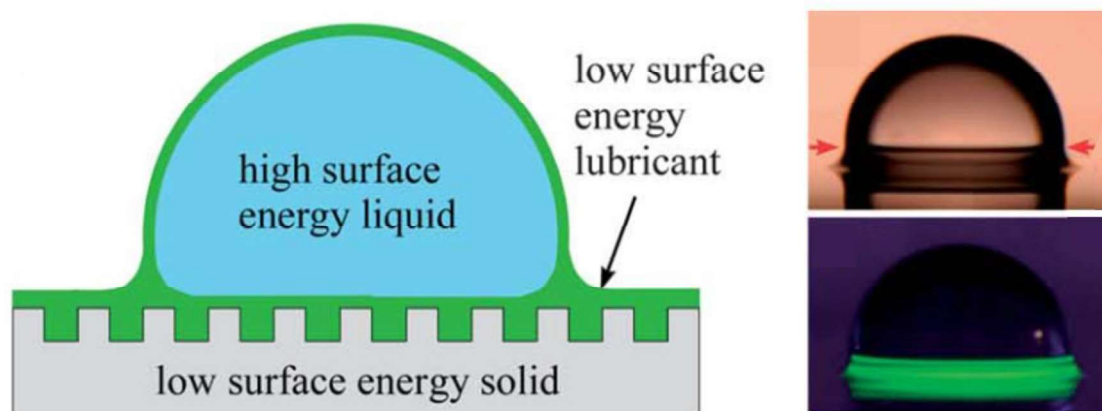


Figure 3.4. The cloaking phenomenon, adapted from Smith *et al.* (2013)²⁵⁷, © The Royal Society of Chemistry, 2013.

Dynamic goniometry showed evidence of an extremely low CAH value ($0.6 \pm 0.2^\circ$), validating the very slippery character of these surfaces. It also brought some information about the infusion state of the surface. Indeed, liquid infused surfaces can be found in different configurations, mainly depending on the mutual affinity of the solid substrate and oil. Smith *et al.* (2013)²⁵⁷ thus described several possible states. On the one hand, the encapsulated state corresponds to the complete coverage of the solid substrate by an oil film. On the other hand, in the impregnated-emerged state, the oil fills in the cavities, but tips of solid are still apparent (Figure 3.5). A very low CAH is more likely to be observed when the surface is encapsulated. Given their goniometry results, it can then be considered that the SLIPS-like surfaces are in the encapsulated state. The SFE value of SLIPS-like surfaces (17.4 ± 3.2 mN/m) also points toward total oil coverage, as it is close to the lubricant's surface tension (around 20 mN/m according to the manufacturer).

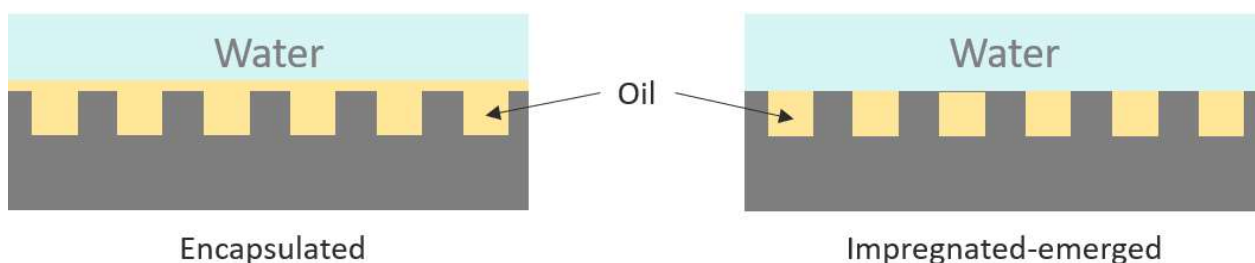


Figure 3.5. Possible Oil-Solid-Water configurations for liquid-infused surfaces. © 2017 ACS.

SLIPS-like surfaces were then tested to fouling in isothermal conditions, without or with further rinsing (SLIPS-r). The results of those tests are presented and discussed in the following section.

1.3. Fouling performances

Figure 3.6 gathers fouling results for reference and SLIPS-like samples tested in the pilot pasteurizer. SLIPS-like surfaces presented good antifouling performances, with a deposit weight reduction of 63 ± 4 wt.-% compared to NAT, even though the electron donor components of NAT and SLIPS-like samples were quite similar (3.5 ± 2.5 mN/m and 3.7 ± 1.0 mN/m, respectively). Given the established importance of this component in fouling regulation¹⁰, the better performance of SLIPS-like surface points out the importance of the interfacial physico-chemistry.

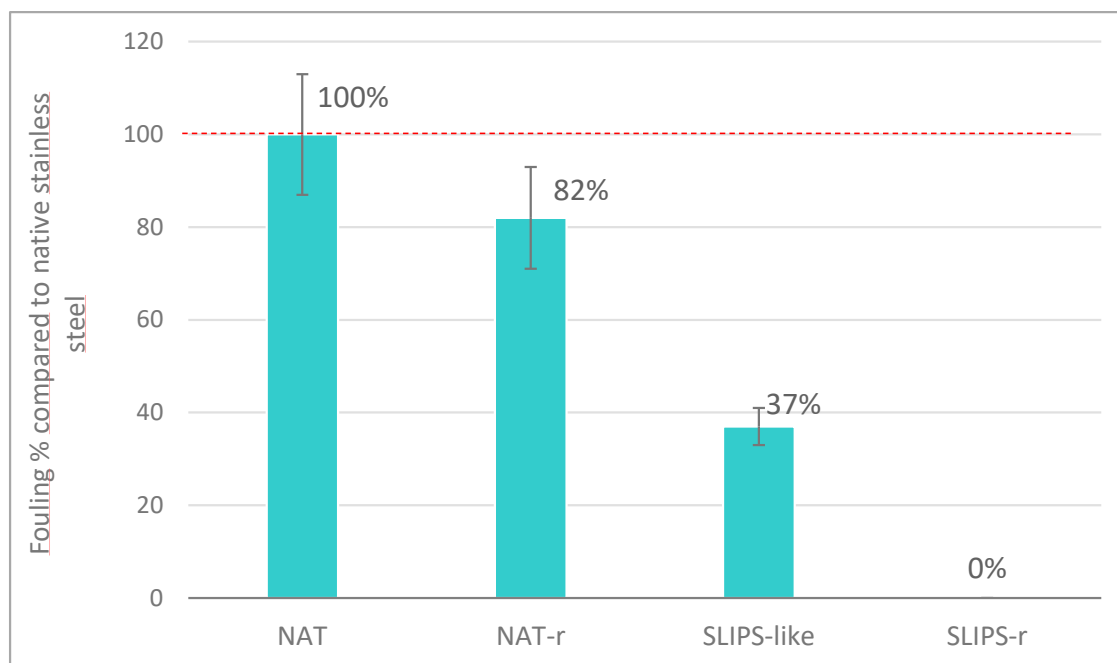


Figure 3.6. Fouling performances (wt.-%) of the different surfaces compared to native stainless steel.

Visual observation of dairy deposits on NAT and SLIPS-like surfaces before rinsing (Figure 3.7) indeed revealed very their different appearances. While the dairy deposit on native SS is dense and rather flat, the deposit on SLIPS-like surfaces presents numerous bubble-like structures, most likely resulting from a lack of adhesion of the deposit to the substrate. Furthermore, the rinsed SLIPS-like surfaces revealed their outstanding fouling-release properties, as no trace of dairy deposit was found on them. This result points out the true potential of liquid-infused surfaces as antifouling in food and beverage industries. Indeed, a simple 20 minutes hot water rinse was enough to eliminate all deposit traces from the lubricated surfaces. In comparison, the rinsing step only allowed removing 18 wt. % of the deposit on NAT samples. Consequently, a full CIP procedure (alkali cleaning, intermediate rinse, acid cleaning and a final rinse) would still be necessary to clean native stainless steel¹⁰. Liquid-infused surfaces could thus lead to significant savings in term of production time, cleaning costs and environmental footprint.

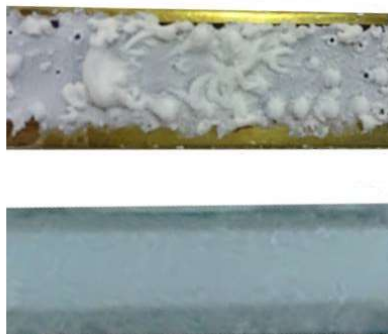


Figure 3.7. Dairy deposits on SLIPS-like sample (top) and native stainless steel (bottom) after 1.5h of fouling in isothermal conditions. © 2017 ACS.

In the light of those promising results and in order to assess their durability, the same surfaces were submitted to a second test and rinsing cycle, with (SLIPS-2-or) and without (SLIPS-2r) oil re-impregnation in between. Figure 3.8 gathers the results of this study.

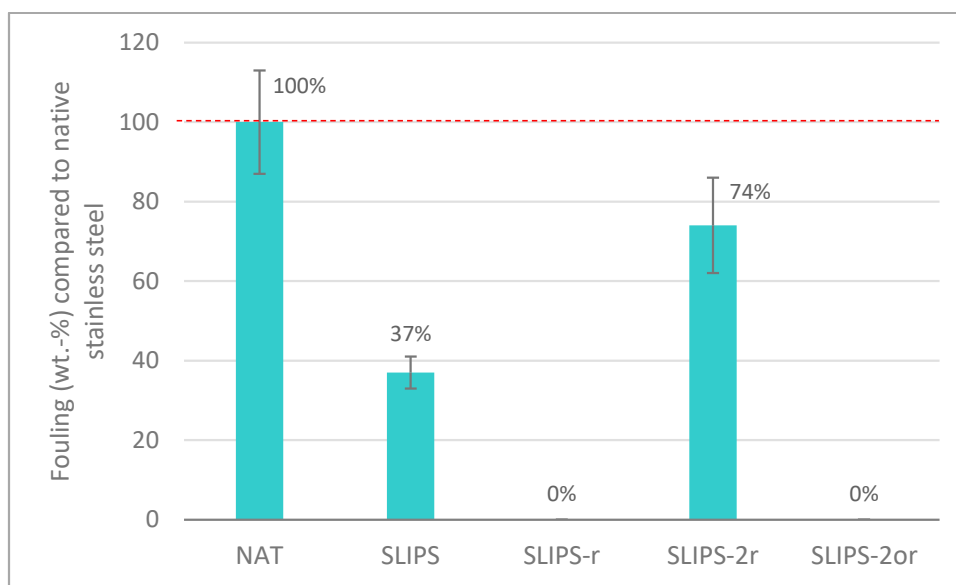


Figure 3.8. Assessment of SLIPS-like samples sustainability. © 2017 ACS.

Re-impregnated SLIPS-like samples (SLIPS-2or) showed the same performance than during their first use: no trace of fouling was found after the rinsing step. On the contrary, SLIPS-2r exhibited a fouling reduction of only 26 ± 12 % compared to the native reference, which is less than the original performance of non-rinsed SLIPS-like surfaces.

To explain this, it is necessary to consider closely the surface/MF (Model Fluid) interface. Indeed, as said earlier, liquid infused surfaces can be in different impregnation states²⁵⁷, which can change

and evolve along the life of the substrate. In the present case of study, and given the dynamic goniometry data (extremely low CAH and slide-off angle, Table 3.1), unused SLIPS-like surfaces are in the encapsulated configuration: they present to the FMF a flat oil interface, inducing scarce and weak deposit adhesion. However, under industrial pasteurization conditions, the high tangential FMF and rinsing water flows are very likely to have caused oil shedding. As a result, the surface configuration evolves from encapsulated to impregnated-emerged (Figure 3.5). Without oil addition to compensate this shedding phenomenon, the surface, during its second use, will present to FMF a composite interface, made partly of oil and partly of emerged cauliflower-like stainless steel. Deposits are then more able to adhere and build-up on the surface than when confronted only to a smooth oily interface. Goniometry confirmed this assumption, and Figure 3.9 clearly shows the difference between the unused SLIPS-like surface showing oil pull-up, and the used one, looking similar to SF-TEX surface (Figure 3.2C). Oil shedding was most likely possible because of the open morphology of SF-TEX surfaces. Consequently, this morphology should be optimized in order to favor oil retention on the substrate. For example, Lee *et al.* (2015)²⁵⁸ proved that oil retention on electrochemically etched porous SS could be enhanced by tuning the etching parameters.

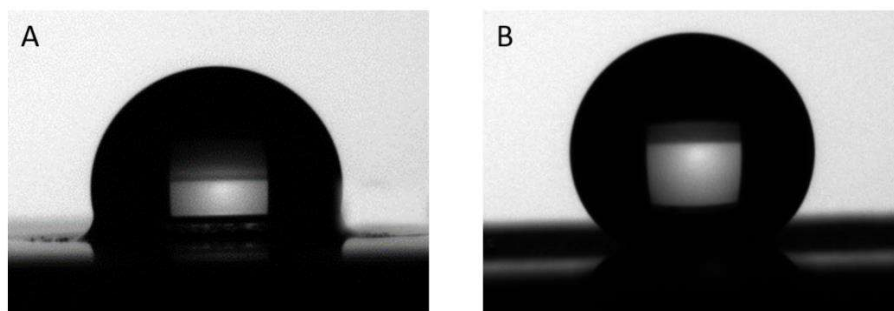


Figure 3.9. Comparative goniometry images of SLIPS-like surfaces, before (A) and after (B) one fouling and rinsing cycle. © 2017 ACS.

However, in the present case, the matter of oil migration into the processed dairy product must be taken into consideration. Indeed, high dosages of fluorine-containing components, like fluorinated aliphatic ethers and esters or fluoride were shown to interact with cellular functions and may put the consumers health at risk^{259,260}. However, even though no study has been carried on possible human toxicity of Krytox 103 GPL, this oil has already been considered for biological

contacting surfaces design^{244,252}. Moreover, Epstein *et al.* (2012)²⁴³ demonstrated that this oil did neither affect bacterial growth nor show any cytotoxicity toward *P. aeruginosa*.

To summarize, SLIPS-like surfaces, designed directly on stainless steel, were proven to possess very interesting fouling-release abilities, due to the presence of low surface energy oil at the substrate/foulant fluid interface. A 20 min rinsing step with only water was sufficient to eliminate all traces of fouling from the SLIPS-like surface, which could represent substantial advantages regarding the economic and environmental cost of cleaning in dairy thermal processing. Although re-use trials revealed the limited lifetime of these SLIPS-like surfaces without oil re-impregnation, those results are encouraging. Further research should focus on optimization of surface morphology to achieve better oil retention and counter lubricant shedding. Furthermore, the adequacy between the lubricant and the target application of impregnated surfaces should be treated with caution. The search for natural or formulated food-compatible lubricants should also be considered for further research.

2. Nanotextured plasma coatings

While the previous section highlighted the advantage of a bio-inspired smooth liquid hydrophobic interface, the present section aims at investigating the behavior of nanostructured hydrophobic biomimetic surfaces. Indeed, Chapter 2 showed that dual-scale lotus-like surfaces exhibited poor fouling results because of their micrometric roughness which induced interlocking between the deposit and the substrate. However, the question of the efficacy of nanometric roughness against fouling remains relevant at this point. Scardino *et al.* (2009)²⁶¹ indeed showed that biomimetic surfaces presenting nanoscale roughness alone deterred the settlement of a broader spectrum of micro-organisms than dual-scale surfaces.

Thus, it seems interesting to generate nanometric structures on stainless steel and to test them against industrial-like dairy fouling. A review by Yan *et al.* (2011)¹¹² stated that plasma processes were frequently used for surface nano-patterning and reported different high-cost techniques, like reactive ion etching^{262,263} or plasma enhanced chemical vapor deposition (PECVD)^{264,265}. Superhydrophobic textured coatings obtained through atmospheric plasma polymerization of silane-containing vapor was also reported as a possible in-line technique²⁶⁶. The use of atmospheric plasma indeed allows for continuous treatment, which cannot be considered with vacuum plasma techniques.

Thus, this section is dedicated to the use of atmospheric pressure plasma spraying (APPS) to design biomimetic nano-rough coatings. Indeed, APPS stands as a very versatile and easily up-scalable process. It has been used to functionalize a vast range of substrates (glass, metal, polymers) for different applications, like enhancement of tribological properties^{267–269}, thermal²⁷⁰ or corrosion protection^{271,272} or adhesion promotion²⁷³ to cite a few. In the following section, siloxane-based APPS coatings on stainless steel, the impact of manufacturing parameters on their surface properties and their behavior towards dairy fouling and bacterial adhesion will be studied. These results were published in *Applied Surface Science* in 2018²³⁷ (Annex IV).

2.1. Atmospheric Pressure Plasma Sprayed Coatings

Plasma coatings were manufactured using a UL-Scan atmospheric pressure plasma spraying device (AcXys Technologies, France) associated with a nebulizing system which allows to spray liquid HMDSO (hexamethyldisiloxane purchased from Fluka) directly into the afterglow of the plasma. The latter results from an electric discharge in pure nitrogen. The plasma nozzle and the precursor nebulizer (Mira-Mist, AnalysenTechnik, Germany) were mounted on a 3-axis automaton (TableTop TT, IAI, Germany) allowing to scan them over the substrate. This set-up (Figure 3.10) allows for several manufacturing parameters to vary and different deposition conditions were thus tested. The varied parameters were: the precursor flow rate Q (g/h), the nozzle-to-substrate distance D (mm) and the scanning speed v (mm/s). All experiments were carried out at room temperature (20°C). Nitrogen was used both as plasmagenic gas and precursor carrier gas, and those flow rates were kept constant in all experiments, at 60 standard liter per minute (slm) and 1.9 slm, respectively.

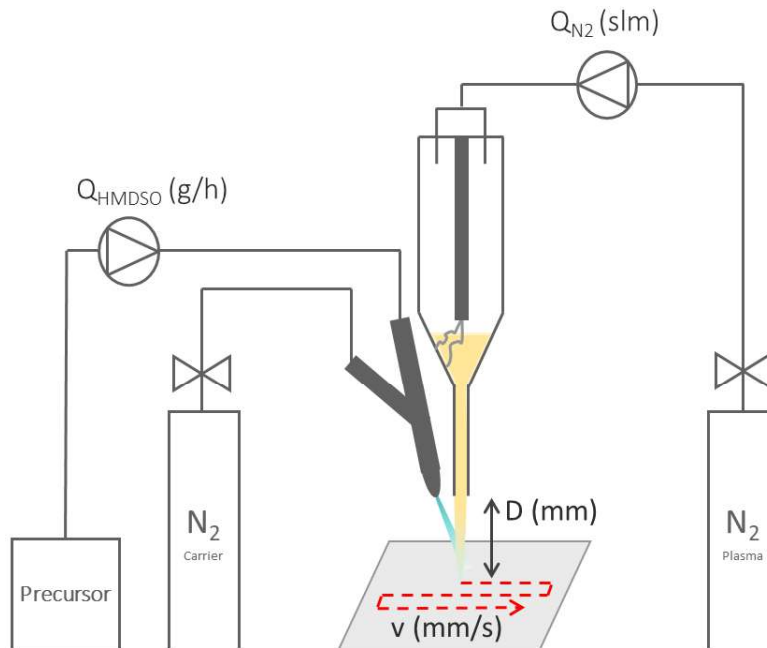


Figure 3.10. Schematic diagram of the UL-Scan device. © 2018 Elsevier.

Substrates were native stainless steel coupons. Prior to modification, they were cleaned according to the protocol detailed in Chapter 2 (p. 61). To enhance the adhesion of the coatings to the substrates, an activation pretreatment, *i.e.* four passes of the plasma jet without precursor spraying (N_2 flow rate= 60 slm, $D= 20$ mm, $v= 100$ mm/s), was applied to all SS surfaces prior coating. The efficiency of such pre-treatments has previously been demonstrated by Regula *et al.* (2009)²⁷¹ and Szabova *et al.* (2009)²⁷⁴.

The temperature of samples after exposure to plasma (T) was measured with K-type thermocouple. After activation, T reached 246°C. The samples were then left 15 min to cool down to room temperature (20°C) before coating. The activated surfaces, *i.e.* exposed to plasma with no precursor spraying, were then coated.

Table 3.2 summarizes all the tested conditions for coating deposition. PL 1 can be considered as the “central” sample, with $Q = 35$ g/h; $D = 20$ mm and $v = 100$ mm/s. For PL 2 to 4, HMDSO flow rate was modified. PL 5 and 6 present nozzle-to-substrate distance variations and finally, PL 7 and 8 present scanning speed variations.

Table 3.2. Deposition conditions for APPS coatings.

Sample ID	Precursor flow rate Q (g/h)	Nozzle-to-sub. distance D (mm)	Scanning speed v (mm/s)	Sample Temperature T (°C)
PL 1	35	20	100	113
PL 2	40	20	100	113
PL 3	30	20	100	133
PL 4	25	20	100	113
PL 5	35	10	100	132
PL 6	35	30	100	107
PL 7	35	20	50	124
PL 8	35	20	150	105

2.2. Influence of the manufacturing parameters on surface properties

WCA, surface energy, roughness and adhesion features of the plasma coatings are gathered in Table 3.3. Considering the nature of the coatings, the OWRK method (Owens, Wendt, Rabel and Kaeble²⁷⁵) was chosen to calculate the surface free energies of PL1 to 8.

Table 3.3. Surface properties of the HMDSO plasma coatings.

Sample ID	Water contact angle (°)	Surface free energy (mN/m)			Arithmetic mean roughness Ra (nm)	Adhesion Grade
		γ^{Total}	γ^{D}	γ^{P}		
Bare SS	84.2 ± 2.6	41.9 ± 4.3	38.2 ± 0.9	3.7 ± 2.5	68 ± 12	/
Activated SS	23.5 ± 0.9	64.7 ± 15.0	35.7 ± 6.3	29.0 ± 9.1	70 ± 9	/
PL 1	95.7 ± 3.3	37.7 ± 1.8	33.8 ± 1.1	3.92 ± 0.7	45 ± 3	5B
PL 2	79.3 ± 4.0	38.4 ± 1.9	35.7 ± 1.0	2.6 ± 0.9	51 ± 1	5B
PL 3	101.2 ± 0.6	44.0 ± 3.7	28.2 ± 1.6	15.8 ± 2.0	43 ± 4	5B
PL 4	101.5 ± 1.0	46.5 ± 3.0	32.0 ± 1.1	14.5 ± 1.8	41 ± 3	5B
PL 5	97.1 ± 0.8	43.3 ± 4.0	36.2 ± 1.1	7.1 ± 2.9	64 ± 5	5B
PL 6	94.3 ± 2.2	41.5 ± 4.7	34.3 ± 2.3	7.1 ± 2.5	49 ± 3	5B
PL 7	95.0 ± 1.3	48.5 ± 7.0	36.1 ± 1.2	12.7 ± 5.8	40 ± 13	5B
PL 8	95.4 ± 1.4	42.3 ± 4.6	32.0 ± 1.3	10.2 ± 3.3	51 ± 4	5B

2.2.1. Effect of the activation step

As expected, the plasma activation of SS significantly decreases the WCA of the substrates from $84.2 \pm 2.6^\circ$ to $23.5 \pm 0.9^\circ$ and consequently increases the SFE value from 41.9 ± 4.3 mN/m to 64.7 ± 15.0 mN/m. It is noticeable that, while the dispersive SFE components of bare and activated SS do not significantly differ from each other (38.2 ± 0.9 mN/m and 35.7 ± 6.3 mN/m, respectively), activation clearly has an effect on the polar component that shifted from 3.7 ± 2.5 mN/m to 29.0 ± 9.1 mN/m. Plasma activation is indeed known to change surface chemistry and to generate reactive groups, like hydroxyls, on the treated substrates²⁷¹. Roughness, on the other hand, was not impacted by activation, as APPS does not deliver enough energy to melt and reshape stainless steel.

2.2.2. HMDSO coatings

Cross-hatch adhesion tests (Table 3.3) revealed that all plasma coatings classify as 5B grade. Thus, activation induced very good adhesion of the coatings to the SS substrate. Similar effect of plasma activation was reported by Regula *et al.* (2009)²⁷¹, who showed better adhesion for HMDSO coatings on silver thanks to the reductive species generated by activation.

Overall, the HMDSO coatings exhibit mild to medium hydrophobicity with WCA comprised between $79.3 \pm 4.0^\circ$ and $101.5 \pm 1.0^\circ$. In all cases except PL 2 (which was obtained with the highest HMDSO flow rate), the coating step increased surface hydrophobicity.

Arithmetic mean roughness was decreased in presence of the coating, regardless of the deposition conditions. This was not surprising as the coating is expected to partly fill in some of the grain boundaries and structural defects of the SS surface.

It is interesting to notice that while total SFE values (γ^{Total}) of bare and coated SS, regardless of the coating conditions, do not present any significant difference, the polar component (γ^{P}) does evolve. PL 3, 4, 7 and 8 indeed exhibit higher γ^{P} values than bare SS. In comparison, Rosmaninho *et al.* (2007)¹²⁷ reported very rough ($R_a = 206 \pm 48$ nm) and rather hydrophilic SiO_x coatings obtained on SS with HMDSO through PECVD (plasma enhanced chemical vapor deposition, *i.e.* low pressure plasma), for which WCA value was of $15 \pm 3^\circ$, γ^{Total} was of 55.6 ± 0.1 mN/m and γ^{P} was of 52.9 ± 1.7 mN/m. Beuf *et al.* (2003)¹¹⁵ also studied PECVD SiO_x coatings from HMDSO on stainless steel. Their coatings were less rough than those of Rosmaninho *et al.* (2007)¹²⁷ and their SFE approached that of SS, as it is the case here. The differences observed between those PECVD coatings and the ones obtained here by APPS, although they originate from plasma deposition of the same chemical precursor, highlight the importance of manufacturing conditions on the final properties of a surface.

Characterizations of the coatings' surfaces and comparisons between each other allowed studying the consequences of deposition parameters modification on the surface properties (Figure 3.11). Those comparisons pointed out that, while the variation of HMDSO flow rate impacts the coating's properties, changes in nozzle-to-substrate distance and scan speed in the studied range do not: indeed, in those cases, variations of WCA, SFE and R_a do not exceed the uncertainty margins (Figure 3.11B and C).

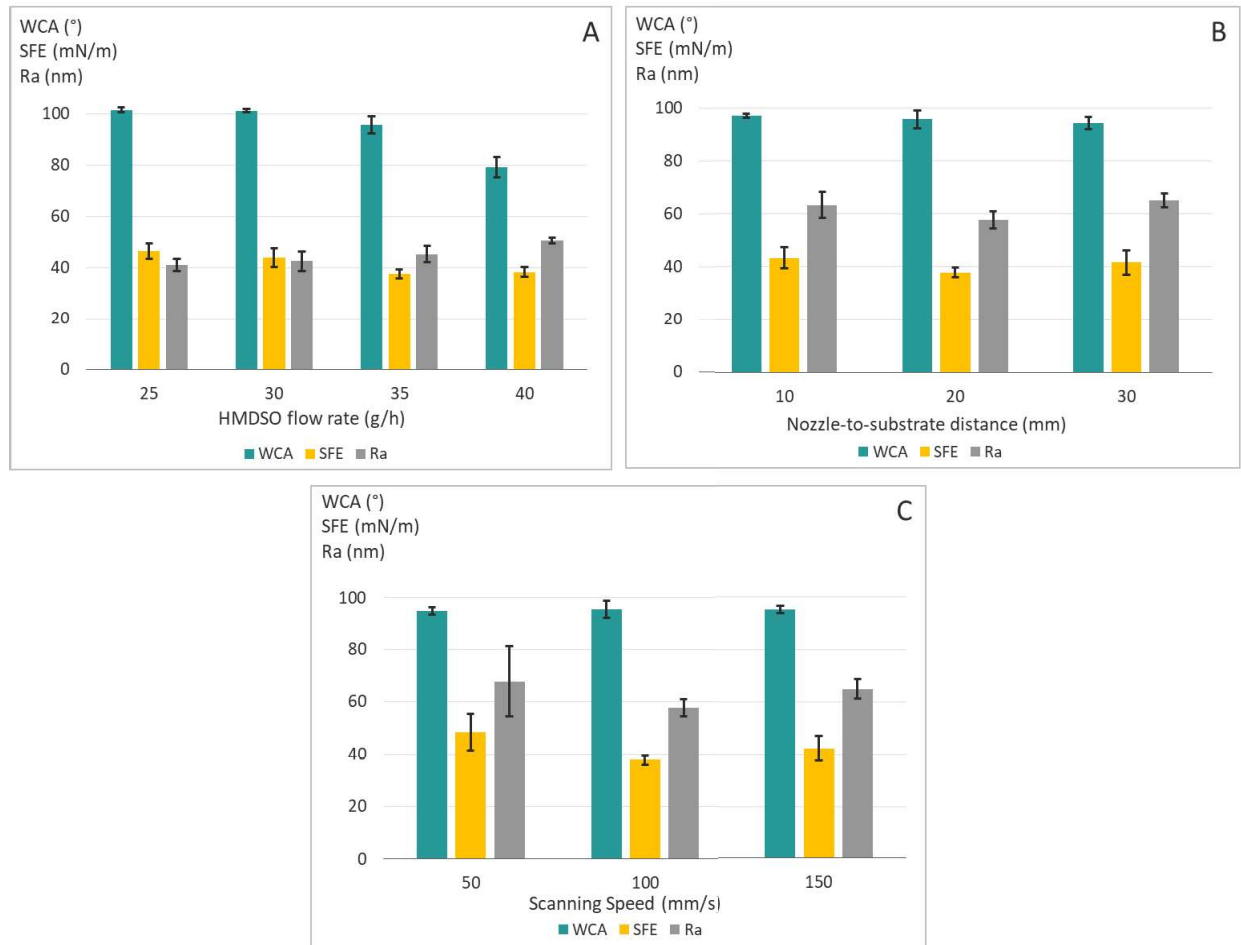


Figure 3.11. Surface characteristics of HMDSO coatings according to HMDSO flow rate (A), nozzle-to-substrate distance (B) and scanning speed (C). © 2018 Elsevier.

Nevertheless, nozzle-to-substrate distance obviously impacts the residence time (t_r) of the precursor in the plasma plume. This residence time can be assimilated to its travel time between the nozzle and the substrate, as HMDSO is nebulized right at the nozzle outlet. t_r value therefore correlates with the plasmagenic gas flow rate – as established by Lommatzch and Ihde (2009)²⁷⁶ – which was kept constant at 60 l/min (10^{-3} m³/s) for all experiments. The speed of the gas can be approximated as the ratio between its flow rate and the nozzle section ($1.3 \cdot 10^{-5}$ m²) to the value of 79.5 m/s. Consequently, for samples PL 1 to 4 and 7 to 8, where D was kept constant at 20 mm, HMDSO took $2.5 \cdot 10^{-4}$ s to reach the substrate surface, which is the t_r . For PL 5 (D = 10 mm) and PL 6 (D=30 mm), t_r was $1.5 \cdot 10^{-4}$ s and $3.9 \cdot 10^{-4}$ s, respectively. Considering that there is no significant difference between PL 1, 5 and 6 in terms of WCA, SFE or roughness (Figure 3.11A), it could then

be concluded that in the present conditions, the precursor reaches its final degradation state within $1.5 \cdot 10^{-4}$ s after penetration in the plasma plume.

On the other hand, the increase of HMDSO flow rate clearly impacts the coatings' WCA and roughness. Nevertheless, the corresponding SFE values do not differ significantly from one another (Figure 3.11C). This can seem surprising, as SFE and WCA are generally considered to vary together (WCA increases as SFE decreases). However, as roughness also fluctuates, the WCA decrease is susceptible to be the consequence of morphological differences between the samples rather than chemical ones. It is indeed known that surface roughness impacts the apparent water contact angle of a surface (Wenzel's equation, Equation 1.4).

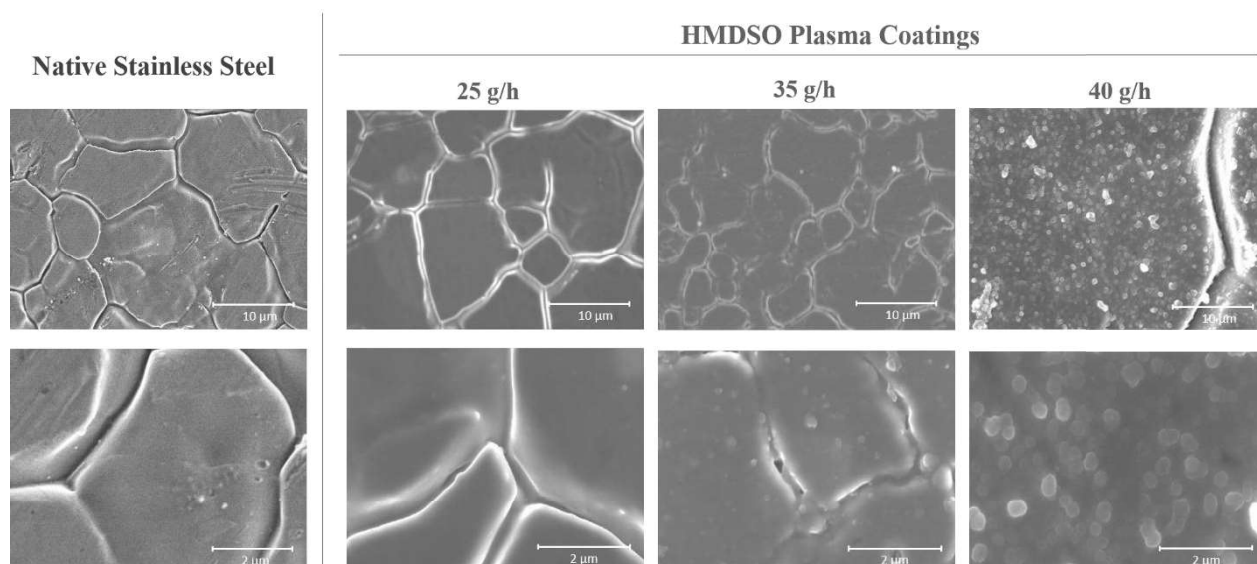


Figure 3.12. SEM surface micrographs of different HMDSO coatings compared to native stainless steel. © 2018 Elsevier.

In the present case, SEM micrographs of coatings (Figure 3.12) generated with three different HMDSO flow rates (25, 35 and 40 g/h respectively) reveal an evolution of the surface morphology vs flow rate increase. At 25 g/h, the surface of the coating looks smooth, but when Q_{HMDSO} rises to 35 g/h, scattered lumps appear. The coating generated with the highest flow rate (40 g/h) has a very grainy, lumpy look which corroborates the existing literature stating that higher precursor flow rate induces the formation of powder in the plasma plume and the integration of particles in the coatings²⁷⁶.

Moreover, FTIR spectra of coated stainless steel with 25 g/h and 40 g/h of HMDSO (Figure 3.13) prove, as expected, that HMDSO flow rate had no significant effect on the coatings' chemistry, which is in accordance with the findings of Lommatzsch and Ihde (2009)²⁷⁶. Consequently, it can be suggested that the WCA changes mainly come from morphological variations.

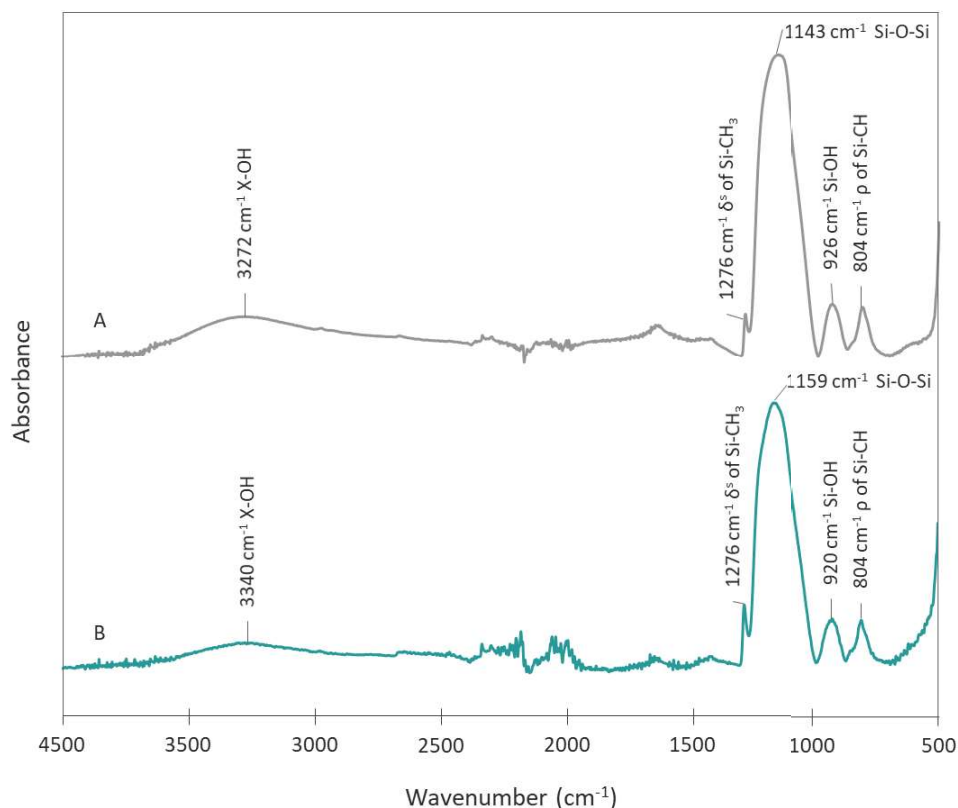


Figure 3.13. FTIR spectra of HMDSO APPS coatings with two different precursor flows, 25 g/h (A) and 40 g/h (B). © 2018 Elsevier.

2.3. Fouling performances of HMDSO coatings

All samples were submitted to two consecutive fouling and rinsing cycles, to study their antifouling performances and to perform a quantitative evaluation of their durability. Native stainless steel was taken as reference in all experiments. Samples were weighted before and after each fouling test and their fouling percentages (F%) were calculated according to Equation 2.1.

After their first use, all HMDSO coatings presented very good antifouling behaviors regardless of the deposition conditions (Figure 3.14), with F% comprised between -90 wt. % and -99 wt. %. The hydrophobic plasma coatings were thus able to significantly reduce dairy fouling in a simulated

pasteurizer holder. In the contrary, Beuf *et al.* (2003)¹¹⁵ and Rosmaninho *et al.* (2007)¹²⁷ reported, on the other hand, that PECVD SiO_x coatings had mediocre to disadvantageous effect on dairy fouling, since the reported coatings in those two studies were rather hydrophilic and rough, which are two fouling-promoting factors²⁰⁶.

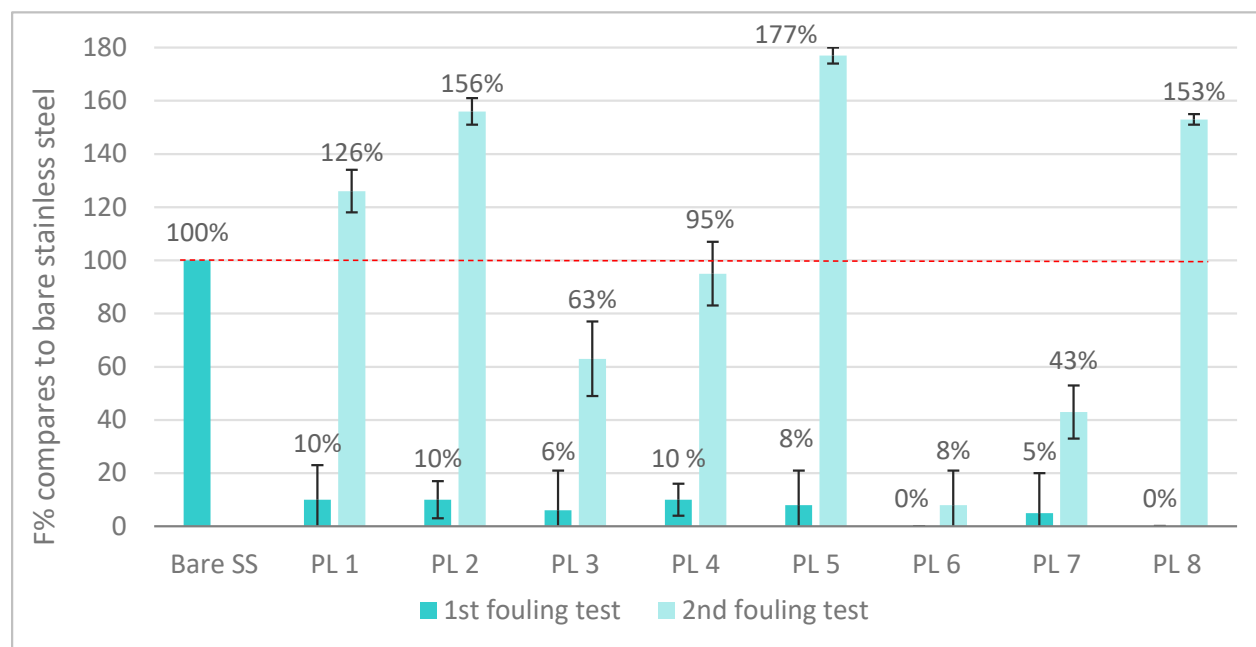


Figure 3.14. Fouling performances of HMDSO APPS coatings.

Table 3.3 shows that the total SFE values (γ^{Total}) of the plasma coatings do not significantly differ from that of bare SS. Additionally, the polar components γ^{p} of plasma coatings are generally higher than the one of stainless steel, which is usually considered as a fouling promoting factor¹²⁷. Consequently, the fouling-release properties of plasma coatings are thus very likely to come with the generally acknowledged chemical inertness of siloxanes allied to surface morphology features.

However, after a second fouling and rinsing cycle, coatings exhibit very variable F%. Particularly, PL 1, 2, 5 and 8 present a fouling increase compared to bare SS whereas PL 3, 4 and 7 exhibit clear losses of fouling-release properties. On the other hand, PL 6 (35 g/h; 30 mm; 100 mm/s) remained close to its original fouling performance.

One possible explanation is that, depending on surface morphology, some deposit from the first use more or less persisted on the coatings and acted as a promoting basis for further deposition

during the second testing run. Indeed, WCA measures carried out on coatings after their first use showed a clear shift for all coatings towards hydrophilicity, except for PL6, whose post-fouling WCA stayed close to its initial value (Table 3.4). Dairy fouling deposits are composed of hydrophilic protein and minerals, and the observed decrease of WCA is consistent with residual deposits on the substrates. By comparison, control measurements carried out on coatings that were immersed in 85°C water for 1.5 h showed WCA very close to the initial values.

Table 3.4. Water contact angle of the coatings in pristine state, after the first fouling test and after a 1.5 h immersion in hot water.

Sample ID	Pristine WCA (°)	WCA after 1 st fouling test	WCA after a 1.5 h immersion in hot water
PL 1	95.7 ± 3.3	68.4 ± 2.2	95.2.5 ± 2.5
PL 2	79.3 ± 4.0	57.0 ± 2.7	76.6 ± 1.7
PL 3	101.2 ± 0.6	61.8 ± 4.0	101.1 ± 1.4
PL 4	101.5 ± 1.0	61.7 ± 4.0	102.4 ± 0.9
PL 5	97.1 ± 0.8	63.0 ± 1.4	97.7 ± 1.5
PL 6	94.3 ± 2.2	93.2 ± 1.1	93.8 ± 2.4
PL 7	95.0 ± 1.3	78.9 ± 0.8	96.1 ± 1.7
PL 8	95.4 ± 1.4	63.1 ± 2.7	94.8 ± 3.8

From this point, the focus will be taken on PL6, in order to elucidate the reasons for its good performances. Figure 3.15 presents cross-section EPMA X-Ray Mappings performed on PL 6 coating after two consecutive fouling runs compared to bare SS. The arborescent look of dairy fouling on native stainless steel and the presence of calcium in forms of particles are consistent with previous observations of isothermal fouling^{32,253}.

The HMDSO coating is apparent and its thickness can be approximated to 150 nm. As a matter of fact, coating thickness did not vary according to manufacturing conditions, probably because the studied flow rate variation range is too small to have a significant impact. The difference between dairy fouling on bare steel and on PL 6 coating is striking. The deposit forms a continuous 250-300 µm-thick film on the reference after one fouling test, whereas only 5 µm-thick isolates are found on PL 6 after two pasteurization cycles.

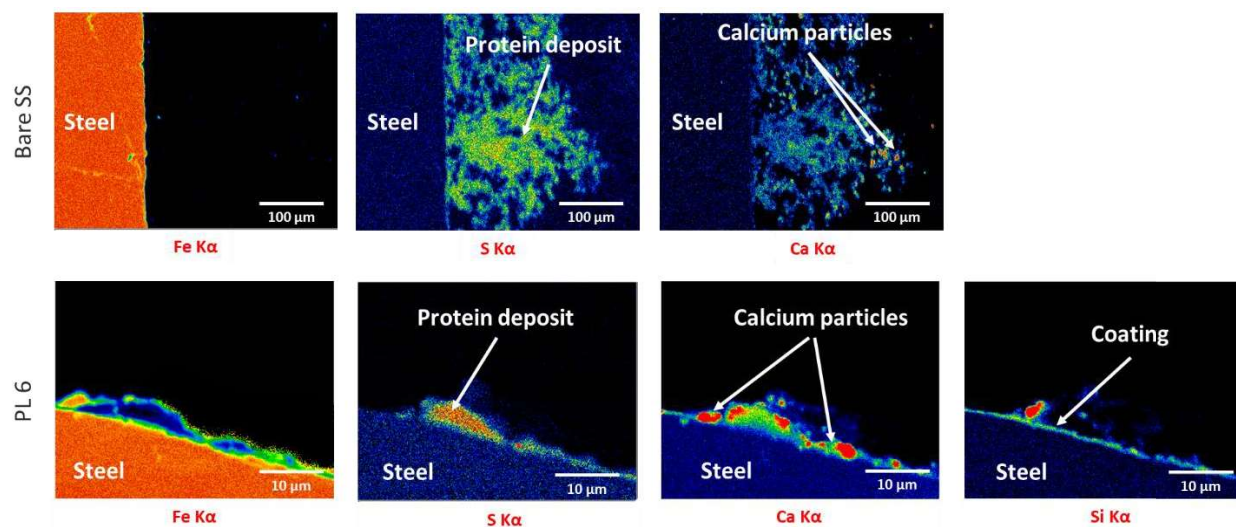


Figure 3.15. Cross-section EPMA X-ray Mappings of one-time fouled bare stainless steel (top row) and two-time fouled PL 6 coating (bottom row). © 2018 Elsevier.

Chemical analysis of PL 6 coating was performed through XPS (Figure 3.16) and showed the presence of oxygen, carbon and silicon, whereas iron, nickel, oxygen and carbon were found on bare SS. Component analysis of the different elements on both surfaces allowed to investigate closely their chemical composition.

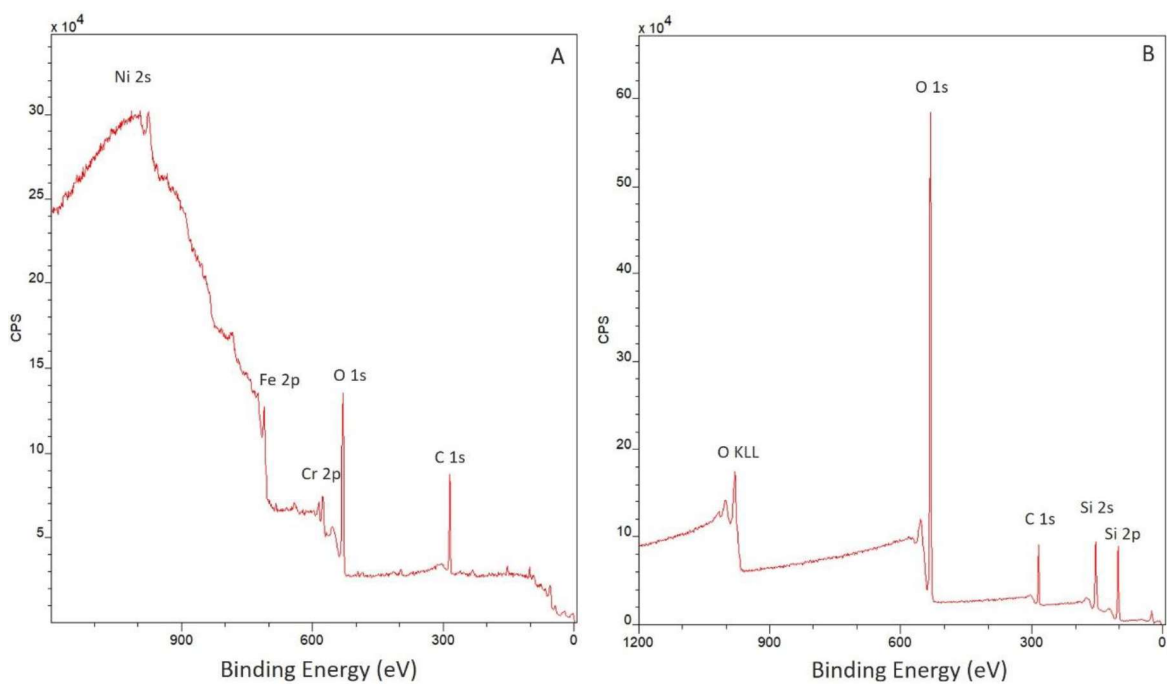


Figure 3.16. XPS surveys of bare stainless steel (A) and PL 6 coating (B). © 2018 Elsevier.

On bare SS, the study of Fe 2p and Cr 2p spectra (Figure 3.17) following the decomposition proposed by Biesinger *et al.* (2011)²¹⁷ revealed the strong presence of iron and chromium oxides, which are electron donor components, and like nickel, very prone to bind with unfolded whey protein³⁹. On PL 6, the Si 2p binding energy (102.8 eV) was found to match exclusively that of siloxane²⁷⁷ and the O 1s binding energy (532.6 eV) to match exclusively that of the oxygen atom of a Si-O-Si group (Figure 3.18)²⁷⁸. The PL 6 coating's surface is thus rich in Si-O-Si groups, which are electron acceptors²⁷⁹. The antifouling properties of PL 6 coatings are thus consistent with the findings of Boxler *et al.* (2013)⁶⁸, who established the antifouling properties of Si-O doped DLC coatings against dairy proteins.

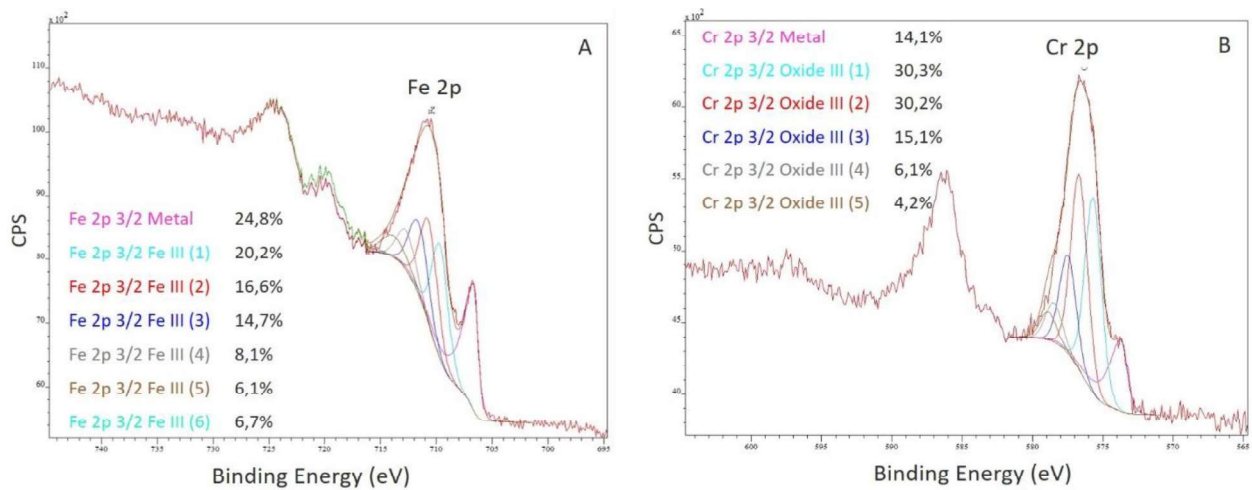


Figure 3.17. XPS Spectra of Fe (A) and Cr (B) in bare stainless steel. © 2018 Elsevier.

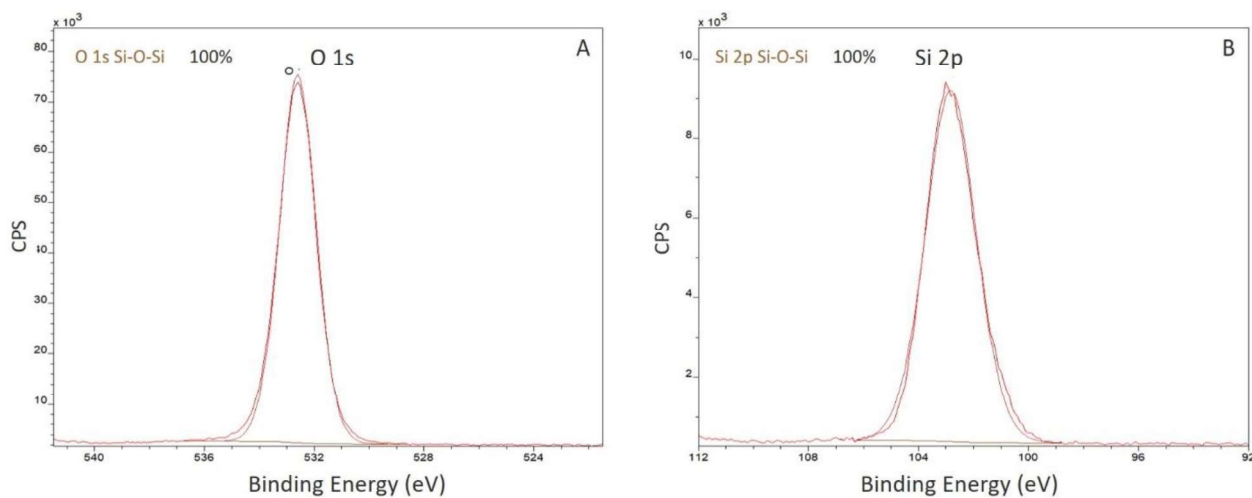


Figure 3.18. XPS Spectra of O (A) and Si (B) in PL 6 coating. © 2018 Elsevier.

Morphology of PL 6 was studied through SEM observations (Figure 3.19) and AFM analysis (Figure 3.20). Although the coating is too thin to fill completely the grain boundaries of the stainless steel substrate (Figure 3.19), AFM revealed the radical change in surface morphology caused by APPS coating. Indeed, while bare SS presents hundred-nanometer deep and wide defects, nano-peaks are visible on PL 6. This nano-roughness is reminiscent of nanotextured and antiadhesive biological surfaces (*e.g.* lotus leaves). In the case of PL 6, this particular morphology, allied to the chemical features mentioned earlier, certainly lowered deposit adhesion and prevented interlocking of dairy foulant particles whose diameters are of 50-60 nm. Previous work indeed pointed out the importance of the relative size of surface relief versus foulants, suggesting that nano-roughness could be beneficial regarding fouling management^{32,253}.

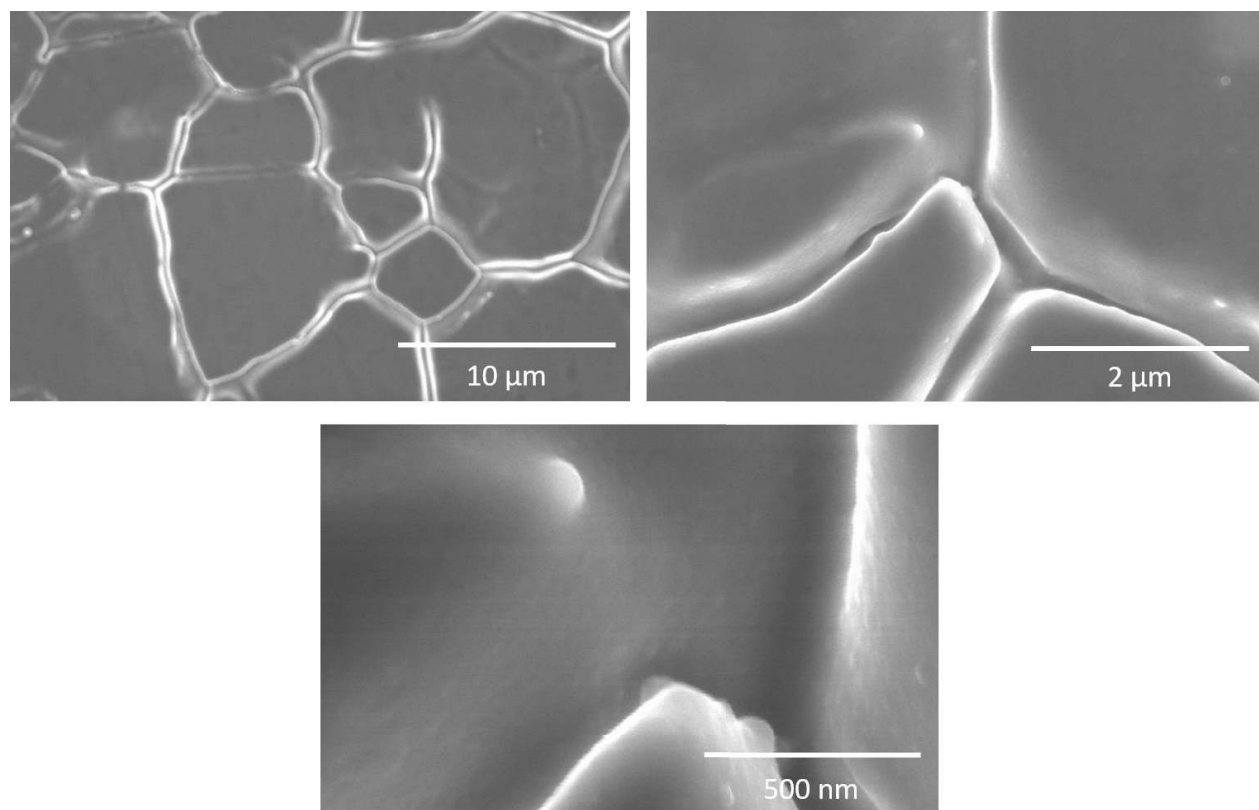


Figure 3.19. SEM micrographs of pristine PL 6 coating. © 2018 Elsevier.

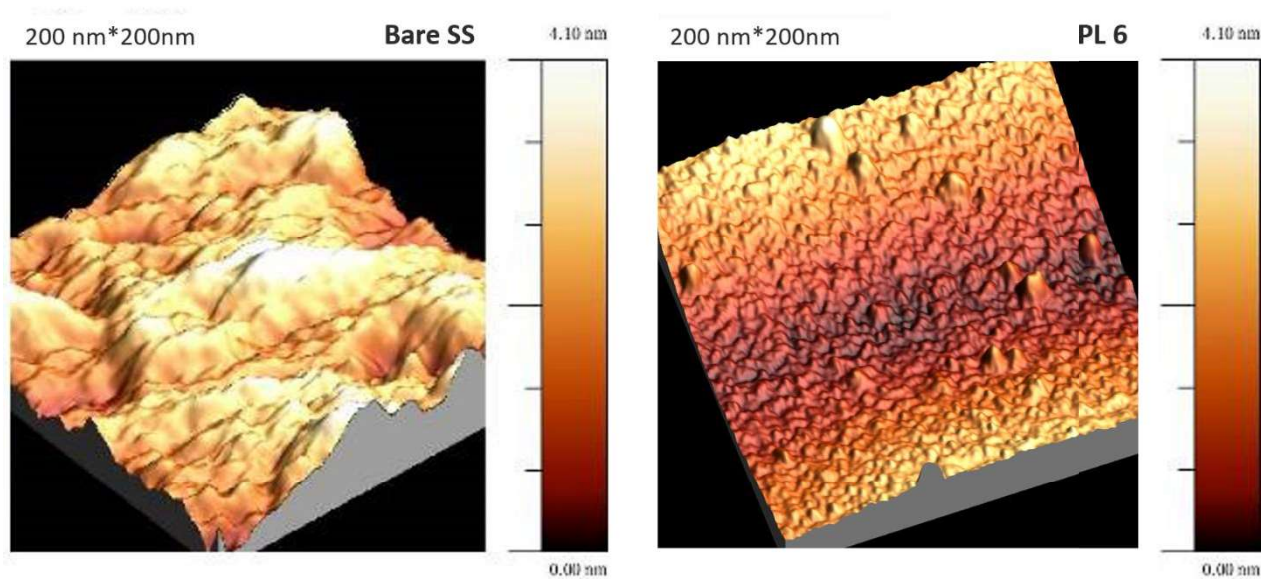


Figure 3.20. AFM pictures of bare SS and PL 6 coating. © 2018 Elsevier.

Overall, the behavior of PL6 surfaces towards protein fouling has been analyzed and explained. It would then be interesting to investigate the effect of the plasma coating on bacterial adhesion. Micro-organisms management is indeed one of the main concerns when dealing with food-contacting surfaces.

2.4. Bacterial Adhesion Assay

Bacterial adhesion tests were carried out as detailed in Chapter 2 (p. 60). The observation and comparison of bare stainless steel and PL6 coating (Figure 3.21) revealed that plasma treatment had a significant impact on bacterial adhesion. Indeed, for all strains, plasma coating reduced cell counts. Fluorescence microscope observations moreover showed that a significant part of adhered cells on PL6 were located in the surface's grain boundaries (Figure 3.21). This impact of surface topography on bacterial adhesion is consistent with existing literature^{280,281}.

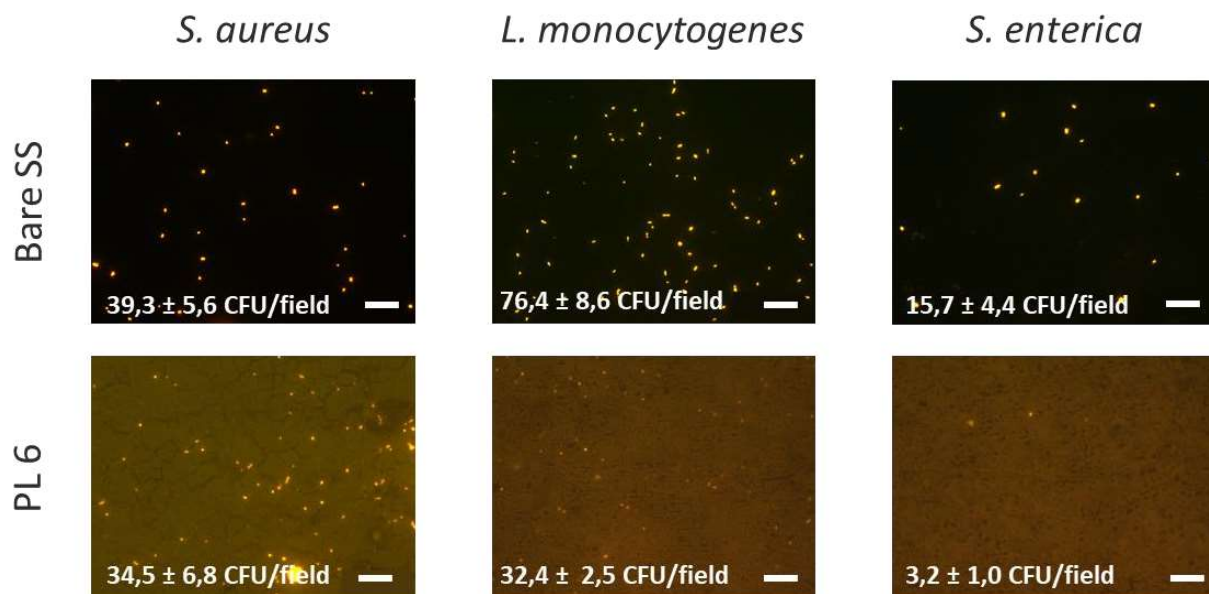


Figure 3.21. Fluorescence microscopy picture of bare SS (left) and PL6 surface (right) after 1 h of *S. aureus* adhesion. Scale bars are 200 μm -long.

To summarize, atmospheric pressure plasma spraying was successfully used to generate thin, very adhesive, hydrophobic silane-based coatings on food-grade stainless steel. Variation of precursor flow was shown to significantly impact surface roughness and morphology of the coatings, as particles are formed in the plasma plume when precursor flow increases. Those particles, included in the film, generate uneven morphologies.

HMDSO coated samples were shown to be efficient antifouling surfaces, however, as expected, the manufacturing conditions impacted the coatings' performances. The best performing coating, which allowed reducing dairy fouling by more than 90 % for two consecutive fouling runs, was closely characterized. Its nanostructured Si-O-Si rich surface was demonstrated to be well fitted for fouling reduction. This plasma treatment also proved to have a significant effect on bacterial adhesion to the substrate.

Further research should be dedicated to the optimization of the manufacturing parameters, e.g. through experimental design, in order to produce coatings with tuned surface properties targeting antifouling in isothermal or non-isothermal conditions. Surface roughness of the treated stainless steel should also be investigated.

3. Amphiphilic environment-responsive coatings

The two previous sections presented hydrophobic surfaces with fouling release properties, which can be considered as suitable for fouling mitigation. However, as discussed in Chapter 1, effective dairy fouling mitigation critically relies on the control and prevention of protein adhesion and associated mineral deposition, which can also be achieved by using hydrophilic materials. Poly(ethylene oxide) (PEO, also called poly(ethylene glycol), PEG), a highly hygroscopic polymer, is indeed widely known for its exceptional antifouling behavior against proteins adsorption and adhesion²⁸². Its ability to tightly bind water molecules induces the formation of a highly hydrated and configurationally mobile polymer layer that prevents protein fouling through steric hindrance^{283–285}. Such coatings could thus be interesting candidates to achieve dairy fouling control. PEO's protein resistance has been primarily established when chains are surface-grafted onto physically stable, model substrates (*e.g.* glass^{286,287} and gold^{288,289}) which are maintained at the surface whatever an air or aqueous environment (Figure 3.22B). However, direct surface-grafting of PEO chains to stainless steel dairy processing equipment is not feasible, necessitating the use of a PEO-containing coating. Silicones are known for their fouling release behavior²⁹⁰ and PEO-modified silicone coatings may be formed *via* simple bulk modification, as proposed by Chen *et al.* (2005, 2005a)^{159,291}, by blending and subsequently curing an RTV (room temperature vulcanizing) silicone with a conventional PEO-silane such as triethoxysilylpropyl PEO monomethyl ether [(EtO)₃Si(CH₂)₃-(OCH₂CH₂)_n-OCH₃] (Figure 3.22A). However, stemming from the low surface energy and high chain flexibility of silicones^{292,293}, reorganization of the PEO to the surface for increased hydrophilicity is highly dependent on the environment (Figure 3.22B and C). These particular PEO-modified silicones have been shown to exhibit not only hydrophobic recovery in air^{159,291} but also poor water-driven migration of PEO to the aqueous interface where fouling occurs^{294–296}. As a result, these bulk PEO-modified silicones exhibit poor anti-fouling behavior^{294,296}.

Instead, biomimetic PEO-modified silicones prepared *via* bulk modification with PEO-silane amphiphiles that include a short siloxane tether [α -(EtO)₃Si(CH₂)₂-oligodimethylsiloxane_m-*block*-(OCH₂CH₂)_n-OCH₃] were reported (Figure 3.22A). The high level of molecular flexibility, induced by

the presence of the siloxane tether, is not without remaining that of fluid-mosaic cell membrane amphiphilic components²⁹⁷. The achievement of water-driven surface restructuration would then allow for antifouling brush-like structures to form only when the surface is placed in aqueous media, as cells are able to express certain molecules on their membranes and modify their interfacial properties when needed²⁹⁷.

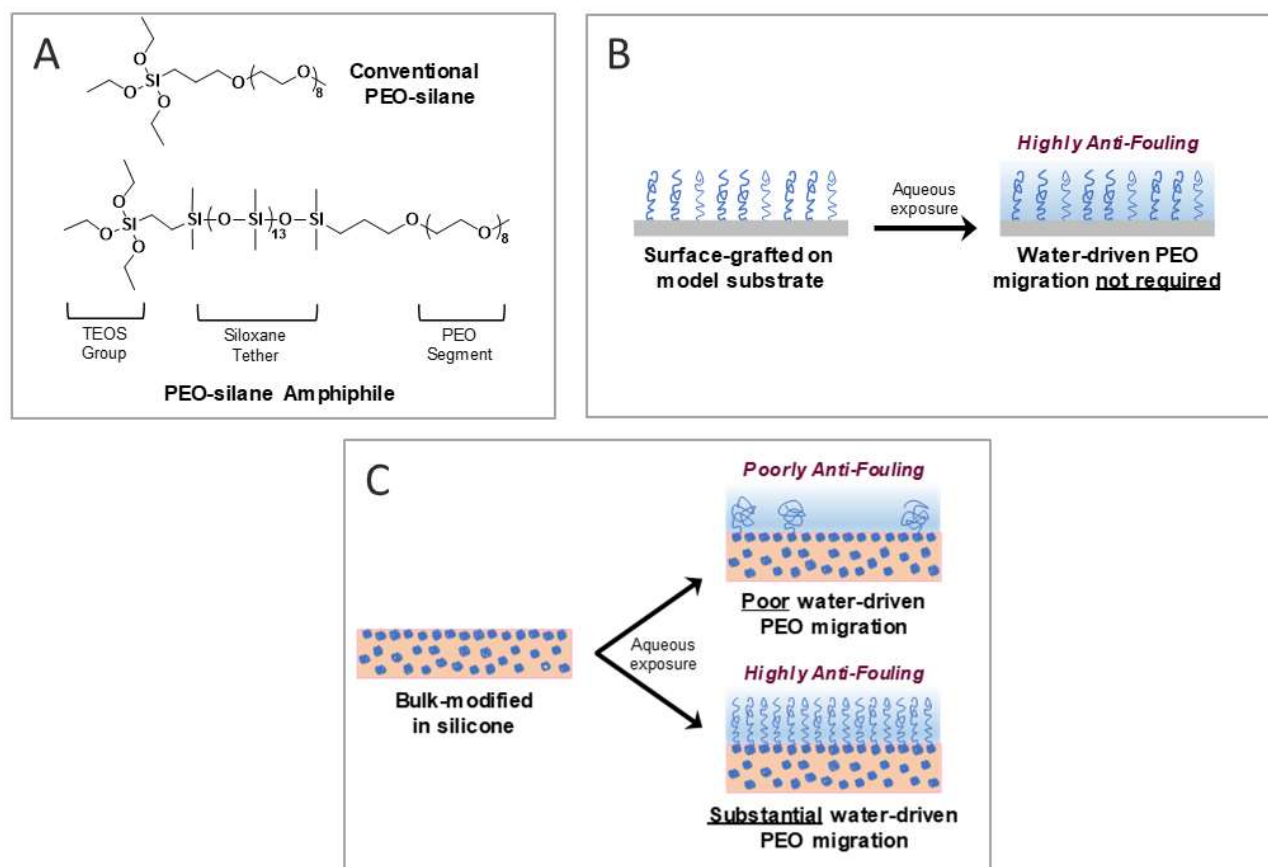


Figure 3.22. Resistance of PEO (A) to fouling requires enrichment at the aqueous interface where fouling occurs. In contrast to surface-grafted model substrates (B), silicones bulk-modified with PEO requires its substantial water-driven migration for effective antifouling behavior (C). Such behavior has been observed for silicones bulk-modified with PEO-silane amphiphiles but not with conventional PEO-silanes (*i.e.* no siloxane tether).

As a matter of fact, for a silica-reinforced RTV silicone modified with PEO-silane amphiphiles, extensive and rapid PEO water-driven surface reorganization was confirmed *via* temporal contact angle analysis^{294–296,298} as well as atomic force microscopy (AFM)²⁹⁹. Their efficacy as surface-modifying additives (SMAs) is attributed to the siloxane tether’s molecular flexibility and similar hydrophobicity to the silicone matrix that enables migration of the tether and attached PEO

segment. As a result, compared to unmodified silicone and those modified with conventional PEO-silanes, silicones modified with PEO-silane amphiphiles demonstrated excellent resistance to plasma proteins^{295,296,298}, bacteria²⁹⁶ and marine organisms^{148,299}. Furthermore, it was demonstrated that water-driven restructuring and protein antifouling behavior appeared particularly effective for a PEO segment length of $n = 8$ and siloxane tether of $m = 13$ ^{294–296}.

The next section will study the surface characteristics of PEO-silane amphiphilic coatings allied to different substrate pre-treatments. The fouling properties of the resulting surfaces in isothermal and anisothermal conditions, as well as their behavior towards bacterial adhesion will then be discussed. This work has been submitted to *Biofouling* and is currently under revision.

3.1. Coatings formulation and surface preparation

3.1.1. PEO-silane amphiphile synthesis

The PEO-silane amphiphile [α -(EtO)₃Si(CH₂)₂-oligo-dimethylsiloxane₁₃-*block*-(OCH₂CH₂)₈-OCH₃] was synthesized at the Biomedical Engineering Department at the Texas A&M University, as reported by Murthy *et al.* (2007)³⁰⁰. Briefly, vinyltriethoxysilane (VTEOS) and α,ω -bis-(SiH)oligodimethylsiloxane₁₃ (ODMS₁₃) were reacted in a Wilkinson's catalyzed regioselective hydrosilylation and the product subsequently subjected to Karstedt's catalyzed hydrosilylation with allyl methyl Polyglykol AM 450 (PEO₈). VTEOS, ODMS₁₃ and Karstedt's catalyst (Pt-divinyltetramethyldisiloxane complex) were obtained from Gelest (USA). PEO₈ was purchased from Clariant (USA). Wilkinson's catalyst (RhCl(Ph₃P)₃) was purchased from Sigma Aldrich.

3.1.2. Preparation of stainless steel coupons for isothermal fouling study

Substrates for the isothermal fouling study and bacterial adhesion study were 10 x 16 x 1 mm³ and 45 x 16 x 1 mm³ 316L 2B stainless steel (SS) coupons (Sapim Inox, France). The substrates were washed before modification following the protocol described in Chapter 2 (p. 61). To enhance the adhesion of PEO-modified silicone coating ("Si-PEO") to SS coupons, several surface pretreatments were evaluated as follows.

3.1.2.1. Plasma activation

SS coupons were activated by atmospheric pressure plasma spot using a UL-Scan device (Acxys Technologies, France), as described previously (p. 98).

3.1.2.2. Polydopamine coating

Polydopamine has been studied for several years as a biomimetic adhesive, inspired from mussels^{301,302}. Studies indeed showed that these animals secreted a catechol and amine-rich mucus to ensure their attachment to a broad spectrum of surfaces^{303,304}. In that context, dopamine (Figure 3.23) was identified as an interesting molecule to mimic mussel's adhesive, as it contains both catechol and amine functions. Therefore, a polydopamine layer was deposited onto stainless steel substrates in order to enhance Si-PEO coating adhesion. Cleaned stainless steel coupons were immersed in a 10 mM TRIS solution containing 2 mg/mL of dopamine (Sigma Aldrich), pH was adjusted to 8.5. The reaction was carried out overnight at RT under stirring (240 rpm). Coupons were then taken out of the solution, rinsed twice in deionized water and cured at 150 °C for 1 hr. The thickness of such polydopamine coatings is usually in the range of 60-70 nm^{305,306}.

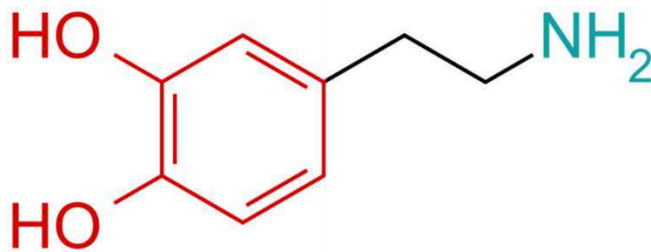


Figure 3.23. Dopamine with its catechol group in red and its amine group in blue.

3.1.2.3. NuSil SP-120 Primer

NuSil SP-120 (NuSil Technology, USA), a silicon-based primer, was applied on the SS substrates with a foam brush and allowed to dry for 30 min before further modification.

3.1.2.4. Preparation of PEO-modified silicone coatings (“Si-PEO”) and unmodified silicone control (“Si-control”) onto SS coupons

PEO-modified silicone coatings and an unmodified silicone control coating were prepared as follows. For the silicone control (“Si-control”), the casting solution was prepared by combining MED-1137 with hexane (1:3 wt:wt) in a sealed glass jar and mixing with a vortexer until a homogeneous solution was produced. For “Si-PEO” coatings, to the aforementioned casting solution was added the PEO-silane amphiphile (50 μmol of amphiphile per 1 g of MED-1137) and lastly mixed under agitation on a shaker plate for 3 h. The casting solutions of a fixed volume (0.1 and 0.4 mL for smaller and larger SS coupons, respectively) were each distributed onto and allow to flow across the different, leveled SS substrates and lastly left to dry in air for 1 week. Table 3.5 summarizes the designations and features of the resulting samples.

Table 3.5. Designation of stainless steel (SS) coupons of various pretreatments coated with PEO-modified silicone (“Si-PEO”) as well as an unmodified silicone control coating (“Si-control”).

Designation	Characteristics
O-(Si-PEO)	Si-PEO coating on native stainless steel
PL-(Si-PEO)	Si-PEO coating on plasma activated stainless steel
PD-(Si-PEO)	Si-PEO coating on polydopamine coated stainless steel
NuSil-(Si-PEO)	Si-PEO coating on NuSil SP120 coated stainless steel
NuSil-(Si-control)	Unmodified silicone coating on NuSil SP 120 coated stainless steel

3.1.3. Preparation of coated stainless steel PHE plates for *in situ* fouling study

Stainless steel V7 heat-exchanger plates from Alfa-Laval (Sweden) (Figure 3.24) were used for the *in situ* study (*i.e.* with fouling on a heated surface, as opposed to the previously described isothermal test). They are 530 x 180 x 0.8 mm³ in dimension and corrugated to optimize flow turbulence and heat transfer.



Figure 3.24. A V7 PHE plate.

The plates were first cleaned according to the previously mentioned protocol and then coated with NuSil SP-120. After 30 min, the PEO-modified silicone coating (“Si-PEO”) was sprayed on the plate with a pressurized gravity-feed Devilbiss Advance GP443-13 spray gun equipped with a 1.3 mm nozzle. The coating was left to cure for 1 week in air before fouling testing.

3.2. Surface properties of PEO-silicone coatings

3.2.1. Surface properties of pre-treated SS coupons

Prior to the application of the PEO-modified silicone coating, SS coupons were subjected to various pre-treatments to potentially improve coating adhesion. The water contact angles were measured and surface free energies (γ) calculated according to the OWRK method for the native, pre-treated and coated SS coupons (Table 3.6).

Table 3.6. Surface characteristics of native, pre-treated and “Si-PEO” coated stainless steel (SS) coupons.

Surface	WCA ₀ (°)*	γ^T (mN/m)	γ^D (mN/m)	γ^P (mN/m)	
Native SS	84.2 ± 2.6	41.9 ± 4.3	38.2 ± 0.9	3.7 ± 2.5	
PL activated SS	23.5 ± 0.9	64.7 ± 1.5	35.7 ± 6.3	29.0 ± 9.1	
PD coated SS	57.7 ± 5.7	35.4 ± 5.6	31.3 ± 3.7	4.1 ± 1.9	
NuSil coated SS	56.2 ± 5.7	58.0 ± 0.6	50.3 ± 0.5	7.7 ± 0.1	
	WCA ₀ (°)*	WCA _{eq} (°)**	γ^T (mN/m)	γ^D (mN/m)	γ^P (mN/m)
O-(Si-PEO)	111.2 ± 2.4	33.6 ± 2.3	51.8 ± 2.4	35.1 ± 1.3	16.7 ± 1.4
PL-(Si-PEO)	106.0 ± 1.1	61.6 ± 3.14	39.1 ± 1.3	29.9 ± 6.6	9.23 ± 0.6
PD-(Si-PEO)	114.8 ± 1.2	30.7 ± 2.9	50.0 ± 2.4	35.9 ± 1.2	14.1 ± 1.2
NuSil-(Si-PEO)	104.9 ± 1.9	28.8 ± 2.5	68.8 ± 1.9	38.7 ± 8.6	30.1 ± 1.1
NuSil-(Si-control)	118.0 ± 0.64	118.0 ± 0.64	14.5 ± 0.7	14.4 ± 0.6	0.1 ± 0.0

*Instant water contact angle, ** Water contact angle 150 s after deposition of droplet, Total surface free energy (γ^T) = dispersive component (γ^D) + polar component (γ^P)

As previously reported, plasma activation substantially reduces the WCA_o of native SS from $84.2 \pm 2.6^\circ$ to $23.5 \pm 0.9^\circ$ and total surface free energy (γ^T) thereby significantly increases from 41.9 ± 4.3 mN/m to 64.7 ± 1.5 mN/m. This change is most likely due to the oxidation and formation of reactive groups induced by plasma exposure at the SS surface³⁰⁷. While not as substantial as for plasma activated SS, polydopamine (PD) deposition also produces a reduction in WCA_o versus native SS, from $84.2 \pm 2.6^\circ$ to $57.7 \pm 5.7^\circ$. This was expected, given that polydopamine coatings are known to be rich in hydrophilic hydroxyl and amine groups^{308,309}. However, despite its lower WCA_o , the γ^T of PD coated SS (35.4 ± 5.6 mN/m) is lower than that of native SS. This was unexpected, given that a lower surface energy is generally associated with greater hydrophobicity (*i.e.* higher WCA). This may be attributed to differences in surface morphology, which is known to impact WCA values⁶⁶. Indeed, SEM images of native SS and polydopamine coated SS revealed the presence of polydopamine nanoparticles on PD coated SS (Figure 3.25), which are commonly observed with polydopamine coatings^{301, 308,310}. Lastly, SS coated with NuSil SP-120 primer exhibited a WCA_o value ($56.2 \pm 5.7^\circ$) similar to that of PD coated SS. Its γ^T was increased (58.0 ± 0.6 mN/m) compared to native SS (41.9 ± 4.3 mN/m).

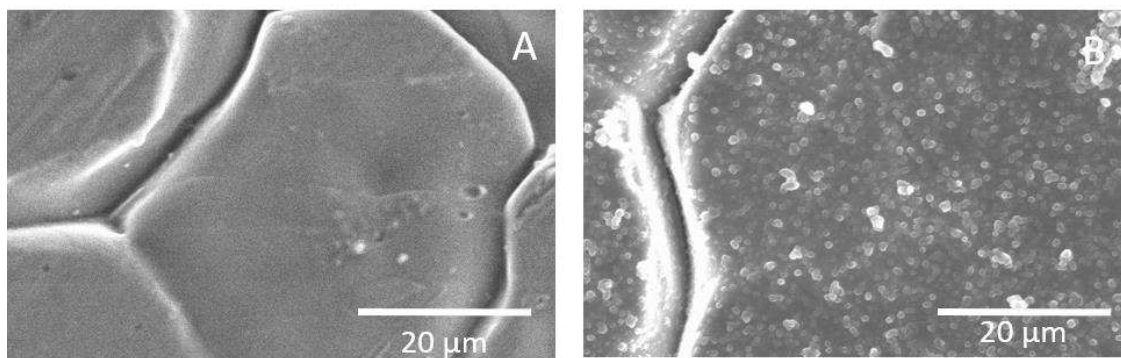


Figure 3.25. SEM micrographs of SS (A) and polydopamine coated SS (B).

3.2.2. Surface properties of Si-PEO coating on pre-treated SS coupons

Silicones bulk-modified with the PEO-silane amphiphile [α -(EtO)₃Si(CH₂)₂-oligodimethyl-siloxane₁₃-*block*-(OCH₂CH₂)₈-OCH₃] have been reported to exhibit a rapid and substantial reduction in WCA of applied droplets^{294–296,298}, indicating water-driven migration of PEO segments to the surface. The exceptional anti-fouling behavior of these surfaces was attributed to this restructuring behavior. However, these prior studies were limited to coatings prepared on native glass

microscope slides. In this work, towards improving adhesion to SS, the PEO-modified silicone coating was prepared on native SS, PL activated SS, PD coated SS, and NuSil primer coated SS: O-(Si-PEO), PL-(Si-PEO), PD-(Si-PEO), and NuSil-(Si-PEO), respectively. In order to evaluate if SS surface pre-treatments would alter the necessary water-driven surface reorganization of the coating, WCA measurements were recorded at 10 sec intervals up to 150 sec, at which point the water-surface interface reaches an equilibrium (*i.e.* WCA_{eq}) (Figure 3.26, Table 3.6). Confirming a lack of substantial evaporation, the volume of 2 μL droplets was monitored over 150 s in the same environmental condition used for WCA assessment and remained constant at $1.72 \pm 0.02 \mu\text{L}$ over the entire period. For all surfaces, the values of WCA_0 were similar (~ 105 to 115°), indicative of very hydrophobic surfaces. It is noteworthy that unmodified silicon coatings (Si-control) present a high WCA value of $118.0 \pm 0.6^\circ$, which stayed constant over the whole measurement time (150 s).

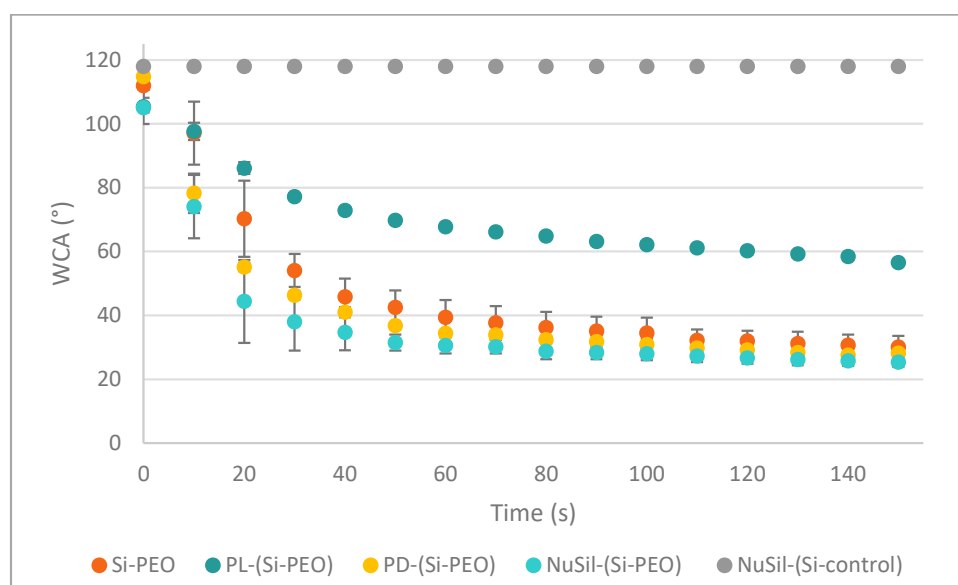


Figure 3.26. Variation of water contact angle (top) with time. (NB: Standard deviation values for WCA of PL-(Si-PEO) surfaces are too small to be correctly presented on the figure (Annex IV).)

Conversely, upon time, WCAs of modified coatings expectedly decreased as the droplets were maintained on the surfaces. For O-(Si-PEO), PD-(Si-PEO) and NuSil-(Si-PEO), WCA_{eq} were reduced to similar WCA_{eq} values of $\sim 30^\circ$, indicative of a PEO-enriched surface. Interestingly, for PL-(Si-PEO), WCA_{eq} was only $\sim 62^\circ$, pointing to a somewhat diminished capacity of the PEO segments to migrate to the aqueous interface. Since the plasma treated SS is the most hydrophilic pretreated surfaces ($WCA_0 \sim 23^\circ$), it may have a stronger affinity to PEO segments of the coating, diminishing the

capacity of PEO to migrate to the aqueous interface. Thus, in terms of restructuring potential of the coating in an aqueous environment, SS treated with polydopamine or NuSil primer are superior substrates.

Interestingly, the contact angle monitoring of non-polar diiodomethane droplets on the different coated surfaces yielded decreasing profiles similar to that observed with water droplets, also pointing toward surface restructuring (see Annex IV). The equilibrium contact angles formed between these surfaces and droplets of diiodomethane further support the lack of affinity of PEO segments with a non-polar environment. This is consistent with previous studies and attributed to surface rearrangements leading to interfacial energy minimization.

3.3. Isothermal fouling study

PL-(Si-PEO), PD-(Si-PEO) and NuSil-(Si-PEO) surfaces were likewise subjected to 1.5 h pasteurization cycle under isothermal conditions, without rinsing. Regardless of the surface pretreatment, no trace of fouling was observed (*i.e.* F% = 0) (Table 3.7).

Table 3.7. Adhesion, roughness (Ra) before and after isothermal fouling, and percent fouling (F%) after each 1.5 hr pasteurization cycle (“isothermal fouling”).

Surface	Adhesion range	Initial Ra (μm)	Ra after final fouling cycle (μm)	F% 1 st cycle	F% 2 nd cycle	F% 3 rd cycle	F% 4 th cycle	F% 5 th cycle
0-(Si-PEO)	1B	0.04 ± 2.10^{-3}	0.2 ± 9.10^{-3}	0 %	Fail	--	--	--
PL-(Si-PEO)	2B	0.03 ± 2.10^{-3}	0.08 ± 4.10^{-3}	0%	0%	Fail	--	--
PD-(Si-PEO)	3B	0.04 ± 0.01	0.1 ± 8.10^{-3}	0 %	0 %	0 %	Fail	--
NuSil-(Si-PEO)	5B	0.02 ± 8.10^{-3}	0.02 ± 5.10^{-3}	0 %	0 %	0 %	0 %	0 %
NuSil-(Si-control)	5B	0.04 ± 0.01	--	90 %	--	--	--	--

Thus, even though the WCA_{eq} of PL-(Si-PEO) was relatively somewhat higher, its similar fouling resistance indicates that sufficient water-driven surface migration of PEO was achieved. However, while superior to that of 0-(Si-PEO), adhesion of the PEO-modified silicone coating to the pre-treated SS coupons varied substantially (Table 3.7), with lack of adhesion limiting the number of pasteurization cycles possible. Crosshatch adhesion tests indeed revealed the impact of SS surface pre-pretreatment on the adhesion of the subsequently applied PEO-modified silicone coating (Table 3.7). For the coating applied directly to native SS (0-(Si-PEO)), adhesion was poor [1B] and

after one fouling cycle, O-(Si-PEO) surfaces showed signs of peeling, and cross-section X-Ray mappings revealed a damaged coating (Figure 3.27). Adhesion increased for all pre-treatments in the order: PL-(Si-PEO) [2B], PD-(Si-PEO) [3B] and NuSil-(Si-PEO) [5B]. Thus, the NuSil primer provided the best and excellent adhesion of the coating to the SS coupon.

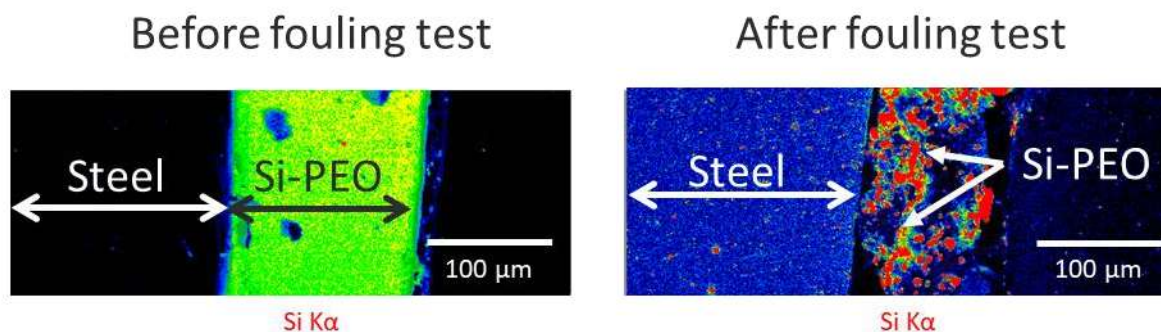


Figure 3.27. EPMA X-Ray mappings on cross-section of representative O-(Si-PEO), before and after one isothermal fouling run (one 1.5 hr pasteurization cycle under isothermal conditions).

Similarly, adhesion failure occurred after two and three pasteurization cycles for PL-(Si-PEO) and PD-(Si-PEO), respectively, and surface roughness (R_a) was also observed to increase, pointing toward coating damage. However, even after five cycles, no peeling as well as no fouling was visually observed on NuSil-(Si-PEO) surfaces (Figure 3.28) nor was there an increase in R_a (Table 3.7).

Figure 3.28 also clearly shows the absence of dairy deposit on the coated surface, whereas native stainless steel exhibits dendritic proteinaceous fouling. By comparison, the unmodified silicone coating showed fouling amounts close to that of native SS, with a fouling density of 54.6 ± 9.3 mg/cm² ($F\% = 90\%$) after only one 1.5 h cycle. This indicates that the antifouling properties of the PEO-modified silicone coatings are due to the water-driven surface restructuring.

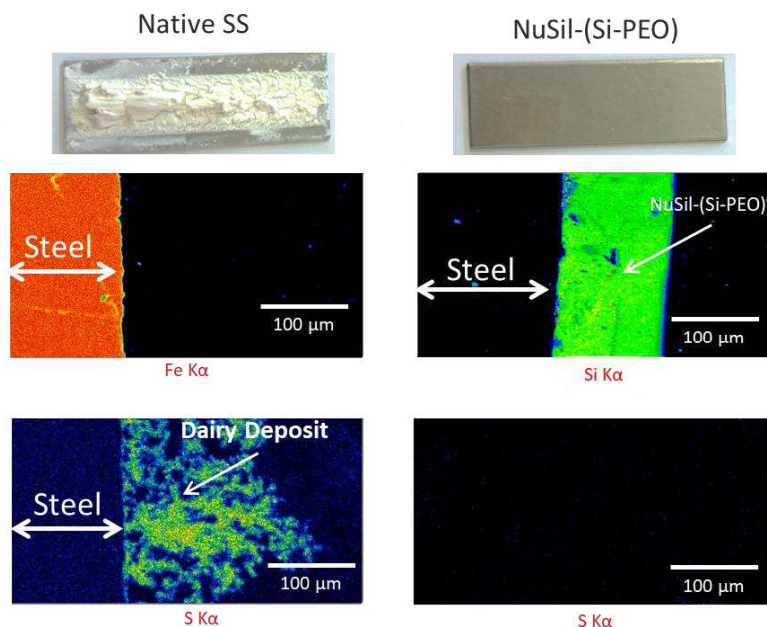


Figure 3.28. EPMA X-Ray pictures of fouled native SS (after one 1.5 hr pasteurization cycle), clean NuSil-(Si-PEO) and fouled NuSil-(Si-PEO) (after five 1.5 hr pasteurization cycles).

Following the five cycles of pasteurization, these coupons were air dried and their WCAs likewise measured (

). WCA_{eq} values of NuSil-(Si-PEO) surfaces after five cycles were similar to those measured prior to fouling testing. Interestingly, the WCA_0 of NuSil-(Si-PEO) decreases from 105° to 46° after five pasteurization cycles. This may be attributed to the lack of removal of surface water that sustains PEO at the surface, eliminating the water-driven PEO migration observed for dry surfaces ¹⁴⁸.

Overall, by staying unfouled for five consecutive 1.5 h fouling test runs (*i.e.* 7.5 h of continuous pasteurization), NuSil-(Si-PEO) surfaces demonstrated the tremendous potential of amphiphilic coatings for dairy fouling management. Research about dairy fouling control has long focused on low SFE fouling-release surfaces, such as fluoropolymers (*e.g.* Teflon)^{117,118, 127,147} or silicone-based surfaces (*e.g.* PDMS)^{24, 55, 106,116}. More recently, Plasma-Enhanced Chemical Vapor Deposition (PECVD) of diamond-like carbon (DLC coatings) were investigated which proved to be more easily cleaned than reference substrates (glass or stainless steel)^{30,31,102}; however, regular cleaning was still required to avoid compromising process efficacy or product quality. By comparison, the present amphiphilic coatings do not need rinsing nor cleaning, enabling longer production runs.

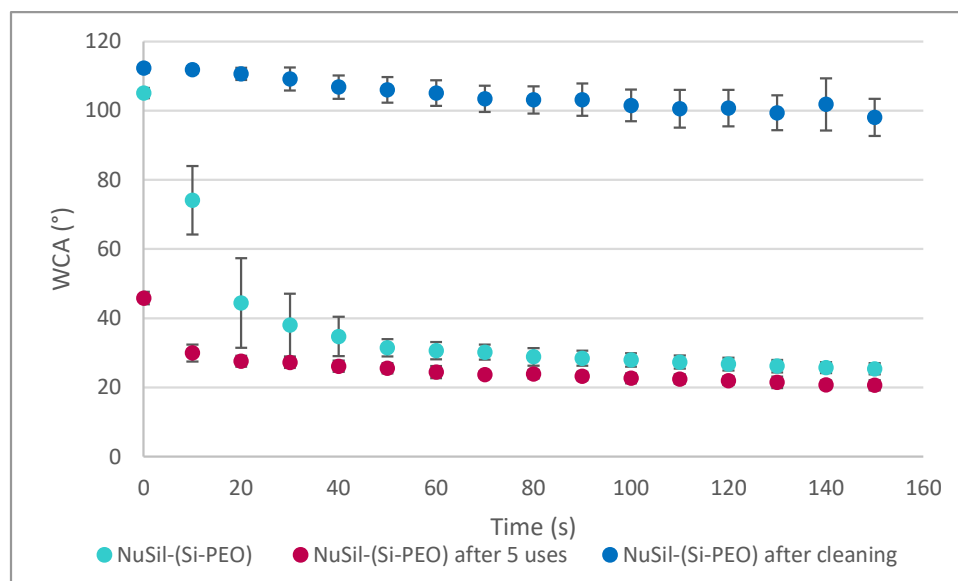


Figure 3.29. Variation of water contact angle (from WCA_0 to WCA_{eq}) with time of NuSil-(Si-PEO) before and after five 1.5 h cycles of pasteurization as well as after subsequent cleaning.

3.4. Clean in place following isothermal fouling study

Due to their excellent fouling resistance and durability during isothermal fouling studies, NuSil-(Si-PEO) surfaces were subjected to a standard clean-in-place procedure (see Chapter 2, p. 57) following the five 1.5 h pasteurization cycles, in order to verify their stability. After exposure to the caustic and acidic cleaning solutions, no visual evidence of peeling was observed. However, it was noted that surface wettability was impacted, as the water contact angle decreased from 112.3° (WCA_0) to only 98.1° (WCA_{eq}) in 150 sec rather than to 21° and 26° prior to and after fouling (Figure 3.29).

Since reduction in surface restructuring hydrophilicity, indicative of a decreased amount of PEO at the interface, may diminish antifouling behavior, a 1.5 h pasteurization cycle was repeated on cleaned NuSil-(Si-PEO) surfaces. While somewhat higher than prior to cleaning, fouling mass was still reduced by 89% compared to bare SS (*i.e.* $F\% = 11$) (Figure 3.30). However, the persistence of the coating's antifouling action (*i.e.* $F\% = 0$) during the original five 1.5 h pasteurization cycles questions the necessity of standard clean-in-place processes.

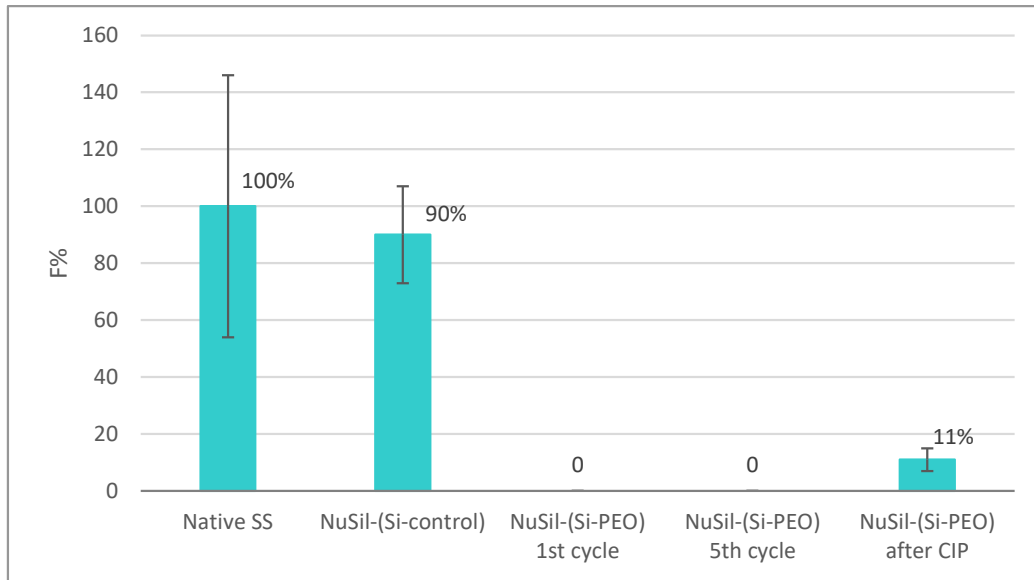


Figure 3.30. Performances of NuSil-(Si-PEO) surfaces compared to native stainless steel (SS).

3.5. *In situ* fouling study

Because of their excellent fouling resistance and durability during isothermal fouling tests, NuSil-(Si-PEO) coating was applied on V7 heat exchanger plates for *in situ* fouling tests. During this fouling test, plates experience non-isothermal conditions as they serve as heat transfer media. The coated plate was placed in PHE 2, in which the model fluid MF is heated to 85 °C (Chapter 2, p. 57) in position number eight among uncoated SS plates (Figure 3.31), with the coated side facing MF.

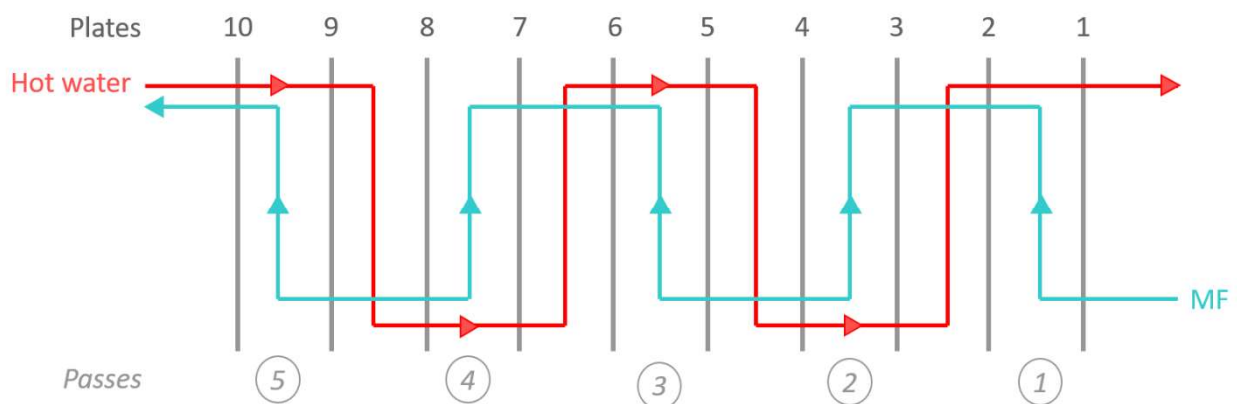


Figure 3.31. Flow diagram of the “heating” plate heat exchanger (PHE).

Plate number eight forms with plate seven the second-to-last MF pass. This particular position was chosen as it was previously demonstrated by Khaldi *et al.* (2015)⁹⁵ that this pass exhibits the largest

amount of fouling. Following one 1.5 h pasteurization cycle, this coated plate remained free of any trace of dairy fouling. In contrast, fouling was evident on all SS plates and was particularly prevalent, as expected on the plate in position seven (Figure 3.32).

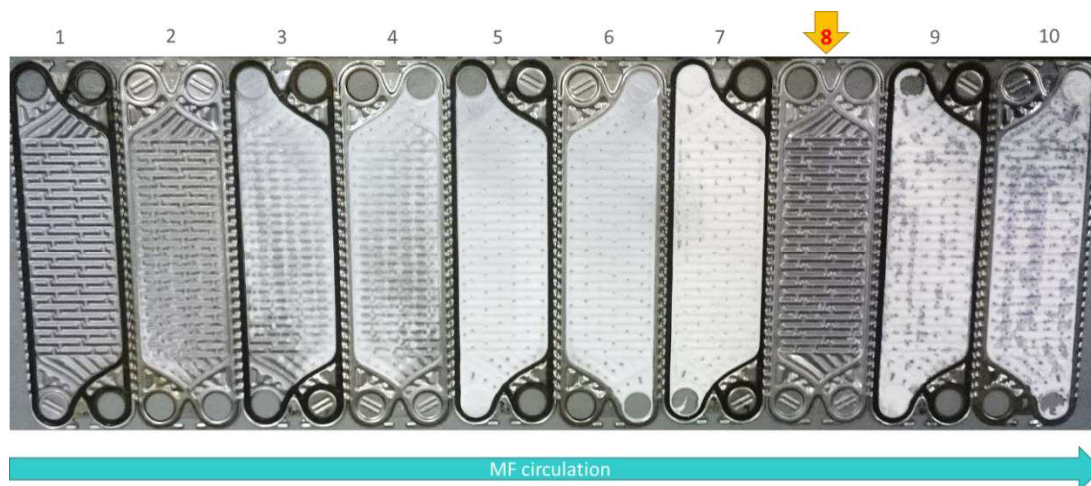


Figure 3.32. Fouling on PHE plates. Plate number 8 (arrow) remained free of deposits, while plate number 7, its counterpart, presents intense fouling.

3.6. Bacterial Adhesion Assay

Similarly to plasma coatings, the adhesion of pathogenic foodborne bacteria *S. aureus*, *S. enterica* and *L. monocytogenes* on NuSil-(Si-PEO) surfaces was evaluated. After 1 h, fluorescence microscopy images revealed no adhered bacterium to this surface regardless of the strain. In contrast bare SS presented 39.3 ± 5.6 , 76.4 ± 8.6 and 15.7 ± 4.4 CFU/microscope field for *S. aureus*, *L. monocytogenes* and *S. enterica* respectively (Figure 3.33). The bacterial resistance of NuSil-(Si-PEO) is consistent with that observed for “Si-PEO” directly coated onto glass substrates against various bacteria²⁹⁶.

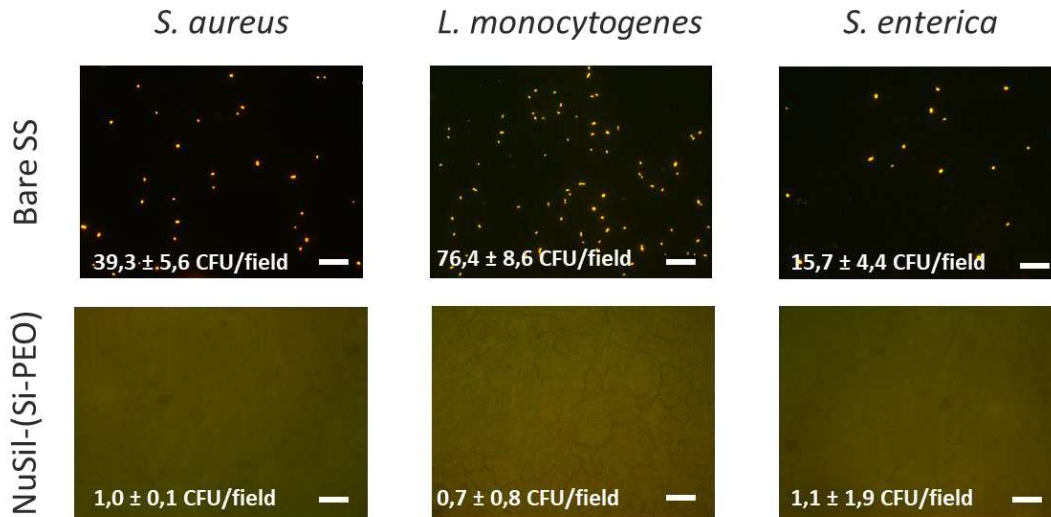


Figure 3.33. Bacterial adhesion on bare stainless steel and NuSil-(Si-PEO) coating. Scale bars represent 200 μm .

To summarize, modification of stainless steel (SS) processing equipment by a biomimetic amphiphilic PEO-silicone coating proved to be a suitable strategy for fouling mitigation. Under isothermal conditions, like those experienced by holding section walls, the coating exhibited no visible sign of dairy fouling during five pasteurization cycles. Additionally, PEO-modified silicone coated on a primed heat exchanger plate was subjected to in situ fouling conditions in the pilot pasteurizer. Likewise, there was no evidence of fouling after one 1.5 h pasteurization cycle. This antifouling behavior indicates that the coating can undergo PEO migration to the surface, even in a dairy fluid-based environment. Adhesion tests moreover showed the very good resistance of the coating to several strains of foodborne pathogenic bacteria, which is a key feature for any food-contacting material.

While not fouled, the coated coupons were subsequently treated by a standard clean-in-place process which somehow impacts the coating's water-driven surface restructuration abilities. Minor amounts of fouling were witnessed on the coating when subjected to an additional pasteurization cycle. However, given that no fouling neither bacterial adhesion was initially observed and, cleaning procedures could undoubtedly be adjusted to milder conditions to not only preserve the coating but to also decrease the use of harsh chemicals.

Conclusions

This chapter reported the surface characteristics and fouling behavior of three different biomimetic surfaces, namely slippery liquid infused surfaces, nano-rough plasma coatings and amphiphilic environment responsive coatings (Figure 3.34). SLIPS-like surfaces showed good fouling-release properties, however their long-term stability is compromised by oil shedding. Furthermore, nano-rough plasma coatings proved that surface nanostructures could considerably impact fouling adhesion on a substrate. Finally, amphiphilic environment responsive coatings exhibited excellent anti-fouling properties through five consecutive isothermal fouling tests and showed similar properties when applied to a heat-transfer surface.

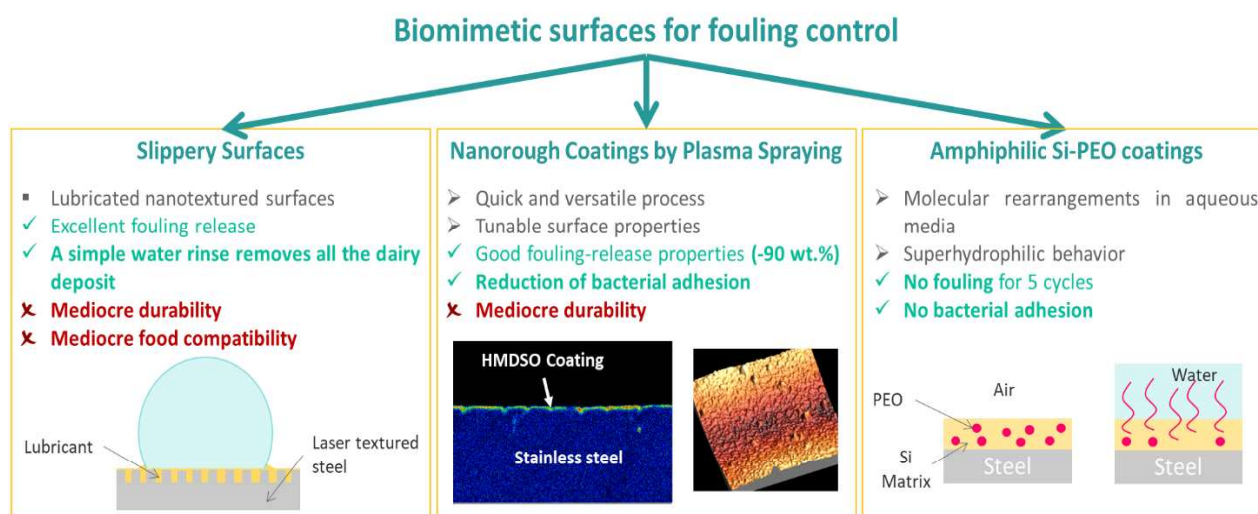


Figure 3.34. Biomimetic surfaces for fouling mitigation.

Overall, the interesting potential of those surfaces for fouling mitigation was demonstrated, although improvements might still be required to enhance their durability and suitability for food-related use. In all cases, the proposed surface modification could lead to significant changes in the CIP procedures, as SLIPS-like and plasma coatings could be cleaned simply with water, while amphiphilic Si-PEO coatings presented the best performance as they did not need cleaning at all and show moreover outstanding antibacterial properties.

Consequently, the use of such a coating in dairy processing could lead to significant financial and environmental saving through the reduction of cleaning costs and effluent production. Nevertheless, it is important to keep in mind that surface modifications themselves induce costs

and environmental impact, which should be considered. The next chapter will thus aim at evaluating the impact of the use of the amphiphilic antifouling coating on the pasteurization process global environmental impact through a Life Cycle Assessment (LCA) approach.

Chapter 4 - INFLUENCE OF SURFACE
MODIFICATION ON THE ENVIRONMENTAL
IMPACT OF PASTEURIZATION

Introduction

Food industries, which must sustain the growing worldwide population, are one of the largest industrial sector and energy consumer of the planet. They consequently are at the center of concerns about liquid, solid and gas waste emissions (*e.g.* CO₂, NO_x, NH₃, CH₄)³¹¹. Simultaneously, consumers, while demanding safe, high-quality products, are increasingly sensitive to the negative effects that current production patterns have on the environment^{312,313}. This growing awareness strengthens their choice of eco-friendly goods³¹². Consequently, manufacturers pay increasing attention to the environmental balance of their processes and need solutions to minimize it.

Life Cycle Assessment (LCA) is a well-known and powerful analytical tool which allows to evaluate the environmental impact of products and processes, while investigating the contribution of each stage of their lifetime, from cradle to grave³¹⁴. A significant number of LCA studies were carried out on milk and dairy processing^{315–319}, and most of them cover dairy production from farming to commercialization. It is thus generally reported that the major contributor to the environmental impact of dairy products is the farming stage^{315,320}. However, the heat-processing stages remains significant, especially regarding CO₂ emissions³¹⁵.

The amphiphilic coating presented in Chapter 3 was proven to have significant impacts on fouling, which could lead to the softening of cleaning conditions and consequently to savings in terms of environmental footprint. However, the coating process itself obviously has its own environmental impact, which should be taken into account when considering the effect of surface modification on pasteurization environmental balance.

Chapter 4 will therefore present an LCA study aiming at quantifying the true effect of antifouling amphiphilic coatings on the environmental balance of a pasteurization process by comparing a reference system (modelled after the pilot pasteurization unit used for fouling testing) to a modified system where the fouling-prone surfaces are coated with this coating.

1. The LCA Approach

1.1. About LCA

Attention have been paid to the impact of human activities on the environment since the XIXth century and the first Industrial Revolution. Ever since, the concept of sustainability (Figure 4.1) was given more and more attention, until becoming one of the main concerns of present-day societies.



Figure 4.1. Sustainability lies at the interface of environmental, economic and social considerations. In 1987, the Brundtland Report¹ stated that “*sustainable development is development that meets the needs of the present without compromising the ability of future generations to meet their own needs*”. This objective, together with the development of Industrial Ecology and Eco-design led to the adaptation and elaboration of several tools, like Functional Analysis and Life Cycle Concept, designed to ease the transition toward sustainable and responsible mass production³²².

Among these tools, Life Cycle Assessment (LCA) (Figure 4.2) is a multi-criteria analysis, which consists in identifying and quantifying all the material and energy flux for a given system, from cradle to grave, and to evaluate them in terms of potential environmental impacts³¹⁴. LCA, which is normalized at the European level by ISO standards 14 040 and 14044 – which can be used for a wide range of products and activities and for different purposes like eco-labeling, product design, hot-spots identification, diagnosis and decision making – rests on a precise and rigorous methodology.



Figure 4.2. The LCA Approach (adapted from Avnir.org³²³).

The first step of an LCA study is to clearly define its scope, paying particular attention to geographical localization, temporality, data representativeness and ground hypotheses³¹⁴. The establishment of clear system boundaries along with judicious ground hypotheses are indeed essential to the pertinence of the study and to the definition of the functional unit (FU). The FU is a key notion in LCA, and is defined as the quantity of service provided by the considered system over a certain amount of time. Thus, the FU allows to normalize the results in order to carry out comparisons with other systems.

The considered system is then subjected to a thorough life cycle inventory (LCI) during which all system inputs and outputs are indexed and quantified. At this point, it is often useful to breakdown the system in pertinent subsystems. Each item is then allocated to the relevant system or subsystem. Allocation is particularly important, especially if the study aims at identifying process hot-spots, *i.e.* steps where eco-optimization is the most needed³²⁴.

The results of the LCA analysis are then calculated through the processing of the LCI by a software which connects every LCI item to its potential environmental impact, by using existing databases and empirical calculation methods (*e.g.* Recipe, Impact2002+...). The environmental effect of each system and subsystem on different indicators (*e.g.* temperature increase, level of fine particulate

matter) is thus calculated, yielding impact scores (measured in points, Pts) in different impact categories (IC) like global warming, particulate matter formation, etc³¹⁴. According to their position in the causality chain, impact categories are generally classified between mid-point and end-point classes. Mid-point indicators quantify the effect of consumed inputs or produced outputs, whereas end-point indicators estimate the damage due to these consumptions or emissions (Figure 4.3). Impact categories are characteristic of a given calculation method, which should be chosen carefully according to their relevance toward the studied systems.

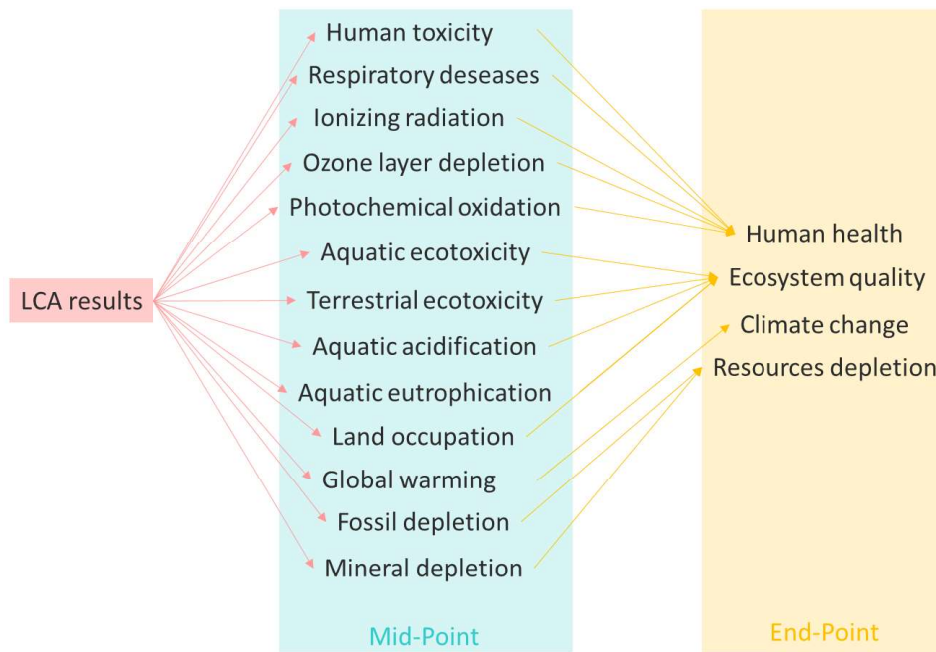


Figure 4.3. Examples of mid-point and end-point indicators.

Finally, the results from the LCA, in the form of scores, can be interpreted, allowing to perform an in-depth environmental diagnosis, to identify hot-spots in order to develop corrective solutions and eco-optimize the system.

1.2. Goals and scope of the present LCA study

The present study aims at performing comprehensive LCAs on two dairy pasteurization systems located in the north of France (Villeneuve d'Ascq) – a reference pasteurization process and a process where fouling-prone surfaces, *i.e.* heat-exchanger plates and holding section, have been

modified with the amphiphilic coating described in Chapter 3 (p. 114) – in order to highlight the effect of an antifouling coating on the environmental impact of a pasteurization unit.

For both systems, the life cycle assessment will consider the impact generated by inputs and outputs from the extraction stage to the waste treatment stage. However, bio-valorization and final wastes will not be taken into account (Figure 4.4).

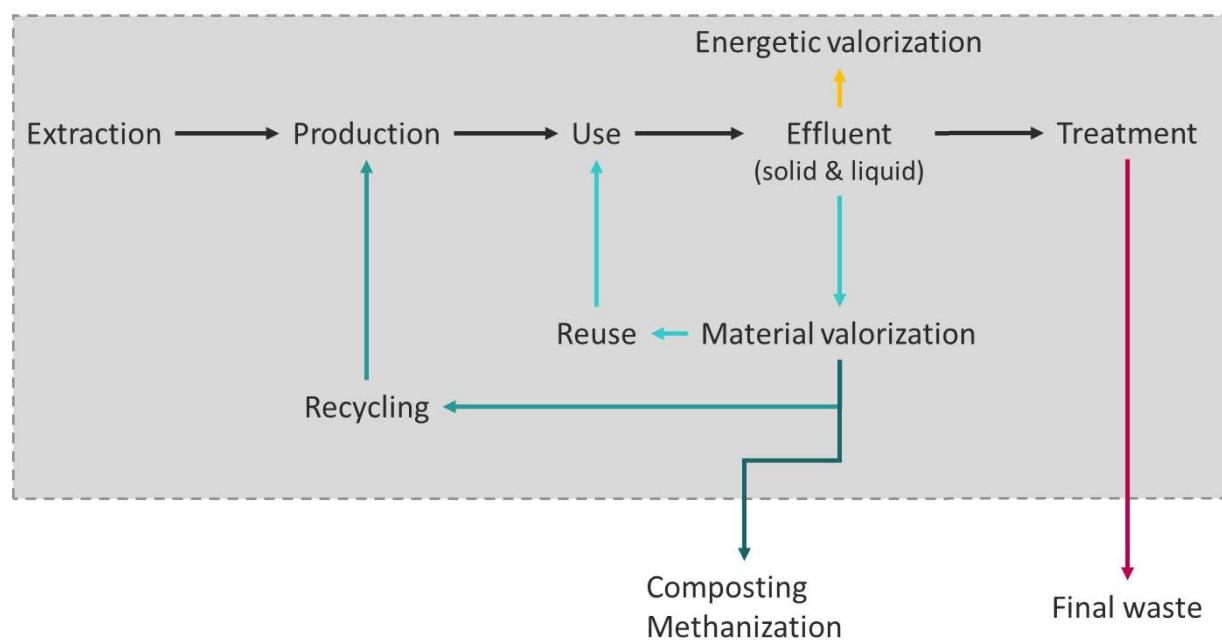


Figure 4.4. Considered aspects of the life cycle.

As previously stated, the careful choice of a functional unit (FU) is crucial for any LCA study. The FU is indeed the standard that will allow for the results to be exploited and compared with existing data. As presented in Table 4.1, the vast majority of dairy-related LCA studies use FUs based on milk or dairy mass or volume, as suggested by the International Dairy Federation (IDF)³¹⁸. It is noticeable that some authors use the notion of fat-and-protein-corrected milk (FPCM) or energy corrected milk (ECM), especially if the study is oriented toward nutritional considerations. Consequently, the FU used in the present study will be defined as 1 kg of pasteurized dairy model fluid (MF), treated in a pilot pasteurization unit located in north of France.

Table 4.1. Functional units used in the literature for LCA in the dairy industry.

Study	Functional Unit	Scope of the Study
Finnegan et al, 2016 ²	Kg of packaged dairy products	LCA of several milk derivatives in Ireland
Rafiee et al., 2016 ³¹⁸	Kg of pasteurized milk at the consumer's gate	LCA of pasteurized milk in Iran
Daneshi et al., 2014 ¹¹⁸	L of packaged medium-fat milk	LCA of packaged fluid milk in Iran
Gonzalez-Garcia et al., 2013 ³²⁵	Kg of ECM* including co-products	LCA of dairy derivatives in Portugal
Thoma et al., 2013 ³¹⁹	Kg of milk consumed in the US	LCA of the production and consumption of milk in the US
Vergé et al., 2013 ³²⁶	Kg of milk Kg of protein content	LCA of milk produced at the farm and processed milk in Canada
Fantin et al., 2012 ³²⁷	Kg of bottled milk	LCA of a dairy factory in Italy
Flysjö et al., 2011 ³²⁸	Kg of ECM* at farm gate	LCA of milk produced at the farm in Sweden
Gerber et al., 2011 ³²⁹	Kg of retailed FPCM**	Comparative LCA of retailed milk, International average vs. US average
Basset-Mens et al., 2009 ³³⁰	Kg of milk at farm gate	LCA of milk produced at the farm in New Zealand
Cederberg, 2009 ³³¹	Kg of ECM* at retail	Sweden, 1990 to 2005
Thomassen et al., 2008 ³³²	Kg of FPCM** at farm gate	Comparative LCA of organic vs. conventional milk in the Netherlands
Foster et al., 2007 ³³³	Kg of FPCM** at farm gate	LCA of processed milk in the UK
Vergé et al., 2007 ³³⁴	Kg of milk at farm gate	LCA of milk produced at the farm in Canada
Basset-Mens et al., 2005 ³³⁵	Kg of milk at farm gate	LCA of milk produced at the farm in New Zealand
Casey and Holden, 2005 ³³⁶	Kg of milk at farm gate	LCA of milk produced at the farm in Ireland
Cederberg and Flysjö, 2004 ³³⁷	Kg of milk at farm gate	LCA of milk produced at the farm in Sweden
Eide, 2002 ³¹⁵	Kg of milk	Comparative LCA of three dairy factories in Sweden
Haas et al., 2001 ²	Kg of milk at farm gate	Comparative LCA of intensive, extensive and organic milk in Germany

*ECM : energy corrected milk; **FCPM: fat and protein corrected milk.

1.3. Description of the investigated systems

For both systems, the LCA study was carried out from plant gate to holding outlet, meaning that the farming and packaging stages were excluded.

1.3.1. Reference pasteurization system (REF)

The reference pasteurization system (REF) is modelled after the pilot pasteurization unit described in Chapter 2 (p. 57) and presented in Figure 2.1. Briefly, it is composed of a stainless steel tank in which the model fluid (1% WPC, 100 ppm calcium in reverse osmosis water) is prepared, of a volumetric pump and of two plate heat-exchangers, PHE1 and PHE2 comprising twenty plates and ten plates, respectively. In both PHEs, the MF is heated by being circulated counter-current to hot water, which is heated in two closed loops circuits (CL1 and CL2) by saturated vapor produced by a boiler. The MF is circulated in the unit at 300 L/h and heated to 60°C by PHE1 and to 85°C by PHE2. At the outlet of PHE2, a holder, *i.e.* a thermally insulated pipe where the MF is maintained at pasteurization temperature during 15 s to ensure the destruction of pathogen micro-organisms, is connected. Due to the accumulation of fouling deposits in the PHEs and holding section, MF circulation must be interrupted every 1.5h and the system cleaned. The cleaning-in-place process involves a water pre-rinse, an alkaline cleaning (2% NaOH w./v), an intermediate water rinse, an acidic cleaning (2% HNO₃ w./v) and a final water rinse, before MF pasteurization can be resumed. The acidic and alkaline cleaning solutions are recirculated during the CIP stage, and fresh 200 L batches of those solutions are prepared every five 1.5 h pasteurization cycles. During thermal treatment and cleaning phases, the operating conditions of the unit are monitored and regulated through an electronic interface, *i.e.* a computer and several sensors (flow, pressure, temperature). REF can thus be broken down into three subsystems, namely “MF preparation”, “thermal treatment” and “cleaning in place” (Figure 4.5). For the smooth running of the study, each subsystem was further divided in sub-assemblies and complete SADT (Structured Analysis and Design Technique) diagrams are available in Annex VI.

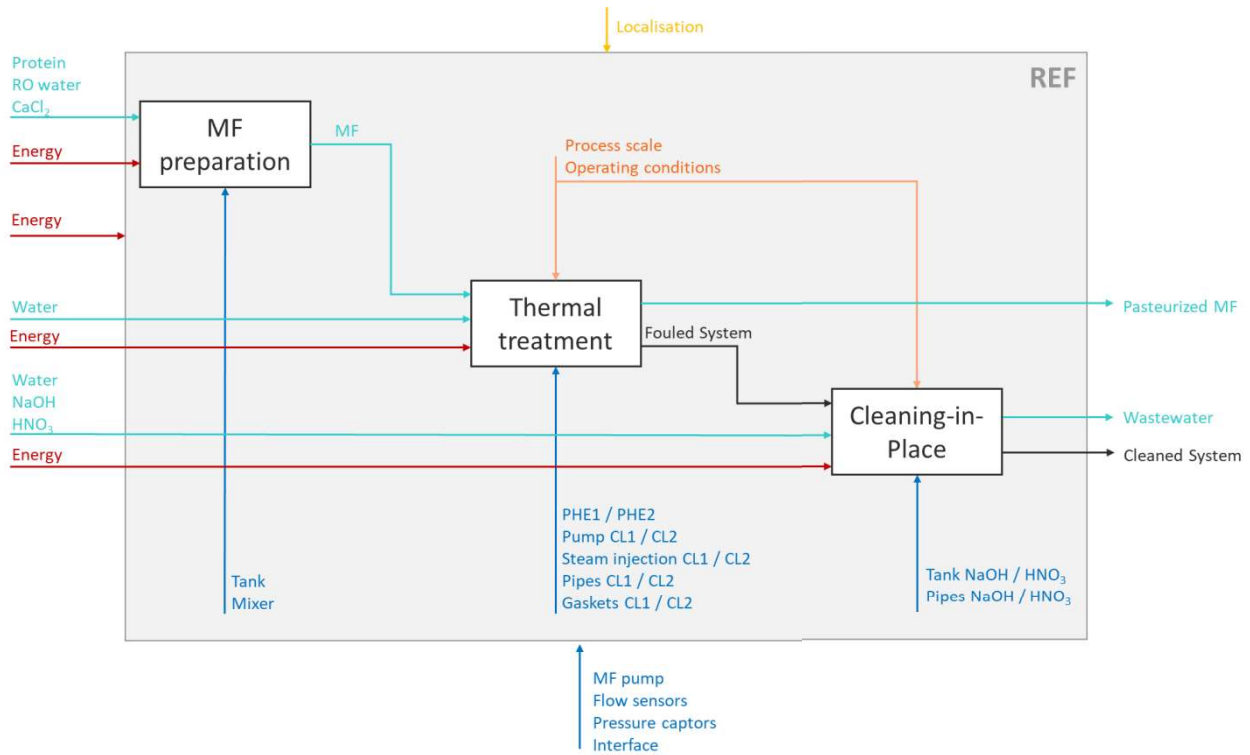


Figure 4.5. SADT diagram of the reference pasteurization system.

1.3.2. Modified System

The system where fouling-prone surfaces were treated with amphiphilic coating will be referred to as “Si-PEO”. In this system, the MF-exposed sides of the heat exchanger plates and the internal surface of the holder are primed with NuSil SP-120 (50 mL/m²) and spray-coated with the amphiphilic coating (300 mL/m²), as described in Chapter 3. The coating mixture is composed of hexane, RTV silicone adhesive MED-1137 and amphiphilic Si-PEO additive. The very good antifouling properties of the coating allow for continuous MF pasteurization during 7.5 h. This duration is a minimum and additional research is needed to apprehend the true lifetime of the coating. The present LCA study will thus consider that the fouling-prone surfaces are rinsed with tap water and re-coated after each 7.5h thermal treatment cycle. The Si-PEO system can thus be divided in four subsystems: “coating” (primer and coating formulations and applications), “MF preparation”, “thermal treatment” and “rinsing” (Figure 4.6).

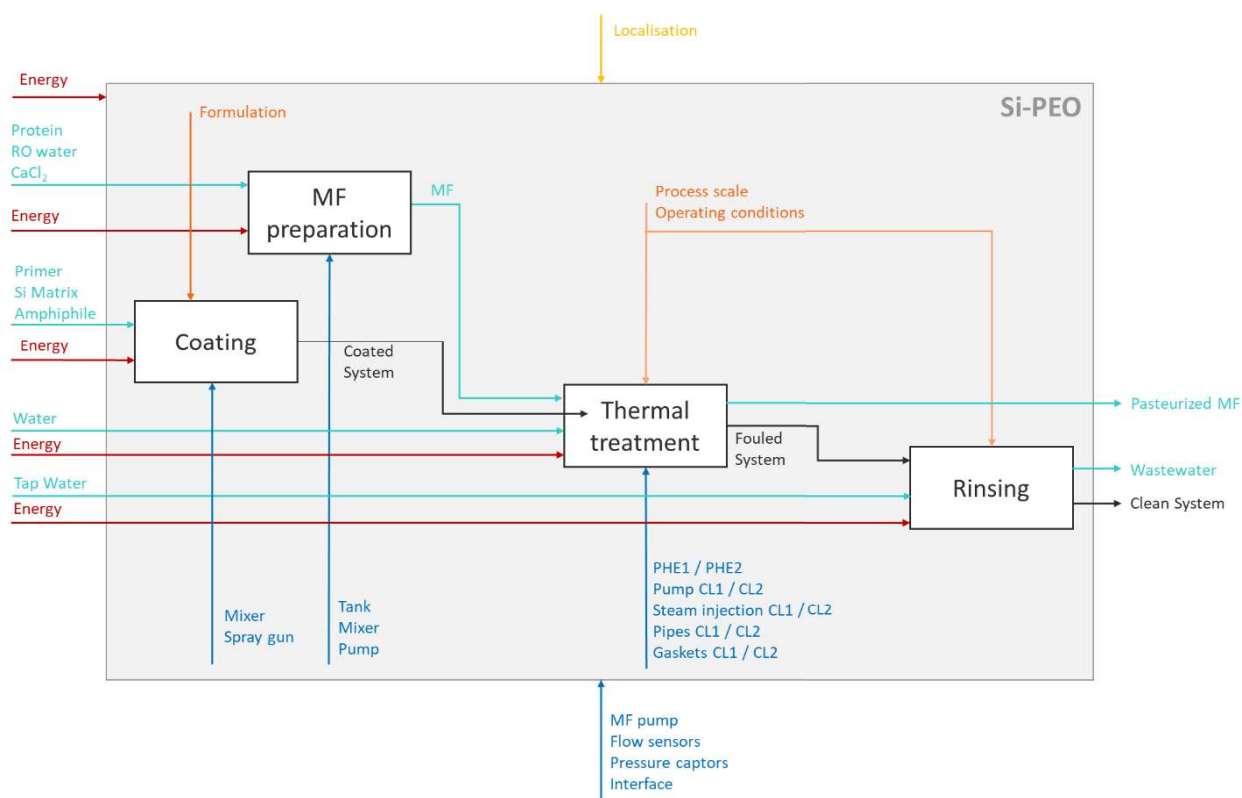


Figure 4.6. SADT diagram for the coated pasteurization system (Si-PEO).

1.4. Life Cycle Inventories (LCIs)

Life cycle inventories are the cornerstone of LCA studies, as they gather every inputs and outputs for each systems and subsystems, quantify them in terms of mass or amount and determines their origin and end of life scenarios. This section aims at presenting the general method and hypotheses used for the LCIs of the two considered systems.

1.4.1. Ground hypotheses

Accessing original data for manufacture, origin or end of life of every input of a system can be difficult, if not impossible in certain cases. Therefore, as established by Rafiee *et al.* (2016)³¹⁸, it is common to use literature data and to formulate hypotheses in order to complete LCA studies. In the present case, most of the data were collected directly from on-site measures and experimental details from the pilot unit. Nevertheless, a certain number of hypotheses still had to be formulated in order to best approach the missing data. They are detailed hereafter.

1.4.1.1. General Life cycle

The total lifetime of the pasteurization unit was estimated to 20 years, with 220 working days per year and continuous production (around-the-clock shifts patterns). The amount of MF pasteurized per day was calculated for each system, according to their respective production and cleaning patterns, which yielded a production rate of 4050 kg/day of pasteurized MF for REF versus 5850 kg/day of pasteurized MF for Si-PEO. These amounts were used in order to normalize the results before comparison. The origins of the supplies, which are directly linked to the environmental footprint of their respective transport stages, were set according to common-sense when not known with certainty. For example, the origin of chemicals like NaOH and HNO₃, purchased from large international companies, was set in Rotterdam (NL), which is the largest commercial harbor in Western Europe.

1.4.1.2. End of life

End of life (EoL) scenarios for metals, rubber and electronics were determined according to the 2014 French Environment and Energy Management Agency (ADEME) guidelines, in regard to the localization of the unit (Villeneuve d'Ascq, FR). Thus, all metallic supplies, like pipes and PHEs, were considered to be transported to the closest waste management facility and recycled at a rate of 50%, while pumps were recycled at a rate of 80%. Rubber supplies were considered to be collected and treated *via* thermal valorization at the same waste management facility. Computer hardwares were considered to be sent in a specialized electric and electronic waste (EEW) facility, located in Lesquin (FR) while other electrical equipment and wires were treated at another EEW facility in Tourcoing (FR). Wastewaters were considered to be treated in the closest municipal sewage treatment plant located in Marquette-lez-Lille (FR).

1.4.1.3. Electrical consumption

Electrical consumptions were calculated according to the devices specifications from manufacturer's sheets and to average data of the French energy mix from the most recent version of the Ecoinvent database.

1.4.1.4. Pasteurization Unit

About the pasteurization unit, metal infrastructures such as pipes or heat exchangers plates as well as pumps were considered to match the lifetime of the pasteurization unit, *i.e.* 20 years. The human labor relative to the building, operation and dismantlement of the unit was not taken into account. Rubber gaskets were considered to be replaced monthly. Reference weights for all electronic supplies (captors, interfaces...) were calculated according to their volume and a filling rate of 25%, among which half was plastic materials and the other half metal and reference electronic materials from the Ecoinvent database.

1.4.1.5. Si-PEO coating step

Synthesis routes were established for each component (hexane, STV silicon adhesive and amphiphile molecule). Only chemicals, solvents and catalysts were taken into account for the life cycle inventory, meaning that operating conditions (heating, stirring) were not. Indeed, these data were not available.

1.4.1.6. Allocation

Careful allocation of inputs and outputs to the right system or subsystem is crucial for result interpretation to be accurate and unbiased, especially when the aim is to identify hot-spots. Generally, allocation can easily be determined following common-sense, *e.g.* the NaOH solution, which is only useful during the CIP phase, should be allocated to the “cleaning-in-place” subsystem. However, the allocation of inputs that are useful in several subsystems can be delicate. Empirical allocation approaches for dairy processes have been developed through collection and compulsion of industrial data^{339,340}, but as they were based on very complex, multi-products plants, they could not be used in the present case. Consequently, it was decided that when it was possible, the problematic inputs would be distributed between the different subsystems proportionally to their respective use. For example, the boiler’s energetic consumption was shared between the “thermal treatment” and the “cleaning-in-place” (REF) or “rinsing” step (Si-PEO), in respect with the duration of each stage. Nevertheless, in some cases, as for the main pump and pressure sensors, this type of divided allocation was not possible. Thus, such items were considered apart from the subsystems to avoid unfair allocation, in a class named “Others”.

1.4.2. An example: LCI of the “thermal treatment subsystem”

For all subsystems of both systems, exhaustive lists of all infrastructure, consumables and energy inputs were realized, and each item allocated to the relevant subsystem. Table 4.2 presents, as an example, the LCI of the “thermal treatment” subsystem.

Table 4.2. Simplified LCI of the “thermal treatment” subsystem.

Input type	Name	Material	Unitary weight/amount	Origin	End of life
Infrastructure	CL1 pump 1 pce	Plastic Metal rubber	82 kg/ pce	Villeneuve d’Ascq (FR)	Recycling (St André, FR)
	CL2 pump 1 pce	Plastic Metal rubber	82 kg/ pce	Villeneuve d’Ascq (FR)	Recycling (St André, FR)
	CL1 pipes 12.17 m	316 L SS	1.7 kg/m	Lund (SE)	Recycling (St André, FR)
	CL2 pipes 12.7 m	316 L SS	1.7 Kg/m	Lund (SE)	Recycling (St André, FR)
	CL1 insulation 12.17 m	Rock wool	2.6 Kg/m	Grande Synthe (FR)	Cement plant (Templemars, FR)
	CL 2 insulation 12.7 m	Rock wool	2.6 Kg/m	Grande Synthe (FR)	Cement plant (Templemars, FR)
	CL1 gaskets 7 pce	Rubber	0.02 kg/pce	Grande Synthe (FR)	Valorization (St André, FR)
	CL2 gaskets 5 pce	Rubber	0.02 kg/pce	Grande Synthe (FR)	Valorization (St André, FR)
	Valves 4 pce	316 L SS	0.3Kg/pce	Villeneuve d’Ascq (FR)	Recycling (St André, FR)
	PHE 1 1 pce	316 L SS	16.64 Kg/pce	Lund (SE)	Recycling (St André, FR)
	PHE 2 1 pce	316 L SS	8.32 Kg/pce	Lund (SE)	Recycling (St André, FR)
	PHE stands 3 pce	316 L SS	1.2 Kg/pce	Lund (SE)	Recycling (St André, FR)
	PHE gaskets 60 pce	Rubber	0.02 Kg/pce	Grande Synthe (FR)	Valorization (St André, FR)
	Holding pipe 1 pce	316 L SS	4.6 Kg/m	Lund (SE)	Recycling (St André, FR)
	Holding insulation 4.4 m	Rock wool	2.6 Kg/m	Grande Synthe (FR)	Cement plant (Templemars, FR)
	Flow captor 2 pce	Plastic	0.17 kg/pce	Rotterdam (NL)	EEW* (Lesquin, FR)

	T° captor 4 pce	Electronic Metal Plastic Electronic Metal	0.14 kg/pce	Rotterdam (NL)	EEW (Lesquin, FR)
	Computer hardware 1 pce	Plastic Electronic Metal	8 kg/pce	Rotterdam (NL)	EEW (Tourcoing, FR)
	Wiring 100 m	Copper Plastic	0.03 Kg/m	Rotterdam (NL)	EEW (Lesquin, FR)
Energy	Electricity for pumps 1 cycle	/	2.4 kWh	French mix	/
	Electricity for boiler 1 cycle	/	53.7 kWh	French mix	/
	Electricity for data recording 1 cycle	/	0.016 kWh	French mix	/

After completing LCIs, data were processed and results classified as described below.

1.5. Method for the LCA analyses.

The LCA calculations were carried out with SimaPro 8.2.3 software and nominal environmental impacts were retrieved from the Ecoinvent 3.4. database. The choice of the calculation method – Recipe E 1.12 (Europe)³⁴¹ – was motivated by the pertinence of its indicators. Rafiee *et al.* (2016)³¹⁸ indeed showed that the most common indicator found in dairy-related LCA studies was global warming (also named “climate change” in some methods), which is one of the main focus of Recipe E. Details about impact categories of Recipe E 1.12 and their characterization can be found in Table 4.3.

Table 4.3. Overview of the chosen mid-point impact categories and their indicators (from Goedkoop *et al.* (2009)³⁴¹).

Impact category	Abbreviation	Indicator	Unit
Climate change (human health)	CCH	Infra-red radiative forcing*	W.yr/m ²
Ozone Depletion	OD	Stratospheric ozone depletion	Ppt.yr
Climate change (ecosystem)	CCE	Infra-red radiative forcing	W.yr/m ²
Human toxicity	HT	Hazard-weighted dose	-
Photochemical oxidant formation	POF	Photochemical O ₃ concentration	kg
Particulate matter formation	PMF	PM ₁₀ ** intake	kg
Ionizing radiation	IR	Absorbed dose	Man.Sv
Terrestrial acidification	TA	Base saturation	yr.m ²
Freshwater eutrophication	FE	Phosphorus concentration	yr.kg/m ³
Terrestrial ecotoxicity	TE	Hazard weighted concentration	m ² .yr
Freshwater ecotoxicity	FEX	Hazard weighted concentration	m ² .yr
Marine ecotoxicity	ME	Hazard weighted concentration	m ² .yr
Agricultural land occupation	ALO	Occupation	m ² .yr
Urban land occupation	ULO	Occupation	m ² .yr
Natural land transformation	NLT	Transformed area	m ²
Metal depletion	MD	Grade decrease	Kg ⁻¹
Fossil depletion	FD	Upper heating value	MJ

*Radiative forcing is the difference between received and emitted radiative energy for a given system, which is directly connected to greenhouse gases rates, **PM₁₀: Particles with diameters inferior to 10 μm.

2. Results of the life cycle assessment.

2.1. Life Cycle Assessment of the REF system.

The LCA study carried out on the reference system first allowed to establish its total environmental score, *i.e.* 62.5 μ pts/pasteurized MF kg. Detailed scores for the whole process as well as for all subsystems are available in Annex VII.

2.1.1. Impact categories selection.

In order to focus on relevant data, the impact categories (IC) representing less than 0.5% of the total “whole process” score were discarded, leaving eight IC to be discussed: Climate Change Human Health (CCH), Human Toxicity (HT), Particulate Matter Formation (PMF), Climate Change Ecosystem (CCE), Marine Ecotoxicity (ME), Natural Land Transformation (NLT), Metal Depletion (MD) and Fossil Depletion (FD).

2.1.2. Interpretation of the LCA results.

In order to demystify the relative contribution of each subsystem to the global impact of the process, the scores of each subsystem in the different IC were assessed (Figure 4.7) and the contribution of the subsystems in each IC (C%) were calculated through Equation 4.1. (Table 4.4).

$$C\% = \frac{\text{subsystem score}}{\text{Whole process score}} * 100 \quad \text{Equation 4.1.}$$

Considering the total impact of the pasteurization process (“whole process” category in the Figures), three impact categories stand out, namely CCH, CCE and HT which gather around 87 % of the global environmental impact. The preponderance of climate change-related scores witnessed here is in good accordance with literature data, as it is generally recognized that the dairy sector deeply impacts climate change through greenhouse gas emissions^{2,318}. It is however noteworthy that, in most reported dairy-related LCA studies, climate change is mainly impacted by the farming stage^{2, 316,318}, while the effect of the processing stage is minor in comparison. This is quite logical, as the cattle food production, which involves intensive cereal production (barley, wheat) and thus

high CO₂ emissions (as well as cattle itself, which produces high amounts of methane³¹⁸), is systematically allocated to the farming stage.

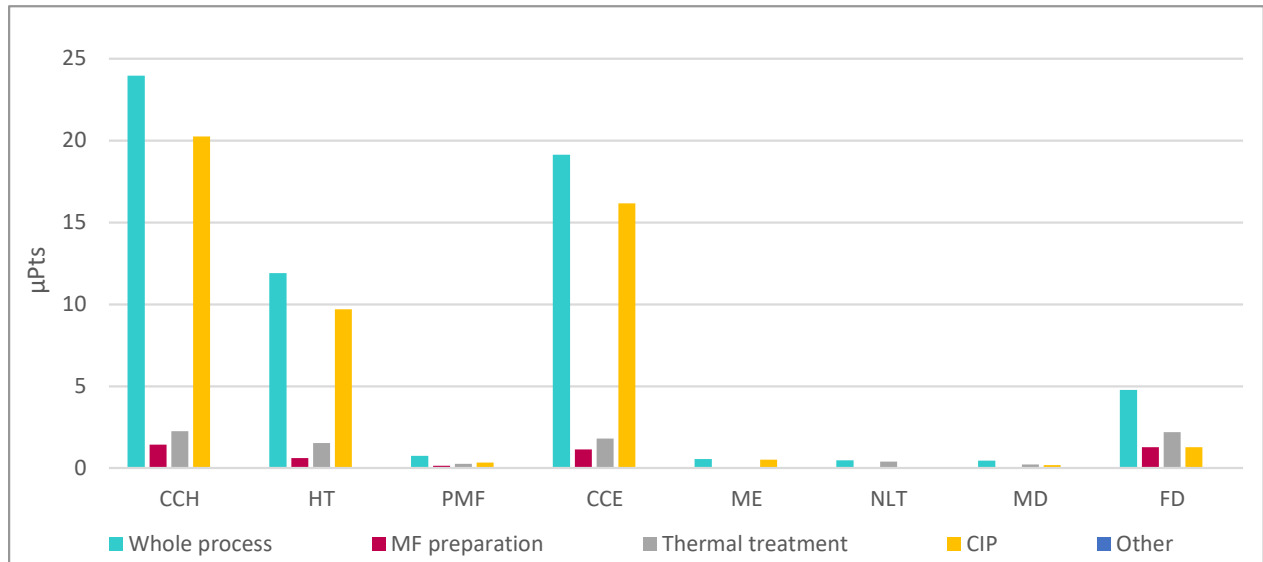


Figure 4.7. Impact of the different subsystems from REF on the selected ICs for 1 kg of pasteurized MF.

Consequently, the intake of processing stages in the climate change categories is seldom visible, superseded by that of farming. However, the present work only considers the pasteurization process, and thus the importance of climate change categories (human health and ecosystems) is well illustrated. CCH and CCE contributions indeed represent 68.8 % of the total environmental footprint of the whole pasteurization process.

The impact of the pasteurization process on HT can be linked to electricity consumption. Indeed, the impact category characterization report of the Recipe E method³⁴¹ states that the indicator of the Human Toxicity is the exposure of the population to carcinogenic substance, mostly from radioactive material and, according to the 2015 report of the French Electricity Transport Network (RTE), the nuclear-based power production represents a significant cut of the French the energy mix (76 %).

Table 4.4. Contribution of REF subsystems to each IC in regard of the total process score.

Impact category	MF preparation	Thermal treatment	Cleaning-in-Place	Other
Climate change Human Health	6.0 %	9,4 %	84,5 %	0,1 %
Human toxicity	5.2 %	12,9 %	81,6 %	0,3 %
Particulate matter formation	18.2 %	35,6 %	45,7 %	0,7 %
Climate change Ecosystems	6.0 %	9,4 %	84,5 %	0,1 %
Marine Ecotoxicity	2.3 %	3,9 %	93,6 %	0,2 %
Natural land transformation	13.0 %	83,7 %	0,5 %	3,0 %
Metal depletion	7.9 %	46,6 %	40,5 %	8,7 %
Fossil depletion	26.9 %	46,0 %	26,7 %	0,5 %
Total impact of the process	8.0 %	14,1 %	77,7 %	0,3 %

When considering the contribution of each subsystem from REF to the global impact of the system, it is clearly visible on Figure 4.7 and Table 4.4 that the CIP stage is by far the largest contributor to the impact of the whole process, as it gathers 77.7% of the total impact. The cleaning-in-place step moreover presents the highest scores in three preponderant impact categories, namely CCH, HT and CCE. These results are in good agreement with the findings of Rafiee *et al.* (2016)³¹⁸, who stated that the retreatment of wastewater from cleaning procedures played a key role in the footprint of dairy processing. Thus, CIP appears to be the hot-spot of the considered system, and the standards of ecological optimization would recommend to act on it, in order to decrease the general environmental footprint of the pasteurization process. Interestingly, this study showed no significant impact of REF on eutrophication. This is surprising, given that most LCA studies carried out on dairy processing report important scores in eutrophication, which is the nutrient enrichment (particularly nitrogen and phosphorus) of the aquatic environment, mostly due to the important production of nutrient-rich wastewater during the CIP stage^{316, 318, 327,330}. However, this IC was not selected for the present study, as the associated scores were too low to be considered significant (Annex VII). This difference from the literature might come from the fact that the implemented method (Recipe E 1.12) under-estimates the impacts linked to eutrophication in the present case. LCA calculation methods are indeed empirical, and rest on ground hypothesis that

shape the relative weight of impact categories. Detailed study of the Recipe E method characterization report indeed revealed that nitrogen emissions from sewage treatment plants (STP) were not considered in the calculation of the freshwater eutrophication impacts, and that only phosphorus emissions were included³⁴¹. Given that the MF used in the present work only contains phosphorus traces, the liquid effluents of REF, unlike classical milk and dairy processing wastewater, present a very low phosphorus content. It seems then logical that eutrophication is not a preponderant IC in the present case. It would then be interesting to process the data with different methods in order to compare the relative importance of the ICs.

The second most important contributor to the global impact of the REF system is the “thermal treatment” phase, presenting significant scores for several ICs, namely CCH, HT, CCE, NLT, MD and FD (Figure 4.7). This not surprising given that the main steel infrastructure of the unit, as well as most of the boiler’s energy consumption, were allocated to this subsystem. It can thus be considered that the impact of “thermal treatment” on NLT and MD are due to metal extraction, which involves intensive mining. The metallurgy processes involved in the fabrication of the metal infrastructures can also explain the high participation of “thermal treatment” on the climate change-related impact categories. The impact of this subsystem on FD is most likely due to the boiler’s electrical consumption, which is higher during the thermal treatment phase than during the cleaning phase. Indeed, cleaning solutions are circulated in close-loops, which means that the feed quickly warms up during the procedure and needs less and less energy to reach the temperature set-points. In contrast, the MF feed always stays cool, and requires more energy to be brought to working temperature. This important electrical consumption also explains the impact of “thermal treatment” on HT, due to the heavy weight of nuclear power production in the French energy mix.

The “MF preparation” subsystem represents 8.0 % of the total environmental footprint of the process. It particularly impacts CCH, CCE and FE, which is undoubtedly due to the allocation of powdered whey protein to this stage of the pasteurization process. This implies that all environmental repercussions of the protein powder production, including milk production at the farm, cattle feed (intensive agriculture) and further processing, are integrated to the “MF

preparation” stage. For similar reasons, “MF preparation” also represents 18.2 % and 13.0 % of the total impacts of the REF system on PMF and NLT respectively (Table 4.4).

2.1.3. End of life

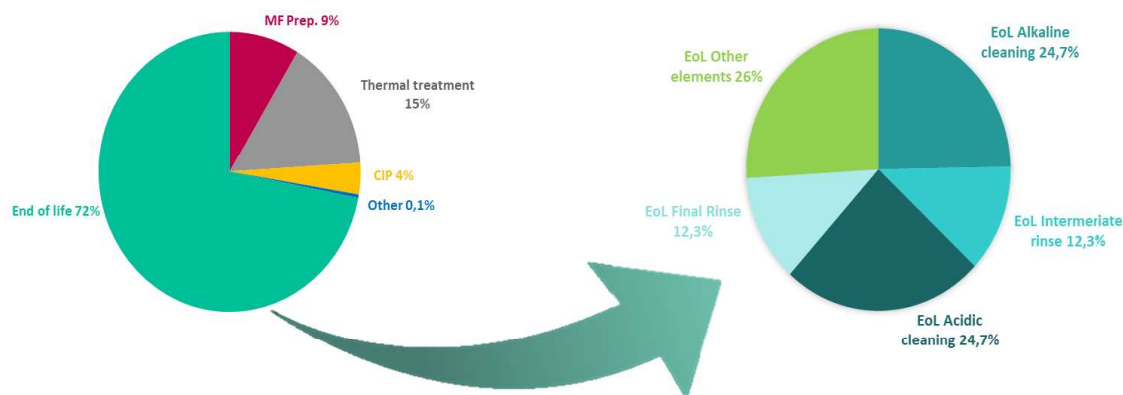


Figure 4.8. Contribution of the end of life to the total environmental impact of the REF system (left) and detailed composition of the end of life impact (right).

Close study of the LCA results demonstrated the preponderance of the end of life (EoL) in the global environmental impact of the pasteurization process, as shown on Figure 4.8, where all EoL-related contributions have been withdrawn from the subsystems contributions and gathered in a total “End of Life” category. Figure 4.8 further shows that 74% of these EoL impacts are due to the CIP stage wastewater retreatment, clearly highlighting how the CIP burdens the environmental footprint of the pasteurization process.

Overall, the LCA analysis carried out on the REF system allowed to highlight the overwhelming impact of the “cleaning-in-place” stage on the global environmental impact of the process, identifying it as a true hot-spot. The investigation of solutions to decrease the environmental footprint of the pasteurization process by modifying cleaning procedures is thus justified. The Si-PEO system, thanks to the antifouling properties of the amphiphilic coating, presents a softer cleaning scenario, i.e. just one tap water rinse every five 1.5h pasteurization cycles instead of a full cleaning-in-place procedure at the end of every 1.5h cycle (Figure 4.9). It may thus allow for a significant reduction of environmental impacts, as the impacts of the coating step do not cancel the benefits from the softening of the cleaning conditions. The following section aims at

answering this question by studying the results of the LCA study of the Si-PEO system and comparing it with that of the REF system.



Figure 4.9. Sequences of action for REF and Si-PEO systems, based on five 1.5h pasteurization cycles.

2.2. Life cycle assessment of Si-PEO system.

2.2.1. Interpretation of the LCA results.

The LCA study on the Si-PEO system allowed to calculate a global environmental score of 14.51 μ Pts/pasteurized MF kg. This represents a substantial decrease compared to that of the REF system (62.51 μ Pts/pasteurized milk kg). Thus, the antifouling properties of the coating allowed to decrease the unit’s environmental impact by 77%. Figure 4.10 moreover shows that Si-PEO is less impacting than REF in every impact category.

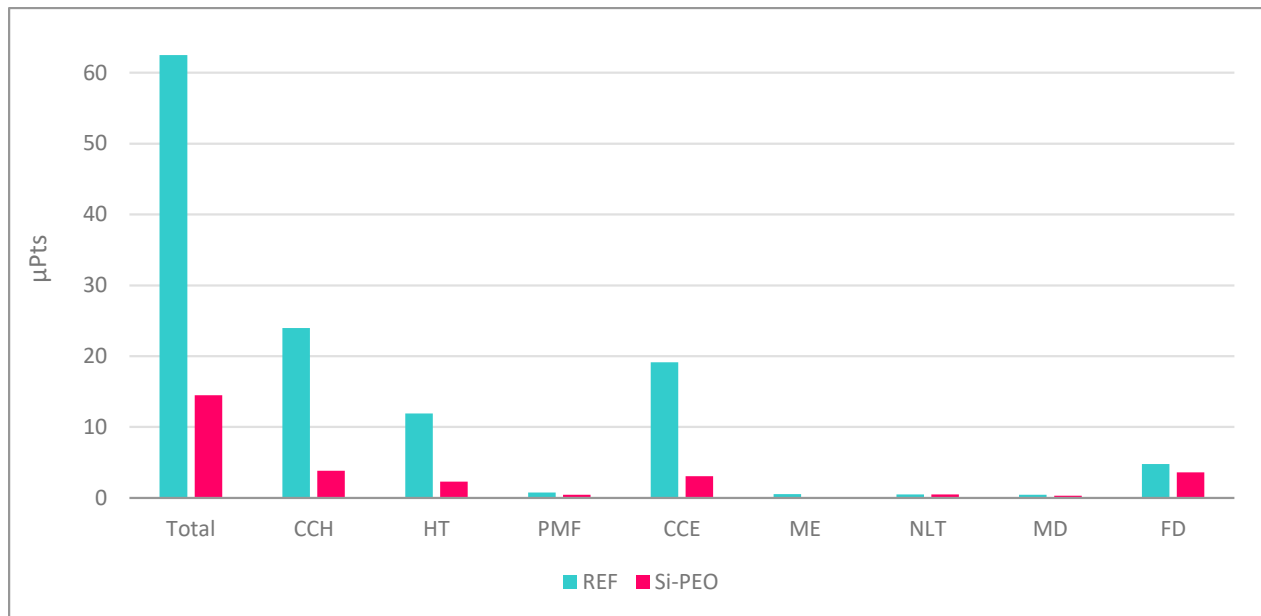


Figure 4.10. Comparison of the environmental impacts of REF and Si-PEO systems.

In order to demystify the causes of this striking decrease, the impact of all Si-PEO subsystems in the chosen IC were assessed (Figure 4.11) and their relative weights for each IC were calculated

(Table 4.5). As in the case of REF, the climate change-related IC (CCH and CCE) are well represented with 47.6 % of the total impact, followed by FD (24.5%) and HT (15.7%).

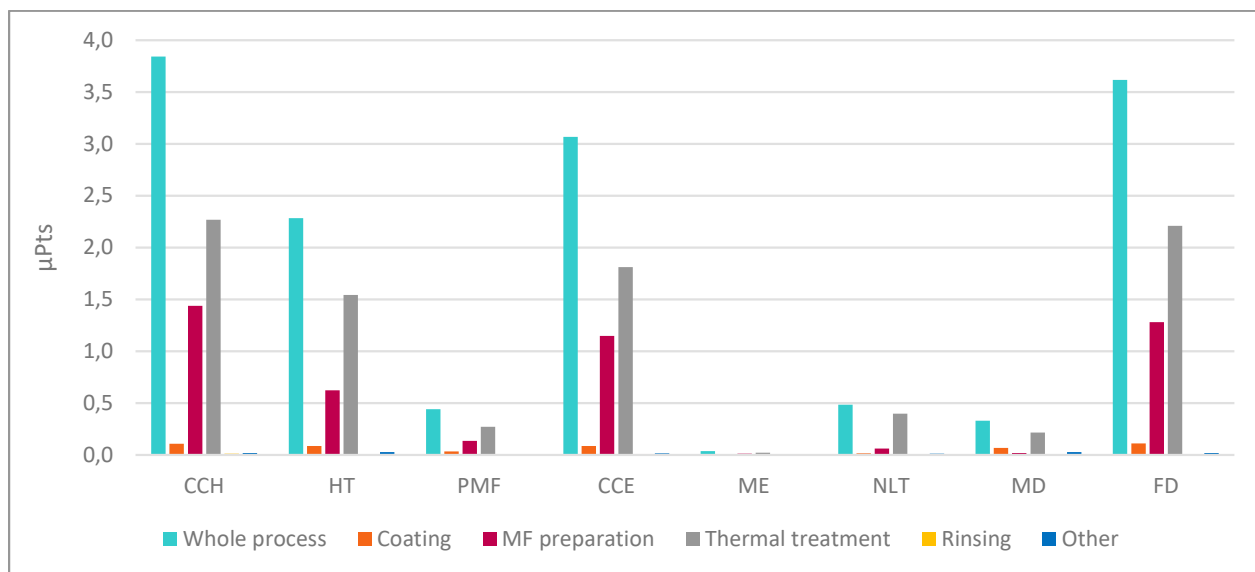


Figure 4.11. Impact of the different subsystems from Si-PEO on the selected ICs for 1 kg of pasteurized MF.

In the Si-PEO system, the “thermal treatment” subsystem is by far the major contributor to all considered impact categories and represents 61.2% of the total impact of the system. As mentioned previously, the impact of “thermal treatment” on NLT and MD can be considered as the consequence of metal mining. Furthermore, the boiler’s energetic consumption can explain the impact of “thermal treatment” on FD, CCH, CCE and PMF. Indeed, the emission of fine particles is strongly linked to energy and infrastructure production.

On the other hand, the high impacts of “MF preparation” (34.3% of the total impact) in all ICs are most likely linked to protein powder production involving traditional dairy farming and milk processing, as it was the case for REF.

By contrast, the “rinsing” step, which was substituted to the CIP procedure thanks to the antifouling properties of the coating, only represents 0.2% of the total impact. Indeed, as no fouling takes place during the pasteurization run, rinsing wastewater is only composed of plain tap water

and presents low nutrient content, requiring minimum treatments at the STP (low BOD and COD*) and inducing low environmental impact. From these results, it is clear that the use of the antifouling coating allowed to substantially reduce the cleaning-related environmental impact of the whole process.

Table 4.5. Impact of each subsystem to each IC for the Si-PEO system.

Impact category	Coating	MF preparation	Thermal treatment	Rinsing	Other
Climate change human health	2.8	37.5	58.9	0.3	0.5
Human toxicity	3.8	27.2	67.4	0.2	1.2
Particulate matter formation	7.2	30.6	61.0	0.1	0.9
Climate change ecosystems	2.8	37.5	58.9	0.3	0.5
Natural land transformation	3.3	12.5	82.1	0.1	2.1
Metal depletion	20.8	5.0	65.6	0.1	8.5
Fossil depletion	3.1	35.3	60.9	0.1	0.4
Total impact of the process	3.6	34.2	61.2	0.2	0.8

The coating step, which includes the synthesis of coating components and of the primer, the elaboration of the mixture and the coating application, represents 3.6% of the total impact. Its larger contribution is to MD (20.8%), most likely due to the use of Karstedt’s and Wilkinson’s catalysts during the synthesis of coating components, which contain platinum and rhodium). Nevertheless, considering all IC, the coating step brings a minor contribution to the total environmental impact.

Contrary to what was observed for the REF system, the EoL only represents a very small portion of the global impact of the Si-PEO environmental impact (Figure 4.12). This can be easily explained by the drastic decrease of wastewater production, due to the modification of the cleaning procedure.

* BOD: Biological Oxygen Demand, COD: Chemical Oxygen Demand

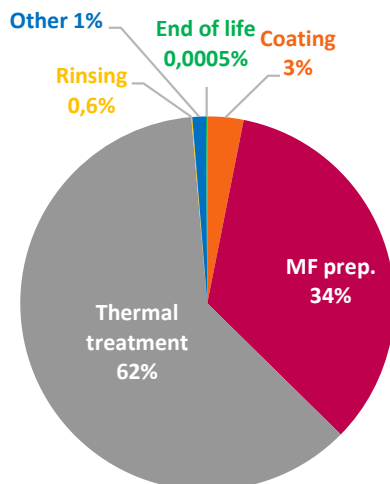


Figure 4.12. Contribution of the end of life to the environmental impact of the Si-PEO system.

2.2.2. Environmental impact of the coating

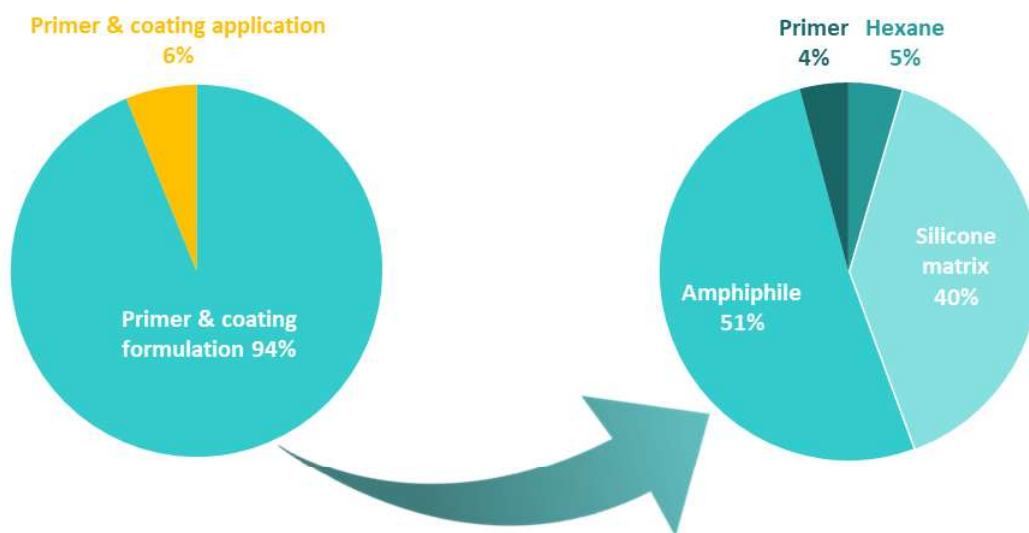


Figure 4.13. Contributions to the environmental impact of the “coating” subsystem (left) and to the primer and coating formulations (right).

Within the coating subsystem, Figure 4.13 shows that syntheses of the silicone matrix and of the amphiphile molecule are by far the most important contributors in terms of environmental footprint, which makes them the hot-spots of the coating stage. Indeed, their synthesis involves a significant number of solvents, petroleum-derived species and catalysts which undoubtedly play a role in this state of fact. In an effort to formulate a more eco-friendly coating, it would then be interesting to investigate greener alternatives for those two inputs.

Conclusions

At first, this LCA study was used for diagnosis purpose on the reference, uncoated pasteurization unit and allowed to emphasize the burden that is cleaning-in-place in the global environmental footprint of the process. It was indeed clearly demonstrated that the end of life of CIP wastewater was the main responsible for the impact of pasteurization on the environment.

The LCA performed on the modified system then permitted to highlight the benefits of fouling mitigation in terms of environmental impacts. Indeed, thanks to the very good antifouling properties of the amphiphilic coating, the Si-PEO system where the CIP hot-spot was replaced with milder and less frequent water rinses presented significantly lower impact scores regardless of the IC. Thus, fouling management and subsequent optimization of the cleaning procedure seem to be appropriate routes toward more ecofriendly pasteurization processes.

On the other hand, the LCA carried out on the Si-PEO system allowed to identify the silicon matrix and the amphiphile molecule as the most important contributors to the coating's environmental footprint. This is undoubtedly due to the involvement of oil-based solvents and chemicals in their synthesis. In order to limit the coating's impact on the environment, further LCA analyses could be carried out as optimization tools, allowing to assess and compare the environmental footprint of different formulations.

CONCLUSIONS AND OUTLOOKS

General Conclusion

The present work aimed at (i) designing novel antifouling surfaces targeting dairy fouling management, (ii) investigating their mode of action and (iii) evaluating the impact of an antifouling surface modification on the environmental footprint of dairy processing, based on a pilot-scale pasteurization unit.

First of all, a **fundamental study**, involving a vast range of advanced characterization techniques, allowed investigating the impact of the substrate's surface properties on isothermal dairy fouling. The analysis of dairy deposit amount and structure on six custom-made stainless steel model surface with different roughness and surface energies lead to the conclusion that surface properties were crucial to control in order to achieve fouling mitigation. Roughness and surface free energy showed significant impact on fouling amount and structure. Particularly, the observation of dairy deposit on textured SS highlighted interlocking phenomena, *i.e.* penetration and settlement of fouling agents inside the relief of a substrate, leading to tremendous increases in fouling amount *via* stabilization and anchorage of the base layers. Conversely, fouling on polished substrates exhibited fragile-looking and heterogeneous structures, due to the lack of anchorage points. On the other hand, reduction of SFE through fluorosilanization led to significant reduction of the fouling amount, regardless of the morphology of the substrate. **Thus, it appears that dairy fouling could be managed through surface modification, by SFE reduction and morphology tuning in order to avoid interlocking.**

In a second time, a biomimetic approach was adopted in order to design antifouling surfaces matching the above mentioned requirements. Three surfaces with different properties, namely liquid-infused surfaces, nano-rough plasma coatings and environment-responsive amphiphilic coatings were tested against isothermal dairy fouling in the pilot pasteurization unit, which allowed examining their antifouling performances and their mechanisms of action.

Liquid-infused surfaces, with their liquid hydrophobic interface, showed both antifouling and fouling release properties. They were cleaned by a simple water rinse, as opposed to the full CIP procedure necessary to get the same result on stainless steel. However, these surfaces exhibited poor durability, because of lubricant loss induced by the exposure to tangential flow. As these

liquid-infused surfaces need to be re-impregnated with oil between two consecutive pasteurization runs, the optimization of oil retention must then be pursued through surface morphology tuning, which could be achieved, for example, through electrochemical etching. Another enhancement axis for those surfaces would be the improvement of food-compatibility by replacing the fluorinated oil by bio-sourced lubricants, more suited to food applications.

Atmospheric pressure plasma spraying of HMDSO also revealed to be a suitable technique for the design of hydrophobic nano-rough coatings. The versatility of the implemented technique allowed to obtain coatings with different surface morphologies, which showed good fouling release properties when confronted to isothermal dairy fouling and allowed to replace classical CIP by a water rinse. Notably, the coating obtained with the PL6 conditions maintained these good performances during two consecutive fouling-rinsing cycles and showed interesting behavior towards bacterial adhesion. However, the other coatings did not manage to keep their fouling-release properties past the first pasteurization run, most likely due to the persistence of traces of fouling materials after the rinsing step, which acted like an anchoring layer for further deposits. Further research should thus focus on elucidating the link between plasma spraying conditions and the characteristics of the resulting coatings, which would lead to the possibility of finely tuning the surface properties and to accurately design functional coatings.

Amphiphilic PEO-modified silicone coatings, exhibiting water-driven surface restructuration, proved to be very efficient against isothermal fouling for five consecutive pasteurization cycles. Indeed, in water-based environment, the surface restructuration leads to the formation of a hydrated PEO layer, which prevents fouling agents from adhering to the substrate. The same performances were observed when the coating was applied to one of the PHE plates, indicating that the antifouling properties were maintained even for a heated substrate. It would then be interesting to assess the impact of the coating on heat transfer. Exposure to a full CIP procedure somewhat impaired the water-driven restructuration process. However, given the ability of this coating to prevent bacterial adhesion, the necessity of the classical CIP procedure is questionable.

Finally, the quantification of the impact of surface modification on the environmental footprint of a pasteurization process was performed by implementing a Life Cycle Assessment approach on two

systems, namely a reference pasteurization unit based on the pilot installation used for fouling testing and a similar unit where fouling-prone surfaces would be modified with the best performing antifouling surface discussed in this work, *i.e.* the amphiphilic PEO modified silicone coating. The results from this study showed that (i) the major part of the reference system's environmental impact was linked to the CIP stage, and that (ii) modifying the relevant surfaces with the antifouling coating allowed to reduce this impact by more than 70%.

Therefore, this work proved that surface modification could be an appropriate pathway toward fouling mitigation. This could lead to substantial reduction of environmental impact through the adaptation of cleaning procedures, which could most certainly benefit from the used of advanced techniques like coda wave interferometry²⁰⁵ or Fluid Dynamic Gauging (FDG)³⁴². Nevertheless, concerns about the long-term durability and food compatibility of the surface modification remain strong, particularly because the risk of contamination of the food product by coating elements stays high. Consequently, other approaches should be taken into consideration, such as the replacement of stainless steel by less fouling-prone materials.

Outlooks

As stated previously, another pathway toward dairy fouling management besides stainless steel surface modification could be the replacement of stainless steel by other heat-conducting materials, like graphite-based composites. Carbonaceous materials have indeed been investigated for heat transfer and processing applications since the 1930's as they are known for their lightness, heat stability, chemical resistance, excellent heat-transfer properties, and competitive prices^{343–347}.

Among others, graphite-polymer composites offer a wide range of possibilities for material and surface properties tuning, as it is possible to conceive a multitude of formulations. For instance, Rabah and El-Dighidy (1990)³⁴⁸ showed that different impregnants (copper, lead, carbon and PTFE) were suitable for block-graphite heat-exchangers design in simulated superphosphate plant. Literature is rich in similar examples of graphite-based materials designed for heat transfers^{349–351}. Moreover, Stancl and Zitny (2010)¹³¹ demonstrated the antifouling properties of a pure graphite electrode for milk direct Ohmic heating in a lab-scale installation. However it appeared that no study has been carried out on the potential antifouling properties of graphite-based composites.

This is why some preliminary experiments were carried out, to see if this concept could work. Two commercial impregnated graphite materials – Graphilor® XC and Graphilor® XTH (Mersen, France) – were submitted to fouling tests and bacterial adhesion tests, in order to assess their fouling behaviors. These results have been submitted to the *International Dairy Journal* and are currently under revision.

Prior to fouling and microbiology testing, the wettability (WCA), surface energy (SFE) and arithmetic mean roughness (Ra) of both composites were assessed. Their surface properties are presented in Table C.1. Bulk densities were calculated on at least 12 measurements for each material, following Equation C.1 where D is the density (kg/m^3), m the mass of a sample (kg), and V its volume (m^3).

$$D = \frac{m}{V} \quad \text{Equation C.1}$$

Obviously, both graphite-based composites exhibit much lower bulk densities than stainless steel, and their values are consistent with the literature³⁵². Lightness is a crucial feature for equipment designers and manufacturers, as it impacts transport and processing costs.

Table C.1. Water contact angle (WCA), total surface free energy (γ^{total}) with dispersive (γ^{D}) and polar (γ^{P}) parts, arithmetic mean roughness (Ra), and bulk density of the studied materials.

Samples	WCA (°)	γ^{total} (mN/m)	γ^{D} (mN/m)	γ^{P} (mN/m)	Ra (μm)	Bulk density (kg/m^3)
NAT	84.2 ± 2.6	39.0 ± 2.6	36.0 ± 0.8	3.1 ± 1.8	0.05 ± 0.01	7701.3 ± 221.9
XC	124.7 ± 2.6	48.8 ± 5.7	48.22 ± 3.6	0.6 ± 2.0	0.54 ± 0.16	1945.0 ± 12.1
XTH	116.8 ± 1.8	49.1 ± 1.7	49.1 ± 1.47	0.0 ± 0.2	0.27 ± 0.06	1972.9 ± 6.4

Drop shape analyses allowed establishing the high hydrophobicity of the two composites with WCA of $124.7 \pm 2.6^\circ$ and $116.8 \pm 1.8^\circ$ for XC and XTH surfaces, respectively. Stainless steel water contact angle was measured at $84.0 \pm 1.6^\circ$, which classifies it as borderline hydrophobic. The SFE of XC and XTH SFE values were found to be higher than that of stainless steel (48.8 ± 5.7 mN/m and 49.1 ± 1.7 mN/m, respectively, versus 39.0 ± 2.6 mN/m), but they exhibit very low polar components (0.6 ± 2.0 mN/m for XC and 0.0 ± 0.2 mN/m for XTH). The arithmetic roughness of the composites (0.54 and 0.27 μm) was found to be significantly higher than that of stainless steel (0.05 μm), in agreement with SEM observations (Figure C.1).

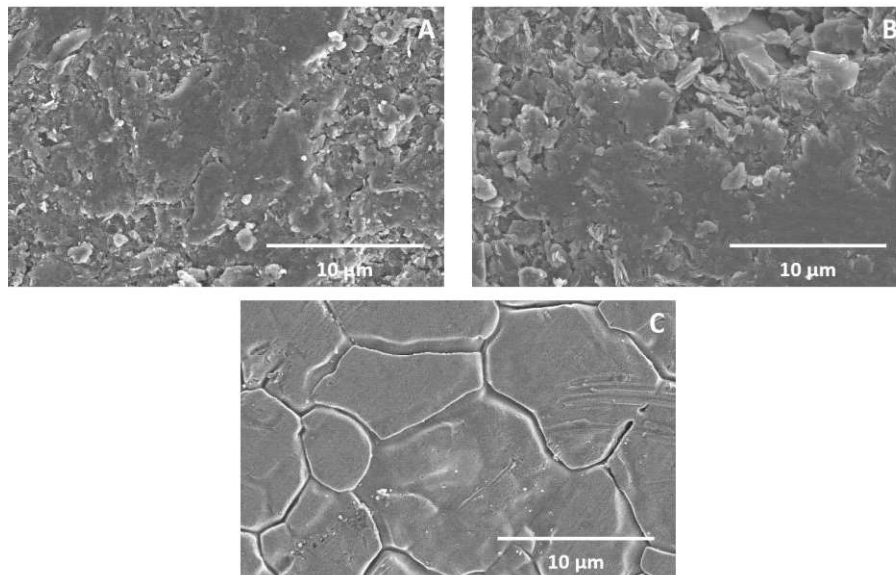


Figure C.1. SEM micrographs of Graphilor® XC (A), Graphilor® XTH (B), and native stainless steel (C).

Both composites and SS reference then underwent isothermal fouling tests with or without rinsing in the pilot pasteurizer. The results of each surface in terms of fouling density (mg/cm^2) as well as the percentage of deposit removed by water rinsing are presented in Table C.2.

Table C.2. Fouling densities of native stainless steel and graphite-based composites, before and after rinsing (mean \pm SD).

Surface	Fouling density (mg/cm^2)	Fouling density (mg/cm^2)	Percentage of deposit removed by rinsing
	Before rinsing	After rinsing	
NAT	92.0 ± 1.5	75.7 ± 1.6	18%
XC	132.4 ± 12.4	7.0 ± 0.9	95%
XTH	91.9 ± 4.0	5.2 ± 0.8	94%

Figure C.2 clearly shows that the graphite-based composites do not present substantial antifouling properties, *i.e.* they do not prevent deposit build-up. Indeed, the fouling density of XTH coupons ($91.9 \pm 4.0 \text{ mg}/\text{cm}^2$) does not significantly differ from that of stainless steel ($92.0 \pm 1.5 \text{ mg}/\text{cm}^2$) and XC surfaces even showed an increased fouling density of $132.4 \pm 12.4 \text{ mg}/\text{cm}^2$. Those results are consistent with the literature, as it has been reported that hydrophobic surfaces, such as PTFE, do not necessary prevent dairy fouling formation and can even enhance fouling amounts^{116,118}. The Ra value of XC, which is higher than that of stainless steel, can also be an explanation for the fouling enhancement. Increased roughness is generally known as a fouling promoting factor^{127, 133, 138,206}. However, the rinsing step revealed noticeable differences between the studied materials. Indeed, the 20 min hot water rinsing only removed 18% of the deposit on SS (fouling density of SS from $92.0 \pm 1.5 \text{ mg}/\text{cm}^2$ down to $75.7 \pm 1.6 \text{ mg}/\text{cm}^2$), while it removed 95% and 94% of the deposits present on XC and XTH, respectively. Thus, both composites exhibit remarkable fouling-release properties. These good performances could have been forecast by considering the low polar components of the composites' surface energy, which is generally known to ease fouling cleaning^{102,127}.

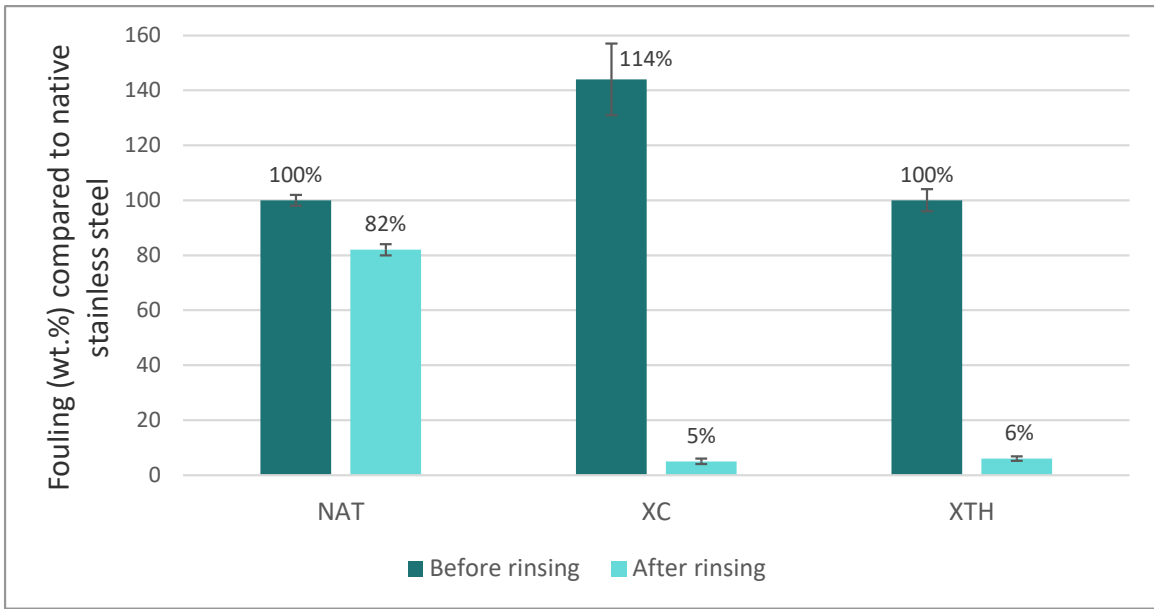


Figure C.2. Fouling performances of native stainless steel (NAT) and graphite-based composites before and after rinsing (XC and XTH).

Cross-section X-ray mappings of fouled stainless steel and composites without rinsing (Figure C.3) allowed to closely examine deposit structure and chemical composition. Native stainless steel exhibits a dendritic-looking deposit. Protein and calcium are found along the same patterns, however Ca particles are well-visible, especially at the top of the fouling layer. This is in good agreement with previous findings on isothermal fouling from similar dairy solutions^{32,206}. Indeed, while studies of long-time fouling on heat-transfer surfaces report calcium accumulation and crystallization near the substrate-deposit interface^{25,66}, Jimenez *et al.* (2013)³² showed that, on a non-heated substrate, proteins deposit first and calcium does not crystallize at the interface but takes part to the build-up as a binder.

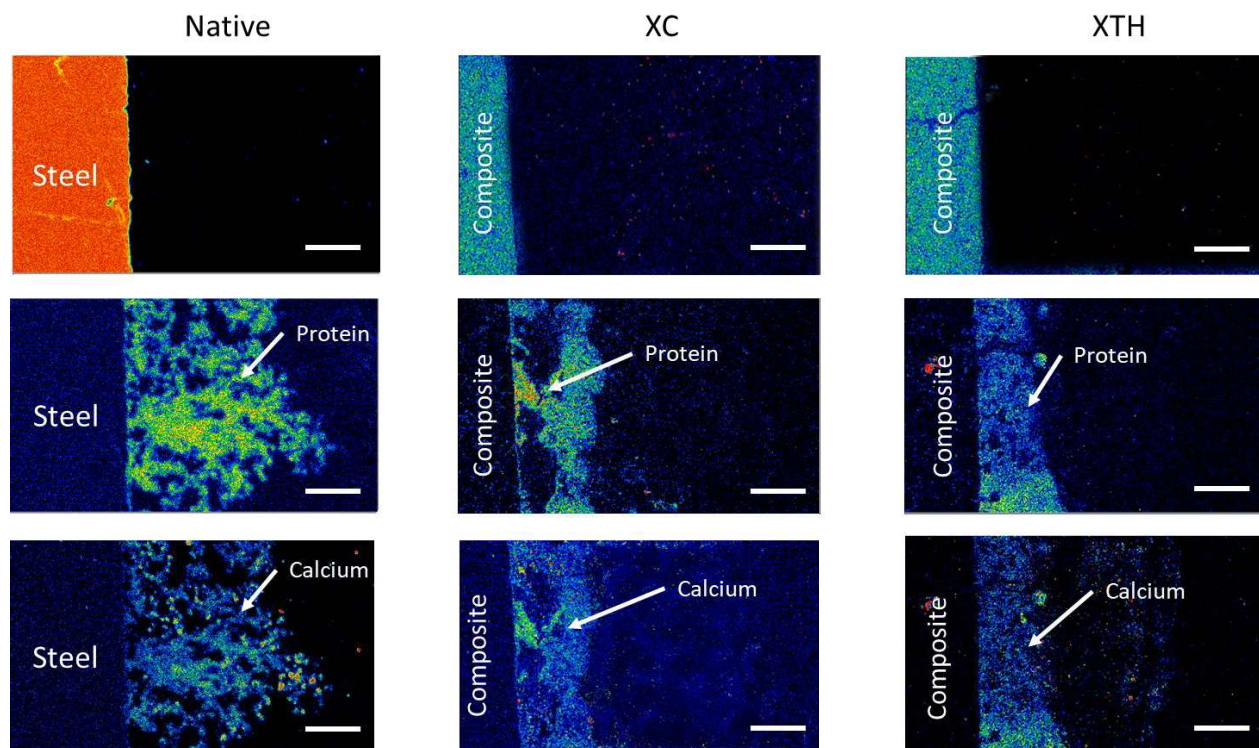


Figure C.3. Cross-section X-Ray mappings of native stainless steel and of both composites (XC and XTH), after fouling.

The aspect of deposits on XC and XTH substrates is radically different. The deposits look heterogeneous, with dense portions and medium (XTH) to large cavities (XC). This type of structure is particularly vulnerable to cohesive failure. It is most likely that this susceptibility to failure, together with the weak substrate-deposit adhesion strength generally attributed to hydrophobic substrates, explains the observed fouling-release properties. From a chemical point of view, fouling on composites is comparable to fouling on stainless steel, except that no calcium particles are found on the composites. Those results are consistent with existing literature, which states that substrate surface properties not only impact the cleanability of fouling, but also its structure and chemistry^{30,132}.

Finally, both composite materials were thus tested for bacterial adhesion, in order to evaluate their hygienic features. Figure C.4 shows that the nature of the surface greatly and significantly impacts bacterial adhesion. First of all, the three studied strains, namely *S. aureus*, *L. monocytogenes* and *Salmonella enterica* showed very different adhesion levels on stainless steel. *L. monocytogenes* presents the highest adhesion rate (76.4 ± 8.6 CFU/microscope field) on native stainless steel

compared to *S. aureus* (39.3 ± 5.6 CFU/microscope field) and *Salmonella enterica* (15.7 ± 4.4 CFU/microscope field).

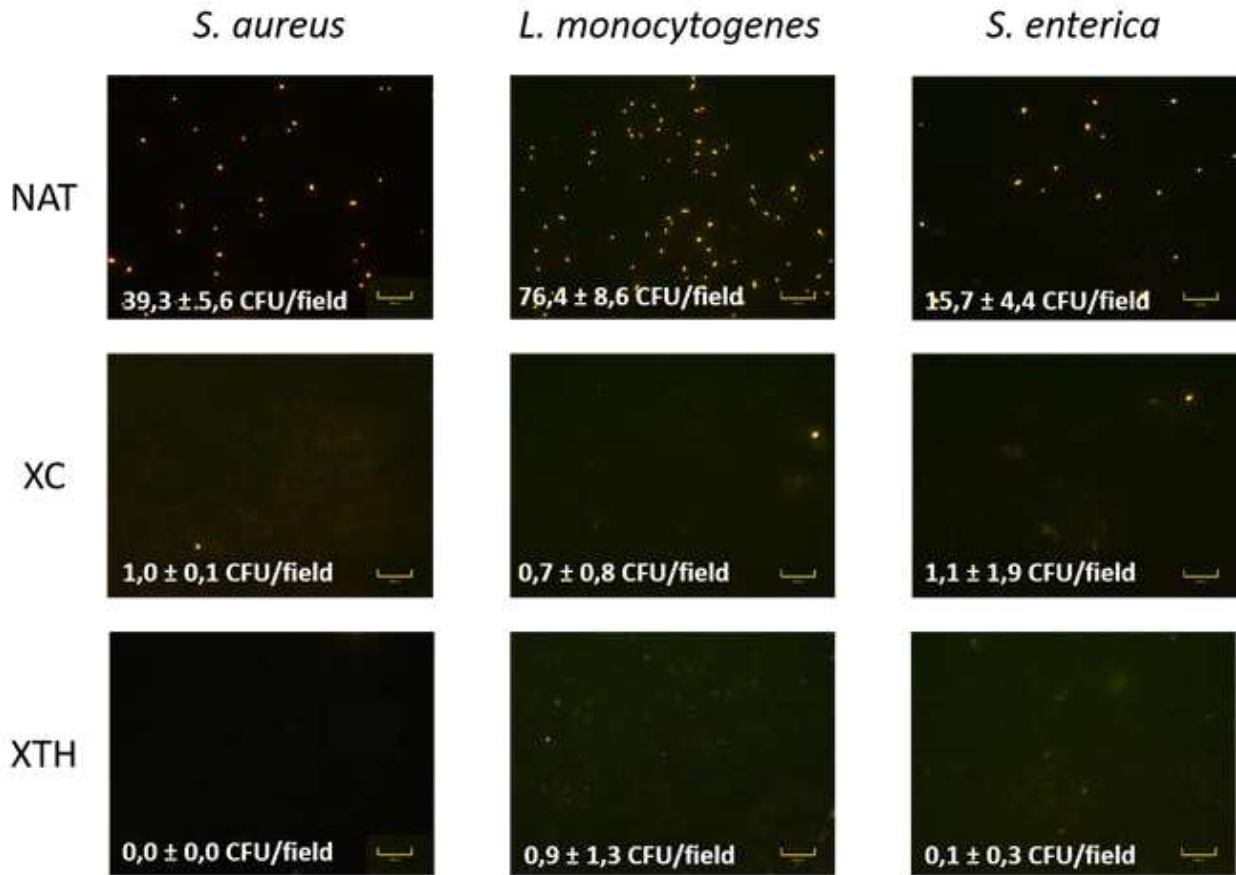


Figure C.4. Fluorescence micrographs and CFU/field values (mean \pm SD) of native stainless steel (NAT) and composites (XC and XTH), after one hour of adhesion with *S. aureus*, *L. monocytogenes* and *S. enterica*. The scale bars correspond to 200 μ m.

On the other hand, both XC and XTH composites exhibited remarkably low CFU counts compared to stainless steel, even though their roughness features were *a priori* rather unfavorable. Medilanski *et al.* (2000)²²⁶ indeed showed that increased roughness induces higher micro-organism adhesion. The present results therefore point toward a great impact of surface properties on bacterial adhesion, which has been previously reported²²⁵. However, other sources stated that surface energy and hydrophobicity cannot be considered as good adhesion predictors. Sinde and Caraballo (2000)²²² indeed witnessed higher adhesion levels of *Salmonella* and *Listeria* strains on hydrophobic rubber and on PTFE. Nevertheless, hydrophobic materials have also been

shown to prevent bacteria persistence through fouling-release properties^{149,227}, which could explain the good performances of XC and XTH surfaces regarding bacterial adhesion.

The strong potential of graphite-based composites for fouling management applications in food processing is established. The tested commercial composites, Graphilor® XC and Graphilor® XTH, indeed exhibited very good cleanability compared to the stainless steel control, in spite of their higher arithmetic mean roughness. Both composites also exhibited remarkably low bacterial adhesion rate. Thus, the combination of good physical properties (lightness and chemical resistance), good thermal conductivity together with the interesting fouling-release and hygienic properties demonstrated here, makes graphite composites promising candidates for the design of cost-effective processes and eco-friendly industrial equipment for thermal processes.

Overall, it seems that surface modification of stainless steel as well as its replacement by other materials are suitable pathways to achieve fouling mitigation in dairy industries. Both approaches have their advantages and drawbacks. Indeed, durability and food-compatibility, which are at the heart of concerns when dealing with surface modifications such as coating, are less problematic when considering material replacement. On the other hand, in this case, main issues would be heat conduction and mechanical properties. Further research should thus pursue both possibilities, while keeping in mind their respective drawbacks, in order achieve efficient, safe and durable fouling mitigation.

REFERENCES

- [1] Delgado. Rising Consumption of Meat and Milk in Developing Countries Has Created a New Food Revolution. *J. Nutr.* **2003**, *133* (11), 3907S–3910S.
- [2] Finnegan, Goggins, Clifford, and Zhan. Global Warming Potential Associated with Dairy Products in the Republic of Ireland. *J. Clean. Prod.* **2016**.
- [3] Food and Agriculture Organization of the United Nations. 2016.
- [4] European Dairy Association. 2018.
- [5] Khaldi. Etude Du Lien Entre La Physico-Chimie de Dérivés Laitiers et Leur Aptitude à l'Encrassement Lors Du Traitement Thermomécanique En Echangeur de Chaleur, 2016.
- [6] Lalande, and Rene. Fouling by Milk and Dairy Product and Cleaning of Heat Exchange Surfaces. In *Fouling Science and Technology*; Melo, Bott, Bernardo, Eds.; NATO ASI Series; Springer Netherlands, 1988; pp 557–573.
- [7] De Jong. Impact and Control of Fouling in Milk Processing. *Trends Food Sci. Technol.* **1997**, *8* (12), 401–405.
- [8] Tamime. John Wiley & Sons, 2009; Vol. 13.
- [9] Özbay, and Demirer. Cleaner Production Opportunity Assessment for a Milk Processing Facility. *J. Environ. Manage.* **2007**, *84* (4), 484–493.
- [10] Boxler. Fouling by Milk Constituents and Cleaning of Modified Surfaces, Technischen Universität Carolo-Whilhelmina zu Braunschweig, 2014.
- [11] Guinée, Heijungs, De Koning, Van, Geerken, Van Holderbeke, Vito, Eder, and Delgado. Environmental Impact of Products (EIPRO) Analysis of the Life Cycle Environmental Impacts Related to the Final Consumption of the EU25. **2006**.
- [12] Sadeghinezhad, Kazi, Dahari, Safaei, Sadri, and Badarudin. A Comprehensive Review of Milk Fouling on Heated Surfaces. *Crit. Rev. Food Sci. Nutr.* **2014**, *12* (55), 1724–1743.
- [13] Georgiadis, Rotstein, and Macchietto. Optimal Design and Operation of Heat Exchangers under Milk Fouling. *AIChE J.* **1998**, *44* (9), 2099–2111.
- [14] Westhoff. Heating Milk for Microbial Destruction: A Historical Outline and Update. *J. Food Prot.* **1978**, *41* (2), 122–130.
- [15] Holsinger, Rajkowski, and Stabel. Milk Pasteurisation and Safety: A Brief History and Update. *Rev. Sci. Tech. Int. des Epizoot.* **1997**, *16* (2), 441–466.
- [16] Augustin, and Udabage. Influence of Processing on Functionality of Milk and Dairy Proteins. *Adv. Food Nutr. Res.* **2007**, *53*, 1–38.
- [17] Van Asselt, Vissers, Smit, and De Jong. In-Line Control of Fouling. *Proc. Heat Exch. Fouling Clean.* **2005**.
- [18] Tuoc. Fouling in Dairy Processes; Elsevier: Amsterdam, 2015; pp 533–556.
- [19] Polat. Integrated Approach to Whey Utilization through Natural Zeolite Adsorption/Desorption and Fermentation. **2009**.
- [20] Havea, Singh, and Creamer. Characterization of Heat-Induced Aggregates of β -Lactoglobulin, α -Lactalbumin and Bovine Serum Albumin in a Whey Protein Concentrate Environment. *J. Dairy Res.* **2001**, *68* (3), 483–497.
- [21] Lindmark-Månsson, Timgren, Aldén, and Paulsson. Two-Dimensional Gel Electrophoresis of Proteins and Peptides in Bovine Milk. *Int. Dairy J.* **2005**, *15* (2), 111–121.
- [22] Dalglish. Denaturation and Aggregation of Serum Proteins and Caseins in Heated Milk. *J. Agric. Food Chem.* **1990**, *38* (11), 1995–1999.
- [23] Jeurnink, Verheul, Stuart, and De Kruif. Deposition of Heated Whey Proteins on a Chromium Oxide Surface. *Colloids surfaces B Biointerfaces* **1996**, *6* (4–5), 291–307.
- [24] Karlsson, Wahlgren, and Trägårdh. β -Lactoglobulin Fouling and Its Removal upon Rinsing and by SDS as Influenced by Surface Characteristics, Temperature and Adsorption Time. *J. Food Eng.* **1996**, *30* (1), 43–60.
- [25] Changani, Belmar-Beiny, and Fryer. Engineering and Chemical Factors Associated with Fouling and Cleaning in Milk Processing. *Exp. Therm. Fluid Sci.* **1997**, *14* (4), 392–406.
- [26] Premathilaka, Hyland, Chen, and Bansal. A Study of the Effects of Surface Chemistry on the Initial Deposition Mechanisms of Dairy Fouling. *Food Bioprod. Process.* **2006**, *84* (4), 265–273.
- [27] Santos, Nylander, Schillén, Paulsson, and Trägårdh. Effect of Surface and Bulk Solution Properties on the Adsorption of Whey Protein onto Steel Surfaces at High Temperature. *J. Food Eng.* **2006**, *73* (2), 174–189.
- [28] Rosmaninho, and Melo. Effect of Proteins on Calcium Phosphate Deposition in Turbulent Flow as a Function of Surface

- Properties. *Exp. Therm. Fluid Sci.* **2007**, *32* (2), 375–386.
- [29] Rosmaninho, and Melo. Calcium Phosphate Deposition from Simulated Milk Ultrafiltrate on Different Stainless Steel-Based Surfaces. *Int. Dairy J.* **2006**, *16* (1), 81–87.
- [30] Mauermann, Eschenhagen, Bley, and Majschak. Surface Modifications—application Potential for the Reduction of Cleaning Costs in the Food Processing Industry. *Trends Food Sci. Technol.* **2009**, *20*, S9–S15.
- [31] Kananeh, Scharnbeck, Kück, and Rübiger. Reduction of Milk Fouling inside Gasketed Plate Heat Exchanger Using Nano-Coatings. *Food Bioprod. Process.* **2010**, *88* (4), 349–356.
- [32] Jimenez, Delaplace, Nuns, Bellayer, Deresmes, Ronse, Alogaili, Collinet-Fressancourt, and Trainel. Toward the Understanding of the Interfacial Dairy Fouling Deposition and Growth Mechanisms at a Stainless Steel Surface: A Multiscale Approach. *J. Colloid Interface Sci.* **2013**, *404*, 192–200.
- [33] Ikeguchi. Transient Non-Native Helix Formation during the Folding of β -Lactoglobulin. *Biomolecules* **2014**, *4* (1), 202–216.
- [34] Tolkach, and Kulozik. Reaction Kinetic Pathway of Reversible and Irreversible Thermal Denaturation of β -Lactoglobulin. *Lait* **2007**, *87* (4–5), 301–315.
- [35] Labouré, Cases, and Cayot. Heat Induced β -Lactoglobulin Polymerization: Role of the Change in Medium Permittivity. *Food Chem.* **2004**, *85* (3), 399–406.
- [36] Relkin, and Mulvihill. Thermal Unfolding of B-lactoglobulin, A-lactalbumin, and Bovine Serum Albumin. A Thermodynamic Approach. *Crit. Rev. Food Sci. Nutr.* **1996**, *36* (6), 565–601.
- [37] Schmitt, and Hardy. Etude de La Coacervation Complexe Entre La Beta-Lactoglobuline et La Gomme d’acacia En Solution Aqueuse, Institut National Polytechnique de Lorraine: Nancy, 2000, Vol. PhD.
- [38] Mulvihill, and Donovan. Whey Proteins and Their Thermal Denaturation—a Review. *Irish J. Food Sci. Technol.* **1987**, *11* (1), 43–75.
- [39] Sakiyama, Tanino, Urakawa, Imamura, Takahashi, Nagai, and Nakanishi. Adsorption Characteristics of Tryptic Fragments of Bovine Beta-Lactoglobulin on a Stainless Steel Surface. *J. Biosci. Bioeng.* **1999**, *88* (5), 536–541.
- [40] Sakiyama, Aya, Embutsu, Imamura, and Nakanishi. Protease Susceptibility of Beta-Lactoglobulin Adsorbed on Stainless Steel Surface as Evidence of Contribution of Its Specific Segment to Adsorption. *J. Biosci. Bioeng.* **2006**, *101* (5), 434–439.
- [41] Gotham, Fryer, and Pritchard. B-lactoglobulin Denaturation and Aggregation Reactions and Fouling Deposit Formation: A DSC Study. *Int. J. food Sci. Technol.* **1992**, *27* (3), 313–327.
- [42] Petit, Six, Moreau, Ronse, and Delaplace. Beta-Lactoglobulin Denaturation, Aggregation, and Fouling in a Plate Heat Exchanger: Pilot-Scale Experiments and Dimensional Analysis. *Chem. Eng. Sci.* **2013**, *101*, 432–450.
- [43] Khaldi, Croguennec, André, Ronse, Jimenez, Bellayer, Blanpain-Avet, Bouvier, Six, and Bornaz. Effect of the Calcium/Protein Molar Ratio on β -Lactoglobulin Denaturation Kinetics and Fouling Phenomena. *Int. Dairy J.* **2018**, *78*, 1–10.
- [44] Xiong. Influence of PH and Ionic Environment on Thermal Aggregation of Whey Proteins. *J. Agric. Food Chem.* **1992**, *40* (3), 380–384.
- [45] Petit, Herbig, Moreau, and Delaplace. Influence of Calcium on β -Lactoglobulin Denaturation Kinetics: Implications in Unfolding and Aggregation Mechanisms. *J. Dairy Sci.* **2011**, *94* (12), 5794–5810.
- [46] Itoh, Nagata, Toyomasu, Sakiyama, Nagai, Saeki, and Nakanishi. Adsorption of β -Lactoglobulin onto the Surface of Stainless Steel Particles. *Biosci. Biotechnol. Biochem.* **1995**, *59* (9), 1648–1651.
- [47] Visser, and Jeurnink. Fouling of Heat Exchangers in the Dairy Industry. *Exp. Therm. Fluid Sci.* **1997**, *14* (4), 407–424.
- [48] Lyster. The Composition of Milk Deposits in an Ultra-High-Temperature Plant. *J. Dairy Res.* **1965**, *32* (2), 203–208.
- [49] Skudder, Thomas, Pavey, and Perkin. Effects of Adding Potassium Iodate to Milk before UHT Treatment: I. Reduction in the Amount of Deposit on the Heated Surfaces. *J. Dairy Res.* **1981**, *48* (1), 99–113.
- [50] Tsuge, Tanaka, Yoshizawa, and Kuraishi. Reactive Crystallization Behaviour of Calcium Phosphate with and without Whey Protein Addition. *Chem. Eng. Res. Des.* **2002**, *80* (1), 105–110.
- [51] Dey, Bomans, Müller, Will, Frederik, and Sommerdijk. The Role of Prenucleation Clusters in Surface-Induced Calcium Phosphate Crystallization. *Nat. Mater.* **2010**, *9* (12), 1010.
- [52] Anema. Effect of Milk Solids Concentration on the PH, Soluble Calcium and Soluble Phosphate Levels of Milk during Heating. *Dairy Sci. Technol.* **2009**, *89* (5), 501–510.
- [53] Wu, Zhuang, and Nancollas. Heterogeneous Nucleation of Calcium Phosphates on Solid Surfaces in Aqueous Solution. *J. Biomed. Mater. Res. Part A* **1997**, *35* (1), 93–99.
- [54] Andritsos, Yiantsios, and Karabelas. Calcium Phosphate Scale Formation from Simulated Milk Ultrafiltrate Solutions. *Food Bioprod. Process.* **2002**, *80* (4), 223–230.

- [55] Morison, and Tie. The Development and Investigation of a Model Milk Mineral Fouling Solution. *Food Bioprod. Process.* **2002**, *80* (4), 326–331.
- [56] Rosmaninho, and Melo. Protein–calcium Phosphate Interactions in Fouling of Modified Stainless-Steel Surfaces by Simulated Milk. *Int. Dairy J.* **2008**, *18* (1), 72–80.
- [57] Khaldi, Blanpain-Avet, Guérin, Ronse, Bouvier, André, Bornaz, Croguennec, Jeantet, and Delaplace. Effect of Calcium Content and Flow Regime on Whey Protein Fouling and Cleaning in a Plate Heat Exchanger. *J. Food Eng.* **2015**, *147*, 68–78.
- [58] O’Kennedy, and Mounsey. The Dominating Effect of Ionic Strength on the Heat-Induced Denaturation and Aggregation of β -Lactoglobulin in Simulated Milk Ultrafiltrate. *Int. Dairy J.* **2009**, *19* (3), 123–128.
- [59] Maas, Lalande, and Hiddink. In *Fouling and Cleaning in Food Processing*; 1985; pp 217–225.
- [60] Epstein. Thinking about Heat Transfer Fouling: A 5×5 Matrix. *Heat Transf. Eng.* **1983**, *4* (1), 43–56.
- [61] Belmar-Beiny, and Fryer. Preliminary Stages of Fouling from Whey Protein Solutions. *J. Dairy Res.* **1993**, *60* (4), 467–483.
- [62] Bohnet. Fouling of Heat Transfer Surfaces. *Chem. Eng. Technol.* **1987**, *10* (1), 113–125.
- [63] Bansal, and Chen. A Critical Review of Milk Fouling in Heat Exchangers. *Compr. Rev. Food Sci. Food Saf.* **2006**, *5* (2), 27–33.
- [64] Toyoda, Schreier, and Fryer. In *Proceedings of Fouling and Cleaning in Food Processing*; 1994; pp 222–229.
- [65] Georgiadis, and Macchietto. Dynamic Modelling and Simulation of Plate Heat Exchangers under Milk Fouling. *Chem. Eng. Sci.* **2000**, *55* (9), 1605–1619.
- [66] Bansal, and Chen. In *ECI Symposium Series : Proceedings of 6th International conference on Heat Fouling and Cleaning Challenges and Opportunities*; Muller-Steinhagen, Malayeri, Watkinson, Eds.; Kloster Isree, Germany, 2005; Vol. RP2, pp 149–157.
- [67] Belmar-Beiny, Gotham, Paterson, and Fryer. The Effect of Reynolds Number and Fluid Temperature in Whey Protein Fouling. *J. Food Eng.* **1993**, *19* (2), 119–139.
- [68] Boxler, Augustin, and Scholl. Influence of Surface Modification on the Composition of a Calcium Phosphate-Rich Whey Protein Deposit in a Plate Heat Exchanger. *Dairy Sci. Technol.* **2013**, *94* (1), 17–31.
- [69] De Jong, Bouman, and Linden. Fouling of Heat Treatment Equipment in Relation to the Denaturation of β -Lactoglobulin. *Int. J. Dairy Technol.* **1992**, *45* (1), 3–8.
- [70] Delplace, Leuliet, and Tissier. Fouling Experiments of a Plate Heat Exchanger by Whey Proteins Solutions. *Food Bioprod. Process. Trans. Inst. Chem. Eng. Part C* **1994**.
- [71] Delplace, Leuliet, and Levieux. A Reaction Engineering Approach to the Analysis of Fouling by Whey Proteins of a Six-Channels-per-Pass Plate Heat Exchanger. *J. Food Eng.* **1997**, *34* (1), 91–108.
- [72] Schreier, and Fryer. Heat Exchanger Fouling: A Model Study of the Scaleup of Laboratory Data. *Chem. Eng. Sci.* **1995**, *50* (8), 1311–1321.
- [73] Grijspeerd, Mortier, De Block, and Van Renterghem. Applications of Modelling to Optimise Ultra High Temperature Milk Heat Exchangers with Respect to Fouling. *Food Control* **2004**, *15* (2), 117–130.
- [74] Lalande, and Tissier. Fouling of Heat Transfer Surfaces Related to β -Lactoglobulin Denaturation During Heat Processing of Milk. *Biotechnol. Prog.* **1985**, *1* (2), 131–139.
- [75] Hege, and Kessler. Deposit Formation of Protein Containing Dairy Liquids. *Milchwiss. (Germany, FR)* **1986**.
- [76] Arnebrant, Barton, and Nylander. Adsorption of α -Lactalbumin and β -Lactoglobulin on Metal Surfaces versus Temperature. *J. Colloid Interface Sci.* **1987**, *119* (2), 383–390.
- [77] Kessler, and Beyer. Thermal Denaturation of Whey Proteins and Its Effect in Dairy Technology. *Int. J. Biol. Macromol.* **1991**, *13* (3), 165–173.
- [78] Blanpain-Avet, André, Khaldi, Bouvier, Petit, Six, Jeantet, Croguennec, and Delaplace. Predicting the Distribution of Whey Protein Fouling in a Plate Heat Exchanger Using the Kinetic Parameters of the Thermal Denaturation Reaction of β -Lactoglobulin and the Bulk Temperature Profiles. *J. Dairy Sci.* **2016**, *99* (12), 9611–9630.
- [79] Chen, Chen, and Wilson. In *Proceedings of the 4th International Conference on Heat Exchanger Fouling—Fundamental Approaches and Technical Solutions*; Davos, Switzerland, 2001; pp 153–162.
- [80] Bansal, Chen, and Lin. Skim Milk Fouling during Ohmic Heating. **2005**.
- [81] Blanpain-Avet, Hédoux, Guinet, Paccou, Petit, Six, and Delaplace. Analysis by Raman Spectroscopy of the Conformational Structure of Whey Proteins Constituting Fouling Deposits During the Processing in a Heat Exchanger. *J. Food Eng.* **2012**, *110* (1), 86–94.
- [82] Mahdi, Mouheb, and Oufier. A Dynamic Model for Milk Fouling in a Plate Heat Exchanger. *Appl. Math. Model.* **2009**, *33* (2), 648–662.

- [83] Jun, and Puri. A 2D Dynamic Model for Fouling Performance of Plate Heat Exchangers. *J. Food Eng.* **2006**, 75 (3), 364–374.
- [84] Jun, and Puri. Plate Heat Exchanger: Thermal and Fouling Analysis. *Comput. Fluid Dyn. Food Process.* **2007**, 417–433.
- [85] Tissier, and Lalande. Experimental Device and Methods for Studying Milk Deposit Formation on Heat Exchange Surfaces. *Biotechnol. Prog.* **1986**, 2 (4), 218–229.
- [86] Britten, Green, Boulet, and Paquin. Deposit Formation on Heated Surfaces: Effect of Interface Energetics. *J. Dairy Res.* **1988**, 55 (4), 551–562.
- [87] Fryer, and Belmar-Beiny. Fouling of Heat Exchangers in the Food Industry: A Chemical Engineering Perspective. *Trends Food Sci. Technol.* **1991**, 2, 33–37.
- [88] Delsing, and Hiddink. Fouling of Heat Transfer Surface by Dairy Liquids. *Netherlands milk dairy J.* **1983**, 37, 139–148.
- [89] Dannenberg, and Kessler. Reaction Kinetics of the Denaturation of Whey Proteins in Milk. *J. Food Sci.* **1988**, 53 (1), 258–263.
- [90] Sandu. In *Fouling and Cleaning in Food Processing*; Druckerei Walch, Augsburg, Germany, 1989; pp 46–56.
- [91] Foster, and Green. A Model Heat Exchange Apparatus for the Investigation of Fouling of Stainless Steel Surfaces by Milk II. Deposition of Fouling Material at 140 C, Its Adhesion and Depth Profiling. *J. Dairy Res.* **1990**, 57 (3), 339–348.
- [92] Fryer. Modelling of Heat Exchanger Fouling, University of Cambridge, 1986.
- [93] Fickak, Al-Raisi, and Chen. Effect of Whey Protein Concentration on the Fouling and Cleaning of a Heat Transfer Surface. *J. Food Eng.* **2011**, 104 (3), 323–331.
- [94] Bansal, and Chen. A Critical Review of Milk Fouling in Heat Exchangers. *Compr. Rev. Food Sci. Food Saf.* **2006**, 5 (2), 27–33.
- [95] Khaldi, Ronse, André, Blanpain-Avet, Bouvier, Six, Bornaz, Croguennec, Jeantet, and Delaplace. Denaturation Kinetics of Whey Protein Isolate Solutions and Fouling Mass Distribution in a Plate Heat Exchanger. *Int. J. Chem. Eng.* **2015**, 2015.
- [96] Guérin, Ronse, Bouvier, Debreyne, and Delaplace. Structure and Rate of Growth of Whey Protein Deposit from in Situ Electrical Conductivity during Fouling in a Plate Heat Exchanger. *Chem. Eng. Sci.* **2007**, 62 (7), 1948–1957.
- [97] Daufin, Labbé, Quemerais, Brulé, Michel, Roignant, and Priol. Fouling of a Heat Exchange Surface by Whey, Milk and Model Fluids. An Analytical Study. *Lait* **1987**, 67 (3), 339–364.
- [98] Roefs, and Kruijff. A Model for the Denaturation and Aggregation of B-Lactoglobulin. *FEBS J.* **1994**, 226 (3), 883–889.
- [99] De Jong, Van Der Horst, and Waalewijn. In *Fouling and Cleaning in Food Processing*; 1998; Vol. 98, pp 39–46.
- [100] Jeurnink. NIZO, 1991.
- [101] Tung. Calcium Phosphates: Structure, Composition, Solubility, and Stability. In *Calcium phosphates in biological and industrial systems*; Springer, 1998; pp 1–19.
- [102] Boxler, Augustin, and Scholl. Fouling of Milk Components on DLC Coated Surfaces at Pasteurization and UHT Temperatures. *Food Bioprod. Process.* **2013**, 91 (4), 336–347.
- [103] Burton. Deposits from Whole Milk in Heat Treatment Plant—a Review and Discussion. *J. Dairy Res.* **1968**, 35 (2), 317–330.
- [104] Lewis, and Heppell. Fouling, Cleaning, and Disinfecting. *Contin. Therm. Process. foods. Gaithersburg, Md. Aspen Publ.* **2000**.
- [105] Yoo, Hardin, and Chen. The Influence of Milk Composition on the Growth of *Bacillus Stearothermophilus*. *J. Food Eng.* **2006**, 77 (1), 96–102.
- [106] Paterson, and Fryer. A Reaction Engineering Approach to the Analysis of Fouling. *Chem. Eng. Sci.* **1988**, 43 (7), 1714–1717.
- [107] Rakes, Swartzel, and Jones. Deposition of Dairy Protein-Containing Fluids on Heat Exchange Surfaces. *Biotechnol. Prog.* **1986**, 2 (4), 210–217.
- [108] Barish, and Goddard. Anti-Fouling Surface Modified Stainless Steel for Food Processing. *Food Bioprod. Process.* **2013**, 91 (4), 352–361.
- [109] Galani. Heat-induced Denaturation and Aggregation of B-Lactoglobulin: Kinetics of Formation of Hydrophobic and Disulphide-linked Aggregates. *Int. J. food Sci. Technol.* **1999**, 34 (5-6), 467–476.
- [110] Brady, and Singer. Mechanical Factors Favoring Release from Fouling Release Coatings. *Biofouling* **2000**, 15 (1–3), 73–81.
- [111] Gadelmawla, Koura, Maksoud, Elewa, and Soliman. Roughness Parameters. *J. Mater. Process. Technol.* **2002**, 123 (1), 133–145.
- [112] Yan, Gao, and Barthlott. Mimicking Natural Superhydrophobic Surfaces and Grasping the Wetting Process: A Review on Recent Progress in Preparing Superhydrophobic Surfaces. *Adv. Colloid Interface Sci.* **2011**, 169 (2), 80–105.
- [113] Bormashenko. Young, Boruvka–Neumann, Wenzel and Cassie–Baxter Equations as the Transversality Conditions for the Variational Problem of Wetting. *Colloids Surfaces A Physicochem. Eng. Asp.* **2009**, 345 (1), 163–165.
- [114] Bico, Tordeux, and Quéré. Rough Wetting. *Europhys. Lett.* **2001**, 55 (2), 214–220.

- [115] Beuf, Rizzo, Leuliet, Müller-Steinhagen, Yiantsios, Karabelas, and Benezech. Fouling and Cleaning of Modified Stainless Steel Plate Heat Exchanger Processing Milk Products. In *Heat Exchanger Fouling and Cleaning: Fundamentals and Applications*; Watkinson, Müller-Steinhagen, Reza Malayeri, Eds.; Kloster Isree, Germany, 2003.
- [116] Yoon, and Lund. Magnetic Treatment of Milk and Surface Treatment of Plate Heat Exchangers: Effects on Milk Fouling. *J. Food Sci.* **1994**, *59* (5), 964–969.
- [117] Gordon, Hankinson, and Carver. Deposition of Milk Solids on Heated Surfaces1. *J. Dairy Sci.* **1968**, *51* (4), 520–526.
- [118] Dupeyrat, Labbé, Michel, Billoudet, and Daufin. Mouillabilité et Interactions Solide-Liquide Dans l'Encrassement de Divers Matériaux Par Du Lactorésum et Du Lait. *Lait* **1987**, *67* (4), 465–486.
- [119] McGuire, and SWARTZEL. The Influence of Solid Surface Energetics on Macromolecular Adsorption from Milk. *J. Food Process. Preserv.* **1989**, *13* (2), 145–160.
- [120] Kirtley, and McGuire. On Differences in Surface Constitution of Dairy Product Contact Materials1. *J. Dairy Sci.* **1989**, *72* (7), 1748–1753.
- [121] Wahlgren, and Arnebrant. Adsorption of β -Lactoglobulin onto Silica, Methylated Silica, and Polysulfone. *J. Colloid Interface Sci.* **1990**, *136* (1), 259–265.
- [122] Murray, and Cros. Adsorption of β -Lactoglobulin and β -Casein to Metal Surfaces and Their Removal by a Non-Ionic Surfactant, as Monitored via a Quartz Crystal Microbalance. *Colloids Surfaces B Biointerfaces* **1998**, *10* (4), 227–241.
- [123] Wu, and Nancollas. Kinetics of Heterogeneous Nucleation of Calcium Phosphates on Anatase and Rutile Surfaces. *J. Colloid Interface Sci.* **1998**, *199* (2), 206–211.
- [124] Wei, Ravn, Gram, and Kingshott. Stainless Steel Modified with Poly (Ethylene Glycol) Can Prevent Protein Adsorption but Not Bacterial Adhesion. *Colloids Surfaces B Biointerfaces* **2003**, *32* (4), 275–291.
- [125] Ramachandra, Wiehe, Hyland, and Bansal. A Preliminary Study of the Effect of Surface Coating on the Initial Deposition Mechanisms of Dairy Fouling. **2005**.
- [126] Parbhu, Hendy, and Danne. Reducing Milk Protein Adhesion Rates: A Transient Surface Treatment of Stainless Steel. *Food Bioprod. Process.* **2006**, *84* (4), 274–278.
- [127] Rosmaninho, Santos, Nylander, Paulsson, Beuf, Benezech, Yiantsios, Andritsos, Karabelas, Rizzo, Muller-Steinhagen, and Melo. Modified Stainless Steel Surfaces Targeted to Reduce Fouling - Evaluation of Fouling by Milk Components. *J. Food Eng.* **2007**, *80* (4), 1176–1187.
- [128] Rosmaninho, Rizzo, Müller-Steinhagen, and Melo. Deposition from a Milk Mineral Solution on Novel Heat Transfer Surfaces under Turbulent Flow Conditions. *J. Food Eng.* **2008**, *85* (1), 29–41.
- [129] Balasubramanian, and Puri. Fouling Mitigation during Product Processing Using a Modified Plate Heat Exchanger Surface. *Trans. ASABE* **2008**, *51* (2), 629–639.
- [130] Balasubramanian, and Puri. Reduction of Milk Fouling in a Plate Heat Exchanger System Using Food-Grade Surface Coating. *Trans. ASABE* **2009**, *52* (5), 1603–1610.
- [131] Stancl, and Zitny. Milk Fouling at Direct Ohmic Heating. *J. Food Eng.* **2010**, *99* (4), 437–444.
- [132] Boxler, Teixeira, Pereira, Mendes, Melo, Augustin, and Scholl. In *Proceedings of 9th International Conference on Heat Exchanger Fouling and Cleaning*; 2011; pp 414–420.
- [133] Jimenez, Hamze, Allion, Ronse, Delaplace, and Traisnel. In *Material Science Forum*; 2012; Vol. 706–709, pp 2523–2528.
- [134] Rungraeng, Cho, Yoon, and Jun. Carbon Nanotube-Polytetrafluoroethylene Nanocomposite Coating for Milk Fouling Reduction in Plate Heat Exchanger. *J. Food Eng.* **2012**, *111* (2), 218–224.
- [135] Patel, Bansal, Jones, and Hyland. Fouling Behaviour of Milk and Whey Protein Isolate Solution on Doped Diamond-like Carbon Modified Surfaces. *J. Food Eng.* **2013**, *116* (2), 413–421.
- [136] Barish, and Goddard. Stability of Nonfouling Stainless Steel Heat Exchanger Plates Against Commercial Cleaning Agents. *J. Food Eng.* **2014**, *124*, 143–151.
- [137] Huang, and Goddard. Influence of Fluid Milk Product Composition on Fouling and Cleaning of Ni-PTFE Modified Stainless Steel Heat Exchanger Surfaces. *J. Food Eng.* **2015**, *158*, 22–29.
- [138] Piepiorka-Stepuk, Tandecka, and Jakubowski. An Analysis of Milk Fouling Formed During Heat Treatment On a Stainless Steel Surface with Different Degrees of Roughness. *Czek J. Food Sci.* **2016**, *34* (3), 271–279.
- [139] Nakanishi, Sakiyama, and Imamura. On the Adsorption of Proteins on Solid Surfaces, a Common but Very Complicated Phenomenon. *J. Biosci. Bioeng.* **2001**, *91* (3), 233–244.
- [140] Van Oss. CRC press, 2006.
- [141] Marsh, Jones, and Sferrazza. Adsorption and Displacement of a Globular Protein on Hydrophilic and Hydrophobic Surfaces.

- Colloids Surfaces B Biointerfaces* **2002**, *23* (1), 31–42.
- [142] Zhao, Liu, Wang, Wang, and Müller-Steinhagen. Effect of Surface Free Energy on the Adhesion of Biofouling and Crystalline Fouling. *Chem. Eng. Sci.* **2005**, *60* (17), 4858–4865.
- [143] Drelich, Chibowski, Meng, and Terpilowski. Hydrophilic and Superhydrophilic Surfaces and Materials. *Soft Matter* **2011**, *7* (21), 9804–9828.
- [144] Dürr. Influence of Surface Roughness and Wettability of Stainless Steel on Soil Adhesion, Cleanability and Microbial Inactivation. *Food Bioprod. Process.* **2007**, *85* (1), 49–56.
- [145] Fang, Kellarakis, Wang, Giannelis, Finlay, Callow, and Callow. Fouling Release Nanostructured Coatings Based on PDMS-Polyurea Segmented Copolymers. *Polymer (Guildf)*. **2010**, *51* (12), 2636–2642.
- [146] Yang, Neoh, Kang, Teo, and Rittschof. Polymer Brush Coatings for Combating Marine Biofouling. *Prog. Polym. Sci.* **2014**, *39* (5), 1017–1042.
- [147] Santos, Nylander, Rosmaninho, Rizzo, Yiantsios, Andritsos, Karabelas, Muller-Steinhagen, Melo, Boulange-Petermann, Gabet, Braem, Tragardh, and Paulsson. Modified Stainless Steel Surfaces Targeted to Reduce Fouling - Surface Characterization. *J. Food Eng.* **2004**, *64* (1), 63–79.
- [148] Faÿ, Hawkins, Réhel, Grunlan, and Linossier. Non-Toxic, Antifouling Silicones with Variable PEO-Silane Amphiphile Content. *Green Matter* **2016**, *4* (2), 53–62.
- [149] Mérian, and Goddard. Advances in Nonfouling Materials: Perspectives for the Food Industry. *J. Agric. Food Chem.* **2012**, *60* (12), 2657–2943.
- [150] Chen, Zeng, Xiang, Luo, and Wang. Polydopamine-Graft-PEG Antifouling Coating for Quantitative Analysis of Food Protein by CE. *Anal. Methods* **2012**, *4* (9), 2852–2859.
- [151] Krishnan, Weinman, and Ober. Advances in Polymer for Anti-Biofouling Surfaces. *J. Mater. Chem.* **2008**, *18* (29), 3405–3413.
- [152] Halperin. Polymer Brushes That Resist Adsorption of Model Proteins: Design Parameters. *Langmuir* **1999**, *15* (7), 2525–2533.
- [153] Dong, Manolache, Somers, Wong, and Denes. Generation of Antifouling Layers on Stainless Steel Surfaces by Plasma-Enhanced Crosslinking of Polyethylene Glycol. *J. Appl. Polym. Sci.* **2005**, *97* (2), 485–497.
- [154] Peng, Su, Shi, Chen, and Jiang. Protein Fouling Resistant Membrane Prepared by Amphiphilic Pegylated Polyethersulfone. *Bioresour. Technol.* **2011**, *102* (3), 2289–2295.
- [155] Norde, and Gage. Interaction of Bovine Serum Albumine and Human Blood Plasma with PEO-Tethered Surfaces: Influence of PEO Chain Length, Grafting Density, and Temperature. *Langmuir* **2004**, *20* (10), 4162–4167.
- [156] Faure, Falentin-Daudré, Jérôme, Lyskawa, Fournier, Woisel, and Detrembleur. Catechols as Versatile Platforms in Polymer Chemistry. *Prog. Polym. Sci.* **2013**, *38* (1), 236–270.
- [157] Chen, Li, Zhao, and Zheng. Surface Hydration: Principles and Applications Toward Low-Fouling / Nonfouling Biomaterials. *Polymer (Guildf)*. **2010**, *51* (23), 5283–5293.
- [158] Li, Meng, Ye, Yang, Tian, and Deng. Surface Modification of PES Ultrafiltration Membrane by Polydopamine Coating and Poly(Ethylene Glycol) Grafting: Morphology, Stability, and Anti-Fouling. *Desalination* **2014**, *344*, 422–430.
- [159] Chen, Zhang, Chen, Brook, and Sheardown. Protein Repellent Silicone Surfaces by Covalent Immobilization of Poly(Ethylene Oxide). *Biomaterials* **2005**, *26* (15), 2391–2399.
- [160] Caro, Humblot, Méthivier, Minier, Salmain, and Pradier. Grafting of Lysozyme and/or Poly(Ethylene Glycol) to Prevent Biofilm Growth on Stainless Steel Surfaces. *J. Phys. Chem. B* **2009**, *113* (7), 2101–2109.
- [161] Khalil, Franzmann, Ramcke, Dakischew, Lips, Reinhardt, Heisig, and Maison. Biomimetic PEG-Catecholates for Stable Antifouling Coatings on Metal Surfaces: Applications on TiO₂ and Stainless Steel. *Colloids Surfaces B Biointerfaces* **2014**, *117*, 185–192.
- [162] Wang, Tan, Kang, and Neoh. Plasma-Induced Immobilization of Poly(Ethylene Glycol) onto Poly(Vinylidene Fluoride) Microporous Membrane. *J. Memb. Sci.* **2002**, *195* (1), 103–114.
- [163] Wu, Timmons, Jen, and Molock. Non-Fouling Surfaces Produced by Gas Phase Pulsed Plasma Polymerization of an Ultra Low Molecular Weight Ethylene Oxide Containing Monomer. *Colloids Surfaces B Biointerfaces* **2000**, *18* (3–4), 235–248.
- [164] Dyer, Ainslie, and Pishko. Protein Adhesion on Silicon-Supported Hyperbranched Poly(Ethylene Glycol) and Poly(Allylamine) Thin Films. *Langmuir* **2007**, *23* (13), 7018–7023.
- [165] Lei, and Ulbricht. Macroinitiator-Mediated Photoreactive Coating of Membrane Surfaces with Antifouling Hydrogel Layers. *J. Memb. Sci.* **2014**, *455*, 207–218.

- [166] Wu, Wang, Wang, Yan, Wang, and Wang. Polyvinylamine-Grafted Polyamide Reverse Osmosis Membrane with Improved Antifouling Property. *J. Memb. Sci.* **2015**, *495*, 1–13.
- [167] Vu, Fouet, Gue, and Sudor. A New and Easy Surface Functionalization Technnology for Monitoring Wettability in Heterogeneous Nano- and Microfluidic Devices. *Sensors Actuators B Chem.* **2014**, *196*, 64–70.
- [168] Wu, Wang, Yan, Wang, Wang, and Wang. Improving the Hydrophilicity and Fouling Resistance of RO Membranes by Surface Immobilization of PVP Based on a Metal-Polyphenol Precursor Layer. *J. Memb. Sci.* **2015**, *496*, 58–69.
- [169] Albert, Augustin, and Scholl. Roughness and Constriction Effects on Heat Transfer in Crystallization Fouling. *Chem. Eng. Sci.* **2011**, *66* (3), 499–509.
- [170] Detry, Sindic, and Deroanne. Hygiene and Cleanability: A Focus on Surfaces. *Crit. Rev. Food Sci. Nutr.* **2010**, *50* (7), 583–604.
- [171] Leclercq-Perlat, and Lalande. Cleanability in Relation to Surface Chemical Composition and Surface Finishing of Some Materials Commonly Used in Food Industries. *J. Food Eng.* **1994**, *23* (4), 501–517.
- [172] Kouider, Hamadi, Mallouki, Bengourram, Mabrouki, Zekraoui, Ellouali, and Latrache. Effect of Stainless Steel Surface Roughness on Staphylococcus Aureus Adhesion. *Int J P App Sci* **2010**, *4*, 1–7.
- [173] Oldham. A Gouy–Chapman–Stern Model of the Double Layer at a (Metal)/(Ionic Liquid) Interface. *J. Electroanal. Chem.* **2008**, *613* (2), 131–138.
- [174] Cai, Fan, Zhao, Hong, Shen, He, Lin, and Chen. Effects of Surface Charge on Interfacial Interactions Related to Membrane Fouling in a Submerged Membrane Bioreactor Based on Thermodynamic Analysis. *J. Colloid an interface Sci.* **2016**, *465*, 33–41.
- [175] McArthur, McLean, Kingshott, St John, Chatelier, and Griesser. Effect of Polysaccharide Structure on Protein Adsorption. *Colloids Surfaces B Biointerfaces* **2000**, *17* (1), 37–48.
- [176] Wu, Jasinski, and Krishnan. Carboxybetaine, Sulfobetaine and Cationic Block Copolymer Coatings: A Comparison of the Surface Properties and Antibiofouling Behavior. *J. Appl. Polym. Sci.* **2012**, *124* (3), 2154–2170.
- [177] Bengani, Kou, and Asatekin. Zwitterionic Copolymer Self-Assembly for Fouling Resistant, High Flux Membranes with Size-Based Small Molecule Selectivity. *J. Memb. Sci.* **2015**, *493*, 755–765.
- [178] Shafi, Khan, Yang, and Gleason. Surface Modification of Reverse Osmosis Membranes with Zwitterionic Coating for Improved Resistance to Fouling. *Desalination* **2015**, *362*, 93–103.
- [179] Meng, Cheng, and Li. Polyacrylonitrile-Based Zwitterionic Ultrafiltration Membrane With Improved Anti-Protein-Fouling Capacity. *Appl. Surf. Sci.* **2014**, *303*, 399–405.
- [180] Bodkhe, Stafslie, Daniels, Cilz, Muelhberg, Thompson, Callow, Callow, and Webster. Zwitterionic Siloxane-Polyurethane Fouling-Release Coatings. *Prog. Org. Coatings* **2015**, *78*, 369–380.
- [181] Huang, Chu, Wang, Li, and Lee. Bioinspired Zwitterionic Surface Coatings with Robust Photostability and Fouling Resistance. *Appl. Mater. Interfaces* **2015**, *7* (42), 22386–23776.
- [182] Chae, Jang, Kim, Sohn, and Rhee. Anti-Fouling Epoxy Coatings for Optical Biosensor Application Based on Phosphorylcholine. *Sensors Actuators B Chem.* **2007**, *124* (1), 153–160.
- [183] Goda, Tabata, Sanjoh, Uchimura, Iwasaki, and Miyahara. Thiolated 2-Methacryloyloxyethyl Phosphorylcholine for an Antifouling Biosensor Platform. *Chem. Commun.* **2013**, *49* (77), 8683–8685.
- [184] Holmlin, Chen, Chapman, Takayama, and Whitesides. Zwitterionic SAMs That Resist Nonspecific Adsorption of Protein from Aqueous Buffer. *Langmuir* **2001**, *17* (9), 2841–2850.
- [185] Chen, Yu, Yu, He, and Jiang. Strong Resistance of a Thin Crystalline Layer of Balanced Charged Groups to Protein Adsorption. *Langmuir* **2006**, *22* (19), 8186–8191.
- [186] Cui, Ju, Liang, Ejima, Lörcher, Gause, Richardson, and Caruso. Nanoscale Engineering of Low-Fouling Surfaces Through Polydopamine Immobilisation of Zwitterionic Peptides. *Soft Matter* **2014**, *10* (15), 2656–2663.
- [187] Rosen, and Gu. Surface Functionalization of Silica Nanoparticles with Cysteine: A Low-Fouling Zwitterionic Surface. *Langmuir* **2011**, *27* (17), 10507–10513.
- [188] Zhao, Zhang, Wei, Li, Zhou, Liu, Liu, and Li. Calcium Alginate Hydrogel Filtration Membrane with Excellent Anti-Fouling Property and Controlled Separation Performance. *J. Memb. Sci.* **2015**, *492*, 536–546.
- [189] Berglin, Lönn, and Gatenholm. Coating Modulus and Barnacle Bioadhesion. *Biofouling* **2003**, *19* (S1), 63–69.
- [190] Stein, Truby, Wood, Takemori, Vallance, Swain, Kavanagh, Kovach, Schultz, and Wiebe. Structure-Property Relationships of Silicone Biofouling-Release Coatings: Effect of Silicone Network Architecture on Pseudobarnacle Attachment Strengths. *Biofouling* **2003**, *19* (2), 87–94.

- [191] Chaudhury, Finlay, Chung, Callow, and Callow. The Influence of Elastic Modulus and Thickness on the Release of the Soft-Fouling Green Alga *Ulva Linza* (Syn. *Enteromorpha Linza*) from Poly (Dimethylsiloxane)(PDMS) Model Networks. *Biofouling* **2005**, *21* (1), 41–48.
- [192] Paul, Jana, Das, Mandal, Halder, Mohapatra, and Mondal. Smart Cleaning-in-Place Process through Crude Keratinase: An Eco-Friendly Cleaning Techniques towards Dairy Industries. *J. Clean. Prod.* **2014**, *76*, 140–153.
- [193] Burfoot, and Middleton. Effects of Operating Conditions of High Pressure Washing on the Removal of Biofilms from Stainless Steel Surfaces. *J. Food Eng.* **2009**, *90* (3), 350–357.
- [194] Fryer, and Christian. Improving the Cleaning of Heat Exchangers. In *Handbook of Hygiene Control in the Food Industry*; Elsevier, 2005; pp 468–496.
- [195] Timperley, and Smeulders. Cleaning of Dairy HTST Plate Heat Exchangers: Comparison of Single-and Two-stage Procedures. *Int. J. Dairy Technol.* **1987**, *40* (1), 4–7.
- [196] Piepiórka-Stepuk, Diakun, and Mierzejewska. Poly-Optimization of Cleaning Conditions for Pipe Systems and Plate Heat Exchangers Contaminated with Hot Milk Using the Cleaning In Place Method. *J. Clean. Prod.* **2016**, *112*, 946–952.
- [197] Piepiórka-Stepuk, Diakun, Jakubowski, Mierzejewska, and Masłowska. Influence of Time and the Cleaning Liquid Flow Velocity on the Effectiveness of Cleaning the Plate Heat Exchanger. *Agric. Eng.* **2012**, *3* (138), 171–176.
- [198] Kolev Slavov. General Characteristics and Treatment Possibilities of Dairy Wastewater—A Review. *Food Technol. Biotechnol.* **2017**, *55* (1), 14–28.
- [199] Lelieveld, Holah, and Napper. Elsevier, 2014.
- [200] Gillham, Fryer, Hasting, and Wilson. Cleaning-in-Place of Whey Protein Fouling Deposits: Mechanisms Controlling Cleaning. *Food Bioprod. Process.* **1999**, *77* (2), 127–136.
- [201] Fryer, Christian, and Liu. How Hygiene Happens: Physics and Chemistry of Cleaning. *Int. J. Dairy Technol.* **2006**, *59* (2), 76–84.
- [202] Jeurnink, and Brinkman. The Cleaning of Heat Exchangers and Evaporators after Processing Milk or Whey. *Int. Dairy J.* **1994**, *4* (4), 347–368.
- [203] Gillham, Fryer, Hasting, and Wilson. Enhanced Cleaning of Whey Protein Soils Using Pulsed Flows. *J. Food Eng.* **2000**, *46* (3), 199–209.
- [204] Chew, Paterson, and Wilson. Fluid Dynamic Gauging for Measuring the Strength of Soft Deposits. *J. Food Eng.* **2004**, *65* (2), 175–187.
- [205] Chen, Moulin, Delaplace, Campistron, Debreyne, and Callens. In *Fouling and Cleaning in Food Processing*; 2018; pp 117–133.
- [206] Zouaghi, Six, Nuns, Simon, Bellayer, Moradi, Hatzikiriakos, Andre, Delaplace, and Jimenez. Influence of Stainless Steel Surface Properties on Whey Protein Fouling under Industrial Processing Conditions. *J. Food Eng.* **2018**, *228*, 38–49.
- [207] Heck, Van Valenberg, Dijkstra, and Van Hooijdonk. Seasonal Variation in the Dutch Bovine Raw Milk Composition. *J. Dairy Sci.* **2009**, *92* (10), 4745–4755.
- [208] Lu, Pickova, Vázquez-Gutiérrez, and Langton. Influence of Seasonal Variation and Ultra High Temperature Processing on Lipid Profile and Fat Globule Structure of Swedish Cow Milk. *Food Chem.* **2018**, *239*, 848–857.
- [209] Indyk, Hart, Meerkerk, Gill, and Woollard. The β -Lactoglobulin Content of Bovine Milk: Development and Application of a Biosensor Immunoassay. *Int. Dairy J.* **2017**, *73* (Supplement C), 68–73.
- [210] Cunault, Faille, Bouvier, Föste, Augustin, Scholl, Debreyne, and Benezech. A Novel Set-up and a CFD Approach to Study the Biofilm Dynamics as a Function of Local Flow Conditions Encountered in Fresh-Cut Food Processing Equipments. *Food Bioprod. Process.* **2015**, *93*, 217–223.
- [211] Kietzig, Hatzikiriakos, and Englezos. Patterned Superhydrophobic Metallic Surfaces. *Langmuir* **2009**, *25* (8), 4821–4827.
- [212] Moradi, Kamal, Englezos, and Hatzikiriakos. Femtosecond Laser Irradiation of Metallic Surfaces: Effects of Laser Parameters on Hydrophobicity. *Nanotechnology* **2013**, *24* (41), 415302.
- [213] Moradi, Kamal, and Hatzikiriakos. Superhydrophobic Laser-Ablated Stainless Steel Substrates Exhibiting Cassie-Baxter Stable State. *Surf. Innov.* **2015**, *3* (3), 151–163.
- [214] Choi, Kawaguchi, and Kato. Self-Assembled Monolayer Formation on Magnetic Hard Disk Surface and Friction Measurements. *J. Appl. Phys.* **2002**, *91* (10), 7574–7576.
- [215] Oldani, del Negro, Bianchi, Suriano, Turri, Pirola, and Sacchi. Surface Properties and Anti-Fouling Assessment of Coatings Obtained from Perfluoropolyethers and Ceramic Oxides Nanopowders Deposited on Stainless Steel. *J. Fluor. Chem.* **2015**, *180*, 7–14.

- [216] Al-Ogaili. Fundamental Approach for Fouling Growth Mechanisms Comprehension at a Stainless Surface: Development of Antifouling Coating for Stainless Steel, Université des Sciences et Technologies de Lille, 2014.
- [217] Biesinger, Payne, Grosvenor, Lau, Gerson, and Smart. Resolving Surface Chemical States in XPS Analysis of First Row Transition Metals, Oxides and Hydroxides: Cr, Mn, Fe, Co and Ni. *Appl. Surf. Sci.* **2011**, 257 (7), 2717–2730.
- [218] Moradi, Hadjesfandiari, Toosi, Kizhakkedathu, and Hatzikiriakos. Effect of Extreme Wettability on Platelet Adhesion on Metallic Implants: From Superhydrophilicity to Superhydrophobicity. *ACS Appl. Mater. Interfaces* **2016**, 8 (27), 17631–17641.
- [219] Ragesh, Ganesh, Nair, and Nair. A Review on “Self-Cleaning and Multifunctional Materials.” *J. Mater. Chem. A* **2014**, 2 (36), 14773–14797.
- [220] Adjonu, Doran, Torley, and Agboola. Whey Protein Peptides as Components of Nanoemulsions: A Review of Emulsifying and Biological Functionalities. *J. Food Eng.* **2014**, 122, 15–27.
- [221] Mafu, Roy, Goulet, and Magny. Attachment of *Listeria Monocytogenes* to Stainless Steel, Glass, Polypropylene, and Rubber Surfaces after Short Contact Times. *J. Food Prot.* **1990**, 53 (9), 742–746.
- [222] Sinde, and Carballo. Attachment of *Salmonella* Spp. and *Listeria Monocytogenes* to Stainless Steel, Rubber and Polytetrafluorethylene: The Influence of Free Energy and the Effect of Commercial Sanitizers. *Food Microbiol.* **2000**, 17 (4), 439–447.
- [223] Fletcher, and Floodgate. An Electron-Microscopic Demonstration of an Acidic Polysaccharide Involved in the Adhesion of a Marine Bacterium to Solid Surfaces. *Microbiology* **1973**, 74 (2), 325–334.
- [224] Lariviere-Gauthier, Letellier, Kerouanton, Bekal, Quessy, Fournaise, and Fravallo. Analysis of *Listeria Monocytogenes* Strain Distribution in a Pork Slaughter and Cutting Plant in the Province of Quebec. *J. Food Prot.* **2014**, 77 (12), 2121–2128.
- [225] Moltz, and Martin. Formation of Biofilms by *Listeria Monocytogenes* under Various Growth Conditions. *J. Food Prot.* **2005**, 68 (1), 92–97.
- [226] Medilanski, Kaufmann, Wick, Wanner, and Harms. Influence of the Surface Topography of Stainless Steel on Bacterial Adhesion. *Biofouling* **2002**, 18 (3), 193–203.
- [227] Sommer, Ekin, Webster, Stafslin, Daniels, VanderWal, Thompson, Callow, and Callow. A Preliminary Study on the Properties and Fouling-Release Performance of Siloxane–polyurethane Coatings Prepared from Poly(Dimethylsiloxane) (PDMS) Macromers. *Biofouling* **2010**, 26 (8), 961–972.
- [228] Bixler, Theiss, Bhushan, and Lee. Anti-Fouling Properties of Microstructured Surfaces Bio-Inspired by Rice Leaves and Butterfly Wings. *J. Colloid an interface Sci.* **2014**, 419, 114–133.
- [229] Jung, and Bhushan. Mechanically Durable Carbon Nanotube–Composite Hierarchical Structures with Superhydrophobicity, Self-Cleaning, and Low-Drag. *ACS Nano* **2009**, 3 (12), 4155–4163.
- [230] Bravo, Zhai, Wu, Cohen, and Rubner. Transparent Superhydrophobic Films Based on Silica Nanoparticles. *Langmuir* **2007**, 23 (13), 7293–7298.
- [231] Mahltig, and Böttcher. Modified Silica Sol Coatings for Water-Repellent Textiles. *J. sol-gel Sci. Technol.* **2003**, 27 (1), 43–52.
- [232] Yu, Gu, Meng, and Qing. Superhydrophobic Cotton Fabric Coating Based on a Complex Layer of Silica Nanoparticles and Perfluorooctylated Quaternary Ammonium Silane Coupling Agent. *Appl. Surf. Sci.* **2007**, 253 (7), 3669–3673.
- [233] Ding, Ogawa, Kim, Fujimoto, and Shiratori. Fabrication of a Super-Hydrophobic Nanofibrous Zinc Oxide Film Surface by Electrospinning. *Thin Solid Films* **2008**, 516 (9), 2495–2501.
- [234] Liu, Du, Wu, and Jiang. Superhydrophobic Gecko Feet with High Adhesive Forces towards Water and Their Bio-Inspired Materials. *Nanoscale* **2012**, 4 (3), 768–772.
- [235] Barthlott, Schimmel, Wiersch, Koch, Brede, Barczewski, Walheim, Weis, Kaltenmaier, Leder, and Bohn. The *Salvinia* Paradox: Superhydrophobic Surfaces with Hydrophilic Pins for Air Retention Under Water. *Adv. Mater.* **2010**, 22 (21), 2325–2328.
- [236] Zouaghi, Six, Bellayer, Moradi, Hatzikiriakos, Dargent, Thomy, Coffinier, Andre, and Delaplace. Biomimetic Nanostructured Surfaces for Antifouling in Dairy Processing. *S6-Microfluidique, nanofluidique écoulements à interface* **2017**.
- [237] Zouaghi, Six, Bellayer, Coffinier, Abdallah, Chihib, André, Delaplace, and Jimenez. Atmospheric Pressure Plasma Spraying of Silane-Based Coatings Targeting Whey Protein Fouling and Bacterial Adhesion Management. *Appl. Surf. Sci.* **2018**, 455, 392–402.
- [238] De Nicola, Castrucci, Scarselli, Nanni, Cacciotti, and De Crescenzi. Super-Hydrophobic Multi-Walled Carbon Nanotube Coatings for Stainless Steel. *Nanotechnology* **2015**, 26 (14), 145701.
- [239] Latthe, Imai, Ganesan, and Rao. Superhydrophobic Silica-Films by Sol-Gel Co-Precursor Method. *Appl. Surf. Sci.* **2009**, 256 (1), 217–222.

- [240] Oldani, Sergi, Pirola, Sacchi, and Bianchi. Sol-Gel Hybrid Coatings Containing Silica and a Perfluoropolyether Derivative with High Resistance and Antifouling Properties in Liquid Media. *J. Fluor. Chem.* **2016**, *188*, 43–49.
- [241] Lafuma, and Quéré. Superhydrophobic States. *Nat. Mater.* **2003**, *2* (7), 457–460.
- [242] Lapierre, Brunet, Coffinier, Thomy, Blosser, and Boukherroub. Electrowetting and Droplet Impalement Experiments on Superhydrophobic Multiscale Structures. *Faraday Discuss.* **2010**, *146*, 125–139.
- [243] Epstein, Wong, Belisle, Boggs, and Aizenberg. Liquid-Infused Structured Surfaces with Exceptional Anti-Biofouling Performance. *Proc. Natl. Acad. Sci.* **2012**, *109* (33), 13182–13187.
- [244] Wong, Kang, Tang, Smythe, Hatton, Grinthal, and Aizenberg. Bioinspired Self-Repairing Slippery Surfaces with Pressure-Stable Omniphobicity. *Nature* **2011**, *477* (7365), 443–447.
- [245] Bohn, and Federle. Insect Aquaplaning: Nepenthes Pitcher Plants Capture Prey with the Peristome, a Fully Wettable Water-Lubricated Anisotropic Surface. *Proc. Natl. Acad. Sci. U. S. A.* **2004**, *101* (39), 14138–14143.
- [246] Wang, Kato, Blois, and Wong. Bioinspired Omniphobic Coatings with a Thermal Self-Repair Function on Industrial Materials. *ACS Appl. Mater. Interfaces* **2016**, *8* (12), 8265–8271.
- [247] Xiao, Li, Mieszkin, Di Fino, Clare, Callow, Callow, Grunze, Rosenhahn, and Levkin. Slippery Liquid-Infused Porous Surfaces Showing Marine Antibiofouling Properties. *ACS Appl. Mater. Interfaces* **2013**, *5* (20), 10074–10080.
- [248] Wang, Zhang, Lu, and Sun. Fabrication of Slippery Lubricant-Infused Porous Surface for Inhibition of Microbially Influenced Corrosion. *ACS Appl. Mater. Interfaces* **2016**, *8* (2), 1120–1127.
- [249] Manabe, Kyung, and Shiratori. Biocompatible Slippery Fluid-Infused Films Composed of Chitosan and Alginate via Layer-by-Layer Self-Assembly and Their Antithrombogenicity. *ACS Appl. Mater. Interfaces* **2015**, *7* (8), 4763–4771.
- [250] MacCallum, Howell, Kim, Sun, Friedlander, Ranisau, Ahanotu, Lin, Vena, Hatton, Wong, and Aizenberg. Liquid-Infused Silicone as a Biofouling-Free Medical Material. *ACS Biomater. Sci. Eng.* **2014**, *1* (1), 43–51.
- [251] Li, Kleintschek, Rieder, Cheng, Baumbach, Obst, Schwartz, and Levkin. Hydrophobic Liquid-Infused Porous Polymer Surfaces for Antibacterial Applications. *ACS Appl. Mater. Interfaces* **2013**, *5* (14), 6704–6711.
- [252] Yin, Mei, Li, Xia, Zhang, and Chu. Self-Cleaning and Antibiofouling Enamel Surface by Slippery Liquid-Infused Technique. *Sci. Rep.* **2016**, *6*, 25924.
- [253] Zouaghi, Six, Bellayer, Moradi, Hatzikiriakos, Dargent, Thomy, Coffinier, André, Delaplace, and Jimenez. Antifouling Biomimetic Liquid-Infused Stainless Steel: Application to Dairy Industrial Processing. *ACS Appl. Mater. Interfaces* **2017**, *9* (31), 26565–26573.
- [254] Nosonovsky, and Bhushan. Lotus Versus Rose: Biomimetic Surface Effects. In *Green Tribology: Biomimetics, Energy Conservation and Sustainability*; Springer-Verlag Berlin Heidelberg: Berlin, 2012; pp 25–40.
- [255] Park, Shin, Kim, Kim, Le, Kang, Kim, Pham, Jung, and Yi. Investigation of 3-Dimensional Structural Morphology for Enhancing Light Trapping with Control of Surface Haze. *Opt. Mater. (Amst)*. **2017**, *66*, 404–409.
- [256] Imamura, Nonaka, Onitsuka, Irishika, and Kobayashi. Light Trapping of Crystalline Si Solar Cells by Use of Nanocrystalline Si Layer Plus Pyramidal Texture. *Appl. Surf. Sci.* **2017**, *395*, 50–55.
- [257] Smith, Dhiman, Anand, Reza-Garduno, Cohen, McKinley, and Varanasi. Droplet Mobility on Lubricant-Impregnated Surfaces. *Soft Matter* **2013**, *9* (6), 1772–1780.
- [258] Lee, Kim, and Kim. Electrochemically Etched Porous Stainless Steel for Enhanced Oil Retention. *Surf. Coat. Technol.* **2015**, *264*, 127–131.
- [259] Barbier, Arreola-Mendoza, and Del Razo. Molecular Mechanisms of Fluoride Toxicity. *Chem. Biol. Interact.* **2010**, *188* (2), 319–333.
- [260] Fischer, and Walther. Acute Toxicity of Some Aliphatic Fluorine Compounds. *Toxicol. Appl. Pharmacol.* **1969**, *14* (1), 114–118.
- [261] Scardino, Zhang, Cookson, Lamb, and Nys. The Role of Nano-Roughness in Antifouling. *Biofouling* **2009**, *25* (8), 757–767.
- [262] Lee, Jung, and Ko. The Effect of the Surface Wettability of Nanoprotrusions Formed on Network-Type Microstructures. *J. Micromechanics Microengineering* **2008**, *18* (12), 125007.
- [263] Lim, Jung, Noh, Choi, and Kim. Simple Nanofabrication of a Superhydrophobic and Transparent Biomimetic Surface. *Chinese Sci. Bull.* **2009**, *54* (19), 3613.
- [264] Balu, Breedveld, and Hess. Fabrication of “Roll-off” and “Sticky” Superhydrophobic Cellulose Surfaces via Plasma Processing. *Langmuir* **2008**, *24* (9), 4785–4790.
- [265] Intranuovo, Sardella, Rossini, d’Agostino, and Favia. PECVD of Fluorocarbon Coatings from Hexafluoropropylene Oxide: Glow vs. Afterglow. *Chem. Vap. Depos.* **2009**, *15* (4-6), 95–100.

- [266] Ji, Kim, Kwon, and Lee. Easy Fabrication of Large-Size Superhydrophobic Surfaces by Atmospheric Pressure Plasma Polymerization with Non-Polar Aromatic Hydrocarbon in an in-Line Process. *Appl. Surf. Sci.* **2009**, 255 (8), 4575–4578.
- [267] Mùgica-Vidal, Alba-Elias, Sainz-Garcia, and Ordieres-Meré. Atmospheric Plasma Polymerization of Hydrophobic and Wear-Resistant Coatings on Glass Substrates. *Surf. Coat. Technol.* **2014**, 259, 374–385.
- [268] Sainz-García, Alba-Elías, Mùgica-Vidal, and Pantoja-Ruiz. Promotion of Tribological and Hydrophobic Properties of a Coating on TPE Substrates by Atmospheric Plasma-Polymerization. *Appl. Surf. Sci.* **2016**, 371, 50–60.
- [269] Mùgica-Vidal, Alba-Elías, Sainz-García, and González-Marcos. Reducing Friction on Glass Substrates by Atmospheric Plasma-Polymerization of APTES. *Surf. Coatings Technol.* **2017**, 309, 1062–1071.
- [270] Wang, Wang, Sun, He, Pan, Zhou, and Wu. Influence of Pores on the Thermal Insulation Behavior of Thermal Barrier Coatings Prepared by Atmospheric Plasma Spray. *Mater. Des.* **2011**, 32 (1), 36–47.
- [271] Regula, Ihde, Keil, Wilken, Hartwig, and Lommatzsch. In *ISPC19*; 2009.
- [272] Lommatzsch, and Ihde. Plasma Polymerization of HMDSO with an Atmospheric Pressure Plasma Jet for Corrosion Protection of Aluminium and Low-Adhesion Surfaces. *Plasma Process. Polym.* **2009**, 6 (10), 642–648.
- [273] Nwankire, Ardhaoui, and Dowling. The Effect of Plasma-Polymerised Silicon Hybride-Rich Polyhydrogenmethylsiloxane on the Adhesion of Silicon Elastomers. *Polym. Int.* **2009**, 58 (9), 996–1001.
- [274] Szabová, Cernakova, Wolfová, and Cernak. Coating of TiO₂ Nanoparticles on the Plasma Activated Polypropylene Fibers. *Acta Chim. Slovaca* **2009**, 2 (1), 70–76.
- [275] Owens, and Wendt. Estimation of the Surface Free Energy of Polymers. *J. Appl. Polym. Sci.* **1969**, 13 (8), 1741–1747.
- [276] Lommatzsch, and Ihde. Plasma Polymerization of HMDSO with an Atmospheric Pressure Plasma Jet for Corrosion Protection of Aluminum and Low-Adhesion Surfaces. *Plasma Process. Polym.* **2009**, 6 (10), 642–648.
- [277] Wagner, Naumkin, Kraut-Vass, Allison, Powell, and Rumble Jr. NIST Standard Reference Database 20, Version 3.4 (Web Version). *Natl. Inst. Stand. Technol. Gaithersburg, MD* **2003**, 20899.
- [278] Beamson, and Briggs. High Resolution XPS of Organic Polymers: The Scienta ESCA300 Database (Beamson, G.; Briggs, D.). *J. Chem. Educ.* **1993**, 70 (1), A25.
- [279] Voronin, Tertykh, Ogenko, and Chuiko. Electron-Acceptor Properties of Silicon Atoms in Surface Chemical Compounds. *Theor. Exp. Chem.* **1978**, 14 (5), 495–500.
- [280] Wirtanen, Ahola, and Mattila-Sandholm. Evaluation of Cleaning Procedures in Elimination of Biofilm from Stainless Steel Surfaces in Open Process Equipment. *Food Bioprod. Process. Trans. Inst. Chem. Eng. Part C* **1995**.
- [281] Flint, Brooks, and Bremer. Properties of the Stainless Steel Substrate, Influencing the Adhesion of Thermo-Resistant Streptococci. *J. Food Eng.* **2000**, 43 (4), 235–242.
- [282] Chen, Yuan, Song, Wu, and Li. Biocompatible Polymer Materials: Role of Protein–surface Interactions. *Prog. Polym. Sci.* **2008**, 33 (11), 1059–1087.
- [283] Knoll, and Hermans. Polymer-Protein Interactions. Comparison of Experiment and Excluded Volume Theory. *J. Biol. Chem.* **1983**, 258 (9), 5710–5715.
- [284] Jeon, Lee, Andrade, and De Gennes. Protein—surface Interactions in the Presence of Polyethylene Oxide: I. Simplified Theory. *J. Colloid Interface Sci.* **1991**, 142 (1), 149–158.
- [285] Lee, Lee, and Andrade. Blood Compatibility of Polyethylene Oxide Surfaces. *Prog. Polym. Sci.* **1995**, 20 (6), 1043–1079.
- [286] Lee, and Laibinis. Protein-Resistant Coatings for Glass and Metal Oxide Surfaces Derived from Oligo (Ethylene Glycol)-Terminated Alkyltrichlorosilanes. *Biomaterials* **1998**, 19 (18), 1669–1675.
- [287] Jo, and Park. Surface Modification Using Silanated Poly (Ethylene Glycol) S. *Biomaterials* **2000**, 21 (6), 605–616.
- [288] Pale-Grosdemange, Simon, Prime, and Whitesides. Formation of Self-Assembled Monolayers by Chemisorption of (Oligo(Ethylene Glycol) of Structure HS(CH₂)₁₁(OCH₂CH₂)MOH on Gold. *J. Am. Chem. Soc.* **1991**, 113 (1), 12–20.
- [289] Prime, and Whitesides. Self-Assembled Organic Monolayers: Model Systems for Studying Adsorption of Protein at Surfaces. *Science (80-.)*. **1991**, 252 (5009), 1164–1167.
- [290] Lejars, Margailan, and Bressy. Fouling Release Coatings: A Nontoxic Alternative to Biocidal Antifouling Coatings. *Chem. Rev.* **2012**, 112 (8), 4347–4390.
- [291] Chen, Brook, and Sheardown. Silicone Elastomers for Reduced Protein Adsorption. *Biomaterials* **2004**, 25 (12), 2273–2282.
- [292] Owen. Surface Chemistry and Applications. In *Siloxane polymers*; Clarson, Semlyen, Eds.; Englewood Cliffs, 1993; p 309.
- [293] Lane. Silica, Silicon and Silicones... Unraveling the Mystery. In *Immunology of Silicones*; Potter, Rose, Eds.; Berlin, 1996; pp 3–12.
- [294] Rufin, Gruetzner, Hurley, Hawkins, Raymond, Raymond, and Grunlan. Enhancing the Protein Resistance of Silicone via

- Surface-Restructuring PEO-Silane Amphiphiles with Variable PEO Length. *J. Mater. Chem. B* **2015**, *3* (14), 2816–2825.
- [295] Rufin, Barry, Adair, Hawkins, Raymond, and Grunlan. Protein Resistance Efficacy of PEO-Silane Amphiphiles: Dependence on PEO-Segment Length and Concentration. *Acta Biomater.* **2016**, *41*, 247–252.
- [296] Hawkins, Schott, Grigoryan, Rufin, Ngo, Vanderwal, Staflieni, and Grunlan. Anti-Protein and Anti-Bacterial Behavior of Amphiphilic Silicones. *Polym. Chem.* **2017**, *8* (34), 5239–5251.
- [297] Nicolson. The Fluid—Mosaic Model of Membrane Structure: Still Relevant to Understanding the Structure, Function and Dynamics of Biological Membranes after More than 40years. *Biochim. Biophys. Acta (BBA)-Biomembranes* **2014**, *1838* (6), 1451–1466.
- [298] Hawkins, and Grunlan. The Protein Resistance of Silicones Prepared with a PEO-Silane Amphiphile. *J. Mater. Chem.* **2012**, *22* (37), 19540–19546.
- [299] Hawkins, Rufin, Raymond, and Grunlan. Direct Observation of the Nanocomplex Surface Reorganization of Antifouling Silicones Containing a Highly Mobile PEO-Silane Amphiphile. *J. Mater. Chem. B* **2014**, *2* (34), 5689–5697.
- [300] Murthy, Cox, Hahn, and Grunlan. Protein-Resistant Silicones: Incorporation of Poly(Ethylene Oxide) via Siloxane Tethers. *Biomacromolecules* **2007**, *8* (10), 3244–3252.
- [301] Lee, Dellatore, Miller, and Messersmith. Mussel-Inspired Surface Chemistry for Multifunctional Coatings. *Science* (80-.). **2007**, *318* (5849), 426–430.
- [302] Jeong, Park, and Choi. Mussel-Inspired Coating and Adhesion for Rechargeable Batteries: A Review. *ACS Appl. Mater. Interfaces* **2018**, *10* (9), 7562–7573.
- [303] Burzio, and Waite. Cross-Linking in Adhesive Quinoproteins: Studies with Model Decapeptides. *Biochemistry* **2000**, *39* (6), 11147–11153.
- [304] Waite, and Qin. Polyphosphoprotein from the Adhesive Pads of *Mytilus Edulis*. *Biochemistry* **2001**, *40* (9), 2887–2893.
- [305] Pérez-Anes, Gargouri, Laure, Van Den Berghe, Courcot, Sobocinski, Tabary, Chai, Blach, and Addad. Bioinspired Titanium Drug Eluting Platforms Based on a Poly-β-Cyclodextrin–Chitosan Layer-by-Layer Self-Assembly Targeting Infections. *ACS Appl. Mater. Interfaces* **2015**, *7* (23), 12882–12893.
- [306] Sobocinski, Laure, Taha, Courcot, Chai, Simon, Addad, Martel, Haulon, and Woisel. Mussel Inspired Coating of a Biocompatible Cyclodextrin Based Polymer onto CoCr Vascular Stents. *ACS Appl. Mater. Interfaces* **2014**, *6* (5), 3575–3586.
- [307] Kato, Uchida, Kang, Uyama, and Ikada. Polymer Surface with Graft Chains. *Prog. Polym. Sci.* **2003**, *28* (2), 209–259.
- [308] Wu, Fan, Chang, and Xiao. Mussel-Inspired Porous SiO₂ Scaffolds with Improved Mineralization and Cytocompatibility for Drug Delivery and Bone Tissue Engineering. *J. Mater. Chem.* **2011**, *21* (45), 18300–18307.
- [309] Xi, Xu, Zhu, Wang, and Zhu. A Facile Method of Surface Modification for Hydrophobic Polymer Membranes Based on the Adhesive Behavior of Poly(DOPA) and Poly(Dopamine). *J. Memb. Sci.* **2009**, *327* (1), 244–253.
- [310] Cheng, Li, Zhao, Wei, Nie, Sun, and Zhao. The Hydrodynamic Permeability and Surface Property of Polyethersulfone Ultrafiltration Membranes with Mussel-Inspired Polydopamine Coatings. *J. Memb. Sci.* **2012**, *417–418*, 228–236.
- [311] Notarnicola, Hayashi, Curran, and Huisingsh. Progress in Working towards a More Sustainable Agri-Food Industry. *J. Clean. Prod.* **2012**, *28*, 1–8.
- [312] Laroche, Bergeron, and Barbaro-Forleo. Targeting Consumers Who Are Willing to Pay More for Environmentally Friendly Products. *J. Consum. Mark.* **2001**, *18* (6), 503–520.
- [313] de Boer. Environmental Impact Assessment of Conventional and Organic Milk Production. *Livest. Prod. Sci.* **2003**, *80* (1–2), 69–77.
- [314] Doglioli, Gambier, Sergent, Braodeaux, and Bronquer. Analyse de Cycle de Vie, Ecobilan. In *Eco-conception: Concept, Méthodes, Outils, Guides et Perspectives*; Vigneron, Patingre, Eds.; Université de Cergy-Pontoise: Paris, 2001; pp 148–163.
- [315] Eide. Life Cycle Assessment (LCA) of Industrial Milk Production. *Int. J. Life Cycle Assess.* **2002**, *7* (2), 115–126.
- [316] Finnegan, Goggins, Clifford, and Zhan. Environmental Impacts of Milk Powder and Butter Manufactured in the Republic of Ireland. *Sci. Total Environ.* **2017**, *579*, 159–168.
- [317] Hospido, Moreira, and Feijoo. Simplified Life Cycle Assessment of Galician Milk Production. *Int. Dairy J.* **2003**, *13* (10), 783–796.
- [318] Rafiee, Khoshnevisan, Mohammadi, Aghbashlo, Mousazadeh, and Clark. Sustainability Evaluation of Pasteurized Milk Production with a Life Cycle Assessment Approach: An Iranian Case Study. *Sci. Total Environ.* **2016**, *562*, 614–627.
- [319] Thoma, Popp, Nutter, Shonnard, Ulrich, Matlock, Kim, Neiderman, Kemper, East, and Adom. Greenhouse Gas Emissions from Milk Production and Consumption in the United States: A Cradle-to-Grave Life Cycle Assessment circa 2008. *Int. Dairy J.* **2013**, *31*, Supple, S3–S14.

- [320] Milani, Nutter, and Thoma. Invited Review: Environmental Impacts of Dairy Processing and Products: A Review. *J. Dairy Sci.* **2011**, *94* (9), 4243–4254.
- [321] World Commission on Environment and Development. 1987.
- [322] Vigneron, Duval, Laclau, Macon, and Fanny. *Ecologie Industrielle*. In *Eco-conception - concepts, méthodes, outils, guides et perspectives*; 2001; pp 14–25.
- [323] Avnir. LCA approach <https://www.avnir.org/>.
- [324] Ekvall. System Expansion and Allocation in Life Cycle Assessment, Chalmers University of Technology, Sweden, 1999.
- [325] González-García, Castanheira, Dias, and Arroja. Using Life Cycle Assessment Methodology to Assess UHT Milk Production in Portugal. *Sci. Total Environ.* **2013**, *442*, 225–234.
- [326] Vergé, Maxime, Dyer, Desjardins, Arcand, and Vanderzaag. Carbon Footprint of Canadian Dairy Products: Calculations and Issues. *J. Dairy Sci.* **2013**, *96* (9), 6091–6104.
- [327] Fantin, Buttol, Pergreffi, and Masoni. Life Cycle Assessment of Italian High Quality Milk Production. A Comparison with an EPD Study. *J. Clean. Prod.* **2012**, *28*, 150–159.
- [328] Flysjö, Cederberg, Henriksson, and Ledgard. How Does Co-Product Handling Affect the Carbon Footprint of Milk? Case Study of Milk Production in New Zealand and Sweden. *Int. J. Life Cycle Assess.* **2011**, *16* (5), 420–430.
- [329] Gerber, Vellinga, Opio, and Steinfeld. Productivity Gains and Greenhouse Gas Emissions Intensity in Dairy Systems. *Livest. Sci.* **2011**, *139* (1), 100–108.
- [330] Basset-Mens, Ledgard, and Carran. In *Proceedings of the Australian and New Zealand Ecological Economics in Action Conference*; Citeseer, 2005; pp 258–265.
- [331] Cederberg, Sonesson, Henriksson, Sund, and Davis. SIK Institutet för livsmedel och bioteknik, 2009.
- [332] Thomassen, Dalgaard, Heijungs, and Boer. Attributional and Consequential LCA of Milk Production. *Int. J. Life Cycle Assess.* **2008**, *13* (4), 339–349.
- [333] Foster, Green, Bleda, and Dewik. Environmental Impacts of Food Production and Consumption: Final Report to the Department for Environment Food and Rural Affairs. **2007**.
- [334] Vergé, Dyer, Desjardins, and Worth. Greenhouse Gas Emissions from the Canadian Dairy Industry in 2001. *Agric. Syst.* **2007**, *94* (3), 683–693.
- [335] Basset-Mens, Ledgard, and Boyes. Eco-Efficiency of Intensification Scenarios for Milk Production in New Zealand. *Ecol. Econ.* **2009**, *68* (6), 1615–1625.
- [336] Casey, and Holden. Analysis of Greenhouse Gas Emissions from the Average Irish Milk Production System. *Agric. Syst.* **2005**, *86* (1), 97–114.
- [337] Cederberg, and Flysjö. Life Cycle Inventory of 23 Dairy Farms in South-Western Sweden. **2004**.
- [338] Haas, Wetterich, and Köpke. Comparing Intensive, Extensified and Organic Grassland Farming in Southern Germany by Process Life Cycle Assessment. *Agric. Ecosyst. Environ.* **2001**, *83* (1), 43–53.
- [339] Feitz, Lundie, Dennien, Morain, and Jones. Generation of an Industry-Specific Physico-Chemical Allocation Matrix. Application in the Dairy Industry and Implications for Systems Analysis (9 Pp). *Int. J. Life Cycle Assess.* **2007**, *12* (2), 109–117.
- [340] Keller, Jungbluth, and Eggenberger. In *proceedings from: The 10th International Conference on Life Cycle Assessment of Food (LCA Food 2016)*; 2016.
- [341] Goedkoop, Heijungs, Huijbregts, De Schryver, Struijs, and Van Zelm. 2009.
- [342] Suwarno, Huang, Chew, Tan, Trisno, and Zhou. On-Line Biofilm Strength Detection in Cross-Flow Membrane Filtration Systems. *Biofouling* **2018**, *34* (2), 123–131.
- [343] Guenbour, Iken, Kebkab, Bellaouchou, Boulif, and Bachir. Corrosion of Graphite in Industrial Phosphoric Acid. *Appl. Surf. Sci.* **2006**, *252* (24), 8710–8715.
- [344] Sari, and Karaipekli. Preparation, Thermal Properties and Thermal Reliability of Palmitic Acid/Expanded Graphite Composite as Form-Stable PCM for Thermal Energy Storage. *Sol. Energy Mater. Sol. Cells* **2009**, *93* (5), 571–576.
- [345] Zheng, Wu, Wang, and Pan. Characterizations of Expanded Graphite/Polymer Composites Prepared by in Situ Polymerization. *Carbon N. Y.* **2004**, *42* (14), 2839–2847.
- [346] Wang, Han, Sommers, Park, T’Joel, and Jacobi. A Review on Application of Carbonaceous Materials and Carbon Matrix Composites for Heat Exchangers and Heat Sinks. *Int. J. Refrig.* **2012**, *35* (1), 7–26.
- [347] Naz, Kausar, and Siddiq. Influence of Graphite Filler on Physicochemical Characteristics of Polymer/Graphite Composites: A Review. *Polym. Plast. Technol. Eng.* **2016**, *55* (6), 604–625.

References

- [348] Rabah, and El-Dighidy. Effect of Impregnants on the Performance of Graphite-Block Heat-Exchangers. *J. Inst. Energy* **1990**, 63 (455), 79–84.
- [349] Eun, Song, Han, Lee, and Kim. Enhancement of Heat and Mass Transfer in Silica-Expanded Graphite Composite Blocks for Adsorption Heat Pumps: Part I. Characterization of the Composite Blocks. *Int. J. Refrig.* **2000**, 23 (1), 64–73.
- [350] Zhang, and Fang. Study on Paraffin/Expanded Graphite Composite Phase Change Thermal Energy Storage Material. *Energy Convers. Manag.* **2006**, 47 (3), 303–310.
- [351] Kapustenko, Perevertaylenko, Khavin, and Arsenyeva. Graphite Plate Heat Exchangers as Energy Saving Tool for Corrosive Media Duties. *Chem. Eng. Trans.* **2007**, 12, 219–224.
- [352] Sengupta, Bhattacharya, Bandyopadhyay, and Bhowmick. A Review on the Mechanical and Electrical Properties of Graphite and Modified Graphite Reinforced Polymer Composites. *Prog. Polym. Sci.* **2011**, 36 (5), 638–670.

ANNEXES

ANNEX I

Journal of Food Engineering 228 (2018) 38–49



Contents lists available at ScienceDirect

Journal of Food Engineering

journal homepage: www.elsevier.com/locate/jfoodeng

Influence of stainless steel surface properties on whey protein fouling under industrial processing conditions



Sawsen Zouaghi ^a, Thierry Six ^{a,b}, Nicolas Nuns ^c, Pardis Simon ^c, Séverine Bellayer ^a, Sona Moradi ^d, Savvas G. Hatzikiriakos ^d, Christophe André ^{a,b,e}, Guillaume Delaplace ^{a,b}, Maude Jimenez ^{a,*}

^a Univ. Lille, UMR 8207 – UMET – Unité Matériaux et Transformations, F-59000, Lille, France

^b INRA, F-59000, Lille, France

^c Univ. Lille, UMR 8181 – UCCS – Unité Catalyse et Chimie du Solide, F-59000, Lille, France

^d The University of British Columbia, Chemical and Biological Engineering Department, V6T-1Z3, Vancouver, BC, Canada

^e Hautes Etudes d'Ingénieur, F-59000, Lille, France

ARTICLE INFO

Article history:

Received 29 July 2017

Received in revised form

9 February 2018

Accepted 12 February 2018

Available online 14 February 2018

Keywords:

Dairy processing

Antifouling

Surface free energy

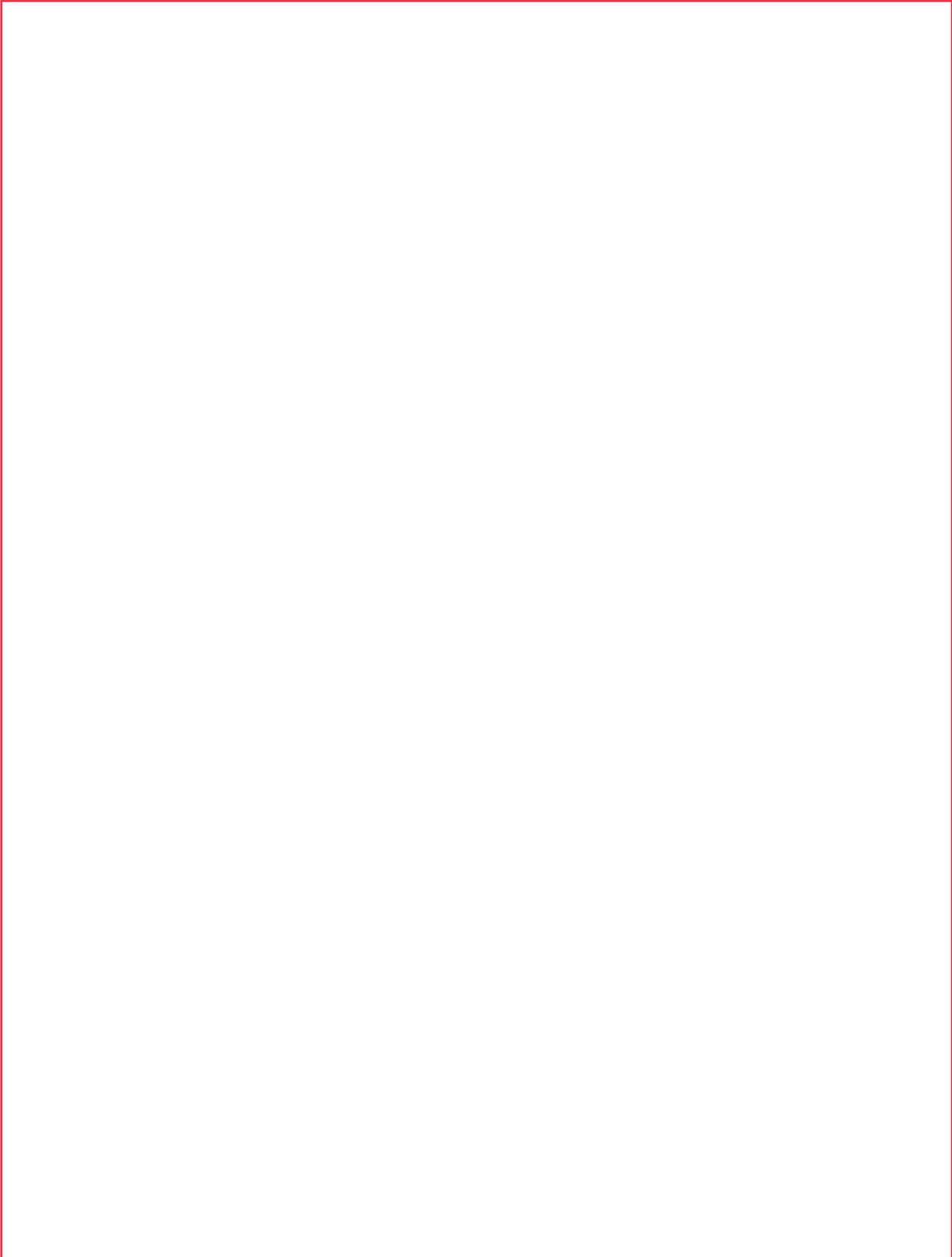
Roughness

Whey protein

ABSTRACT

Heat-induced fouling is a financial and environmental burden for food and dairy industries and its control is therefore desperately needed. A better understanding of the fouling mechanisms and their relation to stainless steel surface properties is thus of considerable interest. This work aims at studying the impact of stainless steel's surface morphology and surface free energy on fouling by a model dairy solution by a close examination of the deposit's growth and adhesion at the substrate-fluid interface. Pristine model surfaces of controlled roughness and surface energy, i.e. native, mirror polished and biomimetic femtosecond laser textured stainless steel surfaces, fluorosilanized or not, were tested under isothermal conditions in a pilot pasteurization facility fed with a model dairy fluid (whey protein and calcium solution). Multi-scale characterizations of those surfaces before and after fouling, using a wide range of analytical tools (goniometry, SEM, ToF-SIMS, EPMA X-Ray mappings) allowed for a better comprehension of the impact of surface energy and morphology modifications on the fouling behavior while highlighting their complex interactions in fouling governance. Lower surface energy was shown to be an asset against deposit growth, as fluorosilanization of native stainless steel allowed to reduce fouling by 72% (wt.%). The relative sizes of surface relief versus fouling agents has been found crucial, as it impacts interlocking phenomena. Textured surfaces have shown a tremendous increase in fouling (+391% for textured, +86% for fluorosilanized textured). However, interesting fouling performances were obtained on smooth, hydrophobic surfaces, as a reduction by 83% of fouling weight was achieved with fluorosilanized polished samples.

Crown Copyright © 2018 Published by Elsevier Ltd. All rights reserved.























ANNEX II

Experimental Methods for Surface Analyses and Characterizations

Water contact angle and surface free energy.

The advancing water contact angles (WCA) of the samples were measured on a DSA100 drop shape analyzer (Krüss, Germany) with 2 μL droplets of deionized water. Surface free energy (SFE) was calculated with Advance 3.0 (Krüss, Germany) following different empirical methods (OWRK, Van Oss, Wu) depending on the considered surface. Three probe fluids were used for SFE calculations: deionized water, formamide (Acros Organics) and diiodomethane (Sigma Aldrich). Their characteristics are listed in Table AII.0-1. All results are representative of at least three measures taken on three independent droplets randomly located on the surfaces.

Table AII.0-1. Values of surface free energy components for water, diiodomethane and formamide.

Fluid	γ^{total} (mN/m)	γ^{LW} (mN/m)	γ^{AB} (mN/m)	γ^+ (mN/m)	γ^- (mN/m)
Water	72.8	51.0	21.8	25.5	25.5
Diiodomethane	50.8	0.0	50.8	0.0	0.0
Formamide	58.0	19.0	39.0	2.3	39.6

Contact angle hysteresis (CAH, *i.e.* the difference between the advancing and the receding angle) of textured samples was measured *via* the tilting method on 5 μL droplets.

Optical microscopy

Optical microscopy pictures were obtained on a Keyence VHZ-1000 microscope, the magnification was x1000.

Scanning Electron Microscopy (SEM)

The SEM used to obtain secondary electron images was a Hitachi S4700 used at 5 kV acceleration voltage and a current intensity of 15 μA , at different magnifications. Prior to observation, the samples were air-dried and carbon-coated in vacuum in a BAL-TEC SDC 005 Sputter Coater.

Electron Probe Micro-Analysis (EPMA) and X-Ray Mappings

❖ Sample preparation

In order to obtain cross-section images, the samples were embedded in epoxy resin cylinders and then polished on a rotary polisher with abrasive silicon carbide paper (grades #180 to #2400) in order to get neat and smooth cross-sections.

When X-ray mappings of thin coatings are needed (below 1 μm), the sample is not embedded in epoxy resin, the cross section is directly polished by the mean of an ion polisher, Fischione 1060 SEM ion milling. A 5 hours polishing process was used, the argon beam was used at 4kv for 4hours for polishing and then at 1kV for 1hour for cleaning.

❖ Analysis

Back scattered electron images were carried out at 15 kV, 20 nA and X-ray mappings were carried out at 15 kV, 40 nA. For X-ray mappings, the crystal used to detect the $K\alpha$ of S (characteristic of protein deposit) and Ca (characteristic of mineral deposit) was PET (pentaerythrol), and a LiF crystal was used to detect the $K\alpha$ of Fe (steel substrate).

Contact Profilometer

Arithmetic mean roughness of the different samples was measured on an AlfaStep IQ surface profilometer (KLA-Tencor). The tip speed was 20 $\mu\text{m}/\text{s}$ and profiles were recorded on 500 μm -long segments. At least three measurements were carried out on each surface.

Atomic Force Microscopy (AFM)

The samples were imaged using a Dimension 3100 model AFM (Veeco) equipped with a Nanoscope IV controller (Digital Instruments) under ambient conditions. Single beam silicon cantilevers (AFM-TM Arrow, Nanoworld) with spring constants of $\sim 42 \text{ Nm}^{-1}$ and resonant frequencies of $\sim 250 \text{ kHz}$ were used. All AFM images were acquired in tapping mode and the image size was $200 \times 200 \text{ nm}^2$.

Fourier-Transformed Infrared Spectroscopy (FTIR)

FTIR spectroscopy of the different coatings was performed on a Nicolet iS-50 spectrometer (Thermo Scientific), in the spectral range 500 to 4000 cm^{-1} . Spectra post-treatment was done with Omnic 9 software.

Time-of-flight Secondary Ion Mass Spectrometry (ToF-SIMS)

ToF-SIMS analyses were performed on both the native steel and modified surfaces obtained after 1 minute fouling. ToF-SIMS spectra measurements were carried out using a ToF-SIMS V instrument (ION-TOF GmbH Germany), equipped with a bismuth liquid metal ion gun (LMIG). Pulsed Bi^+ primary ions were used for analysis (25 KeV, 1 pA). Charging effects, due to the primary ion beam, were compensated using low energy pulsed electrons (20 eV).

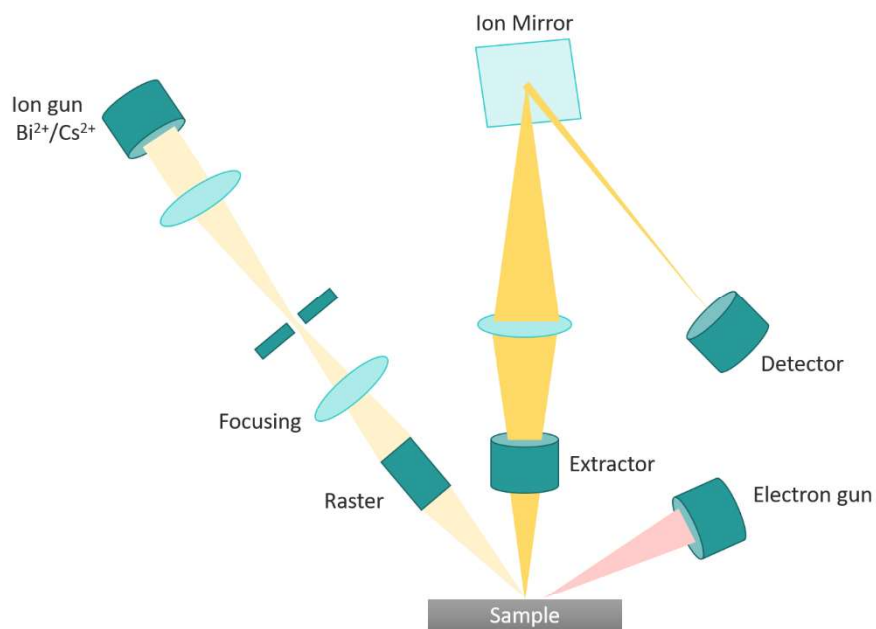


Figure A-II. 1. Schematic representation of key ToF-SIMS components.

Reference mass spectra were established recovering both ion polarities of the whey protein tableted for analysis. Surface spectra were taken from an area of 500 μm x 500 μm by accumulation of 20 scans, 128x128 pixels. Calcium secondary ions were mainly detected in positive polarity, so the depth profiling (non-interlaced mode) was performed only in positive mode on the samples. Cs^+ was used for sputtering (1 kV, 65 nA) and was scanned over an area of 300 μm x 300 μm .

Secondary ions were generated with Bi^+ from an area of $100\ \mu\text{m} \times 100\ \mu\text{m}$ centered on sputter gun crater. CsFe^+ ions were chosen as characteristic of steel substrate and CNCs_2^+ ions as characteristic of dairy deposit. Profiles combined with high lateral resolution secondary ions images were also acquired in the burst alignment mode using Bi^+ as primary ion gun (lateral resolution around few hundreds nm) and Cs^+ (1 kV, 65 nA) for sputtering. Analysis area for Cs^+ and Bi^+ was, respectively, $300 \times 300\ \mu\text{m}^2$ and $20 \times 20\ \mu\text{m}^2$.

X-Ray Photoelectron Spectroscopy (XPS)

XPS analysis were performed on a Kratos AXIS Ultra LDL device with a monochromatic Al K $\text{Al K}\alpha$ X-ray source (10 mA, 12 kV). C 1s, O 1s, Fe 2p, Cr 2p, Ni 2p and Si 2p spectra were obtained using a 40 eV pass energy. Spectra post-treatment was done using Casa XPS software (version 2.3.16, Casa Software Ltd.) All spectra were charge corrected to give the adventitious C1s component a binding energy of 284.8 eV.

Cross-Hatch Adhesion Tests

Coating adhesion on SS substrates was studied following the ASTM D3359-B standard with an Elcometer 107 cross-hatch cutter of 3 mm with 6 teeth. This procedure classifies coatings adhesion from 5B (very good adhesion) to 0B (poor adhesion) ranges.

ANNEX III

Antifouling Biomimetic Liquid-Infused Stainless Steel: Application to Dairy Industrial Processing

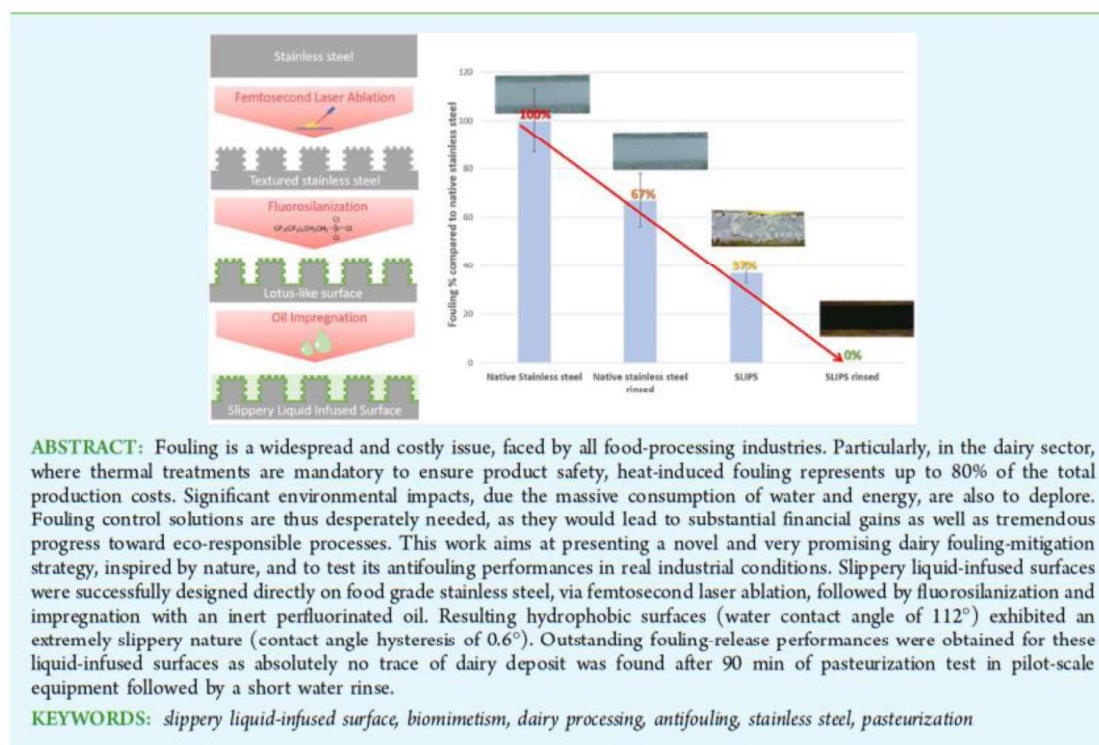
Sawsen Zouaghi,[†] Thierry Six,^{†,§} Séverine Bellayer,[†] Sona Moradi,^{||} Savvas G. Hatzikiriakos,^{||} Thomas Dargent,[‡] Vincent Thomy,[‡] Yannick Coffinier,[‡] Christophe André,^{†,§,⊥} Guillaume Delaplace,^{†,§} and Maude Jimenez^{*,†}

[†]UMR 8207, UMET, Unité Matériaux et Transformations, and [‡]UMR 8520, IEMN, Institute of Electronics, Microelectronics and Nanotechnology, Univ. Lille, F-59000 Lille, France

[§]INRA, F-59000 Lille, France

^{||}Chemical and Biological Engineering Department, The University of British Columbia, Vancouver, BC Canada

[⊥]Hautes Etudes d'Ingénieur, F-59000 Lille, France

















ANNEX IV

Applied Surface Science 455 (2018) 392–402



Contents lists available at ScienceDirect

Applied Surface Science

journal homepage: www.elsevier.com/locate/apsusc

Full Length Article

Atmospheric pressure plasma spraying of silane-based coatings targeting whey protein fouling and bacterial adhesion management

Sawsen Zouaghi^a, Thierry Six^{a,b}, Séverine Bellayer^a, Yannick Coffinier^c, Marwan Abdallah^a,
Nour-Eddine Chihib^a, Christophe André^{a,d}, Guillaume Delaplace^{a,d}, Maude Jimenez^{a,*}

^a Univ. Lille, UMR 8207 – UMET – Unité Matériaux et Transformations, F-59000 Lille, France

^b INRA, F-59000 Lille, France

^c Institute of Electronics, Microelectronics and Nanotechnology, Univ. Lille, UMR 8520 - IEMN, F-59000 Lille, France

^d Hautes Etudes d'Ingénieur, F-59000 Lille, France



ARTICLE INFO

Keywords:

Anti-fouling
Atmospheric pressure plasma spraying
Dairy pasteurization
Silane
HMDSO

ABSTRACT

This work aims at studying the impact of silane-based coatings, generated by atmospheric pressure plasma spraying (APPS) of a liquid precursor (hexamethyldisiloxane – HMDSO), on dairy antifouling and antibacterial properties of food-grade 316L stainless steel. The influence of the manufacturing parameters (precursor flow rate, nozzle-to-substrate distance and scanning speed) on the coatings properties was investigated using a wide range of characterization techniques (drop shape analysis, X-Ray Mappings, Scanning Electron Microscopy, Fourier-Transformed Infrared Spectroscopy, Atomic Force Microscopy). Coating's roughness in particular was shown to strongly increase when precursor flow rate increases. A pilot pasteurizer, fed with a model foulant solution (whey protein and calcium), allowed performing two consecutive industrial-like isothermal dairy fouling tests, revealing the promising anti-fouling properties of the HMDSO-coated steel. A fouling reduction of up to 90% compared to bare stainless steel was achieved after first cycle for all samples. The second fouling run allowed to select the best-performing sample, which kept the same antifouling properties as in the first test. Its mechanism of action was investigated, which revealed that a nanostructured, Si-O-Si rich surface was efficient to prevent isothermal dairy fouling. The adhesion of the pathogenic bacterium *Staphylococcus aureus* also proved to be impacted by this plasma coating, with a significant decrease of adhered cells (~30% compared to native stainless steel).

* Corresponding author.

E-mail addresses: sawsen.zouaghi@ed.univ-lille1.fr (S. Zouaghi), thierry.six@lille.inra.fr (T. Six), severine.Bellayer@ense-lille.fr (S. Bellayer), yannick.Coffinier@univ-lille1.fr (Y. Coffinier), nour-Eddine.Chihib@univ-lille1.fr (N.-E. Chihib), christophe.andre@yncrea.fr (C. André), guillaume.delaplace@lille.inra.fr (G. Delaplace), maude.jimenez@univ-lille1.fr (M. Jimenez).

<https://doi.org/10.1016/j.apsusc.2018.06.006>

Received 20 February 2018; Received in revised form 4 May 2018; Accepted 1 June 2018

Available online 02 June 2018

0169-4332/ © 2018 Elsevier B.V. All rights reserved.

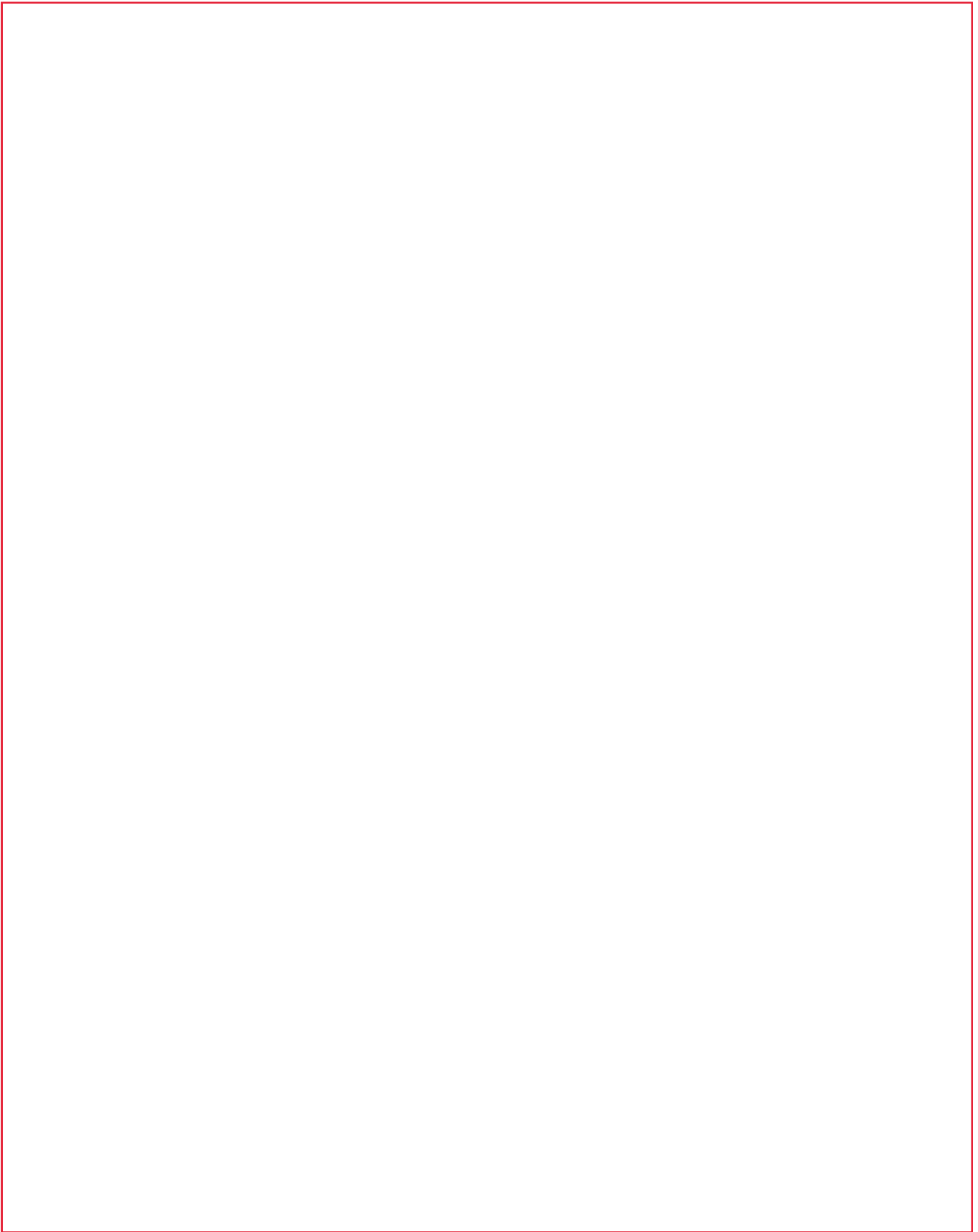




















ANNEX V

*Detailed contact angle values for PEO-modified coatings***Table A-IV.1.** Values of the water contact angle (WCA) of Si-PEO, PL-(Si-PEO), PD-(Si-PEO), NuSil-(PEO) and NuSil-(Si-control) surfaces with time.

Time (s)	O-(Si-PEO)		PL-(Si-PEO)		PD-(Si-PEO)		NuSil-(Si-PEO)		NuSil-(Si-control)	
	WCA (°)	SD	WCA (°)	SD	WCA (°)	SD	WCA (°)	SD	WCA (°)	SD
0	107.2	10.0	108.1	3.2	114.8	1.2	104.9	1.9	118.0	0.6
10	97.1	9.9	97.6	2.7	78.2	6.2	73.7	14.0	118.0	0.6
20	70.2	11.9	86.2	1.8	55.1	1.3	44.3	18.3	118.0	0.6
30	54.1	5.2	77.2	0.5	46.3	1.3	39.3	12.4	118.0	0.6
40	45.9	5.7	72.9	1.2	41.1	1.6	35.5	7.8	118.0	0.6
50	42.5	5.3	69.7	0.9	36.8	0.7	32.0	3.3	118.0	0.6
60	39.4	5.4	67.8	0.6	34.5	0.6	31.2	3.2	118.0	0.6
70	37.7	5.2	66.2	0.8	33.9	1.2	31.1	2.1	118.0	0.6
80	36.2	5.0	64.8	0.8	32.4	1.3	29.8	2.8	118.0	0.6
90	35.1	4.6	63.2	1.1	31.8	1.9	29.2	2.5	118.0	0.6
100	34.4	4.8	62.2	1.1	30.9	1.6	28.7	2.2	118.0	0.6
110	32.5	3.1	61.1	1.1	29.8	2.1	28.0	2.1	118.0	0.6
120	32.0	3.2	60.2	1.1	29.2	1.9	27.4	1.9	118.0	0.6
130	31.2	3.7	59.3	1.0	28.4	1.9	26.9	1.9	118.0	0.6
140	30.6	3.3	58.4	1.0	27.6	1.9	26.4	1.7	118.0	0.6
150	30.1	3.5	56.6	0.2	28.2	0.7	26.0	1.8	118.0	0.6

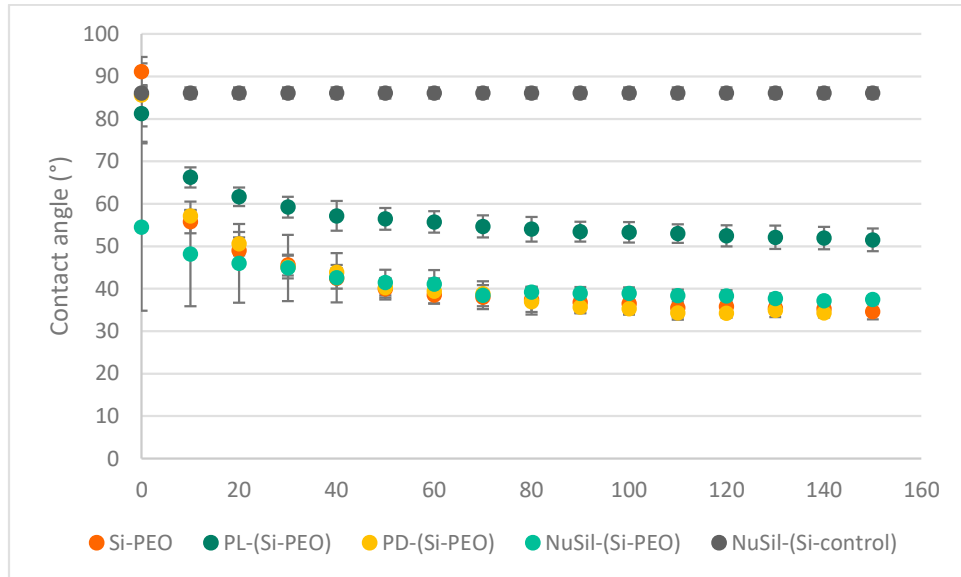


Figure A-IV.1. Variation of diiodomethane contact angle with time of PEO-modified silicone (“Si-PEO”) coated onto stainless steel (SS) substrates having different pretreatments as well as an unmodified silicone coated on NuSil SP 120 treated SS “NuSil-(Si-control)”. (Note: Standard deviation values for WCA of PL-(Si-PEO) and NuSil-(Si-control) surfaces are too small to be clearly presented on the figure (see ESI, Table B).)

ANNEX VI

SADT Diagrams of the different systems and subsystems in the LCA study

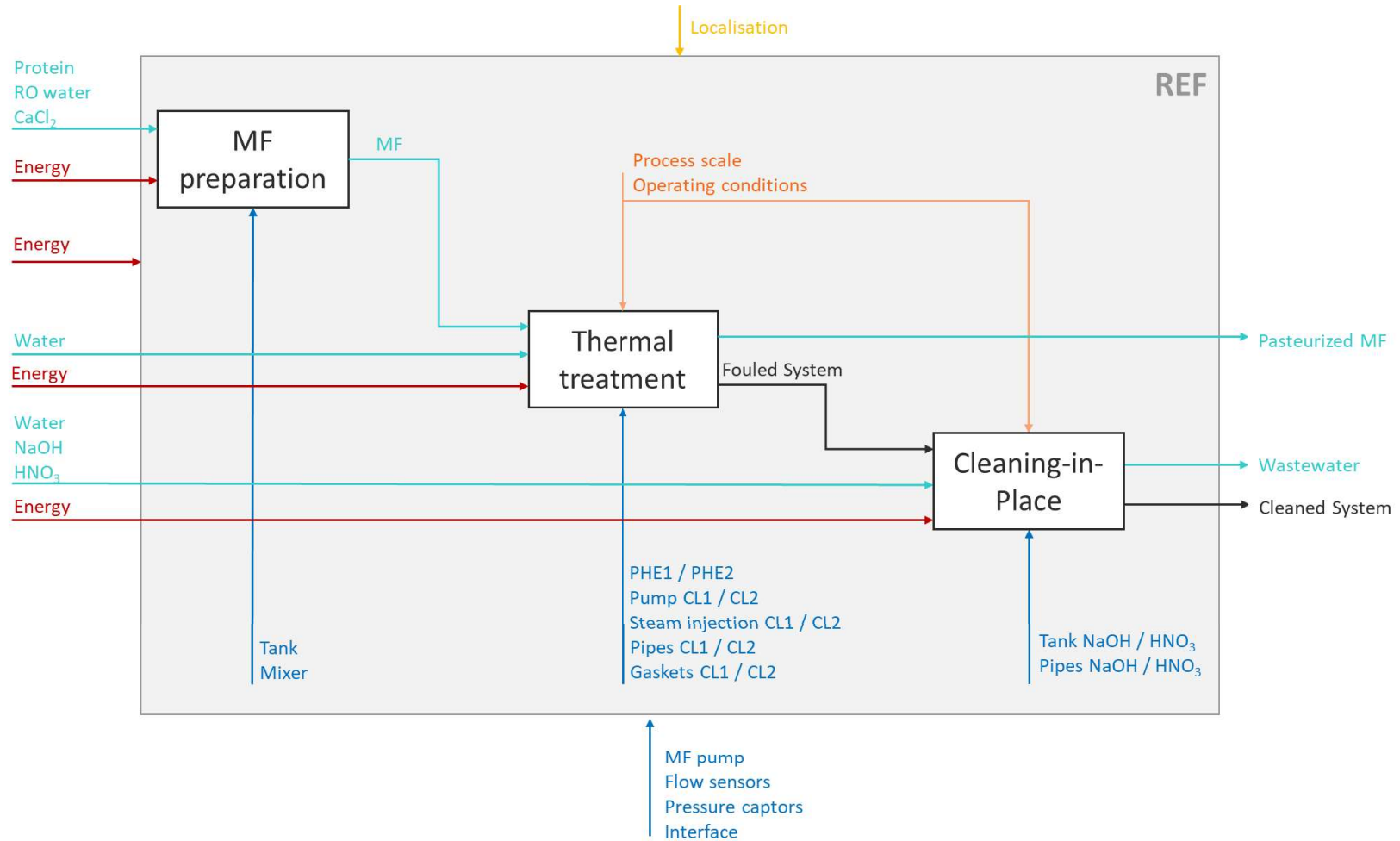


Figure A-VI.1. SADT diagram of the REF system.

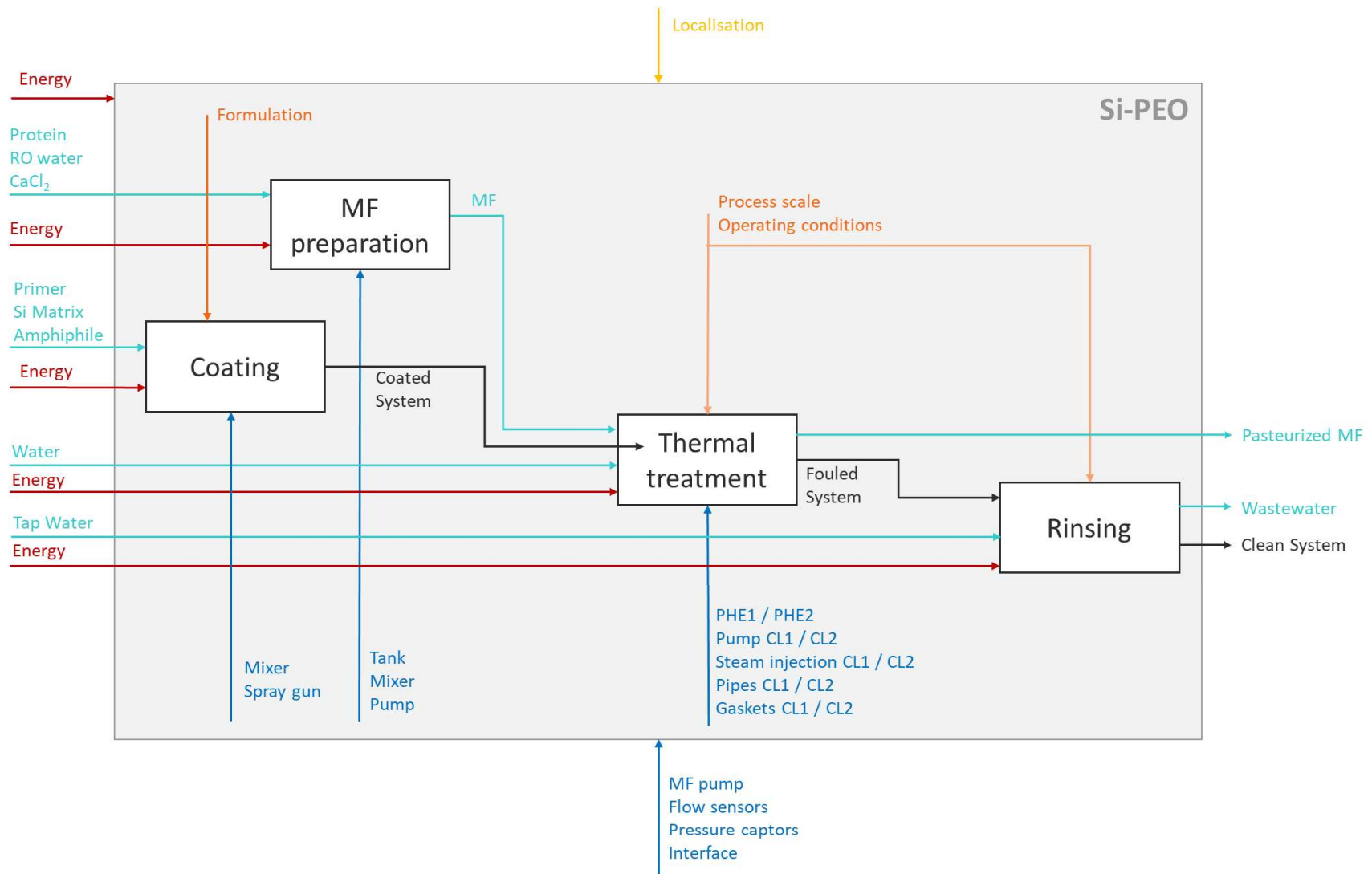


Figure A-VI.2. SADT Diagram of the Si-PEO system.

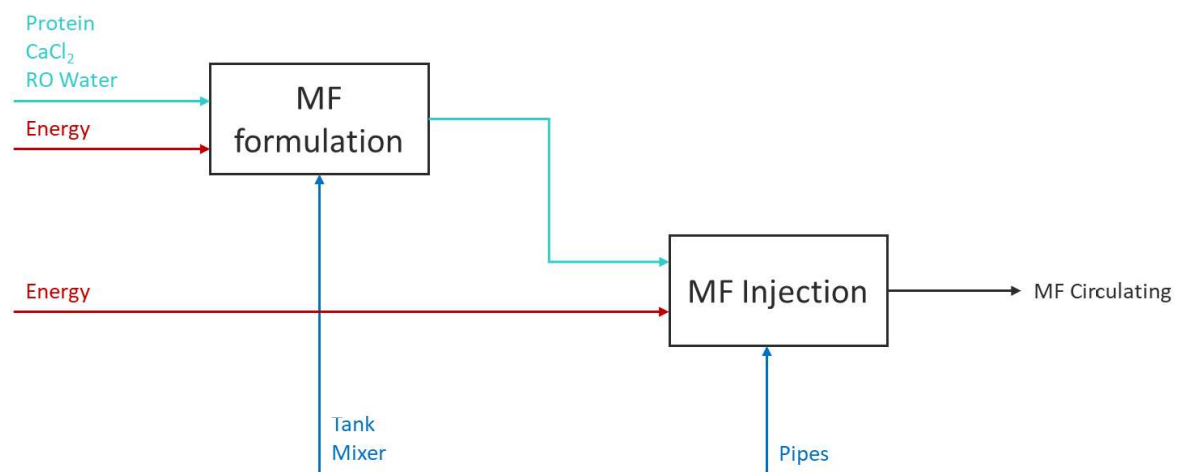


Figure A-VII. 3. SADT diagram of the “MF preparation” subsystem.

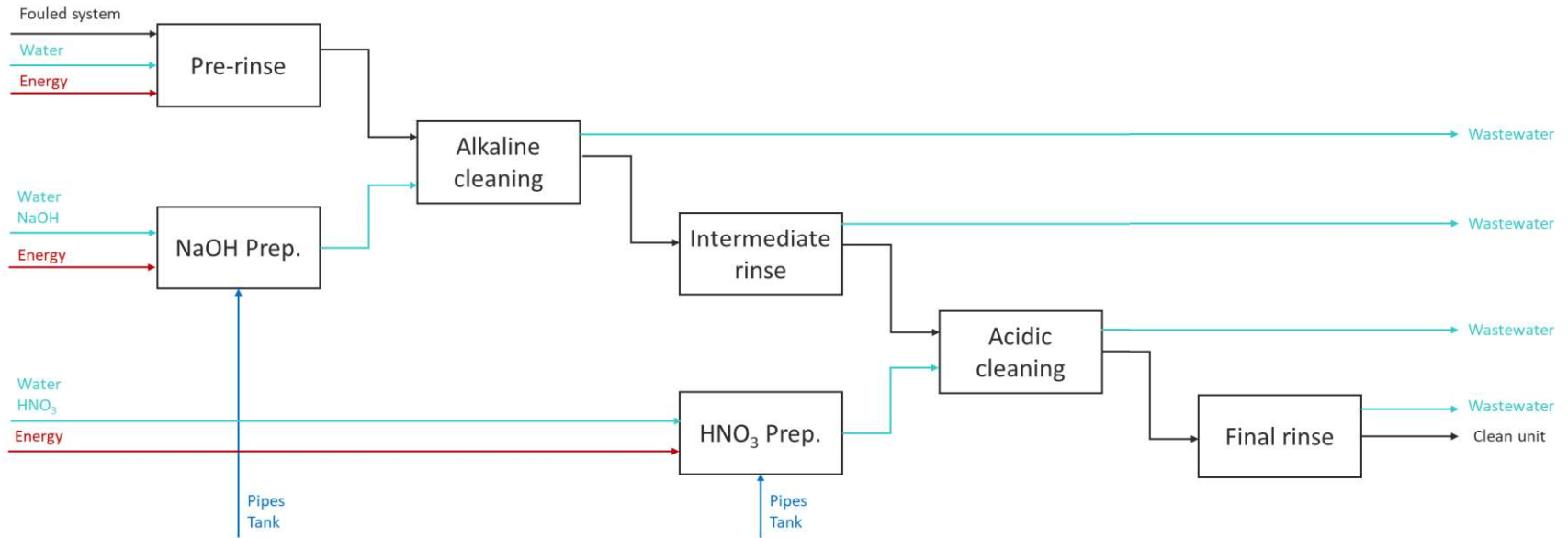


Figure A-VI.4. SADT diagram of the “Cleaning-in-place” subsystem.

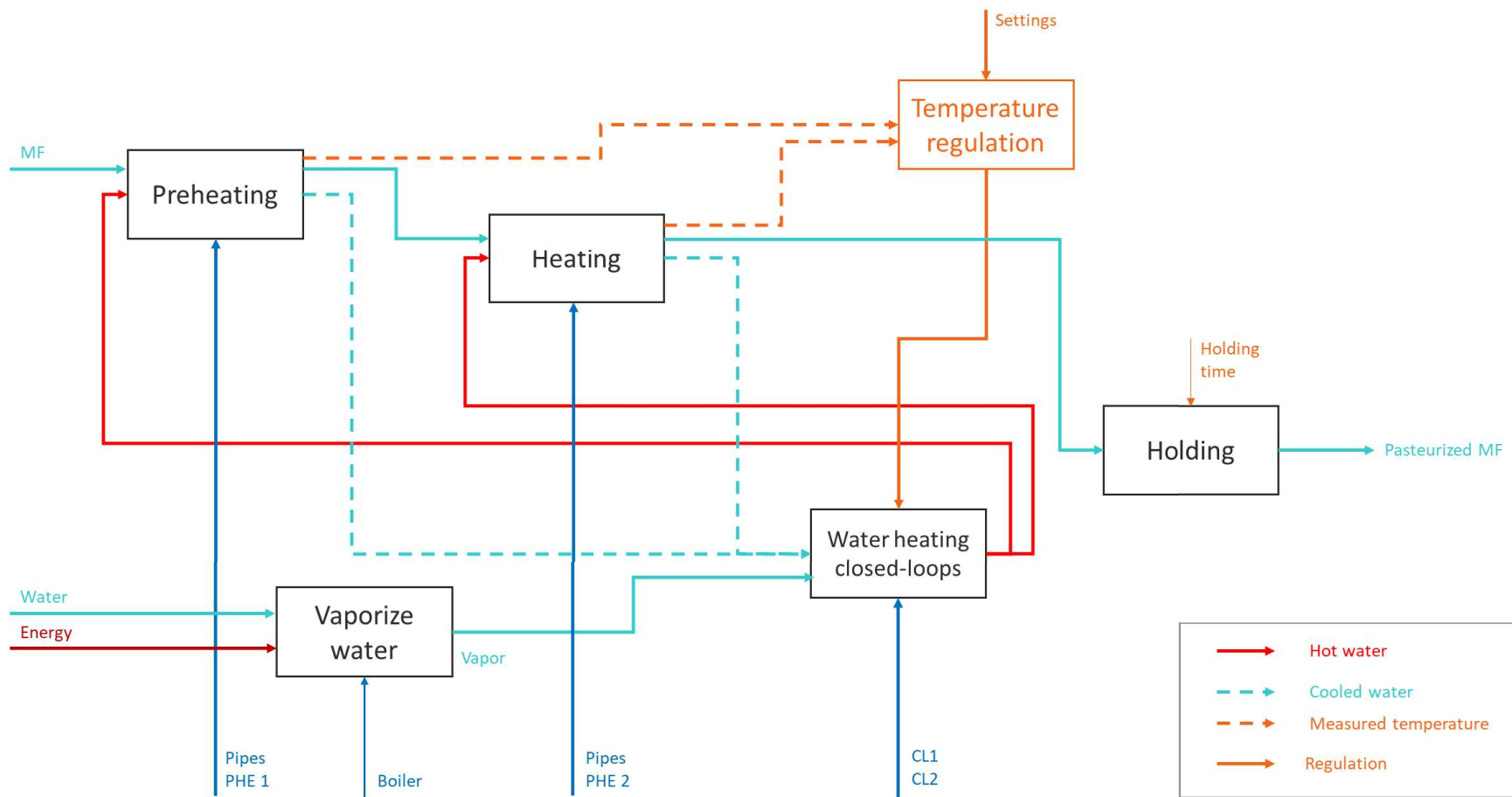


Figure A-VI.5. SADT diagram of the “thermal treatment” subsystem.

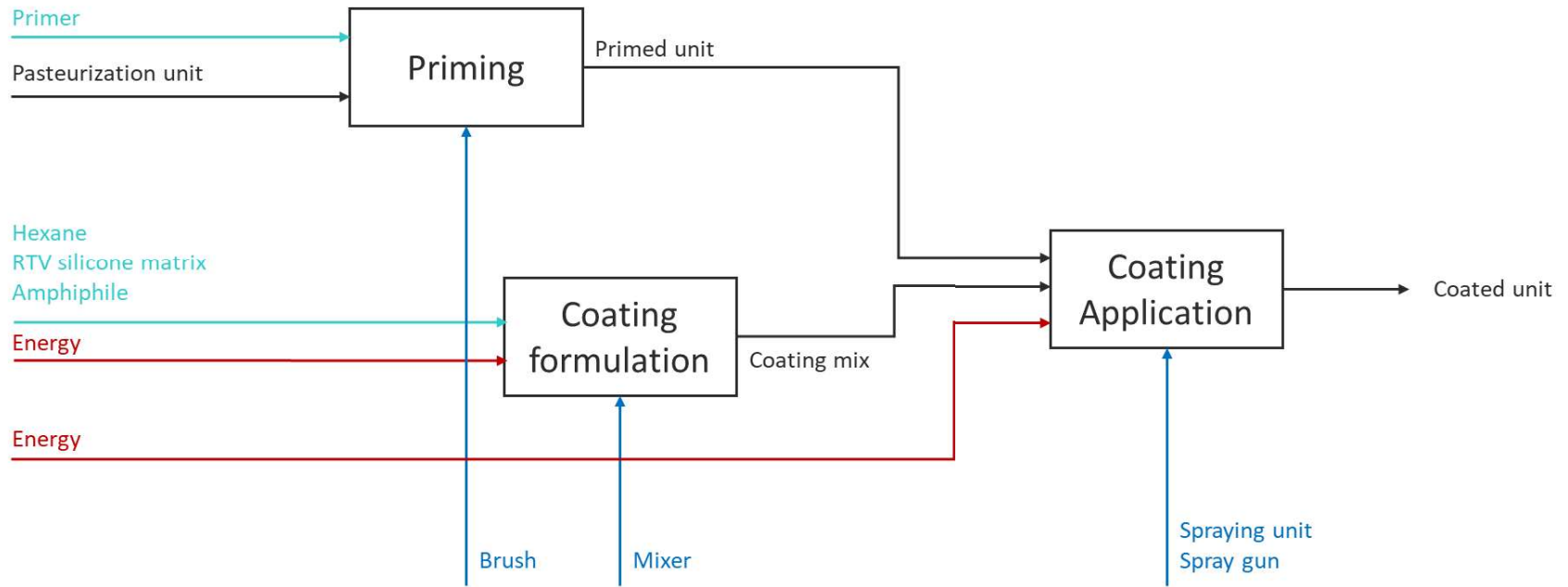


Figure A-VI.6. SADT diagram of the “coating” subsystem.

ANNEX VII

Detailed impact scores of the REF and Si-PEO systems

Table A-VII. 1. Detailed impact scores of the REF system and subsystems.

Impact category	Scores (μ Pts)				
	<i>Whole process</i>	<i>MF preparation</i>	<i>Thermal treatment</i>	<i>Rinsing</i>	<i>Other</i>
Climate change Human Health	23,973	1,440	2,253	20,257	0,026
Ozone depletion	0,002	0,000	0,001	0,000	0,000
Human toxicity	11,902	0,624	1,531	9,710	0,039
Photochemical oxidant formation	0,000	0,000	0,000	0,000	0,000
Particulate matter formation	0,752	0,137	0,267	0,344	0,006
Ionizing radiation	0,016	0,001	0,014	0,000	0,000
Climate change Ecosystems	19,132	1,149	1,798	16,166	0,021
Terrestrial acidification	0,021	0,005	0,007	0,009	0,000
Freshwater eutrophication	0,000	0,000	0,000	0,000	0,000
Terrestrial ecotoxicity	0,078	0,023	0,005	0,049	0,000
Freshwater ecotoxicity	0,006	0,000	0,000	0,006	0,000
Marine ecotoxicity	0,547	0,013	0,021	0,512	0,001
Agricultural land occupation	0,341	0,220	0,108	0,013	0,001
Urban land occupation	0,029	0,002	0,010	0,017	0,000
Natural land transformation	0,472	0,061	0,395	0,002	0,014
Metal depletion	0,463	0,020	0,216	0,188	0,040
Fossil depletion	4,771	1,282	2,194	1,275	0,023
Total	62,506	4,977	8,823	48,549	0,172

Table A-VII. 2. Detailed impact scores of the Si-PEO system and subsystems.

Impact Category	Scores (μ Pts)					
	<i>Whole process</i>	<i>Coating</i>	<i>MF preparation</i>	<i>Thermal treatment</i>	<i>Rinsing</i>	<i>Other</i>
Climate change Human Health	3,84	0,11	1,44	2,27	0,01	0,02
Ozone depletion	0,00	0,00	0,00	0,00	0,00	0,00
Human toxicity	2,28	0,09	0,62	1,54	0,01	0,03
Photochemical oxidant formation	0,00	0,00	0,00	0,00	0,00	0,00
Particulate matter formation	0,44	0,03	0,13	0,27	0,00	0,00
Ionising radiation	0,02	0,00	0,00	0,01	0,00	0,00
Climate change Ecosystems	3,07	0,09	1,15	1,81	0,01	0,01
Terrestrial acidification	0,01	0,00	0,00	0,01	0,00	0,00
Freshwater eutrophication	0,00	0,00	0,00	0,00	0,00	0,00
Terrestrial ecotoxicity	0,03	0,00	0,02	0,01	0,00	0,00
Freshwater ecotoxicity	0,00	0,00	0,00	0,00	0,00	0,00
Marine ecotoxicity	0,04	0,00	0,01	0,02	0,00	0,00
Agricultural land occupation	0,33	0,00	0,22	0,11	0,00	0,00
Urban land occupation	0,01	0,00	0,00	0,01	0,00	0,00
Natural land transformation	0,48	0,02	0,06	0,40	0,00	0,01
Metal depletion	0,33	0,07	0,02	0,22	0,00	0,03
Fossil depletion	3,62	0,11	1,28	2,21	0,00	0,02
Total	14,51	0,52	4,96	8,88	0,03	0,12

Dairy fouling on stainless steel and design of antifouling surfaces

ABSTRACT Fouling is an ongoing issue which burdens the cost of dairy thermal processes as well as their environmental impact. Understanding the fouling phenomena and finding mitigation solutions is therefore of high interest. Consequently, this work aims at: (i) studying the impact of surface properties variation on dairy fouling and (ii) designing and characterizing the mechanisms of action of novel biomimetic antifouling surfaces. It was demonstrated that surface properties were crucial for fouling mitigation, low roughness and low surface energy being the most favorable conditions for fouling reduction. In a second time, three types of biomimetic surfaces, namely slippery liquid infused surfaces (SLIPS), nano-rough atmospheric plasma coatings and amphiphilic environment-responsive coatings were proven efficient against isothermal dairy fouling. The amphiphilic coatings unquestionably presented the best antifouling performances as they totally prevented fouling development as well as pathogenic bacteria adhesion. Such surfaces should allow for significant savings in cleaning costs and environmental impact through the adaptation of the cleaning procedures. In order to assess the real effect of the antifouling coatings on the footprint of the pasteurization process, a Life Cycle Assessment study was carried out. It was demonstrated that the use of such an antifouling coating could lead to the reduction of the environmental impact of a pasteurization process by more than 70%.

RESUME Les traitements thermiques des produits laitiers induisent des phénomènes d'encrassement des échangeurs thermiques, et donc des nettoyages réguliers, qui alourdissent les coûts de production ainsi que l'impact environnemental des procédés. Il est donc important de comprendre ces phénomènes d'encrassement et de développer des stratégies pour les limiter. Cette thèse vise à : (i) étudier l'impact des variations des propriétés de surface sur l'encrassement laitier, (ii) mettre au point des surfaces anti-encrassantes bioinspirées innovantes et (iii) comprendre le mode d'action de ces surfaces. Il a été démontré que les propriétés de surface d'un substrat sont cruciales pour contrôler l'encrassement : la diminution conjointe de la rugosité et de l'énergie de surface sont favorables à la réduction de l'encrassement. Suivant ce constat, d'excellentes propriétés encrassantes ont été obtenues suite à la mise au point de trois surfaces bioinspirées (surfaces lubrifiées « SLIPS », revêtements par plasma atmosphérique et revêtements amphiphiles). Les revêtements amphiphiles ont obtenu sans conteste les meilleurs résultats. Ils préviennent non seulement totalement l'encrassement mais également l'adhésion de bactéries pathogènes. Ce type de revêtement pourrait donc permettre de réaliser des économies non négligeables, non seulement en termes de coût de nettoyage des installations industrielles, mais également en termes d'impact environnemental des procédés. Afin de quantifier l'impact de la modification de surface sur l'empreinte environnementale de la pasteurisation, une étude d'Analyse du Cycle de Vie a été menée et a permis d'établir que l'utilisation d'un revêtement anti-encrassant permettrait de réduire l'impact environnemental d'un procédé de pasteurisation de plus de 70%.

KEYWORDS – MOTS-CLES

Antifouling	<i>Encrassement – Lutte contre</i>	Life Cycle Assessment (LCA)	<i>Analyse du Cycle de Vie (ACV)</i>
Dairy thermal processing	<i>Produits laitiers – Traitement thermique</i>	Slippery Liquid-Infused surfaces (SLIPS)	<i>Surfaces imprégnées de lubrifiant (SLIPS)</i>
Surface modification	<i>Traitement de surface</i>	Atmospheric plasma spraying	<i>Projection au plasma</i>
Biomimetism	<i>Biomimétisme</i>	Amphiphilic coatings	<i>Revêtements amphiphiles</i>
Bacterial adhesion	<i>Bactéries - Adhésivité</i>		